The role of SCN AVP neurons in modulating RP3V kisspeptin neuron activity in physiological and pathological reproductive states

Bradley Jamieson

A thesis submitted for the degree of Doctor of Philosophy

Department of Physiology, University of Otago

Dunedin, New Zealand

May 2020

Abstract

Mammalian fertility is governed by a neural circuit that ultimately controls the activity of gonadotropin-releasing hormone (GnRH) neurons. Activation of GnRH neurons results in the pituitary release of luteinising hormone (LH) and follicle-stimulating hormone. Prior to ovulation, there is a surge in the release of LH, due to the increased activity of afferent kisspeptin neurons in the rostral periventricular area of the third ventricle (RP3V). These kisspeptin neurons are under the control of circadian inputs from the suprachiasmatic nucleus (SCN) and ovarian steroid hormone feedback. One key circadian input to kisspeptin neurons is the vasopressin (AVP) neurons from the SCN. Recent evidence has shown that AVP increases RP3V kisspeptin neuron activity, in relation to the level of ovarian steroids. As such, it is hypothesised that SCN AVP neurons are a key input onto RP3V kisspeptin neurons and their activation underpins the downstream activation of kisspeptin neurons and the resulting preovulatory LH surge.

Using genetically-mediated anterograde viral tract tracing, the projection from SCN AVP neurons was traced in the *Avp-cre* mouse model. *Avp-cre* projections to the RP3V were found in the RP3V and were in close appositions to kisspeptin neurons present. There was a significant correlation between the amount of viral-expression in *Avp-cre* neurons in the SCN to the density of projections seen in the RP3V; there was no correlation between other AVP-expressing regions and the RP3V. This indicates that the *Avp-cre* projection to the RP3V is specifically from the SCN, rather than from other areas if the brain.

To determine whether the *Avp-cre* projections to RP3V kisspeptin neurons were communicating by GABAergic fast-synaptic transmission, a viral vector expressing a channelrhodopsin (ChR2) variant was injected into the SCN of female *Avp-cre:Kiss1-hrGFP* mice. Using short pulses of blue light, the ChR2-expressing projections were optogenetically stimulated while whole-cell electrophysiological recordings were made from identified kisspeptin neurons in the RP3V. Despite the *Avp-cre* appositions to RP3V kisspeptin neurons, very few received inhibitory postsynaptic currents from ChR2-expressing *Avp-cre* projections

in response to optogenetic stimulation. There were no differences to this input across the oestrous cycle.

To determine the contribution of AVPergic to RP3V kisspeptin neurons, high-frequency light stimulation (HFLS) of *Avp-cre* projections was carried out whilst on-cell loose-patch recordings were made from identified RP3V kisspeptin neurons. There was a significant increase in kisspeptin firing rate following HLFS solely in proestrus, which was not seen in other oestrous cycle stages. This response was able to be blocked by the V1R antagonist Manning Compound, indicating it was mediated by AVP release. Surprisingly, a second response was found, solely in oestrus. Rather than a delayed, AVP-mediated excitation of kisspeptin neurons, an immediate inhibition in kisspeptin firing was noted. This response was not seen in other oestrous cycle stages. To determine the potential mechanism of this inhibition, the $GABA_AR$ antagonist, gabazine, was applied throughout HFLS. This inhibited the HFLS-induced decrease during oestrus, suggesting it was mediated by GABA release. Both the excitatory and inhibitory responses seen across the oestrous cycle correlate to time points where the LH surge should and should not be initiated respectively. This points towards a mechanism by which SCN AVP neurons can either trigger or inhibit the onset of the LH surge.

This work was followed by an examination of the SCN-to-RP3V circuit in a mouse model of polycystic ovary syndrome (PCOS), which does not naturally mount an LH surge. In the prenatally androgen-treated (PNA) mouse model, the *Avp-cre* projection to the RP3V was reduced; as was the proportion of close appositions made with kisspeptin neurons. Despite this, kisspeptin neurons from the PNA mouse were able to respond to AVP application.

Overall, this work has confirmed a projection from SCN AVP neurons to RP3V kisspeptin neurons, that comprises an indirect pathway leading to GnRH neuron activation. Activation of this circuit shows oestrous cycle-dependent changes that are consistent with increases in neural activity at the time of the LH surge. Finally, as this circuitry is critical for the timing of the LH surge, its reduction in a clinically relevant mouse model, may be an underlying cause of ovulatory dysfunction seen in PCOS.

Acknowledgements

Firstly, an enormous thank you to supervisors, Richard Piet and Rebecca Campbell. Through this fast-paced rollercoaster of a PhD your support and feedback has been invaluable in shaping not only this work, but my scientific ability as well. Your positivity and dedication to this project, despite our different time zones, has been inspiring and much appreciated.

Many thanks to my advisory committee, Phil Sheard and Brian Hyland. I am grateful for your assistance and convivial approach to this work and its dissemination.

My thanks go out to the members of the Piet Laboratory, particularly Greg Bouwer and Simone Thomas for their never ending support and help with this project; as well to our students Anaëlle Braine, Phebe Lee and Yeri Rim for their help, questions and insight. Further, thanks must go to members of the Campbell Laboratory, Mel Prescott and Amy Ruddenklau, for their help with various aspects of this project; as well as Chris Coyle, Elodie Desroziers, Eulalia Coutinho, Mauro Silva, Chris Marshall, Aisha Sati, Sarah Holland, Phoebe Ross, Monica Hamilton, Nina Donaldson and Renee Masih, for their support and critical insight. I'd also like to extend my gratitude to our visiting professors, Djurdjica Coss and Charles Roselli, both of whom have provided support and insight into not only this project but my ongoing development as a scientist.

Thanks to members of the Centre for Neuroendocrinology, particularly Rachael Augustine, Colin Brown, Jenny Clarkson, Rob Porteous, Su Han, Allan Herbison, Julia Gouws, Betina Nair, Christine Jasoni, and to Andrew McNaughton of the Otago Centre for Confocal Microscopy, for their help with learning and developing new techniques, as well as their help with interpreting the results from then. As well as a thank you to Mum, for her insightful proofreading and interest.

Finally, I would like to thank the Centre for Neuroendocrinology, the Department of Physiology, and the Division of Health Sciences all at the University of Otago; the British Society for Neuroendocrinology; the Physiological Society of New Zealand; and the New Zealand Society for Endocrinology for financial support that has helped support this research and its dissemination at conferences both local and international.

Table of Contents

List of Figures

List of Tables

Abbreviations

(-/-)	Wildtype
(+/-)	Heterozygous
(+/+)	Homozygous positive
3D	Three dimensional
3V	Third ventricle
4-AP	4-aminopyridine
5-HT	Serotonin
AAV	Adenoassociated virus
AgCl	Silver chloride
AHA	Anterior hypothalamic area
AR	Androgen receptor
ARN	Arcuate nucleus
AVP	Arginine-vasopressin
Avp	AVP gene
AVPV	Anteroventral periventricular nucleus
BK	Large-conductance calcium-activated potassium (channel)
BMAL-1	Brain and muscle Arnt-like protein-1
BSA	Bovine serum albumin
$CaCl_2$	Calcium chloride
CALB	Calbindin
CALR	Calretinin
CCK	Cholecystokinin
ChR2	Channelrhodopsin
$ChR2^{(ET/TC)}$	Channelrhodopsin with mutations E123T and T159C
CLOCK	Circadian locomotor output cycles kaput
Clock	CLOCK gene
CRACM	Channelrhodopsin-assisted circuit mapping
Cre	Cre recombinase enzyme
CRY	Cryptochrome protein
cTRIO	Cell-type specific tracing of the relationship between input and output
DHT	5α-dihydrotestosterone
DNA	Deoxyribonucleic acid
DREADD	Designer receptor exclusively activated by designer drugs

E_2	Oestradiol
E*(x)*	Embryonic day *x*
EBox	Enhancer box
ELISA	Enzyme-linked immunosorbent assay
ENK	Enkephalin
ER	Oestrogen receptor (α or β)
ERα	Oestrogen receptor alpha
ERβ	Oestrogen receptor beta
FSH	Follicle-stimulating hormone
FSHR	FSH receptor
g	gram(s)
$G\alpha_q$	G-protein-alpha-q subunit
$G\alpha_s$	G-protein alpha-s subunit
GABA	Gamma-amino butyric acid
$GABA_AR$	GABA receptor A
$GABA_BR$	GABA receptor B
GABAR	GABA receptor (A or B)
GBZ	Gabazine
GC	Genetic copy(-ies)
GDX	Gonadectomise(d)
GFP	Green fluorescent protein
GnRH	Gonadotropin-releasing hormone
Gnrh1	GnRH gene
GnRHR	GnRH receptor
GPCR	G-protein-coupled receptor
GPR54	G-protein-coupled receptor 54 (See also: Kiss1R)
GRP	Gastrin-releasing peptide
H_2O	Water
H_2O_2	Hydrogen peroxide
HCl	Hydrochloric acid
HCN	Hyperpolarisation-activated cyclic-nucleotide-gated ion channel
HEPES	4-(2-hydroxyethyl)-1-piperazineethanesulfonic acid
HFLS	High-frequency light stimulation
HPG	Hypothalamic-pituitary-gonadal
hrGFP	Humanised *renilla* green fluorescent protein

Hz	Hertz
icre	Codon improved cre
IgG	Immunoglobulin
IGL	Intergeniculate leaflet
I_H	Hyperpolarisation-activated cation current
IPSC	Inhibitory postsynaptic current
ir	Immunoreactive, Immunoreactivity
IRES2	Internal ribosome entry site
K2P	Two-pore domain potassium (channel)
KCl	Potassium chloride
kg	Kilogram(s)
kHz	Kilohertz
Kiss1	Kisspeptin gene
Kiss1R	Kisspeptin receptor (see also: GPR54)
KNDy	Kisspeptin-neurokinin B-dynorphin
KO	Knock out
KOH	Potassium hydroxide
LDCV	Large dense-core vesicle
LED	Light-emitting diode
LH	Luteinising hormone
LHA	Lateral hypothalamic area
LHR	LH receptor
LoxP	Locus of X-over P1
M	Molar, Moles per litre
MBH	Mediobasal hypothalamus
MC	Manning Compound, [β-Mercapto-β,β-cyclopentamethylenepropionyl^{1},O-me Tyr^{2}, Arg^{8}]-Vasopressin
mg	Milligram(s)
MgATP	Magnesium adenosine triphosphate
$MgCl_2$	Magnesium chloride
min	Minute(s)
mL	Millilitre(s)
mm	Millimetre(s)
mM	Millimolar, Millimoles per litre
mm^3	Cubic millimetre(s)

mOsm	Milliosmolar**,** Milliosmoles per litre
MRN	Median raphe nucleus
mRNA	Messenger ribonucleic acid
MS	Medial septum
ms	Millisecond(s)
mV	Millivolt(s)
mW	Milliwatt(s)
MΩ	Megaohm(s)
NA	Numerical aperture
Na_2GTP	Sodium guanosine triphosphate
Na_2HPO_4	Disodium phosphate
NaCl	Sodium chloride
NaH_2PO_4	Sodium phosphate
$NaHCO_3$	Sodium bicarbonate
nd	Not detected
NGS	Normal goat serum
NKB	Neurokinin B
nL	Nanolitre(s)
nm	Nanometre(s)
nM	Nanomolar, Nanomoles per litre
NMS	Neuromedin S
NPY	Neuropeptide Y
NT	Neurotensin
ºC	Degrees Celsius
OTR	Oxytocin receptor
OVLT	Organum vasculosum of the lamina terminalis
OVX	Ovariectomise(d)
OX	Optic chiasm
P_4	Progesterone
P*(x)*	Postnatal day *x*
pA	Picoamp(s)
PACAP	Pituitary adenylate cyclase-activating peptide
PBS	Phosphate-buffered saline
PCOS	Polycystic ovary syndrome
PCR	Polymerase chain reaction

PeN	Periventricular nucleus
PER	Period protein
PFA	Paraformaldehyde
***Pha*-L**	*Phaseolus vulgaris*-leucoagglutinin
PK2	Prokineticin 2
PNA	Prenatally androgen-treated
POA	Preoptic area
PR	Progesterone receptor
Prok2	Prokineticin 2 gene
PVN	Paraventricular nucleus
PVP-40	Polyvinylpyrrolidone
PVT	Paraventricular thalamus
QX314-Cl	*N*-ethyllidocaine chloride
RFRP-3	(Arg)(Phe)-related peptide-3
RHT	Retinohypothalamic tract
RMP	Resting membrane potential
ROI	Region of interest
RP3V	Rostral periventricular region of the third ventricle
rPOA	Rostral preoptic area
RRE	REV-ERBα response element
s	Second(s)
SCN	Suprachiasmatic nucleus
SD	Standard deviation(s)
SEM	Standard error of the mean
SITS	4-acetamido-4′-isothiocyanostilbene-2,2′-disulfonic acid
SON	Supraoptic nucleus
SOR	Retrochiasmatic supraoptic group
SP	Substance P
SST	Somatostatin
Syp	Synaptophysin
T	Testosterone
TBS	Tris-buffered sulphate
tdTomato	Tandem-dimer tomato
TGFα	Transforming growth factor alpha
TTX	Tetrodotoxin

V1aR	Vasopressin receptor 1a
V1bR	Vasopressin receptor 1b
V1R	Vasopressin receptor 1 (a or b)
V2R	Vasopressin receptor 2
VEH	Prenatally vehicle-treated
vGAT	Vesicular GABA transporter
VGCC	Voltage-gated calcium channel
VGNC	Voltage-gated sodium channel
VIP	Vasoactive intestinal polypeptide
Vip	VIP gene
vMAT2	Vesicular monoamine transporter 2
VPAC1R	VIP/PACAP receptor 1
VPAC2R	VIP/PACAP receptor 2
VPACR	VIP/PACAP receptor (1 or 2)
$\bar{x}$	Group mean
ZT	Zeitgeber time
µL	Microlitre(s)
µm	Micrometre(s)

Chapter 1:

Introduction

1.0 Preface

Hormones involved in the control of fertility are released under tight circadian control. The circadian system controlling hormone release is within the brain's master clock, an area of the brain known as the suprachiasmatic nucleus (SCN), located at the base of the hypothalamus. Vasopressin (AVP) neurons projecting from the SCN are suspected to exert a circadian tone onto kisspeptin neurons in the rostral periventricular region of the third ventricle (RP3V). These kisspeptin neurons, in turn project to gonadotropin-releasing hormone (GnRH) neurons that ultimately control mammalian fertility. This literature review will look at the role of this circuitry in the control of fertility, and how pathological conditions of endocrine-related infertility such as polycystic ovary syndrome (PCOS) may alter its function.

1.1 The hypothalamic-pituitary-gonadal axis

Mammalian fertility is exquisitely controlled by the sequential release of hormones as part of the hypothalamic-pituitary-gonadal (HPG) axis. Essentially, GnRH is released from GnRH neurons in the hypothalamus into the vasculature of the median eminence. GnRH then travels in the portal vasculature to the anterior pituitary gland where it stimulates gonadotropin cells to release the gonadotropin hormones, luteinising hormone (LH) and follicle-stimulating hormone (FSH). These two hormones enter the peripheral bloodstream and act at either the ovaries or testes (in females and males respectively) to promote gametogenesis and sex steroid synthesis. The secreted sex steroids can then feedback to the hypothalamus and anterior pituitary gland to regulate gonadotropin release (Figure 1.1).

1.1.1 GnRH neurons

At the head of the HPG axis are the GnRH neurons. Unlike most neuroendocrine

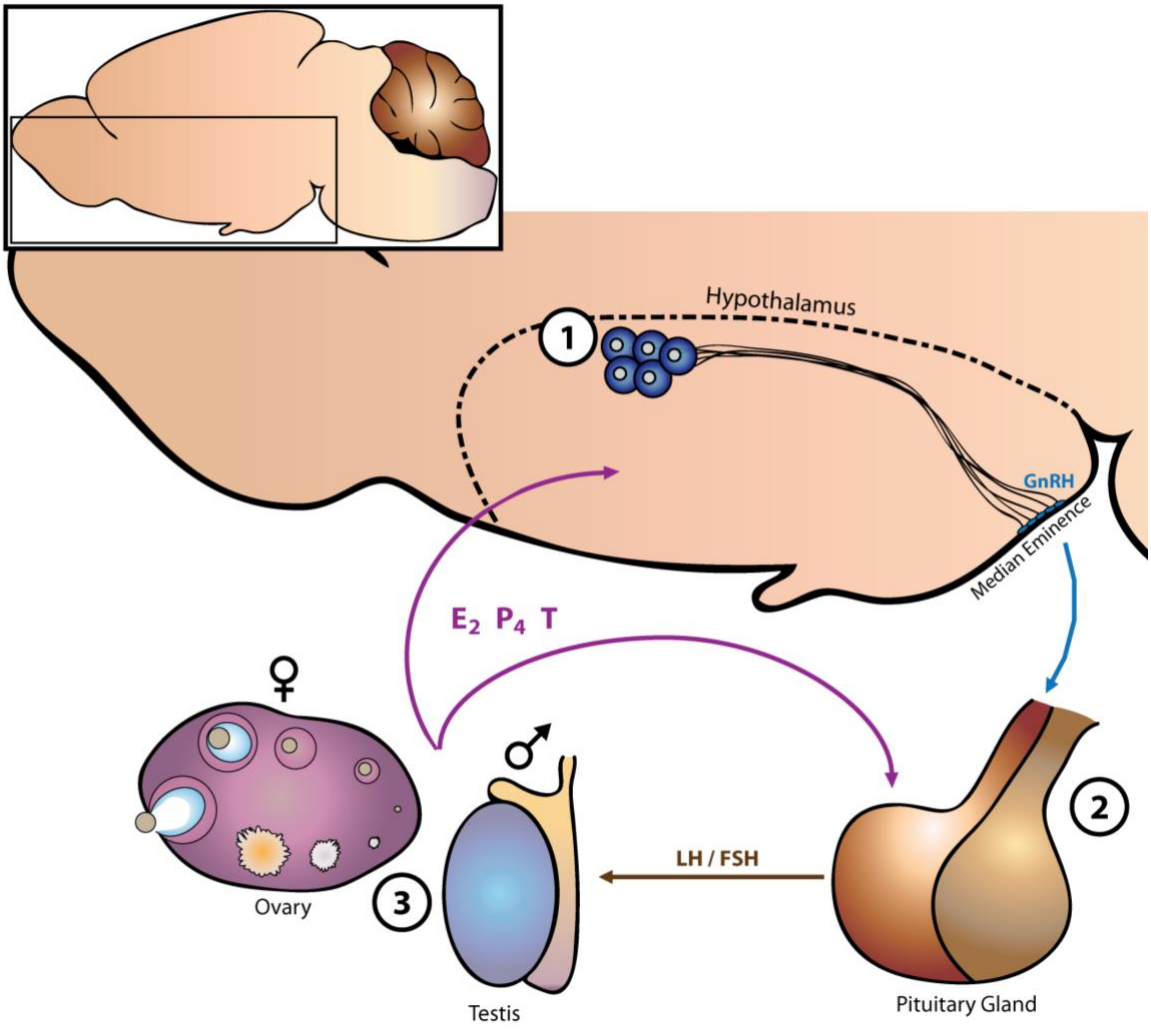

Figure 1.1: The hypothalamic-pituitary-gonadal axis.

At the head of the HPG axis, GnRH neurons in the hypothalamus extend long projections to the median eminence where GnRH peptide is released (**1**). This travels in the blood to the anterior pituitary gland where it stimulates gonadotropin cells to release LH and FSH (**2**). These then act at the ovary or testis to cause the release of sex steroids: oestradiol (E_2), progesterone (P_4) and testosterone (T) (**3**). The sex steroids then act back at the hypothalamus and anterior pituitary gland to regulate the HPG axis.

neurons, which cluster in discrete populations, GnRH neurons show a scattered distribution throughout the forebrain. This is due to their migratory pattern during embryonic development, where they migrate from the nasal placode to the base of the brain (Cariboni *et al.*, 2007). As such, GnRH neurons can be found along a continuum from the olfactory bulb through to the rostral preoptic area (rPOA), before diverging into two paths along either side of the third ventricle into the anterior and mediobasal hypothalamus (MBH) (Herbison, 2015). The key locus of the densest GnRH neuron population differs between species: sheep and rodents have the highest number of GnRH neurons in the rPOA (King & Anthony, 1984; Silverman *et al.*, 1987), while primates show the highest density in the MBH (Silverman *et al.,* 1982; King & Anthony, 1984).

Typical GnRH neurons have a bipolar configuration with a cell body and two opposing dendrites (King & Anthony, 1984; Campbell *et al.*, 2009). Fifty to seventy per cent of the GnRH neurons extend these processes deep into the external zone of the median eminence (Silverman *et al.*, 1987; Merchenthaler *et al.*, 1989). Unlike typical neuroendocrine neurons, this projection is not strictly axonal. GnRH neuron projections near the median eminence can receive synaptic input and propagate action potentials (Herde *et al.,* 2013). Thus, GnRH neuron hypophysiotropic projections are both dendritic and axonal in nature, resulting in their classification as 'dendrons' (Herde *et al.,* 2013). At their distal extent, GnRH dendrons ramify into axon terminals that make contact onto median eminence blood vessels where the GnRH peptide is released (Herbison, 2015).

1.1.2 Anterior pituitary gland and gonads

GnRH peptide travels in the portal bloodstream to the anterior pituitary gland, where it stimulates gonadotropes by binding the GnRH receptor (GnRHR). The GnRHR is a $G\alpha_s$-protein-coupled receptor that drives the secretion of the gonadotropins, LH and FSH, into capillaries within the anterior pituitary gland and, thus, the peripheral bloodstream (Pelletier *et*

al., 1971; Luborsky-Moore *et al.*, 1975). For normal fertility, the release of GnRH and downstream LH must be pulsatile (Belchetz *et al.*, 1978; Clarke *et al.*, 1986). Despite the importance of gonadotropes in the regulation of fertility, it is interesting to note that these only comprise up to 10% of the total anterior pituitary cell number (Yeung *et al.*, 2006). The release of gonadotropins has been shown to faithfully mirror the secretion of GnRH (Clarke & Cummins, 1982; Moenter *et al.*, 1992). It is thought that the frequency and amplitude of GnRH release can preferentially drive the release of either FSH or LH, with high-frequency GnRH release correlating to the preferential release of LH, and low GnRH secretion preferentially causing the release of FSH (Wildt *et al.*, 1981; Savoy-Moore & Swartz, 1987).

Following release, LH and FSH act at their receptors (LHR and FSHR respectively), both of which are $G\alpha_s$-protein-coupled receptors, promoting gametogenesis and steroidogenesis. In the male, LH binds LHRs on interstitial testicular Leydig cells promoting the production of the androgens testosterone, androstenedione and dehydroepiandrosterone. Meanwhile, FSHR activation in testicular Sertoli cells stimulates the secretion of substances that promote spermatogenesis and maintain the health of the developing spermatids (Ramaswamy & Weinbauer, 2015).

Unlike the male, the female has a set amount of immature gametes which require gonadotropin signalling to develop to maturity (Hunzicker-Dunn & Mayo, 2014). FSH initially acts to drive the growth of the follicular cells surrounding the oocyte, while LH drives the later expansion of the antral compartment surrounding the oocyte. Stimulation of the ovarian theca cell by LH drives the activation of enzymes that catalyse the conversion of cholesterol into steroids, particularly androstenedione. Androstenedione is then shuttled to the ovarian granulosa cell where it is converted to testosterone (Young & McNeilly, 2010). FSHR activation on the granulosa cell stimulates the production of aromatase enzymes that convert androgens to oestrogens, particularly 17β-oestradiol (henceforth referred to as oestradiol) (Garzo & Dorrington, 1984). Just prior to ovulation, granulosa cells begin to express greater

levels of LHR (Kumar & Sait, 2011; Yung *et al.*, 2014). This coincides with a higher serum LH concentration, which drives the release of the oocyte from the follicle, known as ovulation. The increase of LHR results in an endocrine change to the follicle. As ovulation is about to occur, the follicle becomes less receptive to oestradiol, decreases oestradiol output, and begins to secrete progesterone (Johnson, 2007b). The hormonal changes in the follicle allow the remaining granulosa cells, post-ovulation, to remodel into a postovulatory structure known as the corpus luteum. The corpus luteum is the main source of progestogens, predominantly progesterone, which are secreted to support the uterine endometrium for implantation should fertilisation occur, and then early pregnancy (Johnson, 2007a).

1.1.3 Gonadal hormone feedback

The production of androgen, oestrogen and progestogen steroids from the gonads is critical for fertility and the support of peripheral reproductive tissues. These steroids regulate the level of GnRH, LH and FSH release from the brain and pituitary respectively to ensure homeostasis of hormone secretion. The roles of these in males and females and their control of the HPG axis will now be discussed.

1.1.3.1 Gonadal hormone action in the male

Testosterone is necessary for the development of secondary sexual characteristics, sexual behaviour and spermatogenesis. Importantly, however, it also acts as part of a negative feedback loop where its release from the testis results in inhibition of GnRH and gonadotropin release (Veldhuis *et al.*, 1993). For negative feedback to occur, the androgen receptor (AR) must be activated by either testosterone or its reduction product 5α-dihydrotestosterone (DHT). Despite being the predominant free androgen in the blood, testosterone has a weaker affinity for AR than does DHT (Grino *et al.*, 1990). Negative feedback mediated by the AR is thought

to rely solely on testosterone rather than its metabolites, as treatment with chemical inhibitors of enzymes necessary for the conversion of testosterone to oestrogens or DHT do not significantly alter the plasma levels of gonadotropins (Sharma *et al.*, 1999). Thus, oestrogen and DHT are unlikely to play a role in regulating GnRH release in the male. Activation of the AR by testosterone is sufficient to decrease the release of GnRH peptide into the median eminence (Caraty & Locatelli, 1988) and repress the *Gnrh1* gene transcript (Brayman *et al.*, 2012). Conversely, the loss of AR in the brain significantly alters gonadotropin release, suggesting a role for AR-mediated negative feedback, particularly at the hypothalamus (Raskin *et al.*, 2009). In the anterior pituitary, ARs expressed by gonadotropes decrease the cellular response to GnRH, further inhibiting the release of LH and FSH (Tobin *et al.*, 1997). In gonadectomised (GDX) males there is also a measurable rise in circulating gonadotropins, which can be attenuated by testosterone replacement (Schanbacher, 1980; d'Occhio *et al.*, 1983; Caraty & Locatelli, 1988). This shows that androgens, particularly those from the testes, are critical for negative feedback of the male HPG axis. The tonic feedback pattern seen in the male does not change over time; in contrast, however, feedback to the HPG axis in females is variable. For the remainder of this thesis, the focus will be on that of hormone changes and action in the female.

1.1.3.2 Gonadal hormone action in the female

Feedback action in the female is variable depending on the stage of the ovarian cycle. Unlike the male, most testosterone synthesised in the gonad (i.e. the ovary) is rapidly oxidised to oestradiol, due to the action of aromatase enzymes. Oestradiol is necessary for the development and maintenance of secondary sexual features, sexual behaviour and maintenance of the oocyte. The levels of oestradiol fluctuate along the course of the ovarian cycle, or oestrous cycle in rodents (Figure 1.2). In the early stages of the follicular phase (equivalent to the rodent

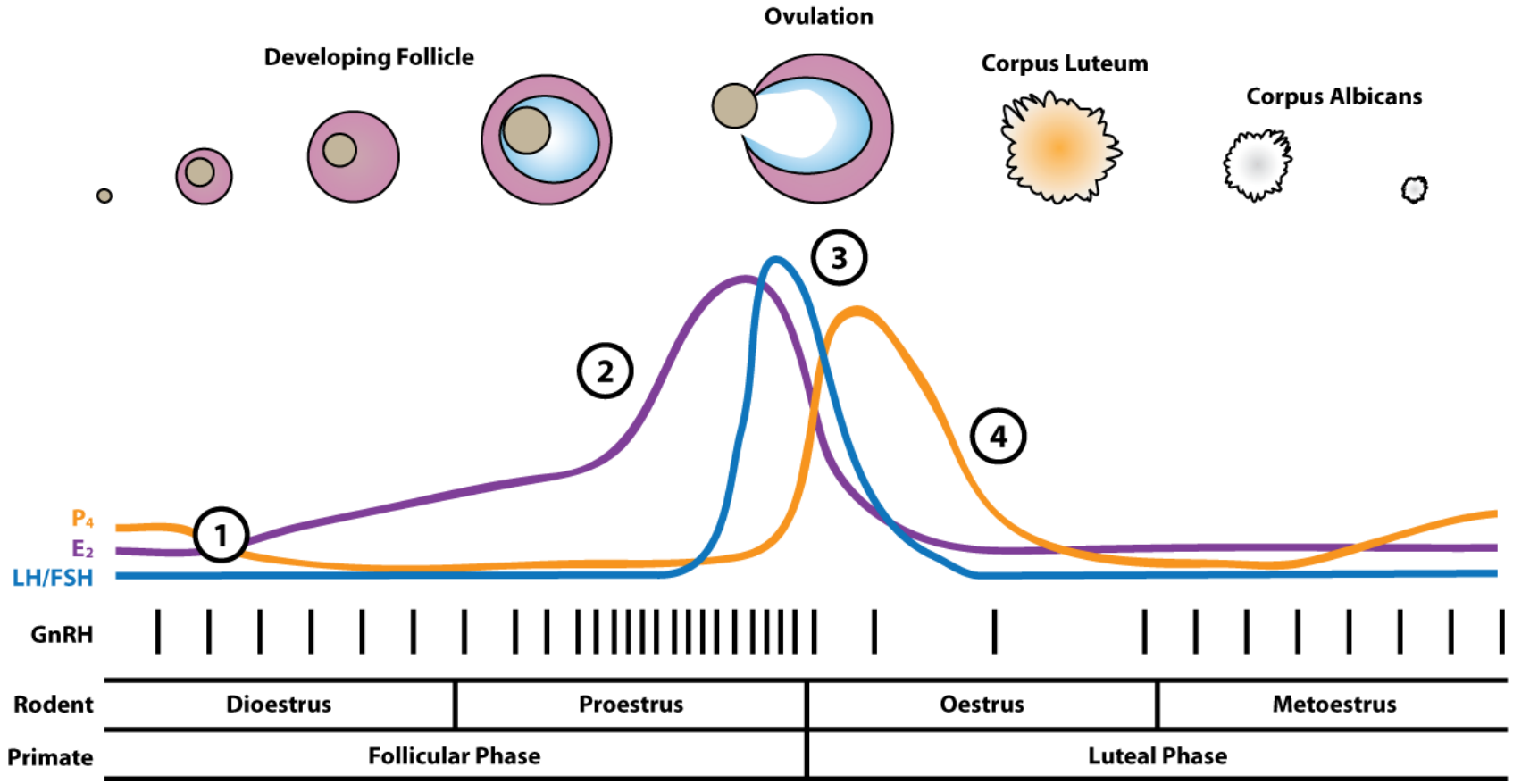

Figure 1.2: The oestrous cycle.

Relative concentrations of oestradiol (E_2), progesterone (P_4) and gonadotropins (LH/FSH); and activity of the GnRH neurons, across the ovulatory cycle in primates and oestrous cycle in rodents. Baseline concentrations of hormones are low. Although not shown here, the release of LH is pulsatile (**1**). As the follicle surrounding the oocyte develops, there is an increase in the serum concentration of E_2 (**2**). Prior to ovulation, when E_2 is at its highest, GnRH neuron activity increases and there is a surge of LH (**3**). E_2, LH and FSH then fall in concentration, while P_4 rises as it is released from the corpus luteum (**4**).

dioestrus), the granulosa cell layer surrounding the oocyte thickens. This increase in the number of aromatase-producing cells drives greater oestradiol synthesis causing the concentration to peak prior to ovulation (during the rodent proestrus). Following ovulation, there is a rapid decline in oestradiol synthesis, as the degenerating granulosa cells become the corpus luteum and steroidogenesis switches mainly to the production of progesterone (the rodent oestrus). Throughout the luteal phase, increased progesterone is important to support the endometrium and, if fertilisation occurs, maintains early pregnancy; it also acts to suppress the release of GnRH, LH and FSH (Skinner *et al.*, 1998). It is important to note here that most spontaneously ovulating rodents lack a true luteal phase, as the rodent metoestrus does not commonly last more than several hours (Smith *et al.*, 1975).

Oestradiol acts at two key nuclear receptors: oestrogen receptor alpha (ERα) and oestrogen receptor beta (ERβ) (Dahlman-Wright *et al.*, 2006); and at two relatively understudied non-nuclear receptors: the membrane-bound oestrogen receptor, and an oestrogen-activated GPCR (Prossnitz *et al.*, 2007; Micevych & Kelly, 2012). ERα is more critical for fertility than ERβ. Seminal work by Lubahn *et al.* (1993) produced a global knockout (KO) of ERα in a mouse line. Female mice display normal external sexual features but have severely hypoplastic uteri with small, cystic ovaries. Conversely, the ERβ-KO mouse shows overtly normal reproductive anatomy and can sufficiently support pregnancy without complication (Krege *et al.*, 1998; Walker & Korach, 2004). These models have proved useful in determining the role that the individual oestrogen receptors may play in fertility. Further to this, the role of oestradiol is complicated by the fact that it does not solely feedback negatively to inhibit the HPG axis. As will now be discussed, the female HPG axis displays two patterns of activity in response to oestradiol feedback.

1.1.3.3 Oestradiol negative feedback

Classically, endocrine homeostasis is considered to be a cycle of hormone release followed by negative feedback into the hypothalamus and pituitary. In the female, this is the case over the majority of the ovarian cycle. Oestradiol synthesised by the granulosa cells negatively feeds back to the hypothalamus to inhibit the release of GnRH (Herbison, 2015). This negative feedback also occurs at the anterior pituitary gland, inhibiting the release of LH and FSH (Shaw *et al.*, 2010). Given that ERβ-KO mice show overtly normal fertility (Cheong *et al.*, 2014), it is likely that oestradiol-mediated feedback or GnRH neuron activity is unaffected in the ERβ-KO mouse (Krege *et al.*, 1998). A mutant rat model with truncated ERβ appears to have attenuated oestradiol feedback but still has recognisable patterns of hormone changes (Rumi *et al.*, 2017). This indicates that ERβ is not likely involved with oestradiol negative feedback in the HPG axis. In contrast, ERα-KO mice have significantly higher serum LH levels (Couse & Korach, 1999; Couse *et al.*, 2003) similar to that of ovariectomised (OVX) mice lacking ovarian tissue necessary for the production of oestradiol (Fink, 1988; Couse & Korach, 1999; Glidewell-Kenney *et al.*, 2007). As such, the high levels of LH in the ERα-KO mouse are indicative of a loss of oestradiol-mediated negative feedback, due to the knockout of ERα. Thus, ERα is likely to be the key receptor involved with oestradiol negative feedback. This negative feedback is unlikely to be direct at the level of the GnRH neurons as it has been shown that GnRH neurons only express ERβ and not ERα (Herbison & Theodosis, 1992; Shughrue *et al.*, 1997). Interestingly, some evidence suggests that the genomic effects of the ERs may be unnecessary, and rather a non-classical action of the ER may be sufficient for negative feedback potentially through a membrane bound ER (Glidewell-Kenney *et al.*, 2007).

1.1.3.4 Oestradiol positive feedback

Unlike males, females show a second pattern of GnRH secretion due to a positive hormonal feedback during the mid-late follicular phase when oestradiol concentrations have

increased. Oestradiol positive feedback occurs in parallel with the increased thickening of the ovarian granulosa cell layer prior to ovulation. The aforementioned negative feedback that maintains LH at a basal concentration is essentially overridden by a positive feedback whereby the serum LH concentration rapidly increases, known as the LH surge. Portal bleeding studies in sheep have revealed that prior to ovulation, GnRH release gradually begins to increase, indicating the replacement of negative feedback by a stronger positive feedback (Caraty & Locatelli, 1988; Evans *et al.*, 1995). Although rodent models are too small to reliably take portal blood to measure GnRH peptide release, they have revealed that at similar time points to the hypothesised increase in GnRH release, there is an increase in the activity of GnRH neurons (Christian *et al.*, 2005) and an increase in GnRH neuron c-FOS expression, as a proxy for increased activity (Lee *et al.*, 1990; Hoffman *et al.*, 1993).

For positive feedback to occur, it is thought that oestradiol must be at a sufficiently high concentration for several hours to trigger the actions of negative feedback (Karsch *et al.*, 1973; Legan *et al.*, 1975; Legan & Karsch, 1975). Studies have shown that implants of oestradiol are sufficient to drive daily positive feedback and increase GnRH and LH release (Kalra & McCann, 1975; Bronson & vom Saal, 1979; Bronson, 1981; Christian *et al.*, 2005). Interestingly, if the oestradiol implants are given and subsequently removed, the LH surge will still occur, indicating that oestradiol exposure makes a prolonged genomic change sufficient to drive several hours of positive feedback necessary for ovulation (Evans *et al.*, 1997). This is dependent on the genetic oestrogen response element as part of the classical actions of oestradiol, rather than at membrane bound receptors (Glidewell-Kenney *et al.*, 2007). Like oestradiol negative feedback, the positive feedback pattern is thought to be mediated by ERα rather than ERβ. As ERβ-KO mice maintain an LH surge and are still fertile (Wintermantel *et al.*, 2006), the necessary positive feedback prior to ovulation likely remains intact (Krege *et al.*, 1998). ERα-KO mice, however, are infertile and do not show changes to GnRH neuron activity

or hormonal increases at the expected onset of positive feedback (Wintermantel *et al.*, 2006; Glidewell-Kenney *et al.*, 2007).

1.1.3.5 Progesterone feedback

During the oestrus stage of the oestrous cycle, there is a marked change in the hormonal profile of the mouse, presenting with higher secretion of progesterone than oestradiol. Progesterone typically inhibits GnRH secretion and thus LH release (Goodman & Karsch, 1980; Skinner *et al.*, 1998), however, GnRH neurons do not express the progesterone receptor (PR) (Skinner *et al.*, 2001). As such, an upstream neuronal population must mediate the effects of progesterone on the suppression of GnRH release. Mice lacking PR expression are unable to suppress LH release in response to progesterone and display significant reproductive abnormalities (Lydon *et al.*, 1995; Chappel *et al.*, 1997).

While it seems clear that progesterone action suppresses the GnRH neuronal network, there is evidence to suggest that PR signalling is also necessary to drive positive feedback. When rodents are primed with oestradiol following OVX, progesterone can mediate an increase in LH release when delivered in a pulsatile manner (Kim & Ramirez, 1982). When PR is specifically knocked out of the hypothalamus, however, this ability is lost (Stephens *et al.*, 2015; Gal *et al.*, 2016). It has been hypothesised that increases in progesterone, prior to ovulation, may be mediated by progesterone synthesised within the brain itself (known as 'neuroprogesterone') (Micevych & Sinchak, 2011). Neuroprogesterone produced in astrocytes, in response to astrocytic and neuronal ERα activation (Micevych *et al.*, 2003; Micevych *et al.*, 2007), could be acting to stimulate afferent neuron activity, thus exciting the GnRH neurons. This would coincide with the timing for oestradiol-mediated positive feedback, implicating both oestradiol and progesterone contribute to the excitation of the GnRH neuronal network.

1.2 Luteinising hormone release patterns

While both FSH and LH are important for fertility, LH release more faithfully mirrors the secretion of GnRH. Thus, LH concentration is typically used as a read out for how the hypothalamus integrates oestradiol feedback. Over the course of the oestrous cycle, LH secretion patterns change in response to gonadal steroid hormone feedback. These different patterns of release will be the focus of the subsequent sections.

1.2.1 Pulsatile LH release

For the majority of the oestrous cycle, LH is released in discrete, roughly hourly, pulses (Czieselsky *et al.*, 2016). This mimics the secretion of GnRH, which in all mammalian species studied to date is also pulsatile (Dierschke *et al.*, 1970; Nankin & Troen, 1971; Butler *et al.*, 1972; Gay & Sheth, 1972; Levine *et al.*, 1982). Pulsatile GnRH release is necessary for appropriate LH secretion, as a constant infusion of GnRH downregulates the release of LH (Belchetz *et al.*, 1978; Clarke *et al.*, 1986). LH pulses have typically been studied in GDX animals in order to remove gonadal hormone negative feedback.

How these pulses are generated has been contentious, however, several hypotheses have been presented. Historically it was suggested that the GnRH neurons themselves form an intrinsic pulse generator, where they are connected to allow synchronous output, where the population can intercommunicate by the release of neurotransmitters in order to coordinate a pulsatile release. In saying this, however, there is very little electrophysiological (or otherwise) evidence supporting a reciprocal communication pathway within the GnRH neuron population (Campbell *et al.*, 2011). The idea of an intrinsic GnRH pulse generator came predominantly from *in vitro* brain slice work or using an immortalised GnRH cell line. These studies showed that GnRH neurons exhibit periods of spontaneous bursting activity (Terasawa *et al.*, 1999a;

Terasawa *et al.*, 1999b; Funabashi *et al.*, 2001; Nunemaker *et al.*, 2001), although this has not been recapitulated *in vivo* (Constantin *et al.*, 2013).

It is more likely that a population of neurons upstream of the GnRH neurons control the pulse generation. Deafferentation of GnRH neurons has proved particularly interesting when studying the external pulse generator. Rat MBH neurons show some contact with GnRH neurons, which, when removed, diminishes the pulse frequency (Halász & Gorski, 1967; Blake & Sawyer, 1974). This is similar to results seen with deafferentation from suprachiasmatic areas (Hoffman & Gibbs, 1982), though neither show complete abolishment of GnRH/LH pulses. Lesions of the rat and monkey arcuate nucleus (ARN) inhibit the occurrence of LH pulses (Plant *et al.*, 1978; Soper & Weick, 1980), indicating the necessity of ARN neurons in pulse generation. Recordings of neurons in the ARN revealed pulsatile bursts as well as transient calcium increases occurring just prior to the onset of an LH pulse (Karsch *et al.*, 1973; Ördög & Knobil, 1995; Clarkson *et al.*, 2017). As such, the pulse generator is thought to reside in the ARN (Clarkson *et al.*, 2017).

1.2.2 The LH surge

Unlike the pulses of LH, the preovulatory LH surge occurs once per oestrous cycle and can last hours such as in the rodent, up to a day in livestock such as sheep or cattle, or several up to several days in humans (Murr *et al.*, 1973; Rawlings & Cook, 1993; McElhinny *et al.*, 1999; Ginther *et al.*, 2013; Czieselsky *et al.*, 2016). As mentioned, oestradiol reaches a threshold to trigger positive feedback and increases the activity, and the output, of GnRH neurons, however, it appears that only GnRH neurons located in the rPOA and around the organum vasculosum of the lamina terminalis (OVLT) express c-FOS (as a proxy for an increase in their activity) during the development of the surge (Lee *et al.*, 1990; Wintermantel *et al.*, 2006). The increasing levels of GnRH cause a massive rise in serum LH concentration,

which is then able to stimulate the induction of ovulation by driving the preovulatory follicle to release the oocyte (Kumar & Sait, 2011).

How the onset of the LH surge occurs is a more difficult question. As discussed, rising oestradiol concentrations are critical in the development of positive feedback (Petersen *et al.*, 1989), particularly through its activity at ERα. GnRH neurons do not express ERα, so an oestrogen responsive brain region expressing ERα, capable of exciting GnRH neurons would be a likely candidate driving the hormonal surge. Lesion studies have indicated that preoptic brain areas are key candidates for the development of the LH surge. A lesion of the area encompassing the anteroventral periventricular nucleus (AVPV) and periventricular nucleus (PeN), which together form a region coined the rostral periventricular region of the third ventricle (RP3V) (Herbison, 2008), results in an inhibition of oestradiol-mediated positive feedback and the loss of the LH surge, but not oestradiol-mediated negative feedback (Wiegand *et al.*, 1980; Wiegand & Terasawa, 1982).

The RP3V lies adjacent to the third ventricle and contains a heterogeneous population of neuronal phenotypes including the well-known kisspeptin neurons, whose specific role is discussed below (Herbison, 2008). Projections from the RP3V are known to project towards GnRH neurons (Polston & Simerly, 2006). Thus, RP3V neurons make perfect candidates for the generation of the LH surge, particularly as c-FOS is present in this area at the onset of the LH surge, indicating their activation (Clarkson *et al.*, 2008). The classification of the neuronal phenotype responsible for GnRH activation includes the ability to classically respond to oestrogen through ERα, as well as forming anatomical and functional projection to GnRH neurons (Clarkson & Herbison, 2009). While the studies looking at the RP3V and its role in the LH surge have mainly been rodent-focussed, this may not be the case for other species (Plant, 2012, 2015).

1.3 The GnRH neuronal network

Although GnRH neurons are considered the head of the HPG axis, it is more correct to consider them as the final output of the brain network regulating fertility. As mentioned, the key driver of homeostatic feedback mediating fertility are the sex steroids, that is, androgens, oestrogens and progestogens. Given that GnRH neurons do not express the AR, ERα nor PR (Herbison & Theodosis, 1992; Huang & Harlan, 1993; Skinner *et al.*, 2001), it is likely the afferent neuronal connections, that drive key changes in GnRH neuron activity, are associated with feedback. The ARN and RP3V regions have been noted as likely sites mediating sex steroid integration for negative and positive feedback resulting in changes in GnRH activity. The following section will introduce the likely neuronal phenotypes involved.

Multiple neurotransmitters and neuropeptides are known to alter the activity of GnRH neurons (Herbison, 2015). To classify these inputs, it is important to consider whether these inputs have a meaningful, functional impact on GnRH neuron activity, as well as whether the neurons that produce the peptides make anatomical inputs to GnRH neurons. Finally, it is necessary to know whether the neuronal afferents are either androgen or oestrogen receptive, to coordinate either negative or positive feedback. Combining these criteria, as well as looking at the neuronal phenotypes in both the ARN and RP3V, one key neuropeptide stands out: kisspeptin.

1.3.1 Kisspeptin

Originally known as metastin, kisspeptin was defined by its inhibition of tumour metastasis (Lee *et al.*, 1996). Isoforms of kisspeptin come in 54- (52- in rodents) 14-, 13- and 10-amino acid sequences, each sharing a conserved C-terminus (Kotani *et al.*, 2001; Bilban *et al.*, 2004). Each isoform of kisspeptin is biologically active, although kisspeptin-10 (commonly referred to as simply kisspeptin) has the strongest action in terms of the GnRH neuronal network (Abbara *et al.*, 2013). The role of kisspeptin in fertility was uncovered when members of two consanguineous families showed inherited defects in the orphan G-protein-coupled receptor

GPR54, (later shown to be the kisspeptin receptor, Kiss1R), and exhibited hypogonadotropic hypogonadism, a disease characterised by failure to go through puberty, and infertility (de Roux *et al.*, 2003; Seminara *et al.*, 2003). The development of the GPR54-KO mouse line corroborated this finding, indicating the evolutionary conservation of Kiss1R as an essential regulator of fertility (Funes *et al.*, 2003; Seminara *et al.*, 2003). Kisspeptin itself must also be functional for adequate fertility. Patients with mutations in the kisspeptin gene, *Kiss1*, show similar patterns of infertility and hypogonadotropic hypogonadism to the Kiss1R mutations (Topaloglu *et al.*, 2012), as do both the GPR54-KO and *Kiss1*-KO mice (Seminara *et al.*, 2003; d'Anglemont de Tassigny *et al.*, 2007; Clarkson *et al.*, 2008).

The question, then, is how does kisspeptin and associated downstream signalling contribute to the development of fertility? Kisspeptin injection *in vivo* is sufficient to drive the release of LH (Gottsch *et al.*, 2004; Thompson *et al.*, 2004; Han *et al.*, 2005; Messager *et al.*, 2005). Well-designed work by Kirilov *et al.* (2013) using a mouse model with Kiss1R restored specifically in GnRH neurons, showed that the action of kisspeptin at GnRH neurons is critical for fertility, rather than elsewhere in the HPG axis. Kiss1R is a $G\alpha_q$-protein-coupled receptor and, as such, drives neuronal depolarisation. In the brain, Kiss1R is most densely expressed through the rostral preoptic area, hippocampus (particularly the dentate gyrus) and cerebellum, along with sparse expression in other hypothalamic and midbrain regions (Herbison *et al.*, 2010). Kisspeptin is the most potent stimulator of GnRH neurons and their electrical activity known to date (Han *et al.*, 2005), causing long-lasting depolarisation of GnRH neurons even at the nanomolar concentration expected *in vivo* (Gottsch *et al.*, 2004; Thompson *et al.*, 2004; Han *et al.*, 2005).This results in the closure of inwardly-rectifying potassium channels (Liu *et al.*, 2008; Zhang *et al.*, 2008), as well as opening the transient receptor potential cationic channel 4, potentiating the depolarising influx of cations (Liu *et al.*, 2008; Zhang *et al.*, 2008).

It is clear that kisspeptin and its signalling through Kiss1R is critical for fertility. As mentioned in the previous section, there are two distinct populations of neurons controlling

either the pulsatile or the surge release of GnRH. Maybe not surprisingly, both the ARN and RP3V contain dense populations of kisspeptin neurons (Clarkson & Herbison, 2009; Yip *et al.*, 2015; Yeo *et al.*, 2016), each of which will now be discussed in turn.

1.3.1.1 KNDy neurons

Within the ARN resides a dense population of kisspeptin neurons, that project to GnRH neurons, within the ARN, to other hypothalamic regions including the PVN and DMH, and the supramamillary nucleus (Yip *et al.*, 2015). As well as being predominantly glutamatergic, arcuate kisspeptin neurons co-express two other functional peptides: neurokinin B (NKB) and dynorphin (Goodman *et al.*, 2007; Navarro *et al.*, 2009; Hrabovszky *et al.*, 2010; Ramaswamy *et al.*, 2010) resulting in their naming as KNDy (kisspeptin-neurokinin B-dynorphin) neurons (Lehman *et al.*, 2010a). These arcuate kisspeptin neurons express the neurokinin 3 receptor and kappa-opioid receptor indicating that they are responsive to locally secreted NKB and dynorphin respectively (Navarro *et al.*, 2009). Electrophysiological recordings of kisspeptin neurons show that NKB stimulates action potentials in KNDy neurons (Navarro *et al.*, 2011; de Croft *et al.*, 2013; Ruka *et al.*, 2013); while dynorphin acts to suppress KNDy neuron activity (de Croft *et al.*, 2013; Ruka *et al.*, 2013).

Similar to GnRH and LH secretion, kisspeptin neuron activity is also pulsatile (Choe *et al.*, 2013; Clarkson *et al.*, 2017), which is thought to be coordinated by the sequential release of NKB and dynorphin. Thus, the proposed mechanism for pulse generation begins with NKB release stimulating surrounding kisspeptin neurons to release kisspeptin at the median eminence GnRH terminals. The increased activity of KNDy neurons then causes the release of dynorphin to rapidly inhibit either itself or surrounding KNDy neurons, ceasing the release of kisspeptin, resulting in a burst of kisspeptin release, causing a pulse-like activation of the GnRH neuron (Navarro *et al.*, 2009; Lehman *et al.*, 2010a). Together, the KNDy neurons form an

interconnected network suspected to be responsible for their pulsatile activity pattern (Burke *et al.*, 2006; Qiu *et al.*, 2016).

1.3.1.2 RP3V kisspeptin neurons

The population of kisspeptin neurons in the RP3V is significantly different from those in the ARN. While the KNDy neurons form a synchronous network to coordinate activity, RP3V kisspeptin neurons do not. Rather, RP3V kisspeptin neurons rely on changes in ion channels and electrical activity dependent on activation of ERα to coordinate their activity (Smith *et al.*, 2005a; Clarkson *et al.*, 2009; Frazão *et al.*, 2013; Piet *et al.*, 2013; Wang *et al.*, 2016). Like the ARN kisspeptin neurons, however, they do project to GnRH neurons, but in a more wide-spread pattern. The RP3V kisspeptin neurons are more likely to project to GnRH neuron somata and proximal dendrites, while the ARN kisspeptin neurons solely target GnRH neuron projections towards the median eminence (Clarkson & Herbison, 2006; Yip *et al.*, 2015). Further, the RP3V kisspeptin neurons also project to the dorsomedial and ventromedial hypothalamus, and bed nucleus of the stria terminalis (Polston & Simerly, 2006; Yip *et al.*, 2015).

The RP3V kisspeptin population is sexually dimorphic. Females have a dramatic ten-fold higher number of kisspeptin neurons throughout the RP3V compared to males (Smith *et al.*, 2005a; Smith *et al.*, 2005b; Clarkson & Herbison, 2006; Kauffman *et al.*, 2007). This is perhaps not surprising, as males do not display an LH surge which is mediated by the RP3V kisspeptin neurons. The activation of RP3V kisspeptin neurons, as demarcated by c-FOS expression, is coincident with the expression of c-FOS in GnRH neurons at the time of the LH surge, indicating their vital role in surge development (Kinoshita *et al.*, 2005; Smith *et al.*, 2006; Clarkson *et al.*, 2008). When this population of kisspeptin neurons are activated optogenetically, there is a surge-like release of GnRH and LH (Qiu *et al.*, 2016; Piet *et al.*, 2018).

1.3.2 Oestrogenic feedback to kisspeptin neurons

The feedback of oestrogen to kisspeptin neurons can easily be studied through OVX, where the endogenous oestrogen from the ovary is removed. OVX leads to ARN *Kiss1* gene expression being massively upregulated (Smith *et al.*, 2005a; Smith *et al.*, 2006). The same holds true for GDX male rodents lacking endogenous testosterone production (Smith *et al.*, 2005b). Steroid negative feedback inhibits the spontaneous activity of ARN kisspeptin neurons and increases postsynaptic inhibitory currents (Frazão *et al.*, 2013). In OVX animals, replacement of oestradiol is sufficient to restore the levels of kisspeptin to that of intact animals (Smith *et al.*, 2005a), indicating a restoration of negative feedback. Further, some studies have suggested that some negative feedback may be independent of ERα (Mayer *et al.*, 2010; Wang *et al.*, 2019).

In contrast to the ARN population of kisspeptin neurons, OVX and the removal of oestradiol decreases RP3V expression of kisspeptin (Smith *et al.*, 2006), and decreases RP3V action potential firing (de Croft *et al.*, 2012). This indicates that RP3V kisspeptin neurons are involved in positive feedback (Figure 1.3). During proestrus, when rodent oestradiol levels are high, RP3V kisspeptin neurons exhibit a higher hyperpolarisation-activated cation current (I_H) (Piet *et al.*, 2013; Zhang *et al.*, 2013; Wang *et al.*, 2016). potentially allowing greater rebound action potential firing and dampening of inhibitory postsynaptic currents. This rebound firing is dependent on transient low-threshold calcium currents, which have also been shown to be upregulated when circulating oestradiol is high (Zhang *et al.*, 2013).

Oestradiol acts as an important mediator of feedback to kisspeptin neurons in female fertility. This project focusses on kisspeptin neurons in the RP3V that regulate positive feedback. Although the oestrogen feedback to the RP3V kisspeptin neuron population is critical, upstream neuronal inputs also regulate kisspeptin neuron activity.

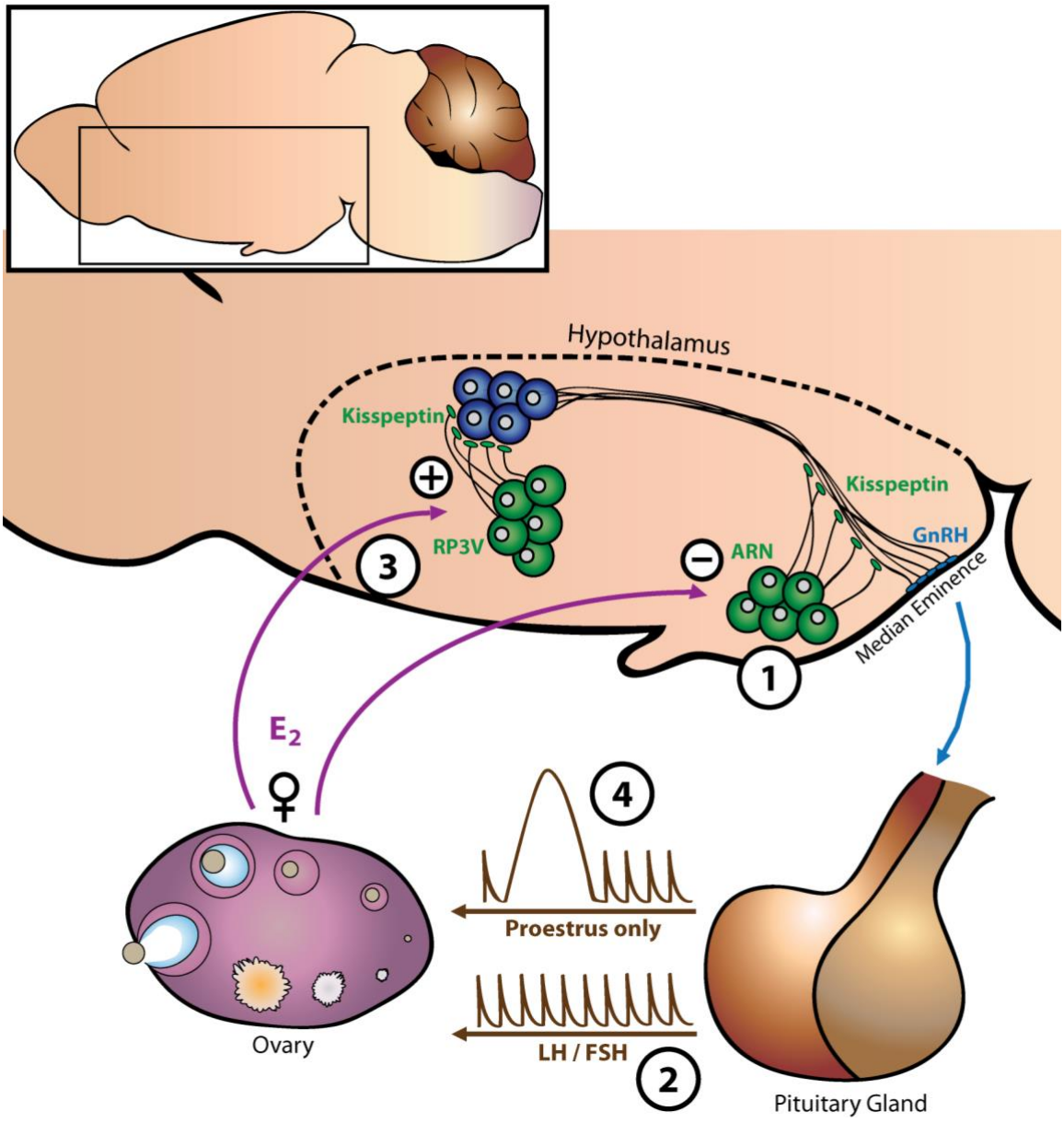

Figure 1.3: Kisspeptin neurons control the hypothalamic-pituitary-gonadal axis.

In the female, oestradiol (E_2) negatively feeds back to the arcuate nucleus (ARN) kisspeptin neurons (**1**) to maintain a low, pulsatile secretion of gonadotropin-releasing hormone (GnRH) and luteinising hormone (LH) from the anterior pituitary (**2**). During proestrus, when circulating E_2 levels rise, positive feedback occurs, stimulating the kisspeptin neurons in the rostral periventricular region of the third ventricle (RP3V) (**3**). This results in an increase in GnRH neuron activity, and the resulting surge output of LH (**4**).

1.4 Circadian regulation of fertility

In rodents, the LH surge is almost perfectly timed to occur prior to the active phase of proestrus (Murr *et al.*, 1973; McElhinny *et al.*, 1999). This allows ovulation to be timed to just before activity and sexual behaviour (McElhinny *et al.*, 1997).

In humans, a timed LH surge is debated. A study by Hoff *et al.* (1983) suggests that the human LH surge is not time-specific, and may occur any time throughout the day before ovulation. Their data, however, suggest that the LH surge is coincident with an exponential increase in serum oestradiol concentration (Hoff *et al.*, 1983). In a more robust study, however, it was shown that the majority of LH surges occur at 0300 ± 1.5 h (Testart *et al.*, 1982), providing some evidence that in humans, similar to rodents, ovulation occurs prior to the awake period. The majority of work looking at this phenomenon corroborates the data for the early morning LH surge in women, suggesting it may occur anywhere between 0000 h and 0900 h (Edwards, 1981; Seibel *et al.*, 1982; Cahill *et al.*, 1998). While the link between oestradiol increase and the LH surge is clear, it is interesting to note that the LH surge is almost perfectly time-locked to the morning peak of cortisol occurring around 0800 h, and the initiation of an increase in serum progesterone (Kerdelhué *et al.*, 2002).

1.4.1 Oestrogenic regulation of a timed LH surge

A link between the timed LH surge and fertility becomes clear with artificial manipulation of hormone levels in OVX animals. After bilateral OVX in the rat, subcutaneous capsules of oestradiol can be implanted, or oestradiol injected, to artificially raise the serum oestradiol concentration. This is thought to prime the RP3V kisspeptin neurons to just prior to the awake phase of the animal, where their activation causes the downstream LH levels to surge (Legan *et al.*, 1975; Bronson & vom Saal, 1979; Christian *et al.*, 2005). This phenomenon of an artificially induced LH surge repeats every 24 hours in the presence of the high concentration

of oestradiol and persists until oestrogen concentrations drop below a critical threshold (Legan *et al.*, 1975; Legan & Karsch, 1975; Christian *et al.*, 2005). This gives rise to the idea that something is timing the LH surge to repeat at a specific time point. Interestingly, this 24-hour repeating phenomenon can be blocked by the administration of barbiturates to the animal (Legan *et al.*, 1975). Similarly, even in rodents without artificially increased oestradiol, barbiturate administration a few hours before the expected LH surge in proestrus delays the LH surge by almost exactly 24 hours (Everett & Sawyer, 1950). Thus, the inhibition of the neuronal component of the HPG axis by barbiturates, even in the presence of high oestradiol, will delay the surge. Further, this provides evidence for a daily signal of neural origin that can time the surge.

The first understanding of how the brain controls the circadian clock came from studies where regions of the brain were lesioned, and the resulting activity of the animal was monitored. Lesions of the rat suprachiasmatic region, including the suprachiasmatic nucleus inhibited the development of an LH surge (Wiegand *et al.*, 1980; Wiegand & Terasawa, 1982), implicating the role of the SCN.

1.5 The suprachiasmatic nucleus

The SCN is the locus of the brain's biological clock. The SCN generates an endogenous circadian rhythm and receives input from neurons responsive to environmental changes, such as light, and synchronises its activity with the environment. A circadian rhythm is an oscillatory rhythm which occurs about a 24-hour time period, synchronised to the Earth's day. Endogenous rhythms occur throughout the body and include behavioural rhythms such as locomotor behaviour, or physiological rhythms such as body temperature changes, hormone release and oestrous cycles (Hastings *et al.*, 2018). The SCN coordinates these endogenous rhythms in response to environmental cues known as zeitgebers. Zeitgebers allow the SCN to synchronise

to external signals by a process known as entrainment. Without any zeitgebers or entrainment, an organism will rely solely on the changes in gene and protein expression occurring in its cells to maintain its rhythms. The most obvious zeitgeber is the change from dark to light as night becomes day. Animals most active in the day, such as humans, are considered to be diurnal species, while animals most active in the night, such as many rodents, are considered as nocturnal species. The introduction, or removal, of a zeitgeber from an organism's environment, can reset the circadian rhythm.

Circadian rhythms originating from the SCN have been extensively studied. When the SCN is lesioned, circadian rhythms are essentially lost (Moore & Eichler, 1972; Stephan & Zucker, 1972; Wiegand *et al.*, 1980; Brown & Nunez, 1986), and the organism is put into a state of arrhythmicity, where it does not respond to any zeitgeber. This reveals changes in locomotor activity, the sleep-wake cycle, and even oestrous cycles (Stetson & Watson-Whitmyre, 1976; Wiegand *et al.*, 1980). In order for these processes to occur, the intact SCN must have an oscillatory activity pattern. This pattern is controlled by a change in genetic and protein expression, known as a transcriptional-translational feedback loop (Welsh *et al.*, 1995; Mohawk & Takahashi, 2011).

1.5.1 Transcriptional-translational feedback loops

Endogenous circadian rhythm is dependent upon changing gene expression and the resulting differences in protein expression. Genetic oscillation is not solely a feature of SCN neurons but occurs throughout cells in the body. Each cell contains a genetic regulatory element known as the enhancer box (EBox) upstream to the clock genes, which is sensitive to proteins vital to circadian rhythms. Circadian locomotor output cycles kaput (CLOCK) and brain and muscle Arnt-like protein-1 (BMAL-1) proteins in the neuronal cytoplasm dimerise, enter the nucleus and activate EBox for each gene. This stimulates the transcription of the REV-ERBα complex and the Period (PER) and Cryptochrome (CRY) proteins (Gekakis *et al.*, 1998).

Throughout the day, REV-ERBα acts at the REV-ERBα response element (RRE) to inhibit the production of BMAL-1; while post-transcriptionally modified PER and CRY, along act to inhibit their own production by inhibiting BMAL-1 and CLOCK binding of their respective EBox (Eide *et al.*, 2005; Partch *et al.*, 2014). Furthermore, BMAL-1 and CLOCK are independently able to regulate the activity of genes within the SCN (Mohawk & Takahashi, 2011). This forms a cycle of proteins being up- and downregulated throughout the course of the day (Figure 1.4a). This transcriptional-translational feedback loop lasts for a period of about 24 hours (Welsh *et al.*, 1995) providing evidence for an internal circadian oscillatory system, both *in vivo* as well as in tissue explants (Welsh *et al.*, 1995; Foley *et al.*, 2011).

1.5.1.1 Electrical activity of the SCN

The relative change in protein expression over the 24-hour cycle results in a change in the electrical activity of SCN neurons. Thus, they act as intrinsic pacemaker cells (Colwell, 2011). SCN neurons can maintain their rhythm *in vivo* (Inouye & Kawamura, 1979), *ex vivo* (Green & Gillette, 1982), and in tissue culture preparations (Welsh *et al.*, 1995). During the day, SCN neurons have high rates of spontaneous action potential firing, which drops off towards the night (Figure 1.4) (Green & Gillette, 1982; Schaap *et al.*, 2003); this is also true regardless of whether the animal is diurnal or nocturnal (Colwell, 2011).

During the day, the majority of SCN neurons are relatively depolarised with a resting membrane potential (RMP) near action potential threshold (~ -45 mV) (Colwell, 2011). The high depolarising drive to SCN neurons even results in a subset displaying an RMP of ≥ -30 mV, functionally inhibiting their ability to fire action potentials (Belle *et al.*, 2009). This depolarisation during the day is attributable to persistent sodium currents driving sodium influx in SCN neurons (Jackson *et al.*, 2004; Kononenko *et al.*, 2004; Flourakis *et al.*, 2015). In order to compensate for the massive Na^+ influx to the cell, the Na^+-K^+ ATPase is more active during

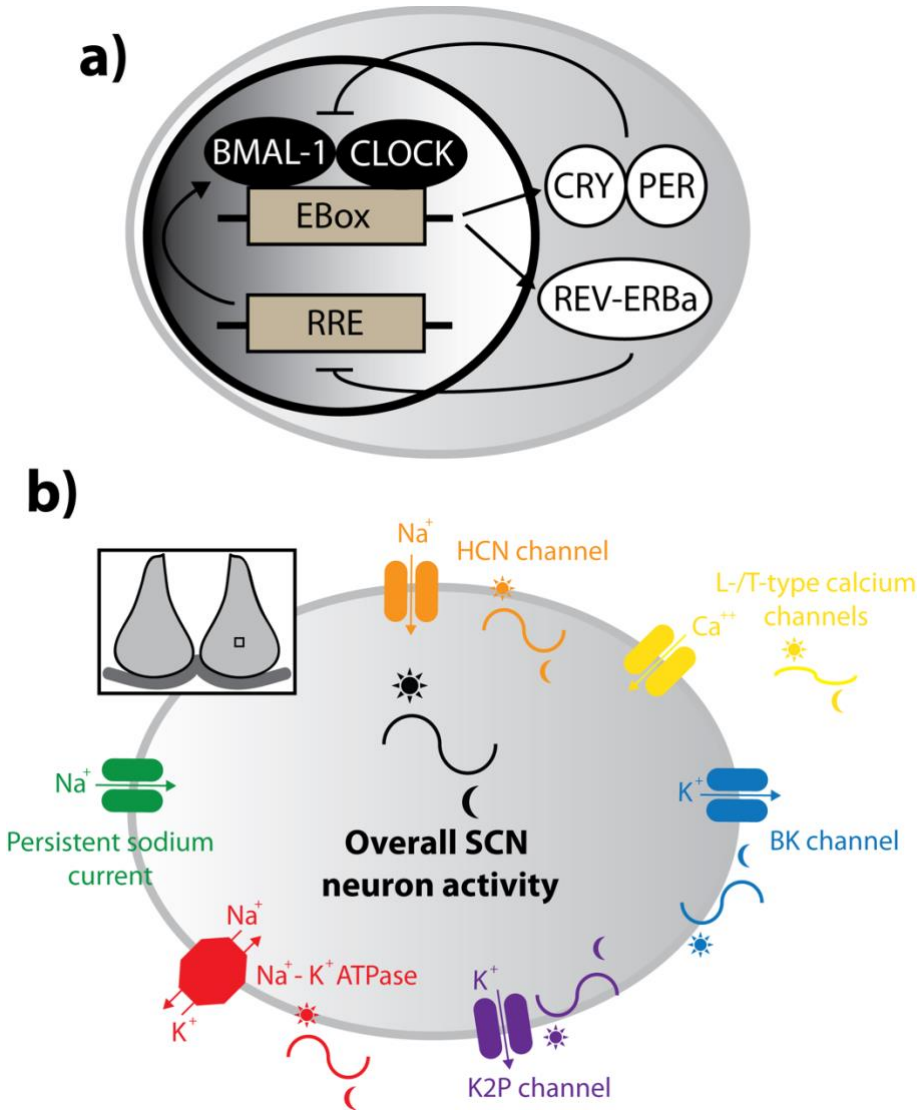

Figure 1.4: Circadian activity of individual SCN neurons.

a) Arrangement of circadian gene expression. The REV-ERBα response element (RRE) drives the production of BMAL-1. BMAL-1 and CLOCK dimerise to activate the EBox. EBox activation results in the production of PER, CRY and REV-ERBα. PER and CRY dimerise to breakdown of CLOCK and BMAL-1, while REV-ERBα binds the RRE to restart the cycle. **b)** Throughout the course of the day, circadian changes in membrane channels in SCN neurons cause alterations in the overall activity of individual SCN neurons. A persistent sodium current (green) drives a high overall resting membrane potential (RMP) in SCN neurons. This is buffered by daily increases in the Na^+-K^+ ATPase (red). The extrusion of Na^+ triggers further Na^+ influx by the HCN channel (orange), also highly expressed during the day. There is also a low amplitude daily increase in L-/T-type calcium channels (yellow), further raising RMP. At night, these channels reduce expression. In turn, these are replaced by K2P channels (purple) and BK channels (blue) which increase the intracellular K^+ concentration. This results in a lowering of RMP. This change in RMP throughout the course of the day results in the circadian changes in overall SCN neuron activity.

the day (Wang & Huang, 2006) to extrude excess Na^+. Following the depolarisation of SCN neurons, there is a hyperpolarisation of the membrane voltage, sufficient to activate hyperpolarisation-activated cyclic-nucleotide-gated ion (HCN) channels. The activation of HCN channels drives an I_H. The I_H causes a rapid influx of Na^+ causing a rebound depolarisation of SCN neurons to maintain the depolarised membrane potential (Akasu *et al.*, 1993; de Jeu & Pennartz, 1997). The activity of HCN channels also shows a diurnal rhythm, potentially contributing to the diurnal excitation of the SCN (Atkinson *et al.*, 2011). The final ionic contribution to the increased SCN activity is due to L- and T-type calcium channels. Although not providing a great contribution to SCN neuron depolarisation, the influx of calcium through L-/T-type calcium channels exhibits a low amplitude circadian oscillation to slightly increase the RMP of SCN neurons during the day (Pennartz *et al.*, 2002; Jackson *et al.*, 2004).

During the night, SCN neurons are essentially silenced by downregulation of HCN and calcium channels resulting in a repolarisation of the RMP (Pennartz *et al.*, 2002; Atkinson *et al.*, 2011). This is coupled with an increase in K^+ channels resulting in an approximate 10 mV decrease in RMP, compared to during the day (Kuhlman & McMahon, 2004). This nightly repolarisation is predominantly driven by an increase in K^+ efflux by K^+ leak currents through the two-pore potassium (K2P) channel. Towards the night, as depolarisation currents decrease resulting in a net repolarisation of SCN neurons, K2P channels become more active, thus, further reducing RMP (Kuhlman & McMahon, 2004; Colwell, 2011; Flourakis *et al.*, 2015). K^+ conductance is further enhanced at night by a peak in expression of Ca^{++}-activated K^+ (BK) channels (Pitts *et al.*, 2006). BK channels respond to any Ca^{++} influx by increasing the K^+ efflux to lower RMP. As such, these circadian changes in SCN neuron conductance underpin the relative changes in excitability, and thus, how the SCN is able to coordinate its output to other brain areas (Figure 1.4b).

1.5.2 SCN anatomy

The SCN comprises a small nucleus (the rat SCN having a volume of ~ 0.07 mm^3 (van den Pol, 1980)) that lies bilaterally at the base of the third ventricle, atop the optic chiasm, in the anterior hypothalamus (Figure 1.5a). It is a dense nucleus consisting of a heterogeneous group of neuronal phenotypes; in saying this, however, the majority, if not all of these neurons, are GABAergic (Moore & Speh, 1993; Castel & Morris, 2000; Abrahamson & Moore, 2001). Despite its small size, the SCN is commonly divided into two sections, the dorsal shell and ventral core regions (Morin & Allen, 2006; Morin, 2013). The division of these regions is traditionally based around the expression of two key neuropeptides: AVP expressed in the shell, and vasoactive intestinal polypeptide (VIP) expressed in the core (Figure 1.5b) (van den Pol, 1980). The SCN, however, does not only produce these two neuropeptides, but also contains a scattering of neurons that produce peptides either co-expressed with AVP/VIP, or discretely. These include gastrin-releasing peptide (GRP), substance P, cholecystokinin, somatostatin, neurotensin, prokineticin 2 (PK2), enkephalin, calretinin and calbindin (Cheng *et al.*, 2002; Morin & Allen, 2006). Further, the SCN produces neuromedin S (NMS) and is the only nucleus in the brain to do so, colocalising with ~ 95% of all AVP and VIP positive cells (Lee *et al.*, 2015).

1.5.2.1 Intra-SCN microcircuits

As there is a clear division in the SCN anatomy, it is important to consider how the two discrete regions coordinate their activity. Early work using electron microscopy revealed that SCN neurons extend local axonal projections which terminate within the opposing division(van den Pol, 1991), likely acting as a neuronal connection between the core and shell (Leak *et al.*, 1999; Yan *et al.*, 2007). Cell-filling data suggests that these axons are a mechanism by which SCN core neurons are communicating with SCN shell neurons (Drouyer *et al.*, 2010). AVP neurons in the SCN shell, however, have vast dendritic branches that extend into the SCN

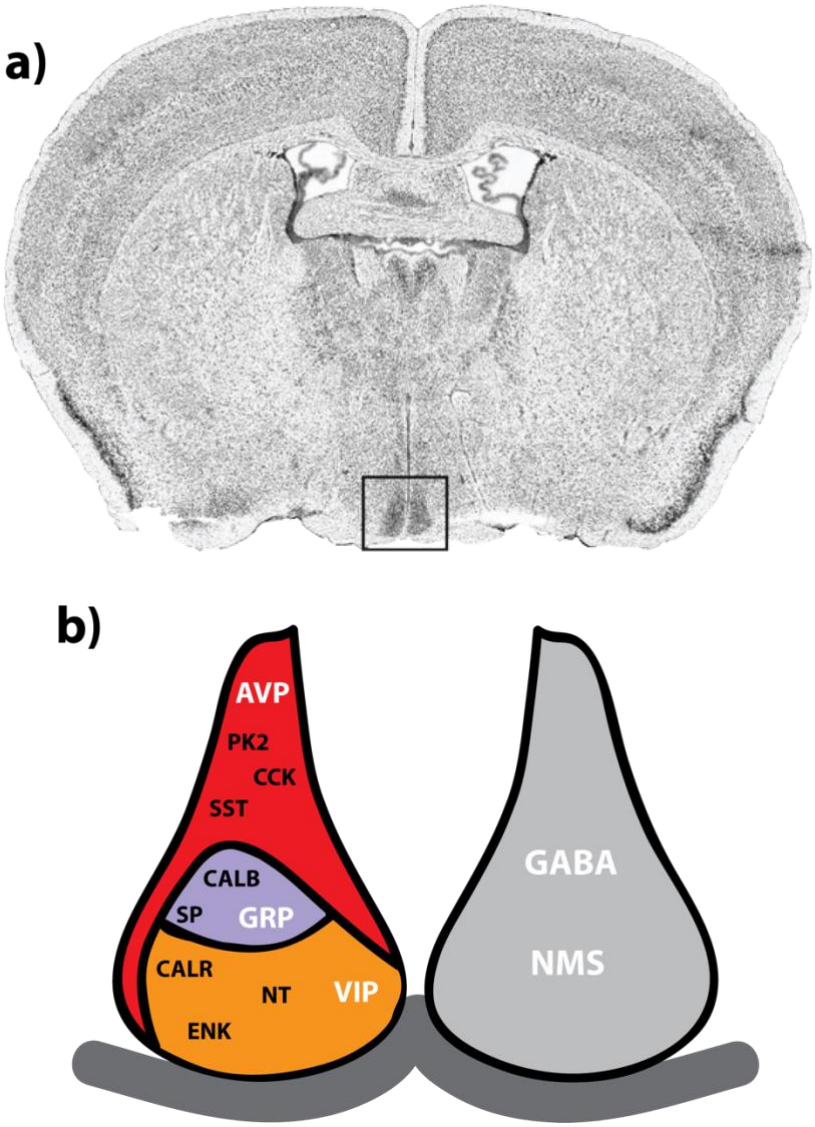

Figure 1.5: The suprachiasmatic nucleus is the locus of the brain's biological clock.

a) Greyscale Nissl-stained coronal brain slice taken at ~ bregma + 0.05 mm. Dense staining at the ventral aspect outlined shows the location of the suprachiasmatic nucleus. Image from Allen Brain Atlas. **b)** Diagrammatic representation of the arrangement of the SCN, with the third ventricle between the two sides, atop the optic chiasm. Red indicates the SCN shell typically demarcated by the presence of vasopressin (AVP) neurons; orange and purple indicate the SCN core, demarcated by the presence of vasoactive intestinal polypeptide (VIP) neurons and gastrin-releasing peptide (GRP). Other neuronal phenotypes are noted in their particular regions. GABA and neuromedin S (NMS), shown on the right, are spread throughout the SCN colocalising with multiple peptides. PK2 = prokineticin 2, CCK = cholecystokinin, SST = somatostatin, CALB = calbindin, SP = substance P, CALR = calretinin, NT = neurotensin, ENK = enkephalin.

core (Pennartz *et al.*, 1998). Whether this is a site for SCN core axonal connections remains unknown. These dendrites may release AVP directly (Castel *et al.*, 1996), similar to the dendrites of AVP neurons in the paraventricular and supraoptic nuclei (PVN, SON) (Ludwig & Leng, 2006). Another feature of intra-SCN connectivity is the presence of gap junctions. Adjacent SCN neurons are electrically coupled by gap junctions (Jiang *et al.*, 1997), however, this appears to be restricted to neurons within either the core or the shell, rather than between the two (Colwell, 2000).

As discussed prior, neurons within the SCN are capable of maintaining individual circadian rhythms, however, analysis of the entire SCN reveals a wave-like pattern of activity throughout the nucleus (Mohawk & Takahashi, 2011). AVP and VIP neurons show subtly different oscillation patterns but remain somewhat coordinated (Schwartz *et al.*, 1983), potentially allowing for differences in their output. When the SCN neurons are dissociated in culture, individual circadian rhythms persist but the synchrony between neurons is lost (Welsh *et al.*, 1995; Herzog *et al.*, 2004). This indicates that cell-to-cell coupling is necessary for the robustness and precision of circadian signals within the SCN (Mohawk & Takahashi, 2011). Synchrony within the SCN is likely coordinated by intra-SCN release of NMS. When NMS neurons are inhibited in the SCN, there is complete desynchronisation of the SCN (Lee *et al.*, 2015). This implicates NMS as a key coordinating molecule of neuronal synchrony in the SCN.

The gap junctions within the SCN are likely to electrically couple nearby SCN neurons as connexin-36-KO mice with functionally ablated gap junctions display dampened circadian behaviour (Long *et al.*, 2005). Studies looking at the communication between the core and shell support the idea that VIP is the most likely neuropeptide coupling the two regions (Aton *et al.*, 2005). VIP application to SCN explants resets the rhythm of SCN neurons (Watanabe *et al.*, 2000), while SCN neurons from VIP receptor-KO and VIP deficient mice are arrhythmic (Harmar *et al.*, 2002; Brown *et al.*, 2007). VIP is likely coordinating the activity of the core and shell, however, their subtly distinct rhythms may be a discrete mechanism of controlling

different outputs to separate efferent targets. The two rhythms could, therefore, provide distinct control over multiple brain regions.

1.5.3 Inputs to the SCN

The activity of SCN neurons is regulated by several inputs, the best characterised being inputs from the retina, the geniculate pathway, and the midbrain raphe nuclei. These brain regions are predominantly those that associate their activity with changes in the environment, particularly with photic cues from the retina.

1.5.3.1 The retinohypothalamic tract

The key environmental zeitgeber is light. Animals detect light by changes in neuronal activity occurring in the retina. These photic inputs activate non-visual melanopsin-positive ganglion cells (Berson *et al.*, 2002; Hattar *et al.*, 2002), whose axons bundle into a large, subcortical pathway, called the retinohypothalamic tract (RHT), and project to within the hypothalamus (Moore & Lenn, 1972). The key termination of the RHT is the SCN, with bilateral innervation from each retina that is predominantly contralateral (Sadun *et al.*, 1984). The RHT further projects to innervate habenular, collicular and geniculate nuclei (Hattar *et al.*, 2006). Here the focus will be on RHT projections to the SCN.

RHT innervation of the SCN is highly variable across species (Morin *et al.*, 2006). The hamster, for example, has a dense RHT innervation of the entire SCN (Pickard & Silverman, 1981), while other rodents tend to show an almost exclusive innervation to the SCN core (Morin & Allen, 2006; Lokshin *et al.*, 2015; Fernandez *et al.*, 2016).

Despite there being no consensus on the exact anatomical innervation of the SCN by the RHT, it is known that the neurotransmitters released from the RHT are capable of entraining SCN rhythms. The primary neurotransmitter released from the RHT is thought to be glutamate

(Hannibal, 2002). Glutamate and ionotropic glutamate receptor agonists are capable of exciting SCN neurons with glutamate receptors being found extensively throughout the SCN (Stamp *et al.*, 1997). The activation of glutamate receptors in the SCN mimics the effect seen in the onset of the light phase (Mintz & Albers, 1997; Mintz *et al.*, 1999). Although these effects are attributed to glutamate receptors, *in vivo* these results may be due to the release of a similar amino acid, aspartate. This is because typical glutamate markers such as the vesicular glutamate transporters are not abundant in the SCN (Fujiyama *et al.*, 2003), thus, aspartate may be having a greater effect on SCN neurons than glutamate (Shibata *et al.*, 1986), and that electrical stimulation of the RHT can cause both glutamate and aspartate to be released (Liou *et al.*, 1986).

Pituitary adenylate cyclase-activating polypeptide (PACAP) is co-expressed in the RHT (Hannibal *et al.*, 1997). PACAP alters the activity of SCN neurons similar to that caused by glutamate/aspartate, although not to such an extent (Hannibal *et al.*, 1997; Harrington *et al.*, 1999). Interestingly, when both PACAP and glutamate are applied together, the resulting phase shift is greater than that caused by the individual neurotransmitters (Chen *et al.*, 1999). Interestingly, the main PACAP receptor, VPAC1R is also activated by VIP, thus, this result may be a modulatory response caused by intra-SCN signalling.

1.5.3.2 Other neuronal inputs to the SCN

While the RHT is the main input to the SCN, there are several other key neural inputs which drive changes in SCN neuron activity (Morin & Allen, 2006). Here, the two key inputs, the intergeniculate leaflet (IGL) and median raphe nucleus (MRN) will be discussed.

The IGL receives input from the RHT, that then, in turn, is passed on to the SCN via the geniculohypothalamic tract, forming an indirect pathway from the retina (Morin *et al.*, 1992). The IGL neurons predominantly produce neuropeptide Y (NPY) (Card & Moore, 1982). The release of NPY within the SCN drives phase advances similar to glutamate/aspartate and PACAP (Biello *et al.*, 1997), likely through the Y5 receptor (Lall & Biello, 2003). While the

retinal input to the IGL is coming from the RHT, the IGL is likely integrating the oculomotor and vestibular activity. This is then directed to the SCN to provide subtle cues to circadian rhythms based on the environmental stimuli (Morin & Blanchard, 2005; Morin & Allen, 2006). Other than the SCN, the IGL projects to other brain regions involved with the maintenance of circadian rhythms, one of which is the MRN (Morin & Blanchard, 2005).

In the midbrain, IGL input to the MRN activates serotonergic neurons (Hay-Schmidt *et al.*, 2003). The release of serotonin (5-HT) from these inputs to the SCN, unlike those mentioned previously, acts to inhibit the SCN neurons resulting in a phase delay (Meyer-Bernstein *et al.*, 1997). The SCN contains at least six different 5-HT receptor types (Morin *et al.*, 2006); that which mediates this effect, however, remains unclear. 5-HT levels in the SCN increase in response to non-photic (i.e. unrelated to light) stimuli, particularly during the night to inhibit SCN activity (Dudley *et al.*, 1998). Although the effect of 5-HT in the SCN is subtle, it is thought to drive motivational cues for changes in behaviour coincident with changes in time, for example (Meyer-Bernstein *et al.*, 1997; Glass *et al.*, 2000).

1.5.3.3 Hormonal inputs

Along with regulating hormonal output, the SCN is under the control of hormonal inputs (Tsang *et al.*, 2014). In terms of circadian regulation, the secretion of the hormone melatonin, driven by SCN activation, acts to inhibit the output of SCN neurons (Liu *et al.*, 1997). Melatonin is released from the pineal gland and acts as an entrainment signal in response to the onset of the dark phase, directly signalling to the SCN through melatonin-1 receptors (Gillette & McArther, 1996). The role of melatonin in resetting circadian period is particularly important in maintaining circadian rhythms, as it is still released in a circadian manner during free-running conditions (Armstrong *et al.*, 1986), and in humans lacking the ability to respond to photic cues (Arendt & Broadway, 1987).

Stress hormones also communicate with the SCN. Projections from the SCN to stress-sensitive neurons in the PVN regulate daily fluctuations in glucocorticoid release (Vrang *et al.*, 1995). The resulting glucocorticoids released from the adrenal gland, however, are unable to feedback into the SCN, due to SCN neurons lacking glucocorticoid receptors (Pezük *et al.*, 2012). As such, glucocorticoids act at peripheral tissues to change their responsiveness to circadian input, as well as indirectly targeting the SCN via other brain circuits, causing the release of hormones, or by subtly changing glucose concentration to change SCN activity (Dickmeis, 2009; Tsang *et al.*, 2014).

The SCN exhibits a somewhat sexually dimorphic pattern of gonadal steroid hormone receptor expression. SCN AR expression is higher in males than females (Wu *et al.*, 1995; Fernández-Guasti *et al.*, 2000; Iwahana *et al.*, 2008), and appears to be localised within the SCN core (Karatsoreos *et al.*, 2007). The ability to relay androgenic signals to the biological clock, however, is not solely at the SCN, with indirect projection regions, such as the IGL and MRN also expressing high levels of AR in the male (Karatsoreos *et al.*, 2007). Activation of the AR in these regions results in less precise entrainment to photic cues (Karatsoreos & Silver, 2007); the physiological relevance of which, however, is yet to be revealed. PRs have been consistently identified in the primate SCN (Goldsmith *et al.*, 1997; Kruijver & Swaab, 2002), although no work has been carried out in the rodent. ERs are expressed consistently higher in the SCN of females than males (Vida *et al.*, 2008). ERα has no, or very little, expression in the SCN (Shughrue *et al.*, 1996; Goldsmith *et al.*, 1997; Shughrue *et al.*, 1997; Vida *et al.*, 2008). ERβ, however, has a 5-fold higher expression than ERα (Kruijver & Swaab, 2002; Vida *et al.*, 2008). In contrast to the AR, ERs are more densely expressed in the SCN shell than the SCN core (Vida *et al.*, 2008). As mentioned, ERβ has little impact on female fertility, thus is unlikely to mediate any oestrogenic feedback of the GnRH neuronal network at the level of the SCN. Interestingly, de la Iglesia *et al.* (1999) report many ERα-expressing afferent neurons which may relay oestrogenic cues to the SCN. It has been suggested that due to the gonadal steroid

receptors in the SCN, gonadal steroids may be influencing certain circadian rhythms (particularly body temperature and sexual behaviour), but it has yet to be shown whether these are direct at the SCN, or acting at afferent populations (Kruijver & Swaab, 2002).

1.5.4 Outputs from the SCN

Research investigating the outputs from the SCN has been significantly hampered by the small size of the nucleus itself. Injection of dyes into the SCN has never been 100% replicable, revealing some targets and not others (Leak & Moore, 2001; Morin & Allen, 2006); while cell filling data only allows individual neurons in brain slices to be targeted at any one time (Yan *et al.*, 2007). Further, little work has looked at the actual functional contributions of neurons from the SCN as part of wider neural networks. As such, the majority of work in this field is purely anatomical with the inference being that SCN neurons are relaying circadian cues to the nuclei to which they project (Morin & Allen, 2006).

1.5.4.1 Axonal outputs from the SCN

Anatomical approaches to studying the efferent SCN connections have predominantly involved the injection of anterograde tracers into the SCN and tracing the axonal outputs; or injection of retrograde tracers into regions thought to be innervated by the SCN and tracing the neurons back to the SCN. More recent immunohistochemical methods, where peptides present in the SCN are labelled and their projections identified, are problematic, as many of these peptides are not exclusively found in the SCN making it difficult to determine their origin (Abrahamson & Moore, 2001).

The majority of SCN projections can be grouped into three categories: rostral projections, dorsal projections, and ventrocaudal projections (Watts *et al.*, 1987). The rostral projections send axons from the SCN to the forebrain, particularly the bed nucleus of the stria

terminalis, ventrolateral septum and the anterior portion of the paraventricular thalamus (PVT) (Watts & Swanson, 1987; Morin *et al.*, 1994; Abrahamson & Moore, 2001; Schwartz *et al.*, 2011). The dorsal SCN projections spread throughout the surrounding hypothalamus, and in general target nearby hypothalamic regions such as the medial preoptic area, PVN, OVLT, PeN and dorsomedial hypothalamus (Watts & Swanson, 1987; Watts *et al.*, 1987; Kalsbeek *et al.*, 1993; Morin *et al.*, 1994; Schwartz *et al.*, 2011). The ventrocaudal projection tracks downwards from the SCN and along the optic tracts to innervate more caudal brain regions such as the posterior PVT and periaqueductal grey (Watts *et al.*, 1987; Morin *et al.*, 1994), as well as those associated with the optic tracts, such as the SON (Kalsbeek *et al.*, 1993; Abrahamson & Moore, 2001). Although some conflict remains between studies about the innervation of some areas by the SCN, this is likely due to differences in technique or particular injection sites between research groups. Table 1.1 provides a more complete list of the areas reported to be innervated by the SCN as well as outlining differences reported between groups and between species.

The peptidergic characteristics of the axonal projections from the SCN remain largely unknown, due to the difficulty in tracing long immunohistochemically labelled fibres throughout the brain. Typically, it is thought that the majority of targets are innervated by both SCN core and SCN shell neurons to some extent (Morin & Allen, 2006). There do appear to be some distinct differences, however; the parvocellular division of the PVN is likely to only be targeted by SCN AVP neurons (Abrahamson & Moore, 2001; Leak & Moore, 2001), while the SON appears to be only targeted by SCN VIP neurons (Kalsbeek *et al.*, 1993; Abrahamson & Moore, 2001). Work by Kalsbeek *et al.* (1993) took a contrasting approach to determine the phenotypic differences in targets; the SCN was lesioned and the absence of peptide-expressing fibres was quantified. Thus, lesioning the SCN provided an indication of whether peptide-expressing fibres detected in a given brain region were of SCN origin.

Brain Structure	Mouse (*Mus musculus*)	Rat (*Rattus norvegicus* or *Arvicanthus niloticus*)	Hamster (*Mesocricetus auratus*)	References
Arcuate nucleus			Yes	e
Bed nucleus of the stria terminalis		Yes (Medial [h])	Yes (Caudal [a])	a, d, g, h
Diagonal band of Broca		Yes		h
Dorsomedial hypothalamus	Yes[†]	Yes[*]	Yes[†*]	a, d, e, f, g, h, i
Intergeniculate leaflet		No (Likely only from the Peri-SCN region [b])	Yes	a, b, c, d, e, h
Medial amygdala			Yes (Sparse [e])	e
Median preoptic area	Yes	Yes[*] (More ventral [a])	Yes[*]	a, d, e, f, g, h
Olivary pretectal area			Yes	e
Organum vasculosum of the lamina terminalis	Yes[*]	Yes	No [a]; Yes[* f]	f, g, h
Parataenial nucleus	Yes[*]	Yes[†]		b, d, f, g, h
Paraventricular nucleus	Yes[*]	Yes (Dense in the dorsal parvocellular division [h], sparse in the magnocellular division [h])	Yes[*] (Dense in the dorsal parvocellular division [a, d, e], sparse in the magnocellular division [a, e])	a, b, d, e, f, h
Paraventricular thalamus	Yes[†]	Yes[*†]	Yes[†] (Rostral [a] but may also be caudal [e])	a, d, e, f, g, h
Periaqueductal grey matter		Yes (Only rostrally [b])	Yes (Sparse [e])	b, e
Periventricular nucleus	Yes[*]		Yes	e, f
Precommisural nucleus		Yes	Yes	a, d
Premammillary area		Yes	Yes	a, d, g
Sub-paraventricular zone	Yes[†]	Yes[*†]	Yes	a, d, e, f, g, h
Supraoptic nucleus	Yes[†] (Sparse [f])		Yes (Sparse [d])	d, f
Ventral preoptic area			Yes	i
Ventrolateral septum	Yes	Yes	Yes	a, b, d, e, f, h, i
Ventromedial hypothalamus	Yes	Yes[†] (Sparse [b], denser medially [g])	Yes	a, b, d, e, f

Table 1.1: Efferent projections from the SCN studied in four model species.

Gaps in the table indicate that the projection has not been reported/examined. **Reference methodologies - a:** Watts *et al.* (1987): Rats of both sexes, injected with *Phaseolus vulgaris* leucoagglutinin (*Pha*-L) into the SCN for anterograde tracing. **b:** Watts and Swanson (1987): Rats of both sexes, retrograde tracing of true blue or SITS injected into regions of interest. **c:** Card and Moore (1984): Rats of both sexes, retrograde tracing of FluroGold or rhodamine-labelled latex beads injected into regions of interest. **d:** Kalsbeek *et al.* (1993): Male hamsters, injected with *Pha*-L into the SCN for anterograde tracing. **e:** Morin *et al.* (1994): Male hamsters, injected with *Pha*-L into the SCN for anterograde tracing. **f:** Abrahamson and Moore (2001): Male mice, immunohistochemical staining for SCN peptides looking in regions of interest. **g:** Leak and Moore (2001): Rats of both sexes, retrograde tracing of cholera toxin-β, FluoroGold, swine herpes virus/pseudorabies virus or biotinylated dextran amine injected into regions of interest. **h:** Schwartz *et al.* (2011): Female rats, injected with biotinylated dextran amine into the SCN for anterograde tracing. **i:** Kriegsfeld *et al.* (2004): Male hamsters, injected with biotinylated dextran amine into the SCN for anterograde tracing. *area reported to be innervated by AVP-expressing neurons; †area reported to be innervated by VIP-expressing neurons.

1.5.4.2 Diffusible outputs from the SCN

As mentioned, the anatomical identity of the SCN outputs is much better understood than their functional relevance. Lesions of the SCN have been a key mechanism in determining not only the presence of a biological clock but how the SCN controls its outputs. Removal of the SCN completely removes an organism's ability to entrain to cues, effectively abolishing typical circadian sleep-wake cycles and circadian locomotor behaviour as well as disrupting circadian endocrine rhythms and oestrous cycles (Wiegand *et al.*, 1980; Wiegand & Terasawa, 1982; Brown & Nunez, 1986; Watts *et al.*, 1989). Silver *et al.* (1996) took this approach a step further, whereby after the SCN was lesioned, a graft of foetal SCN tissue encapsulated in a semi-permeable membrane was implanted into the site of the lesion. Interestingly, the foetal SCN tissue was able to restore locomotor rhythms, but not oestrous cycles (Meyer-Bernstein *et al.*, 1999). The semi-permeable capsule surrounding the foetal SCN tissue inhibited the growth of new axons from the SCN, however, it still allowed small molecules to pass in and out of the graft. As such, it was hypothesised that SCN neurons released a diffusible signal to control some circadian rhythms, but not others. The identity of such a diffusible signal, however, remains unknown. AVP-deficient rats still maintain circadian rhythms, thus ruling out AVP as a candidate (Boer *et al.*, 1999). Other potential signals include transforming growth factor-α (TGFα) and PK2. TGFα displays a circadian expression pattern similar to the circadian locomotor behaviour, which was restored in the foetal SCN grafts (van der Zee *et al.*, 2005). TGFα has also been shown to inhibit locomotion in free running conditions, however (Kramer *et al.*, 2001). PK2 shows the opposite pattern of expression, with very low levels at night when locomotor behaviour is highest (Cheng *et al.*, 2002). Unsurprisingly, PK2 has been shown to inhibit running wheel activity (Cheng *et al.*, 2002). Interestingly, *Prok2*-KO mice are arrhythmic and struggle to entrain to external cues (Li *et al.*, 2006).

To summarise, while circadian rhythms in behaviour are likely controlled by a diffusible signal the axonal outputs from the SCN likely contribute to the control of reproductive status,

if not other endocrine processes as well (Kriegsfeld & Silver, 2006). The role of VIP and AVP as part of these axonal outputs will now be discussed.

1.5.5 The role of VIP

VIP is a 28 amino acid peptide predominantly acting in the digestive system to stimulate smooth muscle relaxation (Umetsu *et al.*, 2011). In the brain, however, VIP is present in neurons in discrete nuclei, though in particularly dense quantities in the SCN (Besson *et al.*, 1986). VIP acts through two receptors, VPAC1R and VPAC2R, both of which are also able to bind PACAP (Usdin *et al.*, 1994). mRNA for *Vip* oscillates within the SCN in a circadian manner (Dardente *et al.*, 2004), indicating that it may act to coordinate circadian outputs from the SCN.

As mentioned, the VIP neurons might be acting as an intermediate between the RHT and the rest of the brain to coordinate this entrainment signal. The SCN contains the densest population of VPAC2R (Usdin *et al.*, 1994) colocalising to ~ 30% of VIP neurons in the SCN, and ~ 50% of AVP neurons (Kalamatianos *et al.*, 2004b; Kalló *et al.*, 2004). As such, VIP is able to influence the neurons within the SCN. VIP signalling is essential to circadian rhythmicity as all VIP- and VPAC2R-KO animal models are unable to maintain circadian locomotor rhythms (Harmar *et al.*, 2002; Colwell *et al.*, 2003). Interestingly, VPAC2R-KO models show a more severe disruption than the VIP-KO animals, potentially underlying a loss of contribution from PACAP signalling (Vosko *et al.*, 2007). Aside from the loss of locomotor rhythms in KO animal models, SCN neurons in culture from VPAC2R-KO mice do not generate oscillations in electrical rhythm (Cutler *et al.*, 2003; Aton *et al.*, 2005), or have appropriate rhythms in their transcriptional-translational feedback loops (Harmar *et al.*, 2002). Therefore, VIP may be necessary for maintaining the circadian rhythm within the intra-SCN circuitry.

SCN VIP neurons extend long projections to neurons mainly involved in neuroendocrine control of homeostasis (Abrahamson & Moore, 2001; Kalsbeek & Buijs, 2002). VIP-immunoreactive (-ir) fibres make close appositions with PVN corticotropin-releasing hormone and thyrotropin-releasing hormone neurons, as well as GnRH neurons in the preoptic area (Kalsbeek & Buijs, 2002). The hormones released from these neuroendocrine neurons are shown to have their own endogenous rhythms, and thus, the neurons may potentially be entrained by VIP signalling from the SCN.

1.5.6 The role of AVP

AVP is a nonapeptide hormone expressed in three main areas of the brain, the PVN, SON and SCN. It is commonly associated with its role in antidiuresis and maintenance of blood pressure, due to its release from PVN and SON magnocellular neurons into the posterior pituitary gland (Bankir, 2001). AVP acts through three main receptors: V1a, V1b and V2 receptors (V1aR, V1bR, V2R). The V2R is predominantly expressed in the lung and kidney tissue to regulate fluid balance (Robben *et al.*, 2004). The V1Rs are localised to the brain, though do have some peripheral effects (Koshimizu *et al.*, 2012). V1aR and V1bR within the brain are found particularly in the hypothalamus and are associated with behavioural responses (Tanoue *et al.*, 2004; Volpi *et al.*, 2004). It is thought, however, that the V1aR, and perhaps to some extent the V1bR mediate the effects of the circadian system (Li *et al.*, 2009; Yamaguchi *et al.*, 2013).

AVP was one of the first neurotransmitters identified within the SCN (Swaab *et al.*, 1975). It shows a circadian pattern of expression with higher mRNA and immunofluorescence noted during the hours following the onset of the light phase and lower expression during the dark phase (Jin *et al.*, 1999; van der Veen *et al.*, 2005; Maruyama *et al.*, 2010), mirrored by its concentration in cerebrospinal fluid (Schwartz *et al.*, 1983). This is due to activation of the *Avp* gene by the CLOCK/BMAL-1 complex (Jin *et al.*, 1999), which accumulates during the day.

This increase in AVP may be synchronising the SCN subregions in response to the onset of the light phase (Maywood *et al.*, 2011). Spontaneous activity of SCN neurons is correlated with the activity of neurons in the surrounding hypothalamus, and this can be abolished by application of an AVP receptor antagonist (Tousson & Meissl, 2004). As such, the activity of AVP neurons is likely to control the surrounding hypothalamic nuclei.

The exact mechanism of AVP control of circadian rhythms is confounded by conflicting results. V1aR-KO mice display impaired circadian locomotor activity (Li *et al.*, 2009), although this is not recapitulated simply by antagonism of V1aRs *in vivo* (Stoynev & Nagai, 1996). Further, AVP-deficient Brattleboro rats do not show any behavioural changes (Groblewski *et al.*, 1981). Therefore, AVP may not be critical in the circadian control of locomotor behaviour. The release of AVP from the SCN is more likely to be important in the circadian control of hormonal release. SCN lesions elevate the levels of corticosterone, as do V1R antagonists (Kalsbeek *et al.*, 1992; Kalsbeek *et al.*, 1996b); thus, AVP may inhibit the release of corticosterone as part of the hypothalamic-pituitary-adrenal axis, likely by changing activity of hypothalamic neurons (Kalsbeek *et al.*, 1996a). In contrast, AVP appears necessary to permit fertility (Funabashi *et al.*, 1999; Palm *et al.*, 1999; Miller *et al.*, 2006) as will now be discussed.

1.6 Mechanisms for the circadian control of the LH surge

The biological clock is clearly implicated in the control of fertility via the HPG axis. GnRH neurons and kisspeptin neurons all express the necessary time keeping genes (as outlined in Section 1.5.1). GnRH and kisspeptin cell lines in culture show oscillations coupled to peptide synthesis (Chappel *et al.*, 2003; Chassard *et al.*, 2015; Jacobs *et al.*, 2016). These changes, however, show more subtle effects in brain slice experiments and *in vivo*, with the circadian responses possibly gating hormone and neuropeptide responsiveness (Cai *et al.*, 2008; Williams *et al.*, 2011; Piet *et al.*, 2016). Further, specific clock gene knock outs from specific cells in the

SCN, kisspeptin neurons, and GnRH neurons, show alterations in the timing (although not the complete inhibition) of the LH surge (Bittman, 2019). Peripherally, clock genes in the pituitary gonadotropes and ovary regulate GnRHR and LHR density (Sellix *et al.*, 2013), respectively. Although these individual clocks may regulate certain circadian aspects of fertility, it is important to remember that when they are intact, but the SCN is lesioned, an LH surge is unable to be initiated. Thus, axonal outputs from the SCN are critical as a true circadian cue for the HPG axis. Anatomical studies of the projections from the SCN have revealed innervation of the GnRH neuronal network at different levels: at the GnRH neuron itself, and the upstream afferents controlling GnRH neuron activity.

1.6.1 Direct circadian control of the HPG axis

The predominant innervation of the GnRH neuron by the SCN is by VIP neurons (Horvath *et al.*, 1998; Kriegsfeld *et al.*, 2002). This forms a direct network by which the SCN can innervate the HPG axis (Figure 1.6). Immunoreactive appositions have been found between VIP-expressing neuronal terminals and GnRH neurons (van der Beek *et al.*, 1997; Horvath *et al.*, 1998; Kriegsfeld *et al.*, 2002; Mahoney & Smale, 2005). At the time of the LH surge, VIP-expressing terminals can also be seen in apposition to GnRH neurons expressing c-FOS, indicating that they may be directly influencing GnRH neuron activity. GnRH neurons express VPAC2Rs (Olcese *et al.*, 1997; Smith *et al.*, 2000), indicating they are responsive to VIP.

The role of VIP in stimulating GnRH release *in vivo* is unclear. Injection of VIP into the brain has been shown to either increase (Vijayan *et al.*, 1979), or decrease the release of LH(Samson *et al.*, 1981; Alexander *et al.*, 1985; Kimura *et al.*, 1987; Akema *et al.*, 1988; Ohtsuka *et al.*, 1988). When VIP is reduced using antibodies injected into animals, or by antisense oligonucleotides, the LH surge is attenuated(Harney *et al.*, 1996; van der Beek *et al.*, 1999; Gerhold *et al.*, 2005). VIP-deficient mice exhibit normal fertility(Colwell *et al.*, 2003),

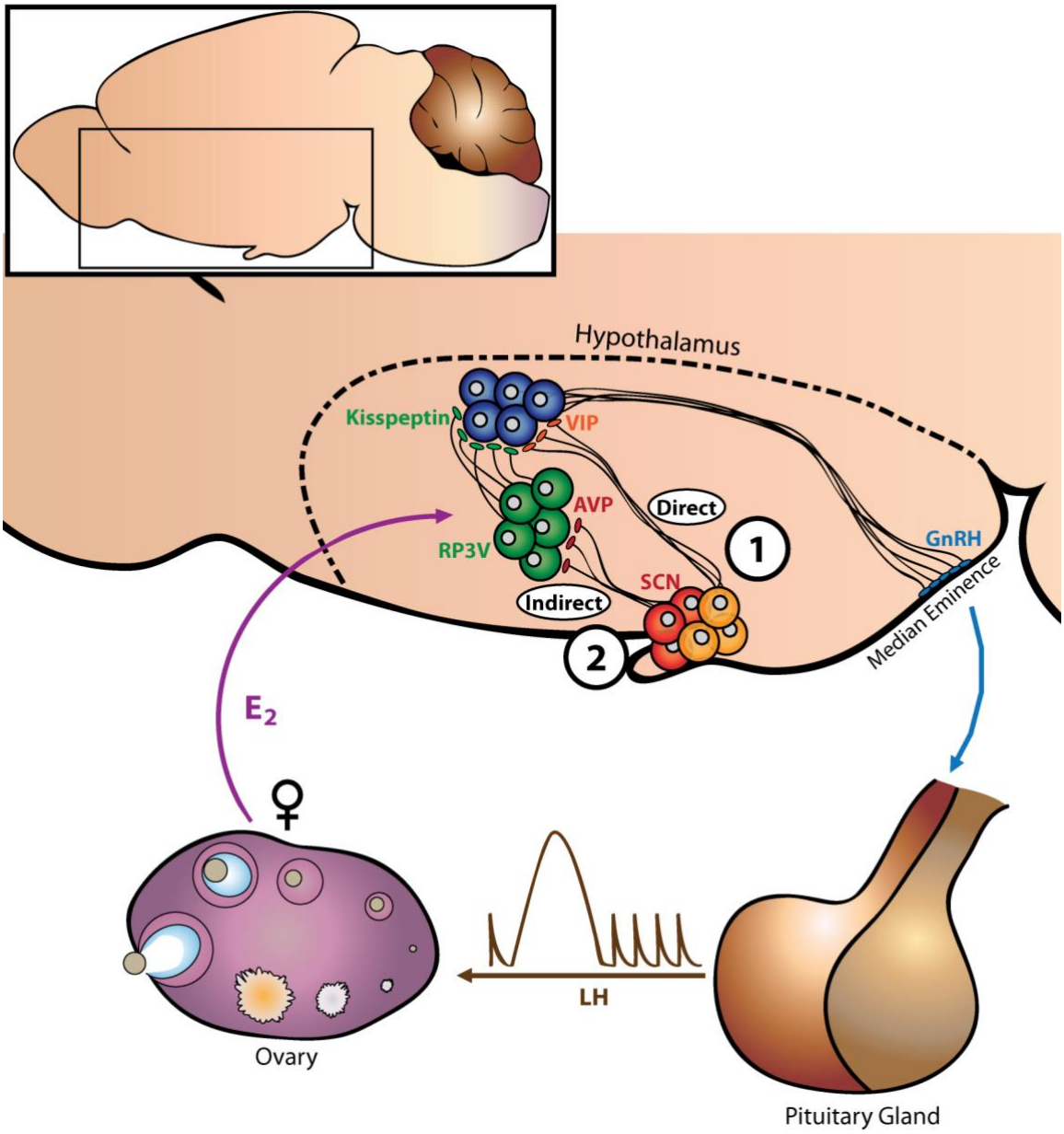

Figure 1.6: SCN neurons control the hypothalamic-pituitary-gonadal axis.

GnRH neurons in rPOA receive direct input from the vasoactive intestinal polypeptide (VIP)-expressing neurons in the SCN (**1**). The vasopressin (AVP)-expressing SCN neurons, however, relay their signal indirectly to the HPG axis via the RP3V kisspeptin neurons (**2**). Kisspeptin neurons act as an integrator for hormonal signals from the ovary such as oestradiol (E_2), as well as circadian signals from the SCN. Together, this may coordinate the timing of the LH surge.

but VPAC2R-KO mice but have irregular oestrous cycles (Dolatshad *et al.*, 2006; Loh *et al.*, 2014). Results *in vitro* are much clearer. VIP, when applied to explants of median eminence can cause the release of GnRH (Samson *et al.*, 1981). This has been replicated in slices of hypothalamus with pituitary attached to show that it also stimulates the release of LH (Ohtsuka *et al.*, 1988). Electrophysiological recordings from GnRH neurons show that VIP excites about half of those neurons tested (Christian & Moenter, 2008; Piet *et al.*, 2016). While appositions between VIP neuron terminals and GnRH neurons has been established, the percentage of GnRH neurons apposed by VIP expressing terminals is significantly lower than the number of GnRH neurons activated at the time of the surge (Williams *et al.*, 2011).

Thus, it is more likely that an indirect pathway is a more potent activator of the LH surge. AVP is likely a contributor to the development of the LH surge (Funabashi *et al.*, 1999; Palm *et al.*, 1999), however, a direct AVP to GnRH neuron projection is unlikely. The relative expression of V1Rs and AVP-ir appositions to GnRH neurons is minimal (Kalamatianos *et al.*, 2004a; Jasoni *et al.*, 2005; Mahoney & Smale, 2005). Further, AVP is unable to excite GnRH neurons (Piet & Herbison, unpublished).

1.6.2 Indirect circadian control of the HPG axis

The indirect pathway between the SCN and HPG axis involves the relay of SCN signals through a secondary neural population. SCN projections to the RP3V have been identified (Watson Jr. *et al.*, 1995; de la Iglesia *et al.*, 1999), with AVP-ir fibres in apposition to kisspeptin neurons (Figure 1.6) (Williams *et al.*, 2011). A second population of neurons expressing (Arg)(Phe)-related peptide-3 (RFRP-3) in the DMH also receive VIP-ir and AVP-ir inputs (Gibson *et al.*, 2008; Russo *et al.*, 2015). Both kisspeptin and RFRP-3 neurons do not show these immunoreactive appositions when the SCN is ablated, indicating their likely origin (Williams *et al.*, 2011; Russo *et al.*, 2015).

RFRP-3 typically inhibits GnRH neurons and LH secretion (Tsutsui *et al.*, 2000; Kriegsfeld *et al.*, 2006; Anderson *et al.*, 2009; Ducret *et al.*, 2009). Thus, RFRP-3 and kisspeptin would act opposite to each other. SCN outputs to the RFRP-3 neurons are likely VIP-mediated, as exogenous VIP inhibits the RFRP-3 neuron activity at the time of the LH surge (Gibson *et al.*, 2008; Henningsen *et al.*, 2017). Despite SCN VIP neurons potentially inhibiting RFRP-3 neurons, there is very little VPACR expression in the DMH (Russo *et al.*, 2015), thus the exact mechanism for inhibition of RFRP-3 neurons remains unknown. Although there are AVP-ir fibres apposed to RFRP-3 neurons, AVP does not appear to affect RFRP-3 neuron activity (Russo *et al.*, 2015). While the SCN may act to disinhibit GnRH neurons (via inhibition of RFRP-3 activity) at the time of the LH surge, it is more likely that SCN neurons stimulate its onset. SCN core rhythms are in phase with kisspeptin neuron activity during the surge (Smarr *et al.*, 2012), and as such, it would seem that SCN AVP neurons acting at RP3V kisspeptin neurons may be playing a more critical role.

The role of AVP in the generation of the LH surge has been studied following dialysis of AVP into the preoptic area (POA) (Palm *et al.*, 1999, 2001). AVP administration to the POA was shown to restore the LH surge in animals with SCN lesions (Palm *et al.*, 1999). This was shown to be time-dependent, only working just prior to the expected onset of the LH surge (Palm *et al.*, 2001). Interestingly, this is similar to mouse models showing *Clock*-gene KO. The *Clock*-KO mouse has disrupted oestrous cycles and is sub-fertile (Miller *et al.*, 2004); and has reduced AVP expression in the SCN (Miller *et al.*, 2006). Administration of AVP to *Clock*-KO mice rescues the LH surge (Miller *et al.*, 2006). The data suggesting that an AVP-induced surge can be blocked with V1R antagonists is conflicting, but may be dependent on the time of administration (Funabashi *et al.*, 2000b; Palm *et al.*, 2001; Miller *et al.*, 2006).

Elegant work by Smarr *et al.* (2012) resulted in the production of a model of SCN desynchronization, where mice housed on an 11-hour light/11-hour dark cycle disrupted the coordination of circadian genes between the SCN core and shell; the individual activity of the

SCN core and shell could then be determined without interference from the other region. They determined that increased activity of the SCN shell occurred at the same time as the initiation of the LH surge (Smarr *et al.*, 2012). This increase in activation was coincident with an increase in *Kiss1* mRNA in the RP3V. There is a putative connection between these effects and AVP, as AVP neurons are found in the SCN shell. Thus, the SCN shell, and potentially the AVP neuron, input activates the RP3V kisspeptin neurons to drive the surge (Smarr *et al.*, 2012). RP3V neurons, as well as identified RP3V kisspeptin neurons, have also been shown to express V1aRs, with their number proportional to the serum concentration of oestradiol (Funabashi *et al.*, 2000a; Kalamatianos *et al.*, 2004a; Williams *et al.*, 2011). Further, they are able to respond to exogenous application of AVP increasing action potential firing (Piet *et al.*, 2015b).

GnRH neuron activation, as stimulated indirectly by SCN AVP output to RP3V kisspeptin neurons, seems to prevail as the key candidate for the integration of hormonal and circadian cues driving the preovulatory surge. The integration of these two cues by RP3V kisspeptin neurons appears to be necessary to stimulate the GnRH neurons to increase their activity resulting in a surge of hormones. As such, this circuit has a high impact for mammalian fertility that has not yet fully been explored.

1.6.3 Circadian-disrupted infertility

As mentioned, lesions of the SCN abolish the oestrous cycle, indicating the SCN is vital for fertility. Changes in an animal's light cycle can also alter ovarian function and oestrous cycles (Lawton & Schwartz, 1967), indicating the role normal circadian patterns have in fertility. In humans, circadian disruption has anecdotally been attributed to changes in female fertility, though scientific evidence for this is not robust (Gamble *et al.*, 2013). Changes in menstrual cycle patterns have been reported in female shift-workers who do not work in typical daylight hours (Gamble *et al.*, 2013). This results in changes reported in pregnancy and the health of offspring (Knutsson, 2003; Bonzini *et al.*, 2011). As such, alterations in circadian

behaviour, or changes to the neural circuitry involved with it, could result in drastic conditions of infertility. One such condition, that may include pathophysiological disruption to this circuit, is PCOS. Women with PCOS show impairments in gonadotropin release and are often anovulatory suggesting impairments in the GnRH neuronal network.

1.7 Polycystic ovary syndrome

PCOS is the most common cause of endocrine-disrupted infertility affecting females worldwide (Azziz *et al.*, 2004). Despite its prevalence, the exact aetiology remains unknown. There are several competing theories for the cause of PCOS, including genetic abnormalities, metabolic abnormalities, and chemical exposure during *in utero* development (Moore & Campbell, 2017). Further, it is still unclear as to whether these changes act alone or whether a combination of factors play into disease development.

PCOS was first characterised by Stein and Leventhal (1935) in women presenting with menstrual abnormalities, androgynous features and the eponymous polycystic ovaries. Despite this, however, PCOS is a much more heterogeneous disease than initially suspected. The current criteria for the broad diagnosis of PCOS were outlined by the Rotterdam Committee (2004) and involve the presence of three cardinal criteria: oligo- or anovulation; hyperandrogenaemia without other explanatory factors such as androgen-secreting tumours; and the presence of fluid-filled cysts on the ovary. Diagnosis by two or three of these criteria results in reportedly 5-20% of women of reproductive age having PCOS (Asunción *et al.*, 2000; March *et al.*, 2010; Yildiz *et al.*, 2012).

Secondary to the cardinal features of PCOS are associated downstream symptoms, particularly those caused by hyperandrogenaemia. These include hirsutism, persistent acne and alopecia (Apridonidze *et al.*, 2005), as well as other hormonal changes such as increased serum concentration of anti-Müllerian hormone (Pigny *et al.*, 2003; Tata *et al.*, 2018). Further, PCOS

is associated with coincident diseases such as obesity, cardiovascular disease and insulin resistance (Apridonidze *et al.*, 2005). To combat the disease, treatment options are symptom based, including hormonal contraceptives and androgen receptor antagonists, anti-diabetic drugs to target metabolic changes, or high concentration hormones to restore ovulation (Ndefo *et al.*, 2013).

In order to help dissect specific causative factors for PCOS, several animal models of the PCOS-like phenotype have been developed (Stener-Victorin *et al.*, 2020). To date, the most common method for this is androgen administration during foetal development – termed prenatal androgen treatment. Prenatal androgen treatment involves delivery of androgens to a pregnant mother where the subsequent hyperandrogenism causes changes to the offspring. The androgen exposure *in utero* causes the female offspring to display their own hyperandrogenaemia later in life (Silva *et al.*, 2018). Prenatally androgen-treated (PNA) models closely resemble the PCOS phenotype, including changes in ovarian function, hyperandrogenaemia and metabolic dysfunction; which have been shown in monkeys (Abbott *et al.*, 2008), sheep (Birch *et al.*, 2003; Smith *et al.*, 2009), rats (Foecking *et al.*, 2005; Wu *et al.*, 2010) and mice (Sullivan & Moenter, 2004; Moore *et al.*, 2013). These changes may be programmed in development from prenatal androgen exposure, or stem from their endogenous hyperandrogenaemia. Although PCOS may classically be thought of as an ovarian disorder, a growing body of evidence now suggests that the prenatal androgen exposure may be altering brain circuits linked to fertility. These may either be organisational (i.e. occurring during development), or activational (i.e. changes due to the resulting hyperandrogenaemia in the offspring) (Figure 1.7).

1.7.1 Neuroendocrine changes in PCOS

For an androgen insult to result in the development of PCOS-like symptoms, AR activation is required. In AR-KO mice, administration of DHT over 3 weeks, to induce

hyperandrogenaemia, does not cause the typical PCOS-like phenotype seen in wild-type mice (Caldwell *et al.*, 2017). Interestingly, in tissue-specific knock-out of AR, it is the brain, rather than the ovary, that requires AR signalling for the full development of PCOS (Caldwell *et al.*, 2017). Thus, it is unlikely that androgen-induced changes at the ovary are necessary to induce PCOS. The potential change in brain circuitry resulting from AR activation, however, is thought to alter the release of gonadotropins. Women with PCOS display markedly higher basal LH secretion, along with high frequency LH pulses (Taylor *et al.*, 1997). As such, defects to the upstream GnRH network are likely to be mediating the alterations in hormone release.

As GnRH neurons do not express AR (Huang & Harlan, 1993). As such, upstream neurons regulating GnRH neuron function are more likely to be altered during development in response to the prenatal androgen exposure. As RP3V kisspeptin neurons are implicated in driving ovulation, it may be expected that periods of anovulation may be due to changes in their activity. Prenatal testosterone treatment of rats changes the organisation of the female RP3V kisspeptin neurons to display a reduced, more masculine-like pattern of *Kiss1* mRNA expression (Kauffman *et al.*, 2007), although this may be due to aromatisation of testosterone causing defeminisation of the neonatal brain. This change in RP3V kisspeptin neuron organisation is not replicated in the PNA (using non-aromatisable DHT) mouse (Prescott & Campbell, unpublished), however changes in kisspeptin inputs and projections have not been investigated in this model. Higher LH concentration and pulse frequency could be attributed to a dysfunction of ARN KNDy neurons, resulting in GnRH neuron hyperactivity. In PNA ewes, KNDy neurons display lower NKB receptor expression, indicating that changes in pulse generation may be occurring (Ahn *et al.*, 2015).

Further investigation into the androgenic changes of the ARN, however, have revealed changes in GABAergic neurons. ARN GABA neurons mostly colocalise with NPY, tyrosine hydroxylase, and neuronal nitric oxide synthase (Marshall *et al.*, 2017). Work by

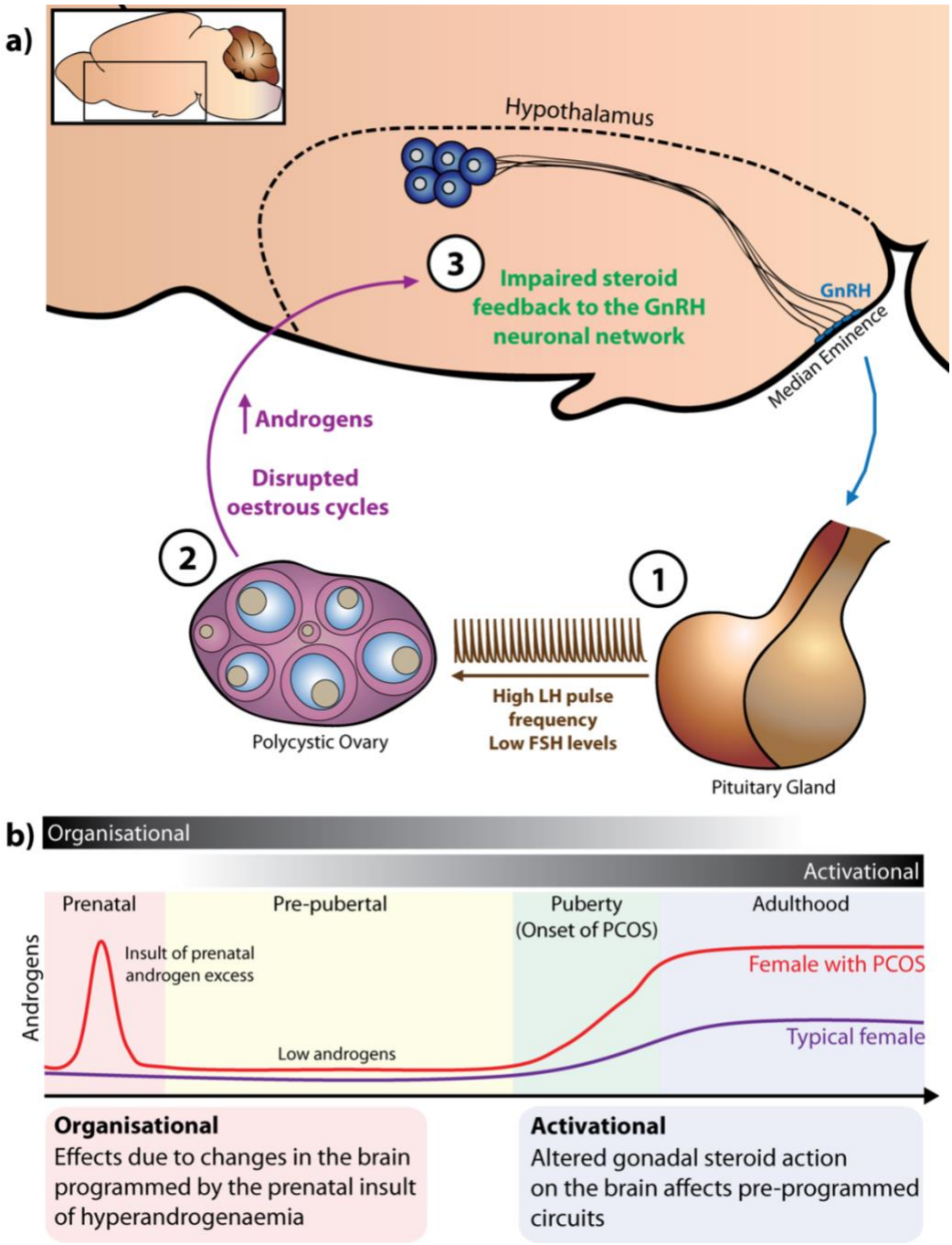

Figure 1.7: Polycystic ovary syndrome as a neuroendocrine disorder.

a) High frequency GnRH release stimulates the pituitary to cause a high frequency release of LH, with little release of FSH (**1**). This potentially results in changes at the ovary presenting with large fluid filled follicles (**2**). The PCOS follicle also synthesises high concentrations of androgens and does not mature normally. The hypothalamus is unable to integrate these changes in gonadal steroid synthesis and thus the feedback to the GnRH neuronal network is impaired (**3**). **b)** A high level of maternal androgens exposes the foetal brain to a prenatal androgen insult it would not otherwise receive. This may change the brain's programming (an organisational effect) to cause the downstream changes seen in PCOS. At puberty, a female with PCOS will have greater androgen synthesis than typical counterparts, leading to higher androgens in adulthood. The high level of adult androgens may also be causing changes to the reproductive axis as an activational effect.

Moore *et al.* (2015) reveals that GABAergic projections arising from the ARN are robustly upregulated in PNA mice. This has since been shown to be the same case for the PNA ewe (Porter *et al.*, 2019). Further, in mice treated with androgens in adulthood, there is an upregulation of a predominately excitatory GABAergic drive to GnRH neurons (Sullivan & Moenter, 2004; Berg *et al.*, 2018), indicating a potentially hyperactive network resulting in greater GnRH neuron output (Dulka & Moenter, 2017; Dulka *et al.*, 2020). While focus has been on this one circuit, there are likely other circuits impacted that have not yet been investigated.

1.8 Is there a role for the SCN in PCOS?

The idea that PCOS may result from underlying changes in brain circuitry (Moore *et al.*, 2013; Caldwell *et al.*, 2017) is a relatively new concept, so very little is known about the role of the SCN in this condition. As a key symptom in PCOS is oligo-/anovulation, it could be that the circuit controlling ovulation, i.e. the SCN-driven preovulatory surge, is disrupted. The link between PCOS and the SCN have not been studied previously, however, OVX mice given testosterone replacement develop a male-like pattern of AR expression in the SCN (Iwahana *et al.*, 2008). This suggests that the SCN is sensitive to androgens via the AR and this sensitivity increases in a high androgen environment. A key organisational change in the PNA mouse brain is the increase in GABAergic appositions to GnRH neurons (Moore *et al.*, 2015; Silva *et al.*, 2018). As the SCN is predominately GABAergic, it may be that changes in the SCN may also occur.

The incidence of PCOS is not significantly higher in women who have disrupted circadian behaviour, such as shift-workers, although there appears to be a trend towards increased symptoms related to PCOS, such as metabolic disturbances (Lim *et al.*, 2016). A common treatment for circadian disruption is melatonin. Interestingly, melatonin has been

shown to reduce menstrual irregularities and hyperandrogenaemia in women with PCOS (Tagliaferri *et al.*, 2018). Further, in a laboratory setting, rats continuously exposed to higher intensity light somewhat unexplainably develop polycystic ovaries (Baldissera *et al.*, 1991). While this may be initial evidence for disrupted circadian rhythms resulting in PCOS-like symptoms, evidence from the behaviour of the PCOS-like animal models is less clear. A mouse model that is treated with androgens at puberty shows changes in ovarian cycling and *Clock*-gene expression in uterine tissue but does not show any defects in other circadian behaviours such as activity patterns (Sellix *et al.*, 2013). It is important to remember that locomotor behaviour is likely controlled by a diffusible SCN signal, while oestrous cycling is controlled by an axonal signal (Silver *et al.*, 1996). As such, hyperandrogenaemia is likely disrupting the axonal, but not the diffusible, output of the SCN. The PNA mouse however, does not show specific clock gene defects in the SCN, but displays peripheral clocks that are not in synchrony (Mereness *et al.*, 2015). This suggests that the output of the SCN may be affected in the PCOS model.

1.9 Research objectives and hypotheses

This project aims **to investigate the role of AVP neurons from the SCN in activating the RP3V kisspeptin neuron population in both normal and pathological reproductive states in the female**. The evidence presented suggests that there is an anatomical and functional relationship between the SCN AVP neuron population, and the RP3V kisspeptin neuron population, however, various technical difficulties call for the re-evaluation of the extent of the SCN-to-RP3V circuit. The exact impact the circuit has is unknown; SCN AVP neurons likely produce both AVP and GABA so it is important to determine how these chemicals may impact the RP3V kisspeptin neurons, and any changes that may occur across the oestrous cycle. Finally, using the PNA mouse model, potential anatomical and functional alterations in the

SCN-to-RP3V circuit will be explored to determine whether they are impaired in a common neuroendocrine disorder associated with an- or oligoovulation.

Therefore, the specific PhD objectives include:

1. To determine the innervation of the RP3V by SCN AVP neurons, and the anatomical relationship of this projection with the kisspeptin neuron population therein.
2. To investigate the functional impact of these projections on the electrical activity of RP3V kisspeptin neurons across the oestrous cycle.
3. To examine how this circuitry may be altered in the PNA mouse model of PCOS.

I hypothesise:

1. There will be a robust anatomical projection from SCN AVP neurons that comes into apposition with RP3V kisspeptin neurons.
2. This projection will have a functional output from SCN AVP neurons to excite kisspeptin neurons, which will be more effective at proestrus.
3. The anatomy and functionality of the projection will be disrupted in the PNA mouse model of PCOS.

Chapter 2:

Materials and Methods

2.1 Animals

All experiments were carried out under either protocol D73/16 or AUP18-180, both of which were approved by the University of Otago Animal Ethics Committee. All mice (*Mus musculus*) used were housed in the Hercus-Taieri Resource Unit (University of Otago, Dunedin, NZ). Mice (age: 2-6 months) were kept in either open-top or individually ventilated cages with sex-matched littermates, in a climate-controlled environment (20ºC/40% humidity) on a 12:12 hour light:dark cycle. Mice were provided an enriched environment with *ad libitum* access to food and water. Original transgenic lines in this study are listed in Table 2.1. All are from a C57Bl/6 genetic background.

Mouse Name in Thesis	Commercial Name	Source	Ref
Avp-cre	B6.Cg-*Avp*$^{tm1.1(cre)Hze}$/J	Jackson Laboratory (Bar Harbour, ME, USA)	1
tdTomato	B6;129S6-*Gt(ROSA)26Sor*$^{tm15(CAG-tdTomato)Hze}$/J	Prof. B. Lowell (Harvard Medical School, MA, USA)	2
Kiss1-hrGFP	C57BL/6-Tg(Kiss1-hrGFP)KG26Cfe/J	Prof. C. Elias (University of Michigan, MI, USA)	3
Nms-icre	C57Bl/6-Tg(Nms-icre)20Ywa/J	Jackson Laboratory (Bar Harbour, ME, USA)	4
Vgat-cre	Slc32a1$^{tm2(cre)Lowl}$/J	Prof. B. Lowell (Harvard Medical School, MA, USA)	5

Table 2.1: Primary mouse strains used in this thesis.
References: 1) Harris *et al.* (2014); 2) Madisen *et al.* (2010); 3) Cravo *et al.* (2013); 4) Lee *et al.* (2015); 5) Vong *et al.* (2011).

Homozygous ($^{(+/+)}$) *Avp-cre* mice were initially bred for use in these studies. However, *Avp-cre*$^{(+/+)}$ mice were found to have diabetes insipidus, likely due to a lack of vasopressin release, and as such, were not used. As such, heterozygous ($^{(+/-)}$) *Avp-cre* mice were bred by crossing *Avp-cre*$^{(+/-)}$ mice onto wildtype ($^{(-/-)}$) littermates.

Secondary mouse lines were produced in house by crossing *Avp-cre*$^{(+/-)}$ mice with either *tdTomato* or *Kiss1-hrGFP*; *Nms-icre* with *Kiss1-hrGFP*; or *Vgat-cre* with *tdTomato*. The resulting offspring were *Avp-cre*$^{(+/-)}$*:tdTomato, Avp-cre*$^{(+/-)}$*:Kiss1-hrGFP*; *Nms-icre:Kiss1-hrGFP*; and *Vgat-cre:tdTomato.* PCR was performed by assistant research fellows in the Piet and Campbell laboratories to confirm the genotype of mice.

2.1.1 Animal husbandry

Mice were weighed daily, and oestrous cycle was determined by vaginal lavage (4 µL H_2O). Aqueous vaginal smears were taken between 0800h and 1100h and placed on a glass microscope slide to dry. They were then stained with toluidine blue (0.5% v/v) for one minute. Light microscopy at 10× magnification was used to examine cells and identify oestrous cycle stage. Proestrous smears showed clustered nucleated cells with no leukocytes; oestrous smears showed dense anucleated, cornified cells, metoestrous smears showed a combination of nucleated and anucleated cells with some leukocytes present; and dioestrous smears showed predominantly leukocytes with few nucleated cells (Caligioni, 2009).

2.1.2 Generation of prenatally androgen-treated offspring

The prenatally androgen-treated (PNA) mouse model of PCOS has been well established (Sullivan & Moenter, 2004; Moore *et al.*, 2013). To generate PNA litters, female *Kiss1-hrGFP* mice were bred on the night of a morning's proestrus smear, with a male *Avp-cre*$^{(+/-)}$*:Kiss1-hrGFP* mouse (Figure 2.1). Following mating, daily weights and vaginal smears were recorded. The day of mating was considered to be day 0 of pregnancy or embryonic day 0 (E0). To determine whether a mating had occurred, seminal plugs were identified the morning after but were not always present to use as an indicator.

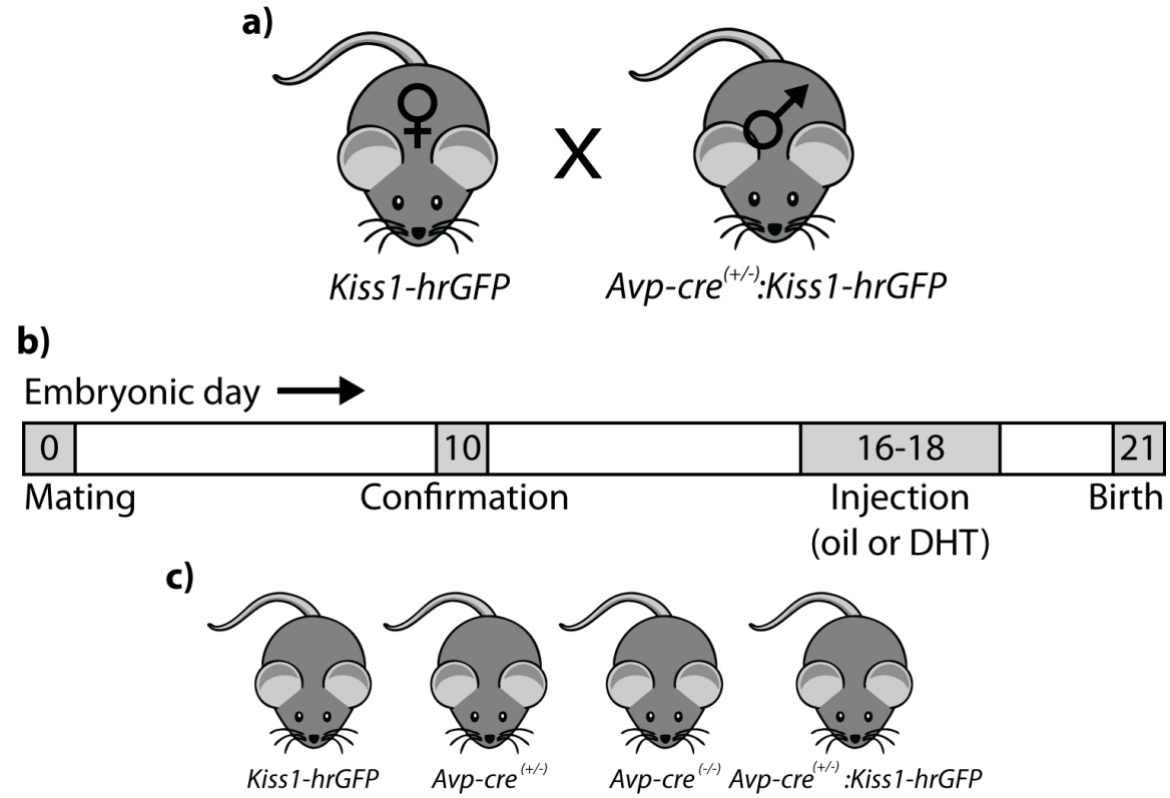

Figure 2.1: Generation of the prenatally androgen-treated mouse model of PCOS.

a) *Kiss1-hrGFP* females were mated on the afternoon of proestrus with *Avp-cre*$^{(+/-)}$*:Kiss1-hrGFP* males. **b)** Embryonic day 0 was considered the day of mating. After daily monitoring of weight and oestrous cycling, pregnancy could be confirmed at day 10. Injections of either DHT (or the sesame oil vehicle) were given in the mornings of days 16, 17 and 18 to prenatally androgen-treat the offspring. Mice typically gave birth on day 21 of pregnancy. **c)** The four genotypes of offspring are shown.

Weight and vaginal smears were taken for another ten days after mating. Pregnancy was confirmed at E10 if a mouse had increased its weight by 2 or more standard deviations from its average pre-mating weight, and if no proestrous smear was observed by that time.

The pregnant females were then treated with 250 µg of dihydrotestosterone (DHT; 100 µL subcutaneous injection) on E16-E18. DHT was prepared as a 10× stock solution in 100% ethanol, and diluted 1:10 in sesame oil on the day of injection. Control groups were injected subcutaneously with 100 µL of the sesame oil vehicle (VEH) on E16-E18, Following the birth of the offspring, pups were weaned at postnatal day 21 and caged as described above until experimentation. PNA and VEH females were used for experimentation. Tail tips were taken at weaning for genotyping to be carried out.

2.2 Surgeries

This section describes the basic procedure for stereotaxic surgery used for the experiments described here. For specific details of particular experiments, please refer to the Methods sections of the relevant chapters.

All surgeries were carried out with sterile instruments and under aseptic conditions. Mice were anaesthetised with 2% isofluorane and placed in a stereotaxic apparatus (Total Lab Systems, Auckland, NZ), with ear bars and nose cone to hold the head in place. Anaesthesia was confirmed by loss of the pedal withdrawal reflex following a toe-pinch with forceps at each paw. Mice were subcutaneously injected with 100 µL of carprofen analgesic (1 mg/kg) and lubricant oil (Polyvisc, Alcon) was placed in each eye to avoid drying during surgery.

2.2.1 Stereotaxic intracerebral injection

The fur covering the scalp was trimmed using small scissors, and 4% hibitane was applied to the exposed skin. A midline incision was made in the skin using scissors, and the

connective tissue covering the skull was cut. The head placement was determined by aligning the sagittal suture perpendicular to the ear bars, and with bregma and lambda being within 0.5 mm of each other in depth. Bregma was then used to zero the stereotaxic apparatus, from which the coordinates of the suprachiasmatic nucleus (SCN) were located. Coordinates were determined initially using Franklin and Paxinos (2008).

A pilot study was carried out to confirm targeting of the SCN by injecting 100 nL of methylene blue dye to determine the location of the needle. While anaesthetised, the mouse was then decapitated and the brain removed. The brain was sliced into 100 µm coronal sections using a vibratome (VT 1200S, Leica) and the location of the injection site with respect to the SCN was observed. Coordinates were then adjusted as necessary. The final coordinates determined for the SCN were as follows: anterior-posterior: + 0.06 mm from bregma, medial-lateral: ± 0.2 mm from bregma, dorsal-ventral: 5.8 mm from the skull surface. Unilateral injections were made at medial-lateral: + 0.2 mm from bregma only, while bilateral injections were made at both ± 0.02 mm.

One or two small holes were bored in the skull using a surgical drill (Technobox 810, Bien Air) at the calculated coordinates. A 25-gauge Hamilton syringe loaded with the viral vector (see Appendix III) was lowered to the dorsal-ventral coordinates and left for 3 minutes. The viral vector was injected at a rate of 100 nL/min. Following injection, needles were left *in situ* for ten minutes, before being slowly raised out of the skull. This was then repeated for the contralateral side. The skin was closed with surgical sutures (Mersilk, Ethicon) and postoperative management procedures, outlined by the University of Otago Animal Ethics Committee, were carried out. Surgery did not affect the animal's oestrous cycle (see Appendix VI).

2.3 Immunohistochemistry

This section describes the basic procedure for immunohistochemistry used within this thesis. For specific details of particular experiments and the antibodies used, please refer to the Methods sections of the relevant chapters.

2.3.1 Transcardial perfusion fixation and brain sectioning

Mice were anaesthetised with a lethal dose of pentobarbital between zeitgeber time (ZT) 4-6 (3 mg/mL, 100 µL intraperitoneal). Following the loss of the pedal withdrawal reflex, animals were placed supine, and the heart was exposed from the ventral aspect. The left ventricle of the heart was punctured at the apex with a 23-gauge needle, and 20 mL of 4% paraformaldehyde (PFA; Appendix I, 1.1/1.2) solution was slowly injected to perfuse the tissue. Brains were then carefully removed from the skull and post-fixed in 4% PFA overnight at 4ºC. The brains were cryoprotected in a 30% sucrose solution (Appendix I, 1.4) for 72 hours at 4ºC. Following cryoprotection, the brains were frozen on dry ice and kept at -80ºC until slicing, or sliced immediately.

For brain sectioning, a flat base was cut coronally through the cerebellum and brainstem allowing the brain to sit upright on a freezing-stage microtome (Leica SM2400). The brains were then frozen to -20ºC and two or three series of 40 µm-thick coronal sections were taken through the forebrain and hypothalamus. The brain slices were stored in cryoprotectant (Appendix I, 1.5) until they were used for immunohistochemistry.

2.3.2 General immunohistochemistry procedure

Brain slices were taken from cryoprotectant and thoroughly washed in tris-buffered saline (TBS; Appendix I, 1.3), 3 times for 10 minutes each, replacing the TBS solution each time. Slices were then placed in blocking solution (Appendix I, 1.6), for 30 minutes at room

temperature. Following this, the brain slices were incubated in blocking solution containing the requisite concentration of primary antibody for 48 hours at 4ºC.

The brain slices were washed in TBS 3 times for ten minutes each, replacing the TBS each time, to remove the primary antibody solution. The brain slices were then placed in incubation solution (Appendix I, 1.7) containing the requisite concentration of secondary antibody for 120 minutes at room temperature. Three times ten minute TBS washes were used to remove the extra secondary antibody. Those brains for which a biotinylated secondary antibody was used were then incubated in a streptavidin-conjugated fluorophore for 60 minutes, before being washed in TBS. Brain slices were mounted on gelatine coated microscope slides and left, protected from light, to air dry overnight at room temperature. The slides were coverslipped with Fluoromount G (ThermoFisher Scientific, MA, USA). Slides were kept in the dark at 4ºC until imaging.

2.4 Confocal image acquisition

Following immunohistochemistry, brain slices were imaged using an inverted Nikon A1R confocal microscope (Nikon Instruments Inc., Tokyo, Japan), with lasers of 488 and 543 nm wavelength. Z-stack images were taken through each region of interest. Images were taken through 10× (1 µm Z-step, 1 AU pinhole, 0.5 NA), 20× (1 µm Z-step, 1 AU pinhole, 0.8 NA) or 40× (0.5 µm Z-step, 1 AU pinhole, 0.9 NA) lenses. Images were acquired using a camera with a further 10× magnification, thus, final images are 100×, 200×, or 400× the original size. Images were saved to a high capacity storage drive for offline analysis.

2.4.1 Confocal image analysis

Images were analysed offline using ImageJ (National Institute of Health, Bethesda, Maryland, USA). Specific procedures for image analysis are outlined in the relevant chapters.

2.5 Electrophysiology

This section describes the basic procedure for electrophysiological experiments used within this thesis. For specific details of particular experiments, please refer to the Methods sections of the relevant chapters.

2.5.1 Brain slice preparation

Mice were euthanised by cervical dislocation at ZT4-6. Following decapitation, the skull was peeled away and the brain was removed, taking care to sever the optic nerves at their rostral extent. The brain was then placed into an ice-cold slicing solution (Appendix I, 1.8). The brain was then removed, the cerebellum was cut in the coronal plane to form a flat base, on which the brain was super-glued to a stage for slicing. The stage and brain were immersed into a bath containing the slicing solution, and 200 μm coronal brain slices from the rostral RP3V to the caudal SCN were taken using a vibratome (VT 1000S, Leica). Brain slices were placed into an artificial cerebrospinal fluid (ACSF; Appendix I, 1.9), warmed to 32ºC, and left to recover for at least one hour.

2.5.2 Brain slice electrophysiology

Individual brain slices were placed in a tissue bath beneath an upright microscope (Slicescope 1000, Scientifica, East Sussex, UK; with Olympus optics), and continuously perfused with ACSF at a rate of 1.5 mL/min. Location of specific brain regions was carried out using differential interference contrast microscopy at 4× magnification (0.1 NA). Individual cells were found using a 40× water-immersion objective (0.8 NA). Fluorophores were briefly excited using an LED (pE-300^{white}, CoolLED) with filter cubes for mCherry (excitation: 562 ±

40 nm; emission: 641 ± 75 nm) or GFP (excitation: 466 ± 40 nm; emission: 525 ± 50 nm). LED light was shone through the 40× objective at an intensity of 20% to excite mCherry, and at 2% to excite GFP (LED intensity/power shown in Appendix IV). Identified cells were approached using infrared differential interference contrast microscopy.

Micropipettes (tip resistance: 2-7 MΩ) were made by pulling borosilicate glass (internal diameter: 1.17 mm; external diameter: 1.50 mm) using a Model P-97 Flaming/Brown micropipette puller (Sutter Instruments Co., USA). Recordings were made between ZT5-10.

2.5.2.1 On-cell loose-patch recording configuration

Micropipettes were filled with ACSF and placed over an AgCl wire to form the recording electrode. They were then lowered into the bath using a micromanipulator (Scientifica, East Sussex, UK) with a small amount of positive pressure applied to displace neuropil. Once a cell was located, the positive pressure was removed allowing some of the neuronal membrane to be sucked into the recording electrode. On-cell loose-patch recordings were carried out at a tip resistance of 12-20 MΩ. Loose-patch recordings were carried out in voltage-clamp mode with no potential imposed on the pipette as not to influence the membrane potential at the tip. The resistance of the seal was measured at the start and finish of the recording. Cells with membrane resistance changes of more than 20%, or if the baseline noise increased significantly throughout the recording, were deemed unfit for analysis as this indicated the pipette seal was breaking down.

Recordings of action potential activity were amplified five times and filtered at a 3 kHz bessel (Multiclamp 700B, Molecular Devices), digitised at a sampling rate of 20 kHz (Digidata 1440a, Molecular Devices), and recorded (Clampex, Molecular Devices) for offline analysis (Clampfit, Molecular Devices). Action potentials were detected using a threshold-crossing method, as the action current is larger than background noise (Figure 2.2). Thus, the individual action potentials were able to be separated from the background.

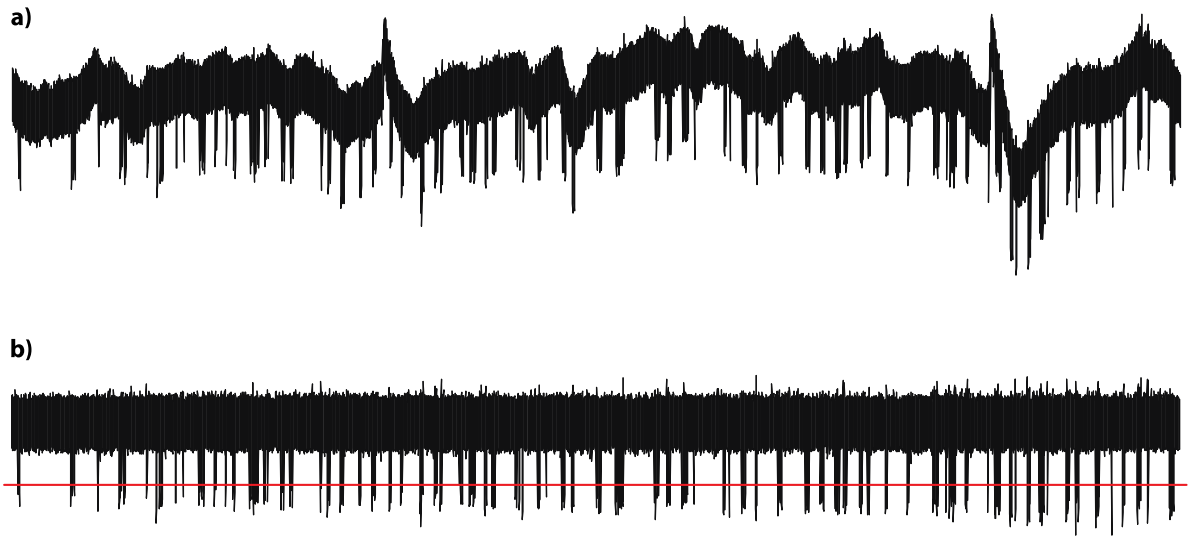

Figure 2.2: 10 Hz high pass filtering.

Example recordings of spontaneous activity from an RP3V kisspeptin neuron before (a) and after (b) passing through a 10 Hz high pass bessel filter. This flattens the trace to remove any mechanical noise. The red line shown in (b) indicates the amplitude of the threshold analysis. Any signal which crosses this threshold (i.e. action potentials) are then recorded for frequency.

2.5.2.2 Whole-cell patch-clamp recording configuration

To look at postsynaptic currents, cells were recorded in the whole-cell voltage-clamp configuration. Micropipettes were filled with a KCl solution (Appendix I, 1.9) and placed over an AgCl wire to form the recording electrode. This allowed the amplification of chloride-mediated signals due to the increased intracellular chloride concentration. They were then lowered into the bath using a micromanipulator (Scientifica, East Sussex, UK) with positive pressure applied to displace neuropil. Once a cell was located, the positive pressure was removed and negative pressure was applied to suck up part of the neuronal membrane and increase the seal resistance. Once a resistance of 1000 MΩ was reached, sharp negative pressure was briefly applied to break into the cell. Whole-cell recordings were carried out in voltage-clamp mode with a holding potential of -60 mV; series resistance was not compensated. Series and input resistance were monitored to ensure recording quality. Postsynaptic currents from individual cells were recorded in 20-second sweeps.

Recordings of postsynaptic currents were amplified ten times and filtered at a 2 kHz bessel (Multiclamp 700B, Molecular Devices), digitised at a sampling rate of 20 kHz (Digidata 1440a, Molecular Devices), and recorded (Clampex, Molecular Devices) for offline analysis (Clampfit, Molecular Devices). For analysis, the 20-second sweeps were overlaid and averaged. Where postsynaptic currents faithfully overlapped was considered a response to optogenetic stimulation.

2.5.3 *In vitro* optogenetic stimulation

In vitro optogenetic experiments were carried out in brain slices of AAV-ChR2 transfected mice. Blue LED light was shone through the GFP excitation filter and the 40× water-immersion objective at an intensity of 20% (Appendix IV).

Refer to individual chapters for specifics on the optogenetic protocols carried out.

2.6 Statistical analysis

Statistical analysis was performed using Prism 7 (GraphPad Software, San Diego, CA, USA). Data sets were also graphed using Prism. Specific statistical tests and graph parameters are outlined in the relevant chapters. Statistical significance was considered as $p < 0.05$.

Chapter 3:

Characterisation of Cre Expression

in the *Avp-cre* Mouse Line

3.1 Introduction

This work has made extensive use of the *Avp-IRES2-cre* mouse model (henceforth referred to as *Avp-cre*). To date, this mouse strain does not have a published characterisation of where cre-recombinase enzyme (cre) is expressed in the adult mouse brain. Therefore, it was pertinent to determine whether this model accurately represents vasopressin (AVP) neurons in the brain, and thus, is suitable for this project. The *Avp-cre* mouse has been mutated to contain a modified internal ribosome entry site (IRES2) downstream of the *Avp* gene. This allows ribosomal translation in the typically untranslated region following the gene. Downstream of the IRES2 construct is the coding sequence for cre (Harris *et al.*, 2014). Due to the proximity of IRES2 and the *Avp* gene, cre is produced when AVP is produced. Thus, the IRES2 allows translation of bicistronic mRNA for both *cre* and *Avp*, within the same cell (Figure 3.1a).

3.1.1 The cre/*loxP* system

Cre is a protein isolated from a bacteriophage that causes cleavage of DNA and recombination between specific locus of X-over P1 (*loxP*) sites (Orban *et al.*, 1992). The cre/*loxP* system has been extensively used in neuroscience to investigate genes of interest and their roles (Han *et al.*, 2018). Transgenic insertion of *loxP* sites surrounding a gene of interest (known as floxed) thus allows removal of floxed gene sequences in cells expressing cre. When mice with floxed genes are crossed to strains expressing cre in genetically-defined cells, cre-dependent excision of the floxed sequence results in the conditional manipulation of a gene in a specific cell type in the offspring (Figure 3.1b) (Bouabe & Okkenhaug, 2013).

The use of the cre/*loxP* system has been extremely fruitful in aiding understanding of brain cells and their circuitry. Cre can be used to turn genes on or off, remove stop sequences, or flip DNA sequences into an appropriate orientation. *LoxP* sites can be targeted to already

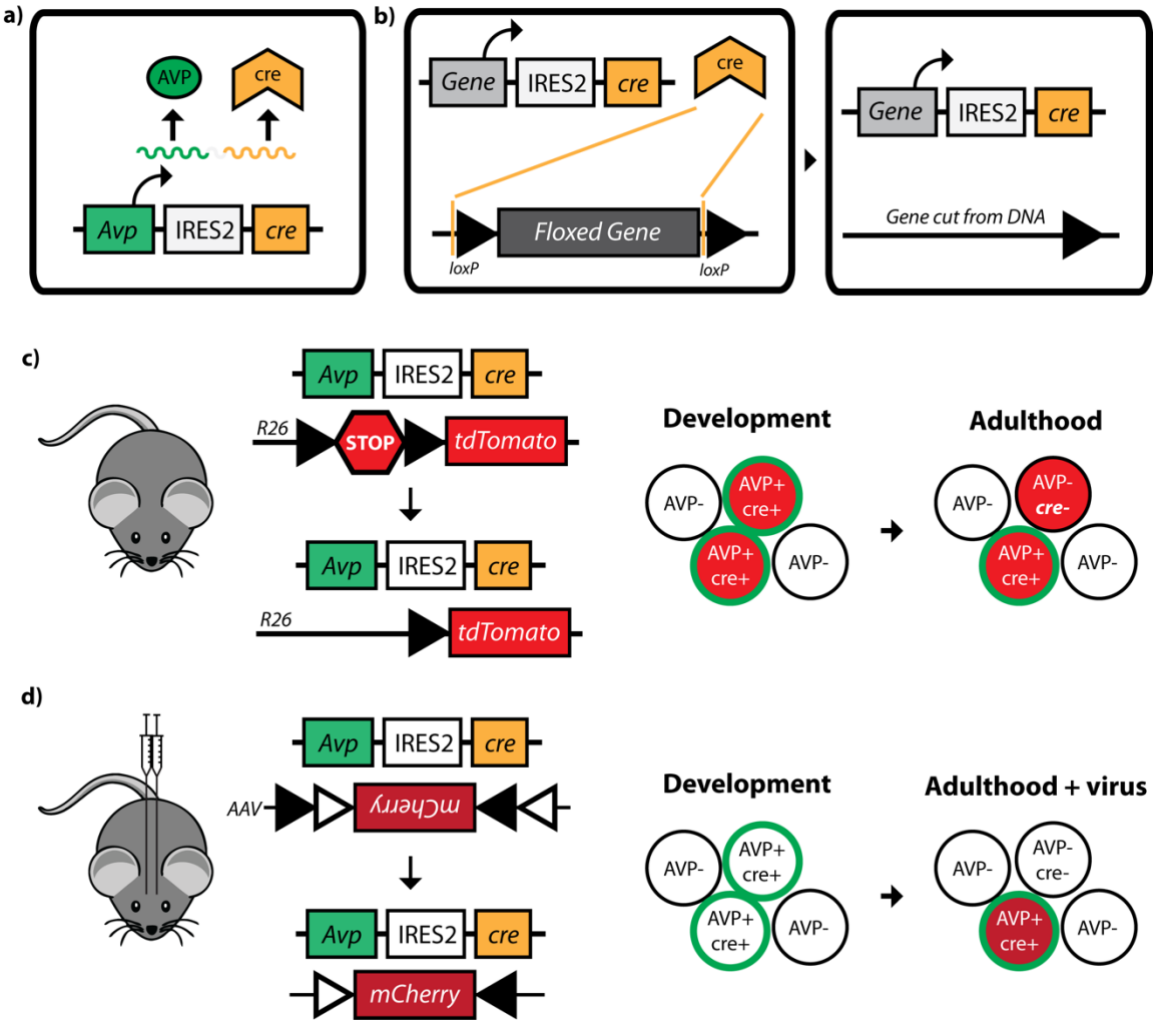

Figure 3.1: Differences in cre-mediated recombination.

a) The *Avp-cre* mouse line produces a bicistronic mRNA strand from one gene locus due to the internal ribosome entry site (IRES2). This allows the production of both AVP and cre. **b)** Insertion of *cre* downstream from a gene of interest allows specific expression of cre conditional to the activation of that gene. When cre is expressed, cre can cleave *loxP* sites excising a floxed gene from the DNA. **c)** An example of this excision is in the *Avp-cre:tdTomato* mouse, where cre excises the floxed STOP sequence resulting in expression of tdTomato in cre-expressing cells. This is driven by the *Avp* gene, turning on tdTomato as soon as it is expressed in development. The pitfall of developmental recombination is that if the *Avp* gene is repressed by adulthood in certain cells, tdTomato remains expressed (red neuron expressing false-positive cre expression (bolded) but not AVP expression). **d)** To overcome this, viral injections of fluorescent reporters (such as mCherry) can be used to determine the pattern of cre expression in adulthood. Cre is able to cleave the viral construct resulting in recombination in the correct orientation for mCherry expression. This method avoids developmental recombination, and provides a more accurate readout of where cre is expressed in adulthood.

a particular gene; and floxed DNA sequences can be added to the genome (knocked-in) to drive expression of reporter proteins, or of a tool to investigate neuronal function, such as a channelrhodopsin for optogenetics (Han *et al.*, 2018). A key caveat, however, arises with genetic recombination: excision of floxed sequences from the genome is irreversible. Thus, in models where mouse strains (one expressing cre and one expressing a floxed sequence) have been crossed together, the recombination will be present from the time that the promoter driving cre expression was first active. For neuroanatomical studies using cre-driven reporter genes, this provides a false-positive readout where the reporter for cre may not be restricted to cells currently expressing the gene of interest. Thus, it is important to accurately characterise cre expression in mouse models.

3.1.2 The *Avp-cre* mouse model

To assess where cre was expressed in the *Avp-cre* mouse, two methods were carried out here; crossing the *Avp-cre* mouse to a cre-dependent reporter strain (showing lifelong cre expression patterns) and viral vector delivery of a cre-dependent reporter (showing the pattern of cre specifically at the time of transfection with the vector). The reporter used was the tdTomato reporter mouse model (see Section 2.1). The *tdTomato* mouse strain contains the genetic sequence for a red fluorescent protein known as tdTomato downstream of a floxed STOP sequence preventing transcription, at a chromosomal locus known as ROSA26 (Figure 3.1c). When the *tdTomato* mouse is crossed to the *Avp-cre* mouse (*Avp-cre:tdTomato*), *Avp*-driven expression of cre should result in excision of the STOP sequence, resulting in AVP neuron-specific recombination and expression of tdTomato. As mentioned, the possibility remains that *Avp* may be transiently expressed prior to experimentation. This would result in the irreversible expression of tdTomato in neurons where AVP is no longer expressed (Figure 3.1c). One way to overcome this and target the cells currently expressing cre is with the delivery of a viral vector carrying a floxed reporter gene. In this case, *Avp-cre* mice were injected with

an adeno-associated virus (AAV) carrying a double-inverted orientation gene for mCherry (Figure 3.1d; henceforth referred to as AAV-mCherry; Appendix III). Viral-mediated transfection of genes provides temporal control as to when genes are inserted into the genome and is more likely to provide an up-to-date readout of cre expression.

3.1.3 Hypothesis and aim

As the *Avp-cre* mouse line has been used successfully for previous investigations, it can be hypothesised that **the *Avp-cre* line displays faithful reporter expression to AVP neurons**. These experiments aimed **to identify the pattern of *Avp*-driven reporter expression (as a proxy for the activity of cre) in the *Avp-cre* mouse model both through development, and at a timepoint in adulthood by viral transfection**. It was particularly necessary to determine the expression within the suprachiasmatic nucleus (SCN), to ensure the reporter-expressing population was representative of AVP neurons; as well as to determine any extra-SCN cre expression which may need to be considered when interpreting later experiments.

3.2 Methods

3.2.1 Animals

General animal information is outlined in Section 2.1. Adult female *Avp-cre* and *Avp-cre:tdTomato* mice (2-6 months old) were used in this study. Oestrous cycle stage was determined by daily vaginal lavage and tissue was collected in dioestrus.

3.2.2 Surgery

The general surgery procedures are outlined in Section 2.2. *Avp-cre* mice were bilaterally injected with 400 nL of AAV-mCherry per hemisphere of the SCN. Mice were left for at least two weeks to allow sufficient viral vector transduction prior to transcardial perfusion.

3.2.3 Immunohistochemistry

The general perfusion-fixation, brain slicing, and immunohistochemistry procedures are outlined in Section 2.3. Primary antibodies used for this chapter include guinea pig anti-AVP (1:2000; Peninsula Laboratories, CA, USA), rabbit anti-VIP (1:5000; Immunostar, WI, USA), rabbit anti-GRP (1:1000; Immunostar, WI, USA), and rabbit anti-mCherry (1:5000; AbCam, UK). Secondary antibodies include donkey anti-guinea pig 488 (1:200, Jackson ImmunoResearch, PA, USA) to visualise AVP-immunoreactivity; donkey anti-rabbit 488 (1:200, ThermoFisher Scientific, MA, USA) to visualise VIP- and GRP-immunoreactivity; or donkey anti-rabbit 568 (1:200, ThermoFisher Scientific, MA, USA) to visualise mCherry-immunoreactivity.

3.2.4 Microscopy and image analysis

The general microscopy methods are outlined in Section 2.4. Images shown herein are maximum projection confocal Z-stack images unless stated otherwise.

For mapping of AVP-immunoreactivity and tdTomato expression, location of neurons in images taken with a 10× objective lens were mapped to mouse brain atlas from Franklin and Paxinos (2008). Bregma coordinates reported in images are taken from Franklin and Paxinos (2008). Five female dioestrus *Avp-cre:tdTomato* mice were used for this mapping.

For experiments to determine colocalisation between AVP immunoreactivity and tdTomato/mCherry, two brain slices through the SCN of individual mice were taken using a

20× objective lens. Images were subject to noise processing using the despeckle function and outlier removal (outliers are at a radius of 2.0 pixels at 50 threshold brightness; Image J, National Institute of Health, Bethesda, Maryland, USA). This removed any brightly labelled fibre projections from the neurons, leaving the cell bodies clearly visible and not masked by fibres. Regions of interesting (ROIs) were drawn in ImageJ around individual AVP-immunoreactive (-ir) and tdTomato/mCherry-ir neurons were marked on ImageJ, in individual confocal planes and colour channels through the Z-stack. Cells for which ROIs overlapped in the two colour channels were considered to colocalise AVP-ir and tdTomato/mCherry-ir. The total number of AVP-ir, tdTomato/mCherry-ir, and colocalised neurons were counted. The specificity of *Avp-cre* and *Avp-cre:tdTomato* models was calculated as the percentage of tdTomato/mCherry-ir neurons colocalising AVP-ir. The percentage of AVP-ir cells colocalising tdTomato/mCherry-ir was termed the efficacy. For VIP- and GRP-ir images, only the neurons that colocalised VIP/GRP-ir and tdTomato were counted.

3.2.5 Statistical analysis

General analysis methods are outlined in Section 2.7. Percentages were compared using a non-parametric comparison using a Wilcoxon signed-rank matched-pairs test. Data are graphed as mean ± SEM. In text, data are reported as mean ± SEM. Where immunohistochemical data are reliant on the success of a viral injection, the range of upper and lower average values has been provided. Individual symbols in graphs represent individual mice and are consistent throughout the chapter.

3.3 Results

3.3.1 Anatomical mapping of cre expression in the *Avp-cre* mouse brain

Broadly, the expression of the tdTomato reporter and AVP-ir neurons, was strictly localised to within the hypothalamus (Figure 3.2). As expected, AVP and tdTomato were expressed in the SCN (Figure 3.2), PVN (Figure 3.3a) and SON (Figure 3.3b) (Sofroniew *et al.*, 1979). tdTomato expression in the SCN was found in a shell-like arrangement with neurons clustered at the rostral/caudal edges (Figure 3.2a, c), and spreading dorsally in the centre of the anterior-posterior axis (Figure 3.2b).

Outside of the SCN, PVN and SON, tdTomato and AVP-ir neurons were seen scattered in the caudal AVPV, dorsal to the SON, SOR, and along the base of the brain (Figure 3.4). No tdTomato expressing cells were found in regions where AVP-ir was not expected.

3.3.2 Characterisation of cre expression in the *Avp-cre* suprachiasmatic nucleus

For this thesis, the SCN AVP neurons are the predominant AVP population of interest. As such, cre expression (as demarcated by the tdTomato reporter) patterns have only been characterised in the SCN, rather than all of the aforementioned AVP-expressing regions. In the SCN, many colocalised cells were visible (Figure 3.5). There were some neurons visible that were only AVP-ir, and others that only expressed tdTomato.

Immunoreactivity for AVP in the *Avp-cre:tdTomato* mouse is colocalised with 44.8 ± 0.8% (n = 5 mice) of the total tdTomato-expressing population in the SCN. Of the AVP-ir population, 60.0 ± 2.0% (n = 5 mice) expressed tdTomato (Figure 3.5; Table 3.1). To determine whether the relatively low specificity of tdTomato expression was due to transient developmental expression of cre, a second experiment was carried out using injections of an

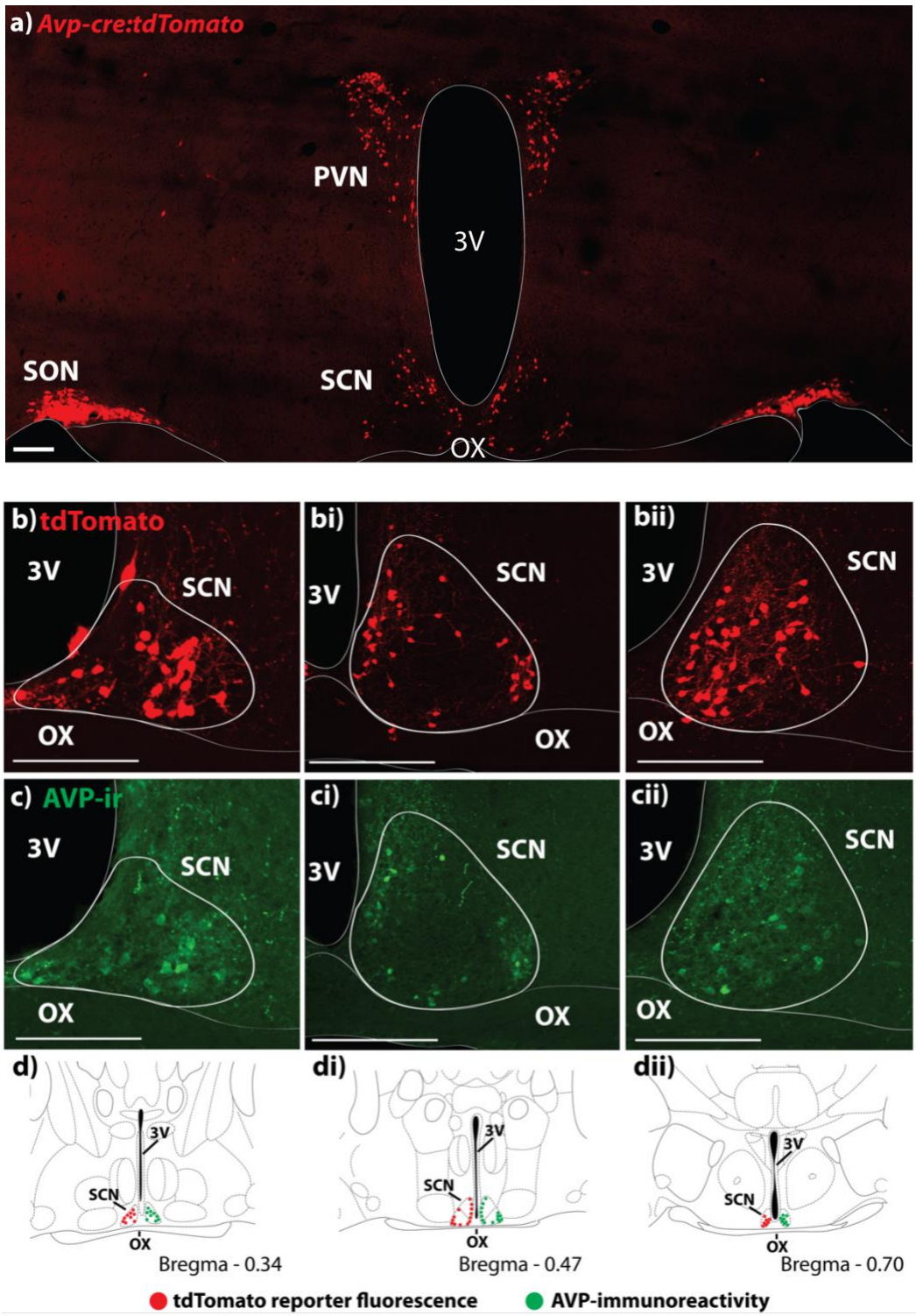

Figure 3.2: SCN distribution of AVP-immunoreactivity and cre expression.

a) tdTomato expression throughout the hypothalamus of the *Avp-cre:tdTomato* mouse. **b-c)** The SCN has a 3D shell-like expression of tdTomato (red) indicating cre activity and AVP-immunoreactivity (green) surrounding the central core. In the rostral-caudal axis, neurons cluster at the rostral (b, c) and caudal (bii, cii) ends, but spread out into a shell around the edges in the centre (bi, ci). **d)** The relative SCN neuron positions have been diagrammatically mapped to Franklin and Paxinos, 2008. Scale bars = 100 µm. 3V = third ventricle. OX = optic chiasm. PVN = paraventricular nucleus. SON = supraoptic nucleus. SCN = suprachiasmatic nucleus.

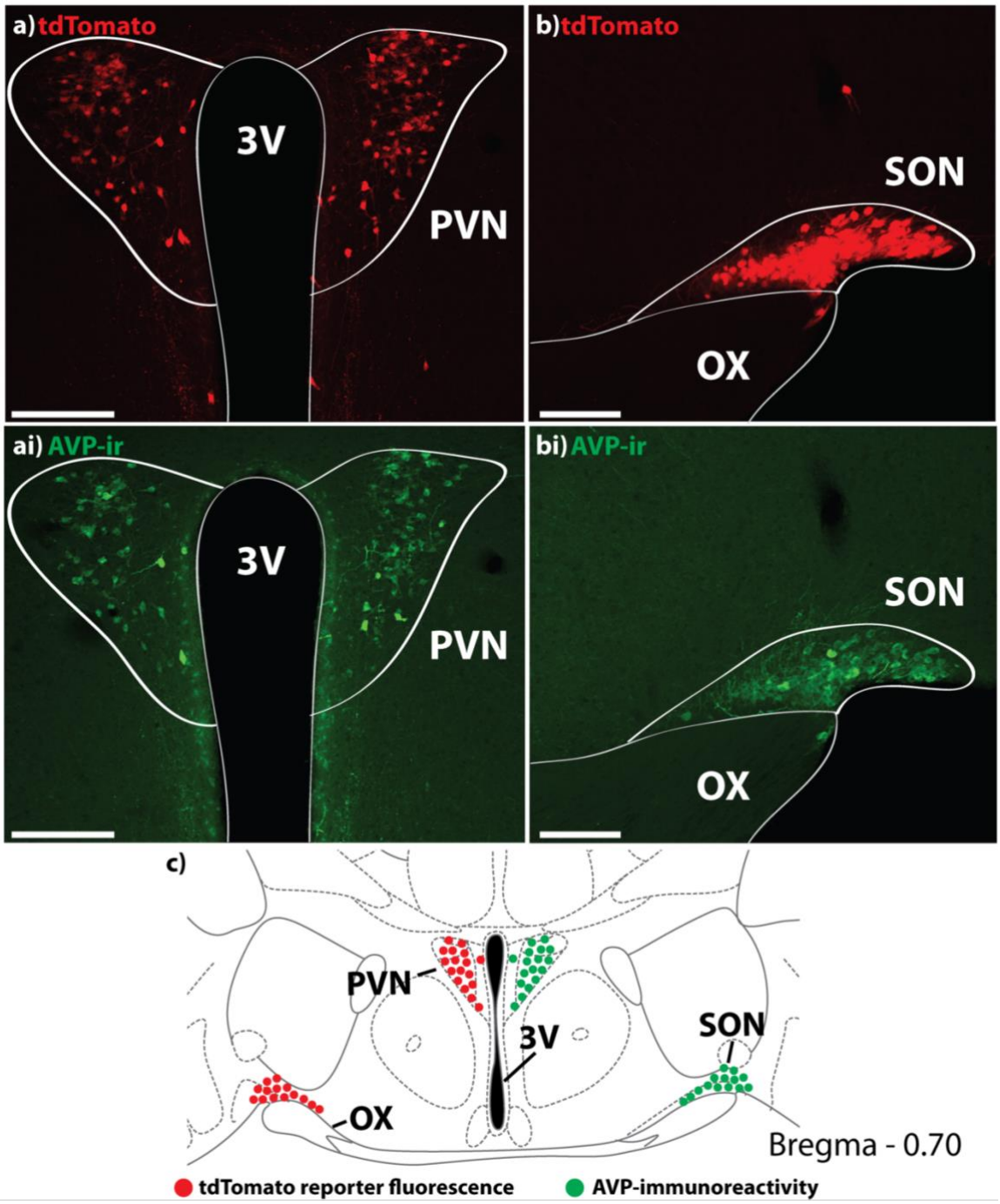

Figure 3.3: PVN/SON distribution of AVP-immunoreactivity and cre expression.

a, b) As expected, tdTomato expression (red) indicating cre activity, and AVP immunoreactivity (green) are seen in magnocellular populations of the PVN (a) and SON (b). **c)** The relative cell positions have been diagrammatically mapped to Franklin and Paxinos, 2008. Scale bars = 100 µm. 3V = third ventricle. OX = optic chiasm. PVN = paraventricular nucleus. SON = supraoptic nucleus.

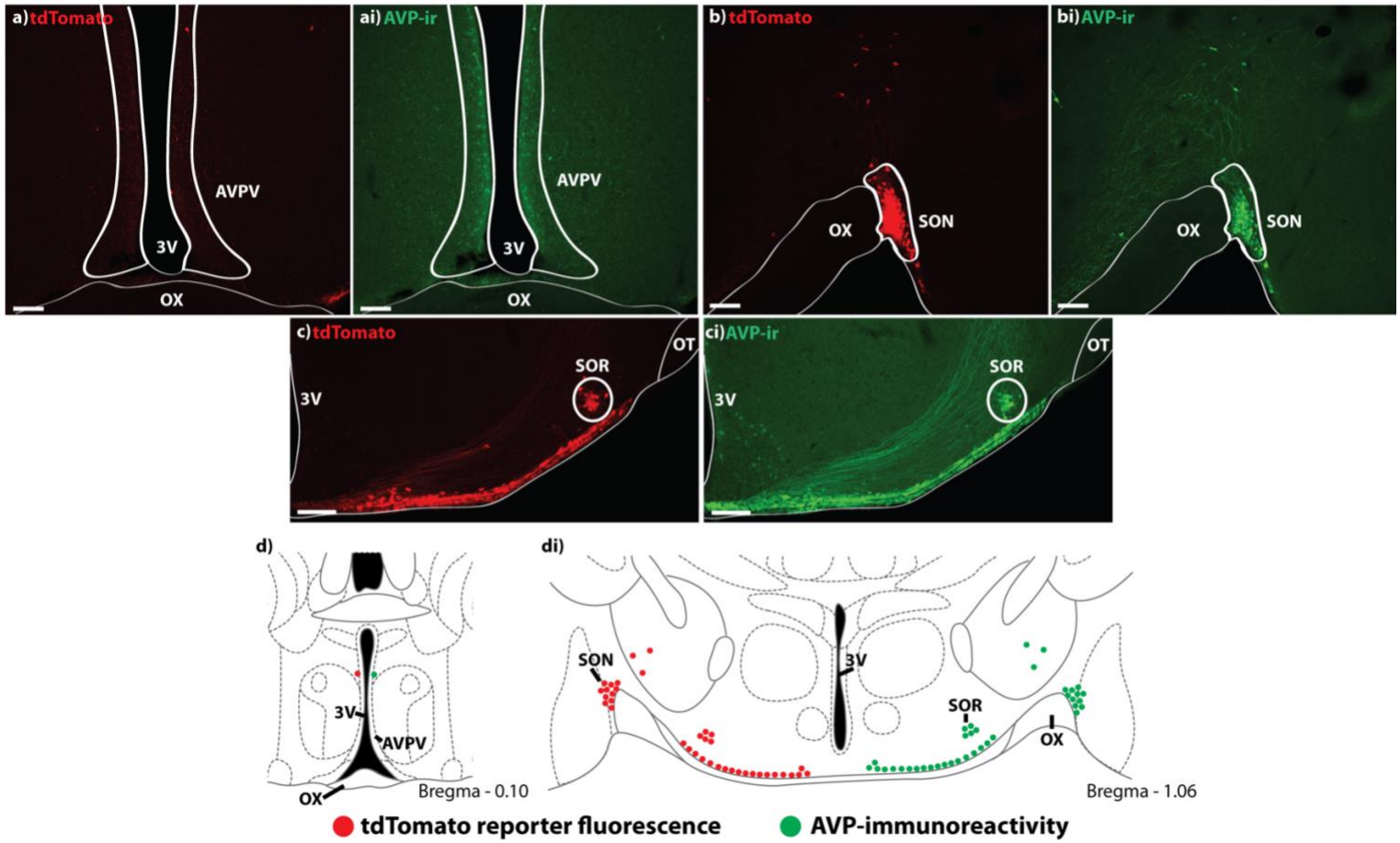

Figure 3.4: Accessory nuclei distribution of AVP-immunoreactivity and cre expression.

a-c) tdTomato expression (red) indicating cre activity, and AVP immunoreactivity (green) can be seen within AVP accessory nuclei. These can be seen in the AVPV (a), dorsal to the SON (b), in the retrochiasmatic supraoptic group and along the base of the brain (c). **d)** The relative cell positions have been diagrammatically mapped to Franklin and Paxinos, 2008. Scale bars = 100 µm. 3V = third ventricle. AVPV = anteroventral periventricular nucleus. OT = optic tract. OX = optic chiasm. SON = supraoptic nucleus. SOR = retrochiasmatic supraoptic group.

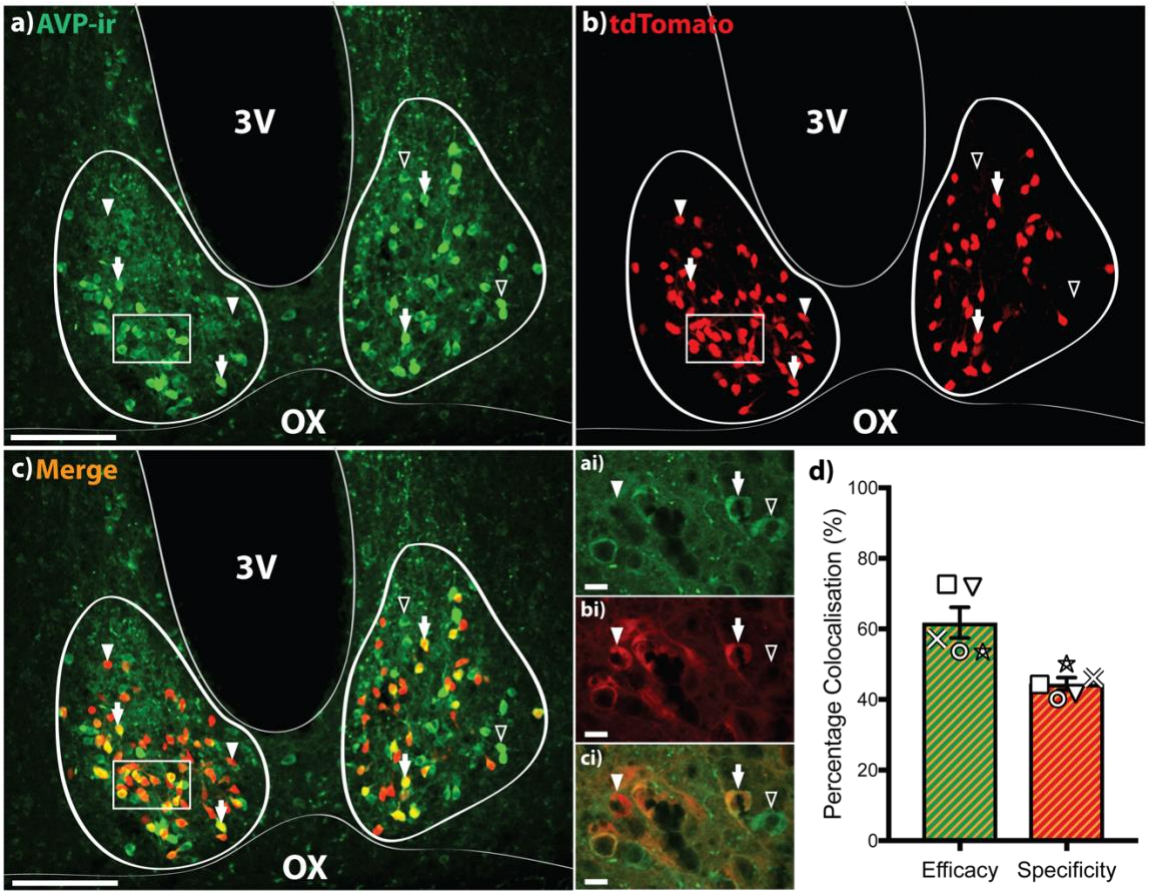

Figure 3.5: Colocalisation between immunoreactive AVP peptide and cre recombinase enzymes as shown by tdTomato.

a-c) Maximally projected Z-stack image of immunohistochemistry showing AVP-ir (green, a) and cre as reported by tdTomato (red, b) in the SCN (thick border). The two images are merged (colocalised neurons in yellow/orange) in c. Boxes in each image are shown in ai-ci as higher magnification images of a single plane in the Z-stack. ai) AVP-ir. bi) tdTomato. ci) merge. Empty arrowheads indicate AVP-ir only neurons. Filled arrow heads indicate tdTomato only neurons. Arrows indicate colocalised cells. **d)** The efficacy of cre expression in AVP neurons indicates how much of the AVP population were expressing cre (as reported by tdTomato); the specificity indicates how specific tdTomato (as a marker of cre expression) was to the AVP population rather than other cells types. Symbols represent individual mice (see Table 3.1 for specific details). Data shown as mean ± SEM. a-c) scale bars = 100 µm. ai-ci) scale bars = 10 µm. 3V = third ventricle. OX = optic chiasm.

	Figure Symbol	Mouse Number	Total AVP-ir neurons counted	Total tdTomato-expressing neurons counted	Total colocalised neurons
tdTomato	■	**13543**	98	160	70
	○	**13544**	108	145	59
	★	**13610**	142	156	76
	▼	**14304**	127	235	94
	×	**14305**	180	209	109

Table 3.1: AVP-ir neurons vs tdTomato expressing neurons in the *Avp-cre:tdTomato* mouse SCN.
Raw numbers of counted neurons either AVP-ir or cre-expressing as marked by endogenous tdTomato fluorescence. Figure symbols are associated with Figure 3.4.

AAV carrying a cre-dependent construct for the red fluorescent reporter, mCherry, to determine the activity of cre at the time of the experiment. In animals injected at the SCN with mCherry, colocalised cells were clearly visible, along with groups of neurons that were only AVP-ir, and groups that were only expressing mCherry (Figure 3.6). The specificity of mCherry expression was 49.7 ± 2.1% (n = 5 mice; range = 30.5% - 55.8%) (Figure 3.6). The AVP-ir population colocalised with 40.3 ± 5.3% (n= 5; range = 23.9% - 52.5%) of mCherry-expressing cells (Figure 3.6; Table 3.2).

There was no difference in the specificity when viral transfection of mCherry is used as a marker of cre expression, compared to the transient reporter expression of tdTomato (Figure 3.6d; p = 0.37, unpaired t-test). The efficacy in the AAV-mCherry infected mice was significantly less than that colocalising with tdTomato (Figure 3.6d; p = 0.014, unpaired t-test). In this case, the efficacy reflects how well the surgery targeted the SCN and *Avp-cre* neurons, rather than how well mCherry reflects cre expression in the neurons.

These data show that cre is expressed in the majority of AVP-ir neurons in the SCN, but also in a proportion of neurons that are not AVP-ir.

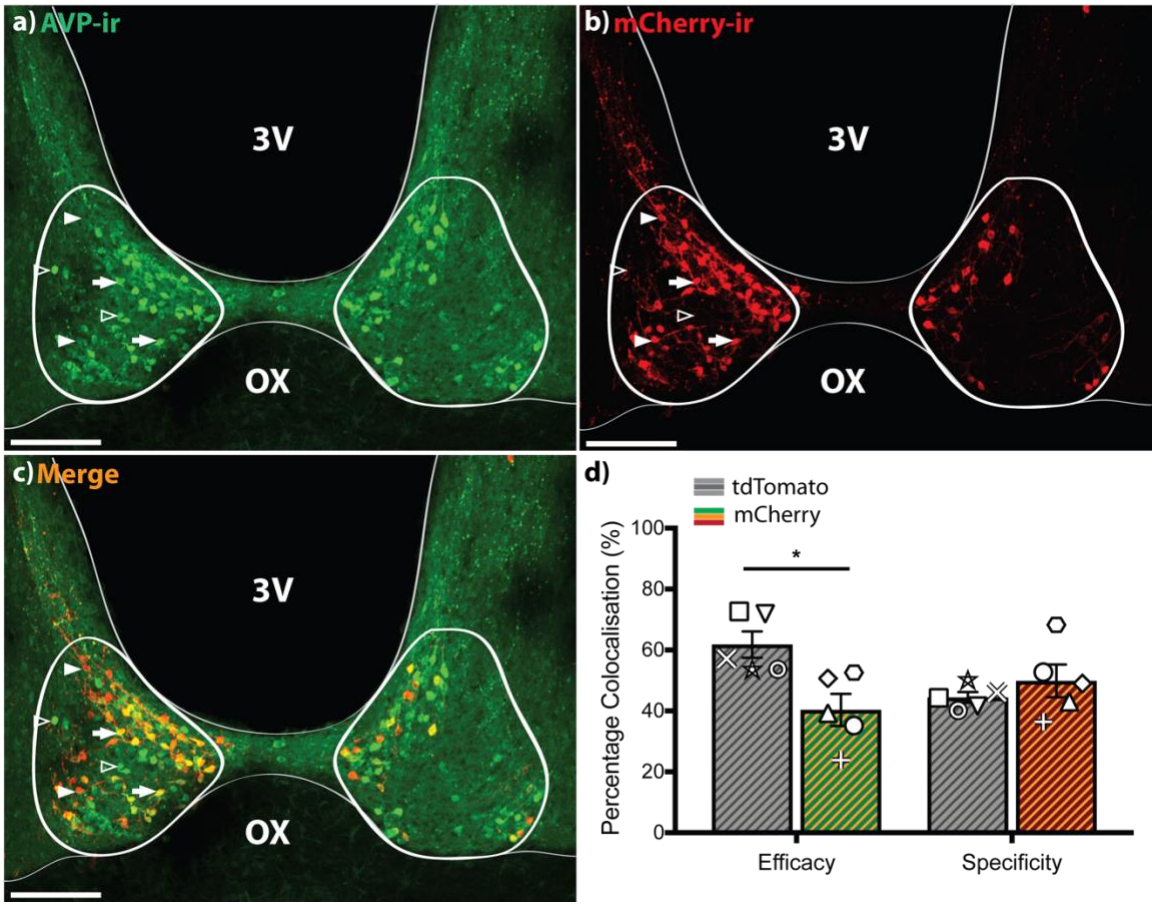

Figure 3.6: Colocalisation between immunoreactive AVP peptide and cre recombinase enzymes as shown by virally transfected mCherry.

a-c) Maximally projected Z-stack image of immunohistochemistry showing AVP-ir (green, a) and cre as reported by mCherry-ir (red, b) in the SCN (thick border). The two images are merged (colocalised neurons in yellow/orange) in c. Empty arrowheads indicate AVP-ir only neurons. Filled arrow heads indicate mCherry-ir only neurons. Arrows indicate colocalised cells. **d)** There is a significant decrease in the efficacy of reporter expression in AVP-ir neurons between the *Avp-cre:tdTomato* and AAV-mCherry transfected *Avp-cre* mouse line. There is no difference in the specificity of the reporter to AVP-ir neurons. Symbols represent individual mice (see Table 3.1/3.2 for specific details). tdTomato data from Figure 3.5. Data shown as mean ± SEM. Scale bars = 100 µm. * $p < 0.05$. 3V = third ventricle. OX = optic chiasm.

	Figure Symbol	Mouse Number	Total AVP-ir neurons counted	Total mCherry-expressing neurons counted	Total colocalised neurons
mCherry	⬢	**14256**	137	95	71
	◆	**14332**	58	44	25
	▲	**14337**	73	63	27
	●	**14360**	139	92	49
	+	**13585**	83	56	20

Table 3.2: AVP-ir neurons vs mCherry-ir neurons in the AAV-mCherry injected *Avp-cre* mouse SCN.

Raw numbers of counted neurons either AVP-ir, or cre expressing as marked by mCherry-ir. Figure symbols are associated with Figure 3.5, and those seen in Chapter 4.

3.3.3 Cre expression in the *Avp-cre:tdTomato* suprachiasmatic nucleus does not colocalise with other SCN peptides

In order to assess the peptide expression of SCN neurons that reported cre, but not AVP-ir, immunohistochemistry for VIP and GRP two well-characterised peptides within the SCN, was carried out. The VIP- and GRP-ir neurons were compared to cre-expression (as reported by tdTomato). It was found that no tdTomato-expressing neuron in the SCN was immunoreactive for VIP or GRP (Table 3.3, Figure 3.7). These data show that the reporter-expressing neurons with unidentified peptide content are not expressing AVP, VIP nor GRP, at the time of euthanasia.

	Mouse Number	Total VIP-ir/tdTomato Colocalised neurons	Total GRP-ir/tdTomato Colocalised neurons
tdTomato	**13032**	0	0
	13698	0	0

Table 3.3: VIP-ir and GRP-ir neurons vs tdTomato expressing neurons in the *Avp-cre:tdTomato* mouse SCN.

Raw numbers of colocalised VIP-ir/GRP-ir neurons with tdTomato. The lack of colocalisation between the two signals can be seen in Figure 3.6.

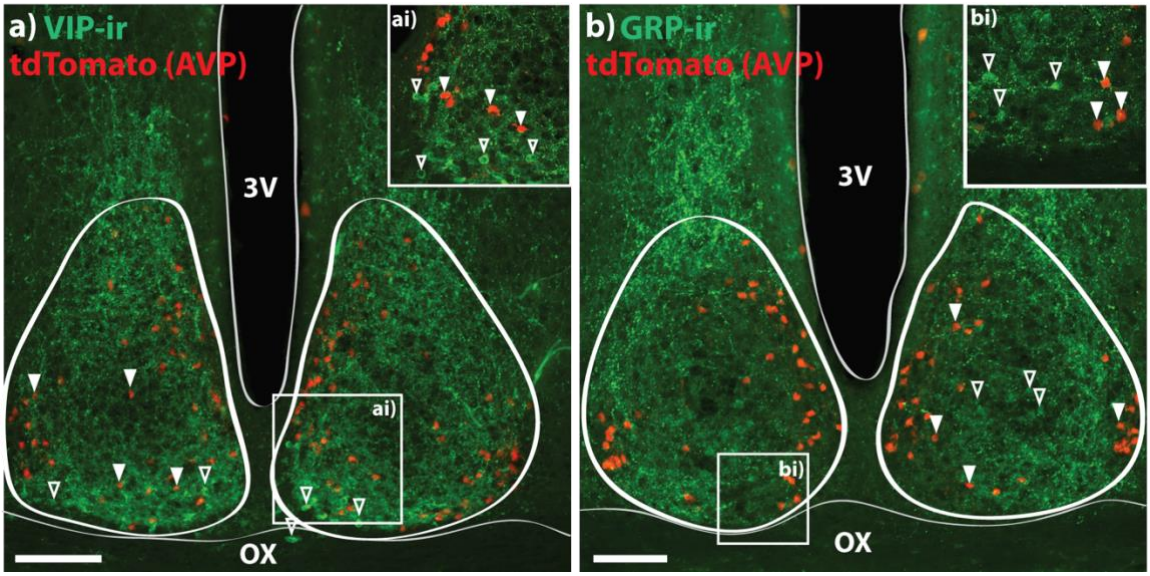

Figure 3.7: No colocalisation between immunoreactive VIP and GRP and tdTomato expression.

a) Maximally projected Z-stack image of immunohistochemistry showing labelling of VIP (green) and endogenous tdTomato (red) in the SCN (thick border). Empty arrowheads indicate VIP-ir only neurons. Filled arrow heads indicate tdTomato only neurons. There is no colocalisation between the two cell types. Inset (ai) shows 40× magnification single plane image of the two cell types. **b)** Maximally projected Z-stack image of immunohistochemistry showing labelling of GRP (green) and tdTomato (red) in the SCN (thick border). Empty arrowheads indicate GRP-ir only neurons. Filled arrow heads indicate tdTomato only neurons. There is no colocalisation between the two cell types. Inset (bi) shows 40× magnification single plane image of the two cell types. For further details, see Table 3.3. Scale bars = 100 µm. 3V = third ventricle. OX = optic chiasm.

3.4 Discussion

This chapter anatomically characterised the expression of cre in AVP neuron populations using two methods of cre-driven reporter expression. Specifically, the location of reporter-expressing cells has been mapped within the hypothalamus, as well as characterising how well reporter-expression maps to AVP-ir cells within the SCN.

3.4.1 AVP-ir neurons and reporters for cre colocalise in the SCN of female *Avp-cre* mice

The work carried out here relied heavily on the use of immunohistochemistry to report for AVP-ir neurons. When AVP-ir was compared to tdTomato that reported cre expression, it was found that the SCN AVP-ir population only accounts for approximately 45% of tdTomato-expressing neurons. Thus, there is a percentage of neurons that express cre, but are not AVP-ir.

A key limitation of immunohistochemistry is that a peptide must be present in the region of interest to be visualised. Staining for AVP in the SCN may be hindered by the fact that *Avp* mRNA and AVP peptide are circadian in their expression (van der Veen *et al.*, 2005; Maruyama *et al.*, 2010; Yoshikawa *et al.*, 2015). Thus, there is a possibility that the mice were euthanised at a time where there is low AVP expression and could not be visualised with immunohistochemistry. The expression of AVP peptide is expected to peak at ZT6-ZT10 (Yoshikawa *et al.*, 2015). These experiments were carried out with that consideration in mind, with tissue collected between ZT4-ZT8. As such, there is a possibility that a low expression of AVP peptide in some cells at that time would result in low to no AVP present to bind to the antibody during immunohistochemistry. *In situ* hybridisation for AVP mRNA, however, could be used to detect changes at the pre-protein level for potentially better specificity.

A second possibility for a low AVP immunoreactivity in the SCN could be that once AVP has been synthesised, the peptide is exported from the cell body to the projections and synaptic terminal. Some cell bodies would, therefore, not be visible by immunohistochemical staining. To overcome the potential export of peptide, intracerebroventricular colchicine treatment could be used to depolymerise microtubules in axons and inhibit the movement of AVP. This would result in its accumulation in the cell body and allow for greater intensity staining in the SCN AVP neuron cell bodies.

Finally, it could be that the tdTomato-expressing neurons that do not colocalise with AVP may not produce AVP at all. The data here have also shown that it is unlikely that they express either VIP or GRP instead of AVP, however.

In comparison to AVP expression, tdTomato expression (as a reporter for cre) has been reported to represent approximately 60% of the SCN AVP-ir neurons. This result is almost 20% greater than what has been reported previously (Gizowski *et al.*, 2016). Thus, there is a group of SCN AVP-ir neurons which are not expressing cre. There is a chance that the *Avp-cre* mouse line does not report all the AVP neurons in the SCN. One cause of a low reporter expression could be the arrangement of chromatin in the neurons may make cre inaccessible to ribosomes for translation, thus would not be able to be reported. Another possibility is that cre could be removed from some neurons during genetic recombination throughout generations. Thus, like AVP-ir neurons, cre expression would also be underreported.

The AAV-mCherry-injected *Avp-cre* mouse does not show a significant difference in cre expression in adulthood compared to what is reported by tdTomato throughout development. This indicates that cre expression likely does not change throughout the SCN over time. Using a viral vector to transfect a reporter into cre-expressing neurons, however, provides an idea of the temporal resolution of SCN cre expression. There is a significant decrease in the efficacy of reporter expression, indicating that less of the total AVP neuron population is being reported. This result, however, is unsurprising as it relies on surgical

technique and the viral vector adequately accessing the cre-expressing neurons. Compared to tdTomato which is inserted into the genome and will be present in all cells, the viral transfection, will only reach a certain spread from the injection site, and may not transfect all the cells in the given area. As such, the lower efficacy is indicative of how well the injection and the virus have targeted the SCN *Avp-cre* neurons. This is further shown by the variability in the efficacy of mCherry, which displays a wider range than the tdTomato. For this thesis, SCN *Avp-cre* neurons will refer to the cre-expressing neurons that can be targeted in this model, where SCN AVP neurons will refer to the general AVP-expressing population in the SCN

3.4.2 Expression of tdTomato and AVP-ir neurons in the hypothalamus of female *Avp-cre* mice

There have been extensive reports surrounding the distribution of AVP neurons, particularly in rodent species (Sofroniew *et al.*, 1979; Rhodes *et al.*, 1981; Hou-You *et al.*, 1986; Rood & de Vries, 2011), with which this work agrees. What has not been reported, however, are the many, seemingly random, expressions of AVP neurons throughout the hypothalamus, such as those seen in the PeN and lateral hypothalamic area. The possibility exists that these populations may produce AVP at the time of experimentation for a yet unknown physiological function; although the expression of tdTomato (indicative of cre expression) matches the distribution of AVP peptide in these mice. A broad overview of tdTomato expression reveals expression in similar areas to that of the AVP peptide. There is clear tdTomato expression in the PVN and SON, which make up the major AVP neuron populations outside the SCN. The tdTomato expression outside of these two nuclei, is along the base of the brain and along the magnocellular projection fibres. These populations are known as the AVP accessory nuclei (Rood & de Vries, 2011). Overall, however, no ectopic tdTomato (in brain areas without AVP peptide) is present in this mouse line.

Of interest to this thesis is the distribution of AVP neurons in the SCN. It has been well reported that SCN AVP neurons form a dorsomedial shell surrounding the core of the SCN (van den Pol, 1980; van der Zee & Bult, 1995; Morin *et al.*, 2006; Rood & de Vries, 2011). Interestingly, it has been shown here that SCN *Avp-cre* neurons are not as well localised to this pattern as has been reported. The typical shell structure only holds true for coronal sections taken through the centre of the SCN. The *Avp-cre* neurons cluster at the caudal and rostral extents. This suggests that the shell is a 3D structure surrounding the entire SCN core. This shell-like structure also does not appear to be strictly dorsomedial as described previously (Morin *et al.*, 2006). A clear ventral layer of *Avp-cre* neurons and a lateral cluster are visible also.

3.5 Summary

To date, this *Avp-cre* mouse model has been used to investigate the physiology and downstream effects of AVP neurons (Gizowski *et al.*, 2016; Jiang-Xie *et al.*, 2019). Despite this, no group has published a full characterisation of cre expression to determine the specificity of the model. It was important to carry out this characterisation, as fluorescent neurons, indicative of cre expression and the resulting viral transfection, will be used as a marker of the AVP population for future experiments. Here, it has been shown that the distribution of AVP neurons in the mouse brain largely reflects cre distribution. In particular, however, cre expressing neurons in the SCN reflect roughly half of the actual SCN AVP population.

Chapter 4:

Anatomical Characterisation of the SCN *Avp-cre* Neuronal Projections to the RP3V

4.1 Introduction

The preovulatory surge of luteinising hormone, necessary for ovulation, is dependent upon RP3V kisspeptin neuron stimulation of GnRH neurons (Smith *et al.*, 2006; Clarkson *et al.*, 2008; Piet *et al.*, 2018). This is regulated by a circadian input, to coordinate the surge to a particular time point (Murr *et al.*, 1973; McElhinny *et al.*, 1999). This circadian network has been shown to originate from the SCN (Wiegand *et al.*, 1980; Wiegand & Terasawa, 1982), most likely axonal projections from the SCN shell where AVP neurons reside (de la Iglesia *et al.*, 2003; Smarr *et al.*, 2012).

4.1.1 Tracing the SCN-to-RP3V network

Previous work to identify the projection between AVP neurons in the SCN and the RP3V kisspeptin neurons has been associated with several challenges. The original lesion studies identified the SCN as the starting point from where the circadian cue for ovulation may originate (Wiegand *et al.*, 1980; Wiegand & Terasawa, 1982). Early tracing studies used the anterogradely trafficked plant lectin *Phaseolus vulgaris* leucoagglutinin (*Pha*-L) injected into the SCN to demarcate its projections (Watts *et al.*, 1987; de la Iglesia *et al.*, 1995; Vida *et al.*, 2010). The projection revealed a dense fibre plexus around the RP3V (Watts *et al.*, 1987), coming into apposition with oestrogen receptor-expressing neurons (de la Iglesia *et al.*, 1995). Neither of these studies, however, determined the peptide content of these projections, so were unable to conclude if these were AVP-expressing fibres. Vida *et al.* (2010) overcame this by coupling injections of *Pha*-L in the SCN with immunohistochemistry for AVP and kisspeptin. Electron microscopy revealed *Pha*-L and AVP coupled projections in apposition to RP3V kisspeptin neurons (Vida *et al.*, 2010). While this provides strong evidence for SCN AVP neurons innervating RP3V kisspeptin neurons, *Pha*-L injections are not specific for defined neuronal populations and can spread throughout brain regions indiscriminately. This can result

in projections from off target neurons being revealed. To determine whether the SCN AVP neurons themselves were those that came into apposition with the RP3V kisspeptin neurons Williams *et al.* (2011) identified that following SCN lesions, AVP-immunoreactive appositions to RP3V kisspeptin neurons were not present, compared to non-lesioned controls.

These studies used different rodent species (mouse, rat and hamster) with known differences in their SCN projections (Table 1.1), thus, for the purpose of this thesis, it was important to map out the extent of the *Avp-cre* projection to RP3V kisspeptin neurons in the mouse. Further, this will establish a tool that allows for a comparisons of *Avp-cre* projections in a pathological condition (Chapter 7).

4.1.2 Genetically mediated viral tract-tracing

To delineate the projections of SCN AVP neurons to RP3V kisspeptin neurons, this work used cre/*loxP* based, viral vector-mediated tract-tracing allowing for the selective targeting of SCN *Avp-cre* neurons. As explained in Chapter 3, the use of the *Avp-cre* mouse provides greater specificity for targeting a single population of neurons to specifically express virally transfected cre-dependent mCherry. This experiment allows us to get a more accurate representation of the projections of SCN AVP neurons to the RP3V. Compared to prior studies, injection of the viral vector causes less damage and less disruption to the animal's physiology than lesions of the SCN. Further, the genetically mediated expression of the fluorescent reporter, mCherry means that projections from cre-expressing neurons will be revealed, independent of the AVP peptide content that immunohistochemistry relies on. The presence of mCherry-expressing fibres within the RP3V and in association with kisspeptin neurons is indicative of a direct anatomical projection from SCN-to-RP3V.

As mCherry expression is through the length of the fibre projection, this allows for visualisation of the projection pattern of the SCN *Avp-cre* neurons. Innervation of the HPG axis by the SCN is thought to be through two pathways: indirectly through RP3V kisspeptin neurons

as discussed, and directly at GnRH neurons (Williams & Kriegsfeld, 2012). While the direct innervation is thought to be VIP mediated (Simonneaux & Piet, 2018), it is unclear whether GnRH neurons are innervated by SCN AVP neurons at all (Mahoney & Smale, 2005).

4.1.3 Hypothesis and aim

Based on the literature presented above, it can be hypothesised that **there will be a robust projection from SCN *Avp-cre* neurons to the RP3V, and they will interact anatomically with RP3V kisspeptin neurons**. These experiments aimed to **determine the extent to which SCN *Avp-cre* neurons project to the RP3V, and the level of interaction these fibres have with the resident kisspeptin neurons**. Further, the interaction the SCN *Avp-cre* projections have with the GnRH neurons was also investigated.

4.2 Methods

4.2.1 Animals

General animal information is outlined in Section 2.1. Adult female *Avp-cre* (2-6 months old) were used in this study. Oestrous cycle stage was determined by daily vaginal lavage and tissue was collected in dioestrus.

4.2.2 Surgery

The general surgery procedures are outlined in Section 2.2. *Avp-cre* mice were bilaterally injected with 400 nL/side of AAV-mCherry at the SCN. Mice were left for at least two weeks to allow sufficient transduction of the viral vector prior to transcardial perfusion.

4.2.3 Immunohistochemistry

The general perfusion-fixation, brain slicing and immunohistochemistry procedures are outlined in Section 2.3. Primary antibodies used for this chapter include rabbit anti-mCherry (1:5000; AbCam, UK), sheep anti-kisspeptin (1:1000; Prof. A. Caraty, INRA, France) and guinea pig anti-GnRH (1:5000, Prof. G. Anderson, University of Otago, NZ). Secondary antibodies include donkey anti-rabbit 568 (1:200, ThermoFisher Scientific, MA, USA) to visualise mCherry and donkey anti-guinea pig 488 (1:200, Jackson ImmunoResearch, PA, USA) to visualise GnRH. Kisspeptin was visualised by the biotinylated donkey-anti sheep secondary antibody (1:1000, ThermoFisher Scientific, MA, USA), followed by a streptavidin-conjugated 488 tertiary antibody (1:1000, ThermoFisher Scientific, MA, USA).

4.2.4 Microscopy and image analysis

The general microscopy methods are outlined in Section 2.4. Images shown herein are maximum projection confocal Z-stack images unless stated otherwise.

4.2.4.1 Fibre density analysis

Two sets of confocal Z-stacks were taken through the rostral and caudal slices of the RP3V using the 10× objective lens. The rostral margin was termed the AVPV, and the caudal termed the PeN. Using ImageJ (National Institute of Health, Bethesda, Maryland, USA), the maximally projected RP3V images were binarised using a threshold function between 1.0 - 1.5%. Binarisation assigns each pixel as either positive for immunoreactivity (black) or negative for immunoreactivity (white). This was used to estimate the transfection level of hypothalamic nuclei (SCN, PVN and SON) and the immunoreactive fibre density in the RP3V. A region of interest (ROI) was drawn around the RP3V (containing 100 µM from the third ventricle) and the measure function was used. This analysed the percentage of black pixels in

the RP3V (representing mCherry-ir fibres) in the ROI. The percentage of pixel density in one slice containing the AVPV and one since containing the PeN per mouse was then averaged for a percentage of total RP3V innervation. This was carried out on both sides of the third ventricle.

The same protocol was applied to a single slice through the centre of the SCN, or in another section through the hypothalamus containing PVN/SON in the same mouse. Each side of the SCN or hypothalamus was analysed to determine the percentage of fluorescence (as a proxy for viral transfection) seen in the individual nuclei. It was empirically determined that successful transfection of a region was considered as greater than 5% area of pixel density in the region of interest. As such, anything less than 5% density was termed a miss. To determine the relative level of transfection, the percentage transfection in the most transfected slice was considered as the upper limit. From this upper limit, 5% was subtracted, and the remainder divided into three. The upper, middle and lower third of this was then considered the high, medium and low (+++, ++ or +) transfection used for Table 4.1.

4.2.4.2 Apposition analysis

As above, two confocal Z-stacks of the RP3V containing AVPV or PeN were imaged using 10× and 40× objective lenses. Using ImageJ (National Institute of Health, Bethesda, Maryland, USA), the kisspeptin neurons in each Z-stack were counted. In individual planes of the Z-stack, each kisspeptin neuron was magnified 4 times, and any appositions with mCherry-ir fibres were counted. A close apposition was defined as an mCherry-ir fibre in the immediate vicinity of a kisspeptin-ir cell body, with no black pixel between the two colour signals. This is based on a method of apposition counting used previously (Moore *et al.*, 2015; Yip *et al.*, 2015). The percentage of kisspeptin neurons with an apposition, and the number of appositions to those kisspeptin neurons, in the AVPV and PeN slice were then averaged for each mouse. This was carried out on both sides of the third ventricle.

For appositions between GnRH-ir neurons and mCherry-ir fibres, one confocal Z-stack from the medial septum (MS), rostral preoptic area (rPOA) and anterior hypothalamic area (AHA) were taken using a 10× objective lens, per mouse. In individual planes of the Z-stack, each GnRH neuron was magnified by 4×, and any appositions to mCherry-ir were counted, as above.

4.2.5 Statistical analysis

General analysis methods are outlined in Section 2.7. Correlation analyses were carried out to compare the mCherry-ir fibre expression, as well as the proportion of kisspeptin neurons with close appositions, to the ipsilateral SCN, PVN and SON, using a linear regression. Data for these experiments are presented as linear regression line ± 95% confidence interval. The percentage of mCherry-ir fibres, percentage of kisspeptin neurons with appositions, and the number of appositions per neuron were compared using a Wilcoxon signed-rank matched-pairs test. In text, these data are reported as mean ± SEM. Where immunohistochemical data are reliant on the success of a viral injection, the range of upper and lower average values has been provided. Individual symbols in graphs represent individual mice and are consistent throughout the chapter.

4.3 Results

4.3.1 The RP3V is densely innervated by SCN *Avp-cre* neuron projections

To determine whether SCN *Avp-cre* neurons project to the RP3V, viral-mediated tract-tracing was carried out by stereotaxic injection of cre-dependent AAV-mCherry into the SCN of female *Avp-cre* mice. Cre-dependent mCherry expression fills the neuron cell body and

fibres allowing the projections to be visualised. Immunohistochemistry against mCherry was used to enhance visualisation of the fibres.

Of the 9 dioestrous females used for this experiment, 7 were transfected by the viral vector. Two mice had less than 5% of mCherry expression in the SCN and were considered as misses (i.e. the injected viral vector had not transfected the SCN; Table 4.1). Due to the proximity of the SCN with the SON and PVN, in which AVP and cre are also expressed, it was difficult to solely target the SCN with stereotaxic surgery. Thus, most mice expressed mCherry in the SCN as well as the SON and/or PVN (Table 4.1).

Figure Symbol	Mouse Number	SCN Transfection	PVN Transfection	SON Transfection
■	**14078**	+++	++	+++
●	**14360**	+++	+	+
▲	**14337**	++	-	+
▼	**13585**	++	+	-
⬢	**14256**	++	++	-
◆	**14332**	++	-	+++
★	**13584**	++	+++	+
O	**14255**	-	+++	++
×	**14333**	-	+	-

Table 4.1: *Avp-cre* mice injected for viral tract tracing.

Mice injected with AAV-mCherry were unlikely to only transfect the SCN. This table outlines the AVP-expressing nuclei in the brain, and the relative level of transfection (+++, ++ or +) in each where - indicates no transfection, ipsilateral to the most densely transfected half of the SCN. The figure symbols indicate the individual mice seen in the graphs shown in the figures of Chapter 4.

In mice where the SCN *Avp-cre* neurons sufficiently expressed mCherry (Figure 4.1a), mCherry-ir fibres were found densely surrounding the third ventricle in the RP3V (Figure 4.1ai). The mCherry-ir fibre density in the RP3V was 10.5 ± 2.1% (Figure 4.1c; n = 7 mice, range = 3.8% - 19.3%). There was a similar mCherry-ir fibre density in the anatomical subdivisions of the RP3V (Figure 4.1c; AVPV: 9.6 ± 2.8%, n = 7 mice, range = 3.6% - 25.0%; PeN: 11.3 ± 2.5%, n = 7 mice, range = 0.6% - 20.9%; p = 0.58, Wilcoxon signed-rank matched-

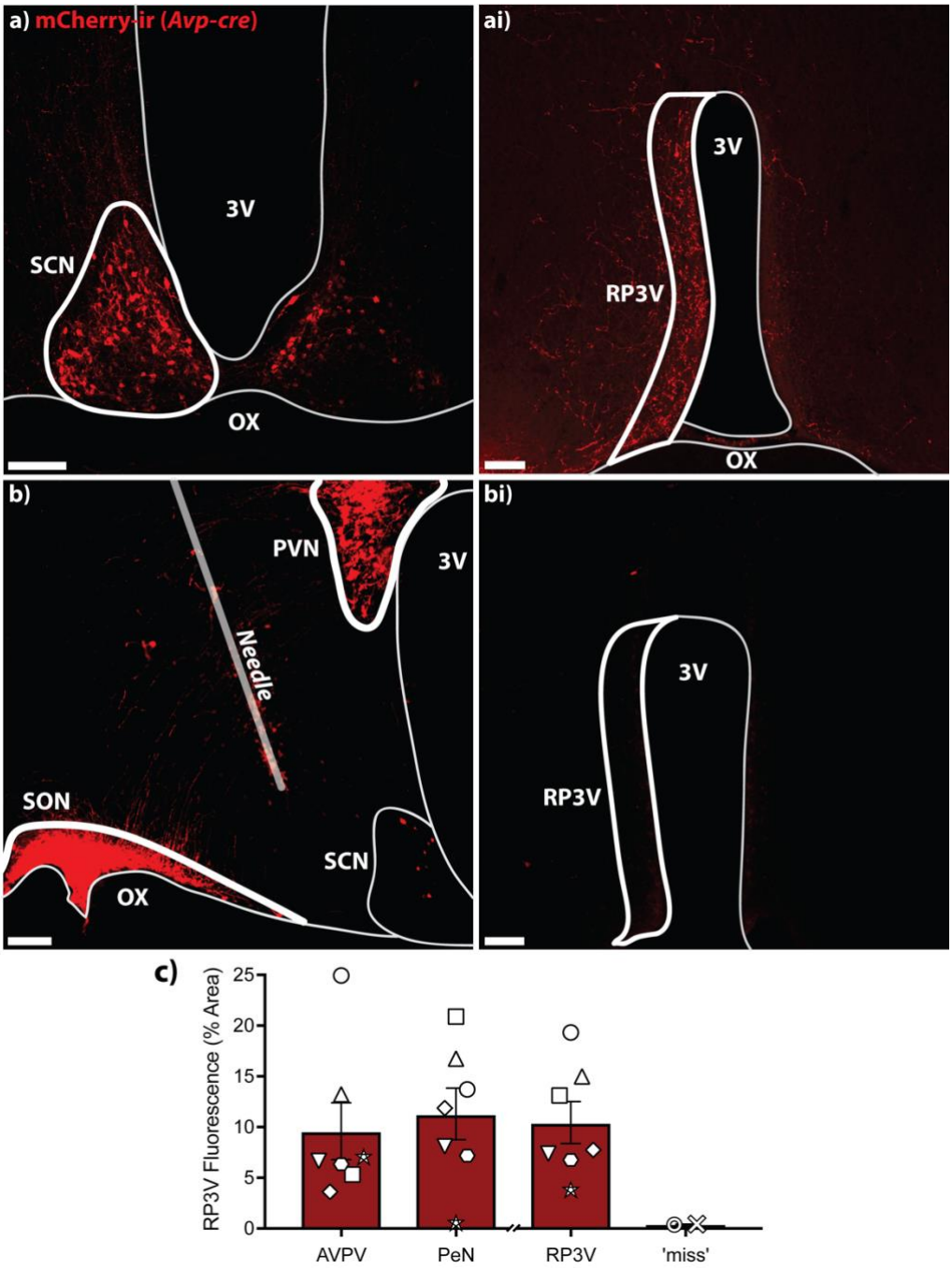

Figure 4.1: Viral vector-mediated tract tracing reveals SCN *Avp-cre* neurons project to the RP3V.

a) Accurate targeting of the SCN shows mCherry expression in the typical shell pattern of *Avp-cre* neurons. **ai)** Confocal Z-stack image of the RP3V from the same animal in a). The mCherry-ir fibres are visible along the edge of the third ventricle within the RP3V. **b)** An example of an animal with poor mCherry expression in the SCN due to inaccurate needle placement. Notice the high level of mCherry expression in the PVN and SON. **bi)** Confocal Z-stack image of the RP3V from the same animal in b). Little to no mCherry-ir fibres can be seen in the RP3V. **c)** The percentage area of RP3V innervation is similar in the AVPV and the PeN. Mice with a poorly transfected SCN ('miss') have little RP3V fluorescence. The thick white boundaries in the confocal images represent the regions of interest used for pixel density analyses. Symbols represent individual mice. Data shown as mean ± SEM. Scale bars = 100 µm. 3V = third ventricle. OX = optic chiasm.

pairs test). In mice where the SCN was not accurately targeted (Figure 4.1b), there was little to no mCherry-ir fibres visible in the RP3V (Figure 4.1bi; 0.40 ± 0.02% pixel area, n = 2 mice, range = 0.38% – 0.43%). As mentioned, injection of the viral vector often resulted in expression of mCherry in SON and PVN *Avp-cre* neurons. As such, it was important to determine the exact origin of the fibre projection seen in the RP3V. A linear regression analysis was carried out to correlate the amount of mCherry expression seen in the SCN, PVN and SON with the density of mCherry-ir fibres in the RP3V. A positive correlation between transfection in the SCN and RP3V density was found (Figure 4.2a, b; n = 9 mice, $p < 0.0001$, $R^2 = 0.70$, linear regression). This indicates that greater targeting of the SCN with the mCherry vector results in greater mCherry-ir fibre density in the RP3V. In contrast, neither transfection in the PVN nor in the SON showed any correlation to innervation of the RP3V by mCherry-ir fibres (Figure 4.2c; PVN: n = 9 mice, $p = 0.92$, $R^2 = 0.001$; Figure 4.2d; SON: n = 9 mice, $p = 0.15$, $R^2 = 0.12$, linear regression). This suggests that mCherry-ir fibres in the RP3V may originate in the SCN, and not in the PVN or SON.

Specific attention should be drawn to mouse 14255 (indicated by the empty arrowhead in Figure 4.2) that showed high mCherry expression in the PVN/SON but not the SCN. When compared to mouse 14360 (indicated by the filled arrowhead in Figure 4.2), it appears that relatively high mCherry expression in the PVN/SON does not contribute to the innervation of the RP3V by mCherry-ir fibres. As mouse 14360 shows relatively high mCherry expression in all three nuclei analysed, and a high level of fibre density in the RP3V, it is unlikely that the confounding influence of PVN/SON transfection would contribute to mCherry-ir fibre density. As such, these data show that the mCherry-ir fibres within the RP3V likely come solely from the SCN *Avp-cre* neurons, rather than the those in the PVN or SON.

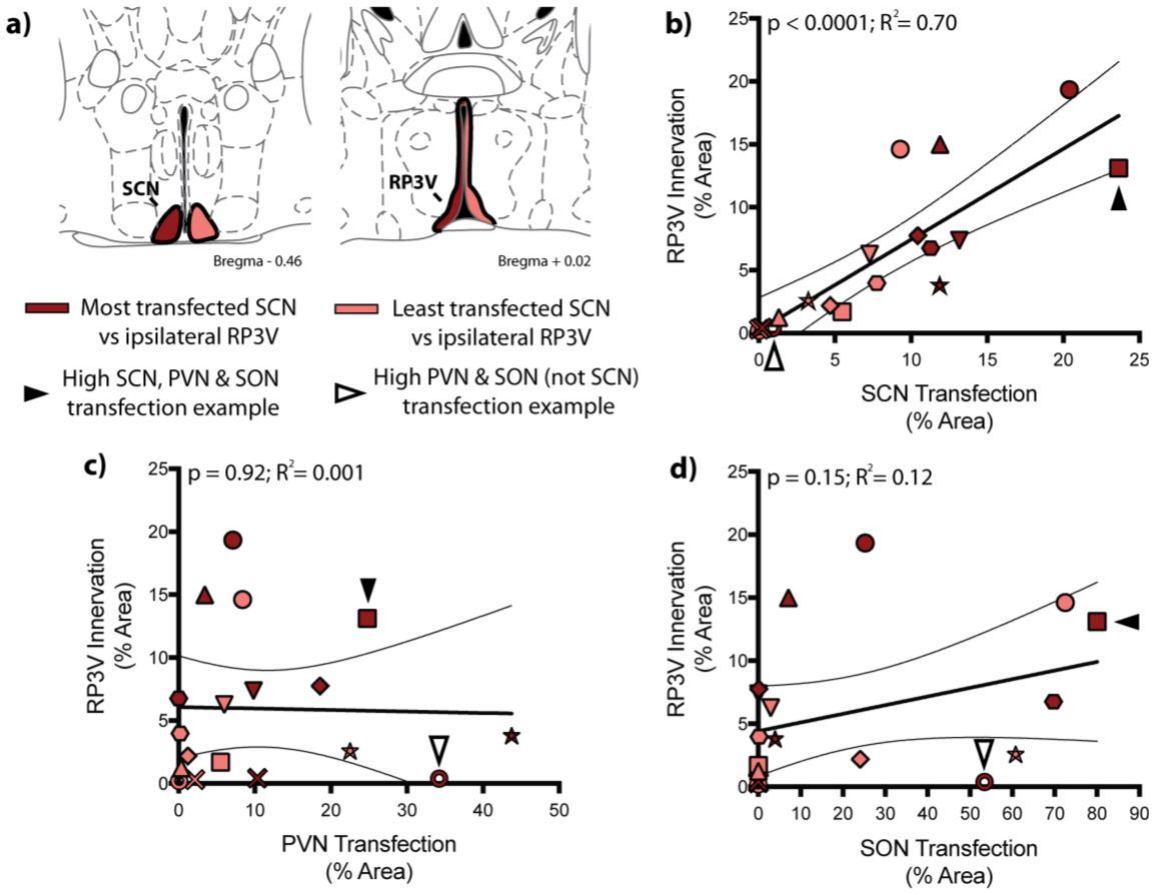

Figure 4.2: *Avp-cre* neurons from the SCN, but not PVN or SON, project fibres into the RP3V.

a) Schematic representation of the analysis. Dark red indicates the most densely transfected half of the SCN, while the light red is the least densely transfected half of the SCN. The density of mCherry expression in the PVN and SON, ipsilateral to the SCN half, were also compared to the mCherry-ir fibre density in the RP3V. **b)** Linear regression analysis reveals a positive correlation between transfection in the SCN and the fibre density in the RP3V. **c, d)** There is no such correlation between the transfection of the PVN or SON and the respective RP3V fibre density. Data shown as line of best fit ± 95% confidence interval. Representative brain slices taken from Franklin and Paxinos (2008).

4.3.2 Kisspeptin neurons in the RP3V are closely apposed by SCN *Avp-cre* neuron projections

As the SCN *Avp-cre* expressing neurons are clearly projecting to the RP3V, it was important to determine their anatomical interaction with the kisspeptin neurons. Dual fluorescence immunohistochemistry for kisspeptin and mCherry showed that mCherry-ir fibres in the RP3V form a dense plexus surrounding the kisspeptin-ir neurons (Figure 4.3b).

Closer inspection of the RP3V revealed that the mCherry-ir fibres made close appositions to 44.6 ± 6.6% of the kisspeptin-ir neurons in the RP3V ipsilateral to the most transfected SCN half (Figure 4.3c; n = 6 mice, range= 22.3% - 68.6%). Similar proportions of kisspeptin neurons were apposed by mCherry-ir fibres in the AVPV and PeN (Figure 4.3c; AVPV: 40.5 ± 6.2%, range = 16.7% - 53.3%; PeN: 48.7 ± 8.7%, range = 18.8% - 83.9%; p = 0.69, Wilcoxon signed-rank matched-pairs test). Of the RP3V kisspeptin neurons apposed by mCherry-ir fibres, there were 1.40 ± 0.13 close appositions per neuron (Figure 4.3d). Again, no difference was found between the anatomical subdivisions of the RP3V (Figure 4.3d; AVPV: 1.33 ± 0.09/neuron; PeN: 1.48 ± 0.17/neuron, p = 0.16, Wilcoxon signed-rank matched-pairs test). Consistent with these fibres originating in the SCN, the proportion of RP3V kisspeptin neurons receiving close appositions was positively correlated with the transfection in the ipsilateral SCN; that is to say, more viral transfection in the SCN revealed more close appositions to RP3V kisspeptin neurons (Figure 4.3e; n = 6 mice, p = 0.0003, R^2 = 0.74, linear regression).

These data suggest that SCN *Avp-cre* neurons may establish synaptic inputs onto approximately half of RP3V kisspeptin neurons.

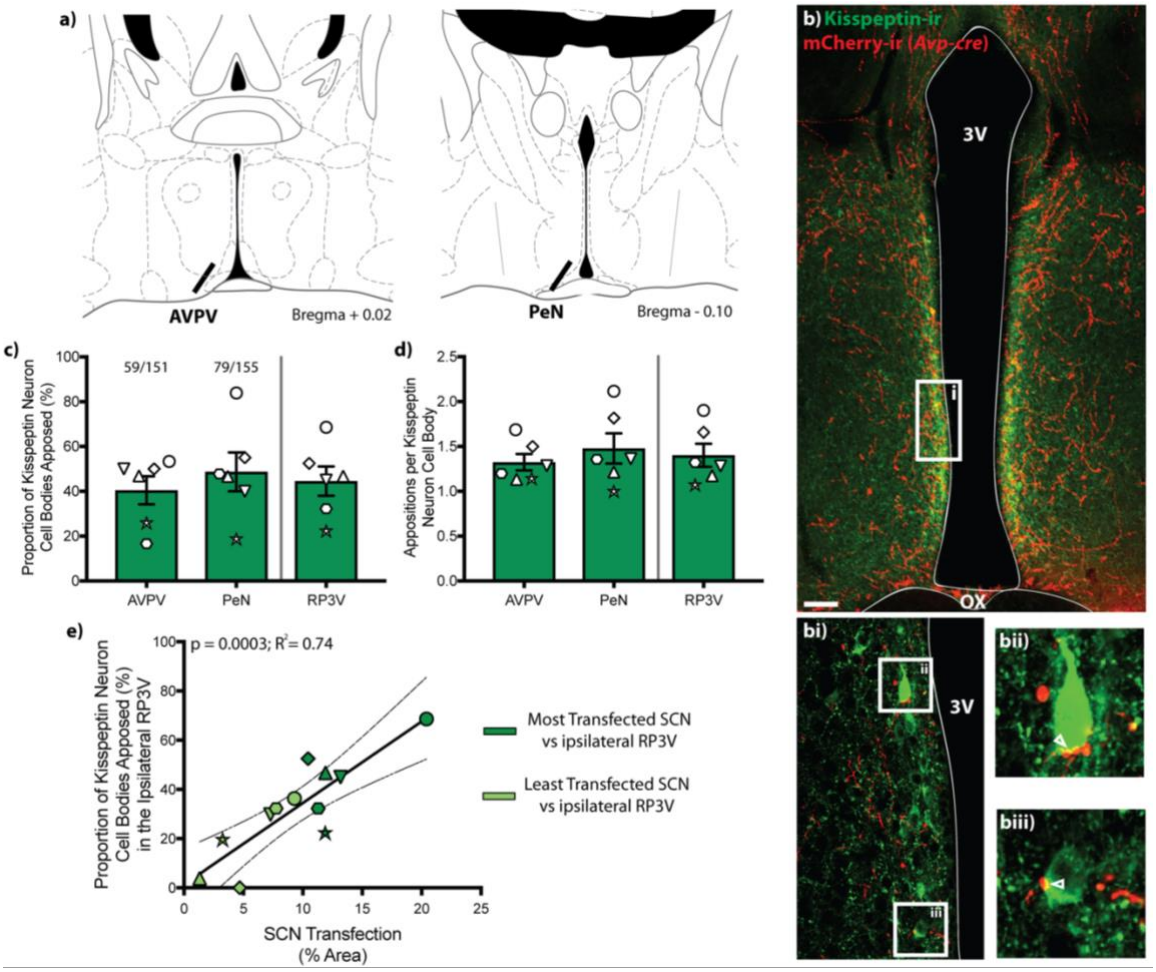

Figure 4.3: SCN *Avp-cre* neurons make putative synaptic inputs onto RP3V kisspeptin neurons.

a) Relative brain positions from where mCherry-ir appositions to kisspeptin neuron were taken. **b)** Confocal Z-stack image of the RP3V showing kisspeptin-ir neurons (green) with the mCherry-ir fibres (red) innervating the region. bi) Single confocal plane image of the RP3V alongside the third ventricle showing kisspeptin neurons with the mCherry-ir fibres coming into close apposition. Close appositions to kisspeptin neuron somata (empty arrowheads) are shown in bii) and biii). **c)** Proportion of kisspeptin neurons apposed in either the RP3V subdivision (with the fraction of the total counted above), and for the entire RP3V. **d)** The number of appositions per apposed kisspeptin neuron in either the RP3V subdivisions, and for the entire RP3V. **e)** There is a positive correlation between the fluorescence of the transfected SCN to the proportion of kisspeptin neurons apposed in the ipsilateral RP3V. Symbols represent individual mice. Dark and light green indicate measurements taken ipsilateral to the most and least transfected side of the SCN, respectively. Data shown as mean ± SEM, or linear regression ± 95% confidence interval. Scale bar = 100 µm. 3V = third ventricle. OX = optic chiasm. Representative brain slices taken from Franklin and Paxinos (2008).

4.3.3 SCN *Avp-cre* neurons do not appose GnRH neurons

Viral tract-tracing was used to determine whether SCN *Avp-cre* neurons project directly to GnRH neurons, in addition to the RP3V kisspeptin neurons. GnRH neurons are scattered across the rostral hypothalamus (Herbison, 2015). As such, brain slices containing the MS, rPOA and AHA were chosen for examination of the GnRH neurons (Figure 4.4a). In each of these areas, there was very little mCherry-ir innervation (Figure 4.4c-e). Of all the GnRH neurons analysed, only 4/74 (5.4%) showed close appositions to mCherry-ir fibres (Figure 4.4b; MS: 1/25 (4.8%) neurons apposed; rPOA: 2/30 (6.7%) neurons apposed; AHA: 1/19 (5.6%) neurons apposed; n = 3 mice). As these animals were also used in Section 4.3.2, it is interesting to note that they had 32.2 – 52.5% of RP3V kisspeptin neurons with close appositions. This indicates that the SCN *Avp-cre* neurons do not directly innervate GnRH neurons in the mouse, supporting the proposed model (Williams & Kriegsfeld, 2012; Simonneaux & Piet, 2018).

4.4 Discussion

To determine whether SCN AVP neurons project to the RP3V and its resident kisspeptin neurons, the cre expressing neurons in the *Avp-cre* mouse SCN were targeted for viral tract tracing. Here it has been shown that there is a dense fibre projection to the RP3V from SCN *Avp-cre* neurons and that their projection fibres come into close apposition with kisspeptin-ir neurons. It has also been shown that this is not the case for GnRH neurons.

4.4.1 SCN AVP neurons innervate the RP3V

Rather than examining the projection from the entire SCN, as in previous studies

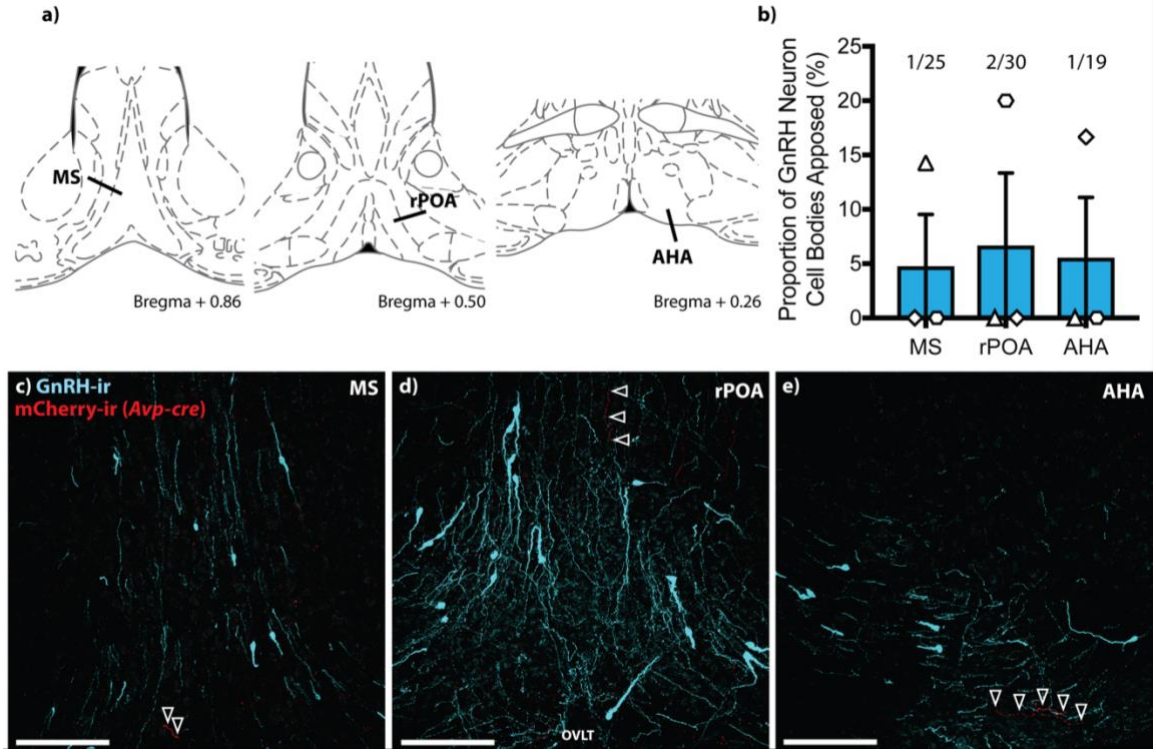

Figure 4.4: GnRH neurons show few close appositions from SCN *Avp-cre* neuron projections.

a) Relative brain positions from where GnRH neuron counts were taken. **b)** Quantitative analysis of the proportion of GnRH neuron cell bodies apposed by mCherry-ir fibres. Numbers above bars represent the number of neurons with a close apposition to a mCherry-ir fibre as a fraction of the total neurons counted. **c-e)** Cyan pseudocoloured GnRH neurons in the MS, rPOA and AHA show almost no appositions with mCherry-ir fibres. Thin projection fibres are present in each area and are indicated by arrowheads along their length. Symbols represent individual mice. Data shown as mean ± SEM. Scale bars = 100 µm. AHA = anterior hypothalamic area. MS = medial septum. OVLT = organum vasculosum of the laminar terminalis. rPOA = rostral preoptic area. Representative brain slices taken from Franklin and Paxinos (2008).

(de la Iglesia *et al.*, 1995; Vida *et al.*, 2010), the viral tract tracing method used here allows specific tracing of a genetically defined population of neurons, to investigate the input from the SCN *Avp-cre* neurons to the RP3V. These findings are consistent with others showing innervation of RP3V kisspeptin neurons by AVP (Vida *et al.*, 2010; Williams *et al.*, 2011). Further, these findings reveal a higher proportion of innervation to RP3V kisspeptin neurons (roughly 33% and 37% in Vida *et al.* (2010) and Williams *et al.* (2011), respectively), likely due to the more specific tract tracing rather than immunohistochemical methods. Interestingly, the potential AVPergic innervation of the RP3V appears to be solely from the SCN, although it is impossible to determine whether these projections are solely ipsilateral, due to transfection across hemispheres. The method used here allows selective targeting of regions of interest and provides evidence that the AVP-expressing neurons in the PVN and SON do not innervate the RP3V. This supports previous immunohistochemical work by Vida *et al.* (2010), where co-staining of peptides was used to discriminate between the magnocellular and suprachiasmatic projections. As the PVN/SON neurons do not appear to innervate the RP3V, this provides a level of confidence that any effect caused by AVP neurons at the level of RP3V kisspeptin neuron (particularly for later chapters), must be originating from the SCN AVP population.

4.4.2 SCN AVP neurons indirectly target GnRH neurons

The tract tracing shown here provides evidence that the SCN *Avp-cre* neurons do not substantially innervate the GnRH neurons. This, however, is based on appositions at the level of the cell body. GnRH neurons have been shown to receive synaptic input along their projection fibres (Campbell *et al.*, 2009; Herde *et al.*, 2013) that may have been missed in this analysis. As the projection pattern of SCN AVP neurons is more typically dorsal/rostral (Rood & de Vries, 2011), it is unlikely that they would innervate the caudal projections of GnRH neurons. Consistent with the lack of innervation, GnRH neurons lack V1Rs (Kalamatianos *et al.*, 2004a; Jasoni *et al.*, 2005), and a do not respond to AVP application (Piet & Herbison,

unpublished). Despite this, dialysis of AVP into the preoptic area can trigger the LH surge via excitation of the GnRH neuronal network (Palm *et al.*, 1999, 2001). This work provides evidence that the SCN *Avp-cre* neurons are in apposition to RP3V kisspeptin neurons, which may then relay circadian cues necessary for generating the LH surge. The viral tract-tracing work confirms the model that SCN *Avp-cre* neurons are in apposition to kisspeptin neurons, but not GnRH neurons. This is indicative of a direct circuit from SCN AVP neurons to RP3V kisspeptin neurons, and an indirect pathway which mediates the excitation of GnRH neurons and thus, the LH surge.

4.4.3 SCN *Avp-cre* neurons appose RP3V kisspeptin neurons

Almost half of the RP3V kisspeptin neurons appear to be in apposition to mCherry-ir fibres from the SCN, however, as mentioned above in regard to GnRH neurons, these appositions are only taken at the level of the cell body. There is a possibility that the SCN may be innervating kisspeptin neurons at more distal dendritic regions, resulting in an underestimation of the apposed kisspeptin neurons. Given the characterisation of the mouse model from Chapter 3, *Avp-cre* mCherry-ir fibres are likely to represent 60% of the SCN AVP neurons potentially underrepresenting the true number of close appositions from SCN AVP neurons to kisspeptin neurons.

The appositions at kisspeptin neurons are defined as those lacking a black pixel between fibre and cell body in the images. However, an apposition is not definitive as a functional synapse. It could be that these projections, although coming close to kisspeptin neurons, are not establishing an actual synapse in the RP3V. Due to the brain having been sliced, it is impossible to determine whether the fibres are ending at the RP3V, or passing by. An immunohistochemical stain for a synaptic marker such as synaptophysin, electron microscopy, or a transsynaptic retrograde viral tracer would provide greater evidence for synaptic contact between mCherry and kisspeptin. There is also a possibility that a potential input from the SCN

AVP neurons may not be strictly synaptic. Magnocellular and SCN AVP neurons have been shown to release peptides in a non-synaptic manner from the dendrites (Pow & Morris, 1989; Castel *et al.*, 1996). Thus, it could be that these neurons release their content in an extrasynaptic manner near to kisspeptin neurons as opposed to synaptically.

4.5 Summary

SCN AVP neurons are thought to be critical for the timing of the LH surge. Here, the projection from cre-expressing neurons from the SCN of the *Avp-cre* mouse has been traced to show an anatomical pathway between the SCN and RP3V. This provides evidence for a potential pathway by which the SCN may relay circadian cues to kisspeptin neurons. As GnRH neurons receive no such innervation from SCN *Avp-cre* neurons, this confirms an indirect pathway from SCN neurons to GnRH neurons, via the RP3V kisspeptin neurons. Further, these experiments have shown that at least half of these kisspeptin neurons are potentially innervated, a greater proportion than previously suspected.

Chapter 5:

Examination of Fast Synaptic Communication Between SCN *Avp-cre* neurons and RP3V neurons

5.1 Introduction

The previous chapter provided anatomical evidence that SCN *Avp-cre* neurons project to, and come into close apposition with, RP3V kisspeptin neurons. This suggests that a synaptic circuit may exist between the SCN AVP neurons and RP3V kisspeptin neurons. The experiments in this chapter aimed to determine whether this anatomical projection is functionally active, communicating with RP3V kisspeptin neurons by the release of fast neurotransmitter.

Functional communication between the two populations of neurons is typically synaptic, relying on the release of neurotransmitter to either excite or inhibit the postsynaptic target. In brief, an influx of sodium drives action potentials which propagate along neuronal projections to activate voltage-gated calcium channels in presynaptic terminals. The influx of calcium to presynaptic terminals drives vesicles containing neurotransmitter/neuropeptides to the synaptic membrane where they can be released into the synaptic cleft. Their binding to postsynaptic receptors allows for the transmission of the electrical message across the synapse, resulting in postsynaptic currents (Figure 5.1).

Neurons within the SCN are thought to be GABAergic (Card & Moore, 1984; Okamura *et al.*, 1989; Moore & Speh, 1993; Gao & Moore, 1996; Abrahamson & Moore, 2001), along with co-expressing neuropeptides, thus may release GABA onto postsynaptic targets. Released GABA binding to $GABA_A$ receptors ($GABA_ARs$) typically causes the influx of chloride resulting in an inhibitory postsynaptic current (IPSC). Recording IPSCs from the postsynaptic neuron, in response to presynaptic depolarisation, is the easiest method to determine whether two neuronal populations are synaptically linked. Therefore, recording GABAergic neurotransmission onto RP3V kisspeptin neurons, in response to SCN *Avp-cre* neuron stimulation would provide irrefutable evidence that these neurons establish synaptic input in the RP3V.

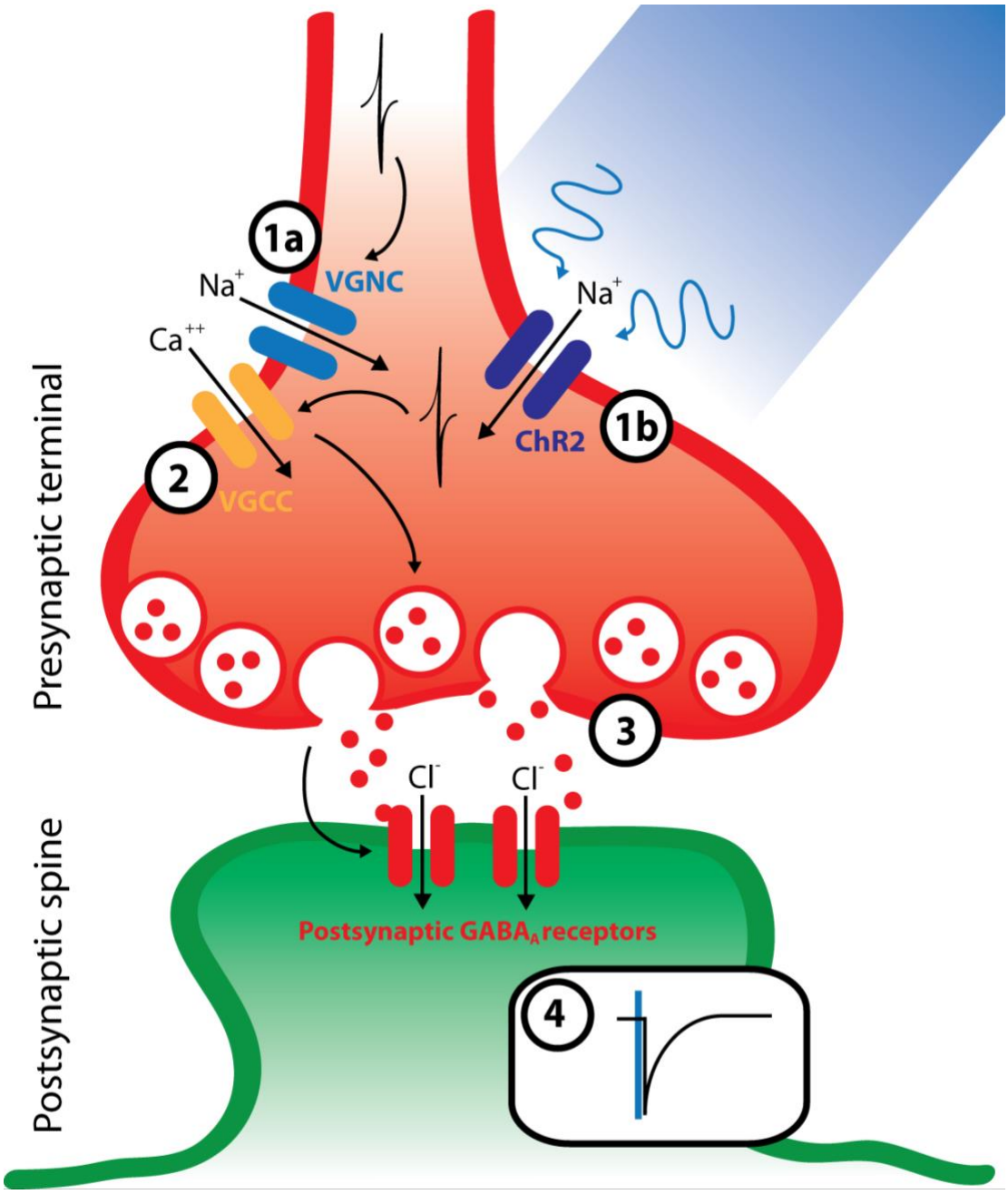

Figure 5.1: The mechanism of neurotransmission.

Electrical stimulation of a presynaptic neuron opens voltage-gated sodium channels (VGNC) which drives the generation of action potentials (**1a**). Optogenetic activation of neurons by blue light through channelrhodopsins (ChR2) also drives the influx of sodium to evoke action potentials (**1b**). This results in depolarisation of the presynaptic terminal. The depolarisation opens voltage-gated calcium channels (VGCC) to drive the influx of calcium (**2**). Calcium causes the vesicles at the membrane bind and release their content into the synaptic cleft (**3**). The released transmitters bind postsynaptic receptors, opening an ion channel (letting chloride ions through in the case of the $GABA_A$ receptor). The resulting postsynaptic current can be detected using whole cell voltage clamp electrophysiology (**4**). In optogenetic experiments, recorded postsynaptic currents occurring with a short and constant latency provide evidence that the presynaptic light stimulation evokes neurotransmitter release and thus evidence of the presence of functional synaptic connections.

5.1.1 Channelrhodopsin-assisted circuit mapping

Over the past decade, optogenetics has proved to be a critical method to help define neuronal circuitry. Optogenetics is a powerful method whereby genetically defined populations of neurons can be activated in a non-invasive manner using light (Fenno *et al.*, 2011). Typically, light-sensitive proteins are expressed by a viral vector into neurons of interest, which can then be activated by specific wavelengths of light to selectively excite or inhibit neurons (Han *et al.*, 2018). One specific method of optogenetics uses channelrhodopsin (ChR2), a blue light-gated non-selective cation channel. Light stimulation opens the channel causing movement of Na^{+} and Ca^{++} into, and K^{+} out of the neuron. This results in positive charge entering the cell to cause depolarisation of the membrane and, if this depolarisation is strong enough, activation of voltage-dependent ion channels for the generation of action potentials (Figure 5.1). Here, a double mutant channelrhodopsin known as $ChR2^{(ET/TC)}$ has been used. The double mutant speeds up ChR2 kinetics and enhances ChR2 conductance (Berndt *et al.*, 2011). This advantage allows for high-fidelity responses to fast light stimulation and precise stimulation of action potentials.

Channelrhodopsin-assisted circuit mapping (CRACM) takes advantage of this light sensitivity to non-invasively depolarise neuron terminals whilst electrophysiological recordings are carried out in putative downstream neuronal populations (Petreanu *et al.*, 2007). The detection of post-synaptic currents evoked by light-stimulation thus provides unequivocal functional evidence that there is an input from one neuronal population to the next.

CRACM is an invaluable tool when coupled with the cre/*loxP* system. Here, cre-dependent viral vector for $ChR2^{(ET/TC)}$ (Appendix III; herein referred to as AAV-ChR2) was injected into the *Avp-cre* mouse SCN to enable specific expression of ChR2 in cre-expressing SCN neurons. As ChR2 spreads along the neuronal projections (analogous to the tract-tracing experiments from Chapter 4) and inserts into the membrane, ChR2-expressing axons will still

be present and functional even when severed from their cell bodies. Although the full circuit is not intact, potential synaptic inputs would still be detected in the neurons of interest (Petreanu *et al.*, 2007; Betley & Sternson, 2011; Lim *et al.*, 2013), in this case, RP3V kisspeptin neurons. Using CRACM with the *Avp-cre* mouse model provides a level of specificity that would not be attained using more electrical stimulation, which activates axons indiscriminately (Yizhar *et al.*, 2011).

5.1.2 The *Kiss1-hrGFP* mouse model

To carry out experiments recording from kisspeptin neurons specifically in living brain slices, this work used the *Kiss1-hrGFP* mouse. The mouse line was generated by insertion into the mouse genome of a bacterial artificial chromosome containing parts of the kisspeptin gene, modified to contain a humanised *renilla* (hr) GFP cassette (Cravo *et al.*, 2013). The *Kiss1-hrGFP* model has been characterised in ovariectomised conditions by *in situ* hybridisation (Cravo *et al.*, 2013). Immunohistochemical analyses of GFP to kisspeptin-ir were carried out in intact mice, in the Piet laboratory by Anaëlle Braine. It was found that 86.5 ± 2.4% of kisspeptin-ir neurons expressed GFP, while 64.4 ± 3.2% of GFP-expressing cells were kisspeptin-ir (Appendix VII), identifying this as a good model to visualise kisspeptin neurons.

When the *Kiss1-hrGFP* mouse is crossed to the *Avp-cre* mouse strain, the offspring (*Avp-cre:Kiss1-hrGFP*) makes a perfect model for interrogating how stimulation of *Avp-cre* neurons affects RP3V kisspeptin neurons. Here, CRACM has been carried out with ChR2-transfected *Avp-cre* neurons, whilst recording from identified *Kiss1-hrGFP* neurons in brain slices.

5.1.3 Oestrous cycle-dependent changes in input activity

Changes in neuronal electrical activity have been reported in females across the oestrous cycle, particularly in the way that neurons respond to upstream activity. Differences have been recorded in the hippocampus (Warren *et al.*, 1995; Scharfman *et al.*, 2003), nucleus accumbens (Proaño *et al.*, 2018), and in the hypothalamus (Liu & Herbison, 2011). The changes in electrical activity across the oestrous cycle provide a mechanism by which neurons might regulate the activity of their downstream targets or may change their receptivity to incoming signals. This could be particularly important at proestrus as a mechanism to help elicit the LH surge.

As activity of neurons in the RP3V is highly influenced by the sex steroid environment, it may be that changes in hormone concentration may affect how the neurons integrate upstream signals. At the ultrastructural level, synapses to RP3V neurons change in number across the oestrous cycle, with an increase at oestrus, and a decrease at met-/dioestrus (Langub Jr. *et al.*, 1994). Vida *et al.* (2010) have also shown that AVP-immunoreactive appositions to kisspeptin neurons increase with oestradiol treatment in OVX mice. It remains to be determined, however, if these appositions are synapses, and whether any functional plasticity exists across the oestrous cycle. Any plasticity, particularly around proestrus when the LH surge is generated would be relevant to the neuroendocrine regulation of ovulation. Here, recordings over different stages of the oestrous cycle indicate any potential change that could be occurring in the way that RP3V kisspeptin neurons integrate synaptic signals from the SCN *Avp-cre* neurons.

5.1.4 Hypothesis and Aim

Due to the anatomical interactions presented in Chapter 4, it was hypothesised that **these close appositions will be points of fast synaptic communication between SCN *Avp-cre* neurons and RP3V kisspeptin neurons**. The experiments in this chapter aimed to **determine whether RP3V kisspeptin neurons respond to GABAergic synaptic transmission from**

SCN *Avp-cre* neurons and to whether there may be synaptic plasticity due to the changing hormonal environment across the murine oestrous cycle.

5.2 Methods

5.2.1 Animals

General animal information is outlined in Section 2.1. Adult female *Avp-cre*, *Avp-cre:Kiss1-hrGFP, Vgat-cre:tdTomato* and *Nms-icre:Kiss1-hrGFP* mice (2-6 months old) were used in this study. Oestrous cycles were determined by daily vaginal lavage and tissue was collected in oestrous stages outlined in each experiment.

5.2.2 Surgery

The general surgery procedures are outlined in Section 2.2. For Section 5.3.1, *Avp-cre* mice were unilaterally injected with 400 nL of AAV-ChR2 at the SCN. For the remainder of experiments, mice were injected bilaterally with 400 nL/side of AAV-ChR2 at the SCN. Mice were left for at least two weeks to allow sufficient transduction of the viral vector prior to experimentation.

5.2.3 Acute brain slice preparation

The brain slicing procedure for electrophysiology is outlined in Section 2.5.1.

5.2.4 Brain slice electrophysiology

The general brain slice electrophysiology procedure and recording configurations are outlined as part of Section 2.5.2. Prior to experimentation, the level of ChR2 transduction was determined by examining mCherry expression in the SCN. Mice were used for experiments when mCherry expressing neurons were easily visible in the SCN.

5.2.5 Optogenetic and electrophysiological protocols

5.2.5.1 Identification of kisspeptin neurons

By using blue light to excite the GFP in kisspeptin neurons, a significant issue could be encountered whereby the light may also activate the blue-light sensitive ChR2. This issue has been encountered previously (Qiu *et al.*, 2016; Piet & Herbison, 2018; Piet *et al.*, 2018), and has been mitigated by two key approaches used here. First, identification of kisspeptin neurons was carried out at the lowest light intensity sufficient to excite GFP (in this case 0.8 mW). This light intensity limits the level of ChR2 activation as the intensity may not be high enough to stimulate some/all of the ChR2 present. Secondly, the wait time following blue light stimulation (5-10 mins) ensures the recovery of the system. Identification of kisspeptin neurons, followed by the recovery period ensures that 1) ChR2 and ChR2-expressing projections fully recover from activation, 2) the effects of any neurotransmitters or neuropeptides released during the illumination would have subsided, and 3) the potentially released chemicals would have been cleared from the extracellular space (Piet *et al.*, 2018). Thus, the combination of brief illumination and the recovery period minimised potential unwanted effects of ChR2 activation.

5.2.5.2 Characterisation of ChR2 function

To carry out a characterisation of the efficacy of the ChR2 at responding to light stimulation, ChR2-transfected SCN neurons, as identified by mCherry expression, were

targeted for on-cell loose-patch electrophysiological recordings. Trains of ten 5 ms blue light (14.1 mW) pulses at 1, 2, 5, 10, 20 and 50 Hz were shone onto the SCN, and the resulting action potentials were recorded. All neurons recorded were stimulated at each frequency in a random order but finishing with 50 Hz. The recordings were examined to determine when light pulses faithfully elicited action potential firing. Where an action potential followed a light pulse (within 10 ms), this was considered a response.

5.2.5.3 Fast synaptic responses

Neurons in the RP3V were targeted for whole-cell patch-clamp electrophysiological recordings. As a control for the issue of potential ChR2 excitation whilst identifying GFP-expressing neurons, unidentified RP3V neurons, from *Avp-cre* mice that did not express the *Kiss-hrGFP* transgene, were targeted to determine their response. Once a whole-cell patch configuration was attained, the neurons were left to recover for several minutes prior to baseline recordings for two minutes. Two pulses of blue light were then shone onto the RP3V for 5 ms each, with 200 ms between pulses (5 Hz). This was repeated every 20 s, 25-50 times per neuron.

5.2.5.4 Testing for a monosynaptic circuit

To determine whether the input from ChR2-transfected SCN neurons was monosynaptic, a protocol modified from Petreanu *et al.* (2009) was used. Once a postsynaptic response was measured, tetrodotoxin (0.5 µM; TTX) was bath applied resulting in inhibition of that postsynaptic response. 4-aminopyridine (100 µM; 4-AP) was then bath applied with TTX and the continued inhibition or restoration of the postsynaptic current was measured.

5.2.6 Immunohistochemistry

The general perfusion-fixation, brain slicing and immunohistochemistry procedures are outlined in Section 2.3. The antibodies used in this Chapter have been reported in Chapter 3.

5.2.7 Microscopy and image analysis

The general microscopy methods are outlined in Section 2.4. General colocalisation analysis methods are outlined in Section 3.2.4. ChR2-expressing neurons were imaged in the SCN using a 20× objective for Figure 5.2. For Section 5.3.3, AVP-ir neurons were counted and the proportion colocalised with tdTomato (as a marker of the vesicular GABA transporter, vGAT) was determined. Images shown herein are maximum projection confocal Z-stack images unless stated otherwise.

5.2.8 Statistical analysis

General analysis methods are outlined in Section 2.7. The recorded sweeps were overlaid and inspected to determine the presence of a time-locked postsynaptic current (within 10 ms of the light stimulation onset). Neurons that showed time-locked IPSCs in response to light stimulation were considered as ‘responding’ neurons. Those neurons that did not show IPSCs in response to light stimulation were termed ‘non-responding’. Comparisons of the proportions of responding and non-responding neurons across transgenic mouse strains were carried out using a chi-squared test. In this chapter, where n-values are reported, n refers to neurons recorded, while N refers to the number of animals used in the experiments.

5.3 Results

5.3.1 Characterisation of ChR2 function in *Avp-cre* neurons

First, it was necessary to determine whether SCN *Avp-cre* neurons expressed functional ChR2. mCherry (a reporter of ChR2 transduction) was expressed in SCN neurons in acute brain slices, indicating that the viral construct was successfully transfected. mCherry-expressing *Avp-cre* neurons were recorded in the on-cell loose-patch configuration and stimulated with 10-pulse trains of blue light illumination delivered at various frequencies (Figure 5.2a). Blue light elicited action potentials in SCN *Avp-cre* neurons with perfect fidelity at all frequencies from 1-20 Hz. At the highest frequency tested (50 Hz), the fidelity of the response was still near perfect at 95.3 ± 3.2% success (Figure 5.2b, c; n = 7 neurons, N = 3 dioestrous mice). As such, ChR2 can successfully be transfected in SCN *Avp-cre* neurons and action potential firing can be reliably controlled over a range of frequencies by blue light-stimulation.

5.3.2 SCN *Avp-cre* neurons do not communicate with RP3V kisspeptin neurons via fast-synaptic transmission

GFP-expressing neurons in the RP3V were recorded using whole-cell patch-clamp electrophysiology. The ChR2-expressing projections were then stimulated with paired pulses of blue light to evoke neurotransmitter release (Figure 5.3a). Interestingly, only 1 out of 14 kisspeptin neurons from mice in dioestrus (7.1%) was found to respond to a fast-synaptic input from SCN *Avp-cre* neurons (Figure 5.3b, c; N = 4 dioestrous mice). This response was inhibited by gabazine (GBZ), showing it was mediated by activation of $GABA_AR$ (Figure 5.3c).

It has been suggested that elevated oestrogen can increase the innervation of RP3V kisspeptin neurons by AVP neurons (Vida *et al.*, 2010). Thus, at proestrus when circulating oestrogen is higher there could be more fast-synaptic transmission from the SCN *Avp-cre* neurons to RP3V kisspeptin neurons. However, it was found that only one out of 12 recorded kisspeptin neurons (8.3%) from proestrus mice, received fast synaptic input (Figure 5.3d;

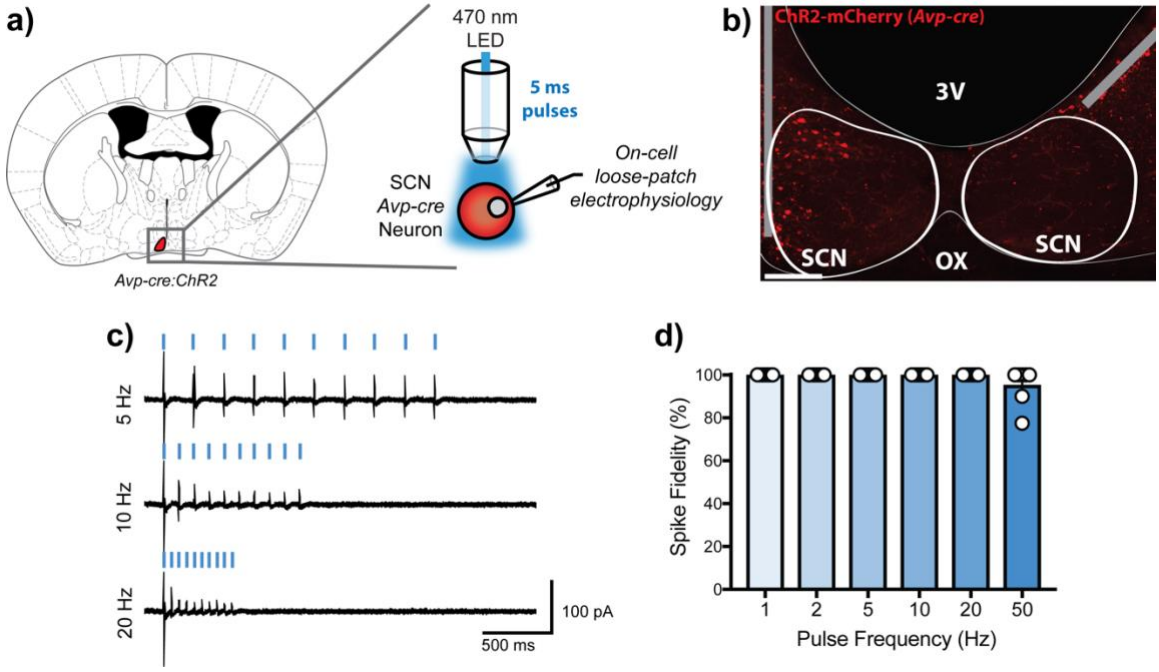

Figure 5.2: ChR2 function in the *Avp-cre* mouse SCN.

a) Experimental setup. **b)** Maximum projection image of a confocal Z-stack of the SCN showing ChR2 expression (from a bilaterally injected mouse) as demarcated by mCherry. ChR2/mCherry-expressing neurons can be seen in the left SCN along the upper and left-hand sides, outlining the SCN shell. Grey bars indicate positions of the needle track. **c)** Example recordings showing 5, 10 and 20 Hz stimulation of ChR2 transfected SCN AVP neurons. Blue lines indicated 5 ms light pulses. Sharp deflections in the trace indicate action potential firing. **d)** Quantification of the fidelity of action potential firing in response to 1, 2, 5, 10, 20 and 50 Hz stimulations. Data shown as mean ± SEM. Scale bar in b) = 100 µm. 3V = third ventricle. OX = optic chiasm. n = 7 neurons, N = 3 mice. Representative brain slice taken from Franklin and Paxinos (2008).

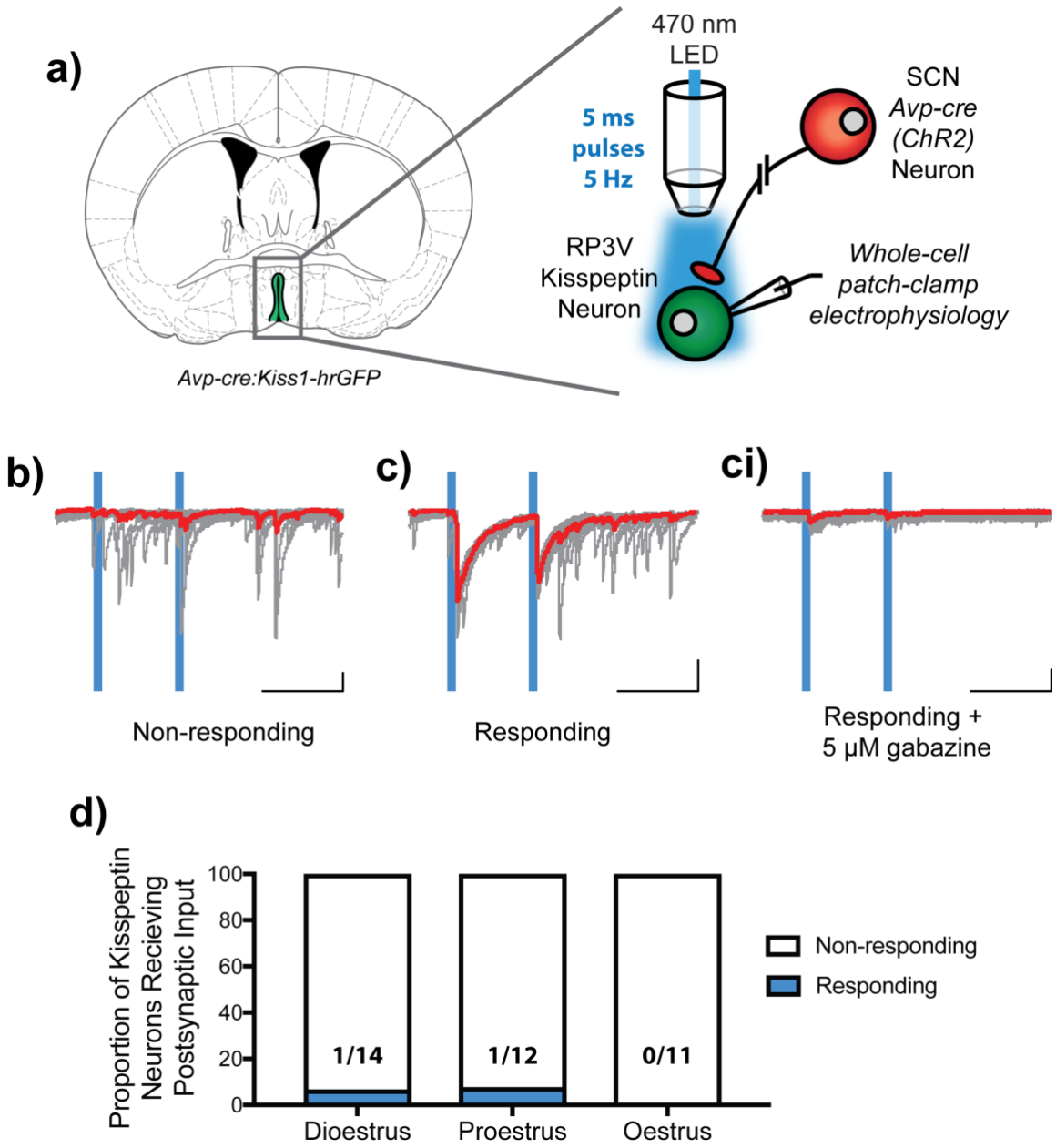

Figure 5.3: RP3V kisspeptin neurons rarely exhibit fast synaptic input from SCN *Avp-cre* neurons. **a)** Experimental setup. **b)** Example traces of a non-responding RP3V kisspeptin neuron. **c)** One recorded kisspeptin neuron exhibited IPSCs in response to blue light stimulation of the ChR2-expressing *Avp-cre* projections. This response was blocked by the $GABA_AR$ antagonist gabazine (ci) indicating this is a GABA-mediated postsynaptic current. **d)** There was no difference in the proportions of responding kisspeptin neurons over different stages of the oestrous cycle. Traces displayed as 10 sweeps with the average overlaid in red. Scale bars = 200 ms/50 pA. Di: N = 4 mice, Pro: N = 4 mice, Oestrus: N = 4 mice. Representative brain slice taken from Franklin and Paxinos (2008).

N = 4 proestrous mice). Later in the oestrous cycle, during oestrus when oestradiol levels are low, none of the ten recorded kisspeptin neurons displayed blue-light evoked postsynaptic input (Figure 5.3d; N = 4 oestrous mice). There was no difference between the proportion of neurons responding in any stage of the oestrous cycle (Figure 5.3d; dioestrus vs proestrus: $p = 0.91$; dioestrus vs oestrus: $p = 0.90$; proestrus vs oestrus: $p = 0.98$; chi-squared tests).

As GFP and ChR2 have overlapping excitation spectra, there is a chance that the blue light needed to identify GFP-expressing neurons may deplete neurotransmitters in synapses. In dioestrous *Avp-cre* mice not expressing the *Kiss1-hrGFP* transgene, unidentified RP3V neurons were recorded using whole-cell patch-clamp electrophysiology. (Figure 5.4a). Following paired-pulse blue light stimulation of ChR2-expressing projections, it was found that only one of the 14 recorded neurons (7.1%) displayed fast synaptic input from SCN *Avp-cre* neurons (Figure 5.4b, N = 6 mice). This response was blocked by application of GBZ (Figure 5.4c). These results are not different to that seen in the *Avp-cre*:*Kiss1-hrGFP* mouse (Figure 5.4d; $p = 0.83$, chi-squared test), with GFP expression in kisspeptin neurons.

5.3.3 SCN AVP neurons colocalise with the vesicular GABA transporter

Although *Avp-cre* neurons form putative inputs to RP3V kisspeptin neurons, there is a rarely fast synaptic transmission occurring. One potential possibility may be that these *Avp-cre* neurons do not release GABA. In order to be released at synapses, GABA must be packaged into vesicles by the vesicular GABA transporter (vGAT). Thus, absence or presence of vGAT in SCN AVP neurons would indicate whether or not these neurons are equipped to release GABA. In dioestrous *Vgat-cre:tdTomato* mice, where vGAT expression is reported by red fluorescent tdTomato (Vong *et al.*, 2011), immunohistochemistry was carried out to determine

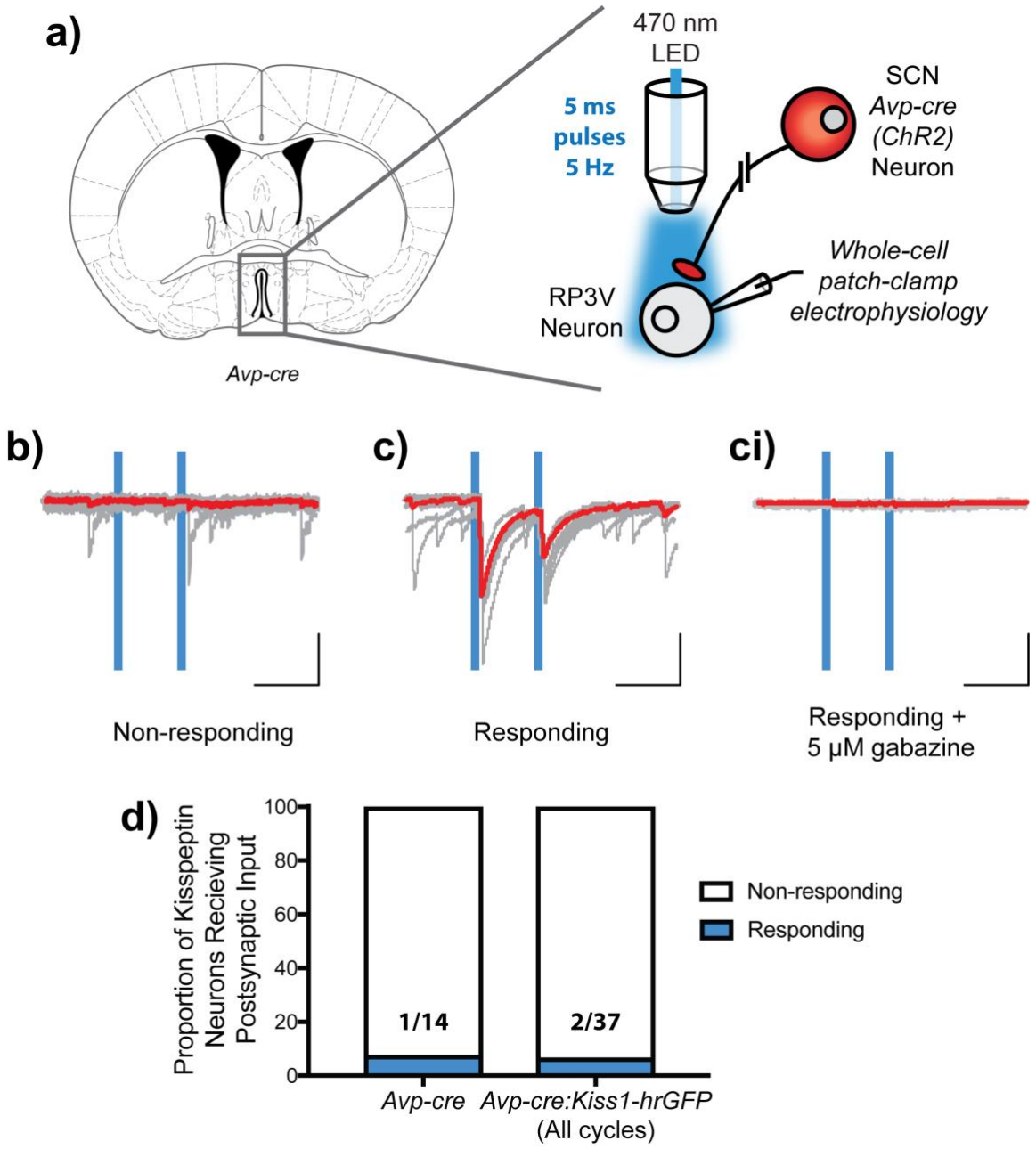

Figure 5.4: Unidentified RP3V neurons rarely exhibit fast synaptic input from SCN *Avp-cre* neurons.

a) Experimental setup. **b)** Example traces from a non-responding RP3V neuron. **c)** One recorded RP3V neuron exhibited postsynaptic currents in response to blue light stimulation of the ChR2-expressing *Avp-cre* projections. This response was blocked by the $GABA_AR$ antagonist gabazine (ci). **d)** There was no difference in the proportions of responding neurons seen in the *Avp-cre* or the *Avp-cre*:*Kiss1-hrGFP* mouse. Traces displayed as 10 sweeps with the average overlaid in red. *Avp-cre:Kiss1-hrGFP* data from Figure 5.3. Scale bars = 200 ms/50 pA. *Avp-cre:* N = 6 mice, *Avp-cre:Kiss1-hrGFP:* N = 12 mice. Representative brain slice taken from Franklin and Paxinos (2008).

whether SCN AVP neurons express vGAT. It was found that 58.7 ± 2.8% of AVP-ir neurons in the SCN colocalise with tdTomato (Figure 5.5; N = 4 mice). This indicates that a majority, but certainly not all, of the SCN AVP neurons express vGAT, and are equipped to release GABA. Absence of vGAT, therefore, perhaps does not fully account for the lack of fast synaptic transmission between SCN *Avp-cre* neurons and RP3V kisspeptin neurons.

5.3.4 *Nms-icre* neurons make monosynaptic inputs onto RP3V kisspeptin neurons

Due to the lack of blue light-evoked postsynaptic currents in RP3V kisspeptin neurons, as well as evidence suggesting that the majority of SCN AVP neurons can package GABA into vesicles for release, it was necessary to ensure that the light stimulation of ChR2 could drive neurotransmitter release onto RP3V kisspeptin neurons. Preliminary findings in the Piet laboratory suggest that SCN NMS neurons release GABA onto RP3V neurons. Therefore, *Nms-icre*:*Kiss1-hrGFP* mice were used as a positive control to determine whether the experimental approach was technically sound. As mentioned in Chapter 1, the NMS-expressing neurons of the SCN are thought to comprise up to 40% of SCN neurons and 96% of the SCN AVP neuron population, as well as producing NMS (Lee *et al.*, 2015).

Paired-pulse blue light stimulation of ChR2-expressing *Nms-icre* axons and terminals (Figure 5.6a) resulted in IPSCs in 11 of the 13 (84.6%) kisspeptin neurons recorded (Figure 5.6b; N = 1 proestrous and 2 dioestrous mice). This proportion was significantly greater than that seen in the *Avp-cre* and *Avp-cre*:*Kiss1-hrGFP* mouse models (Figure 5.6c; $p < 0.0001$ vs *Avp-cre*, $p < 0.0001$ vs *Avp-cre*:*Kiss1-hrGFP*, chi-squared tests).

To determine whether the NMS projection to the RP3V was direct, a second experiment, similar to that by Petreanu *et al.* (2009), was carried out. In RP3V neurons in which IPSCs

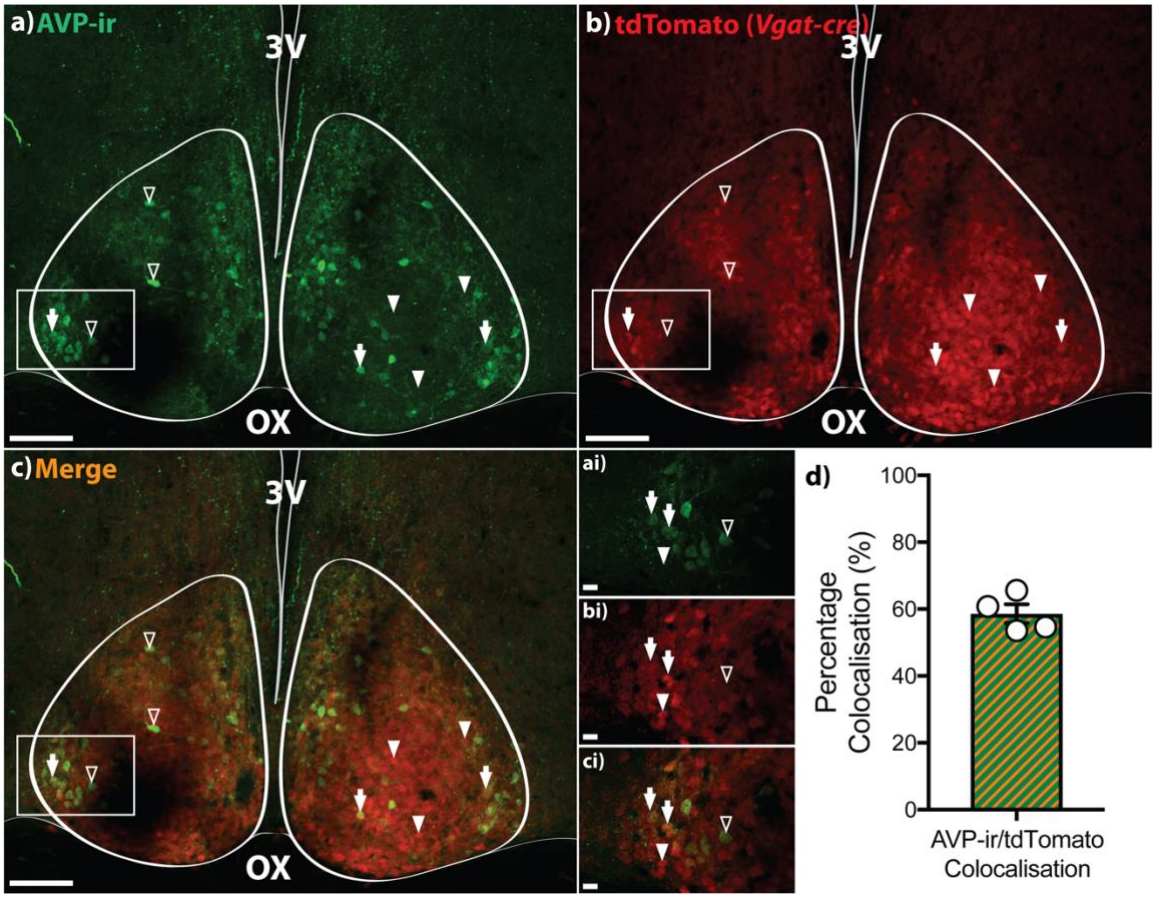

Figure 5.5: Over half of SCN AVP neurons colocalise the vesicular GABA transporter, vGAT.

a-c) Maximally projected Z-stack image of showing immunolabelling of AVP (green, a) and endogenous tdTomato fluorescence (red, b) in the SCN (thick border). The two images are merged (colocalised neurons in orange) in c. Box insets show higher magnification single plane images of AVP-ir (ai), endogenous tdTomato fluorescence (bi) and merged labels (ci). Empty arrowheads indicate AVP-ir only neurons. Filled arrow heads indicate tdTomato only neurons. Arrows indicate colocalised cells. **d)** Colocalisation of AVP-ir with tdTomato fluorescence. Data shown as mean ± SEM. a-c scale bars = 100 µm. ai-ci scale bars = 10 µm. 3V = third ventricle. OX = optic chiasm.

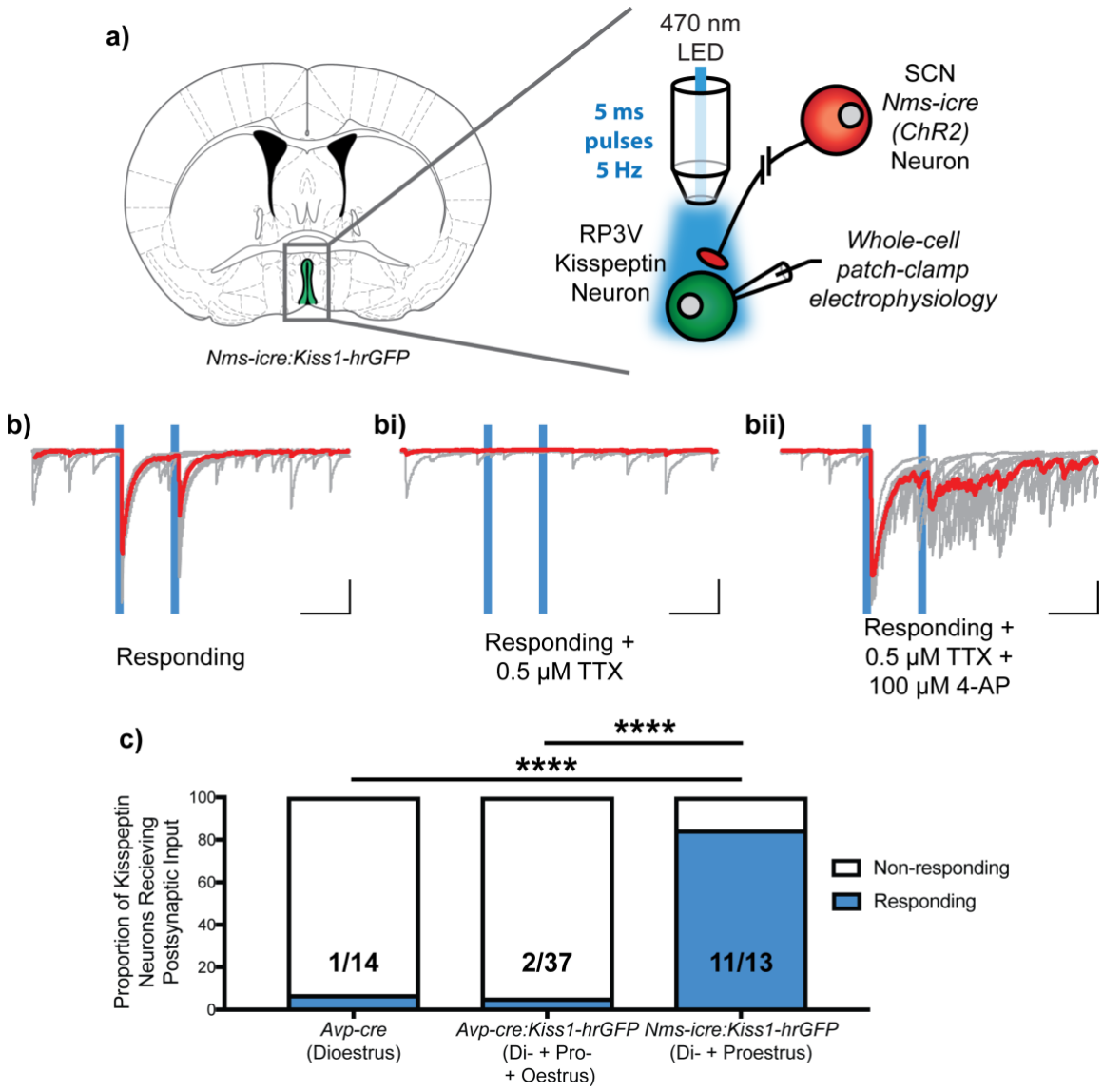

Figure 5.6: RP3V kisspeptin neurons receive monosynaptic fast synaptic input from SCN *Nms-icre* neurons.

a) Experimental setup. **b)** Blue light stimulation of ChR2-expressing *Nms-icre* projections evokes IPSC in a kisspeptin neuron, which was blocked by application of TTX (bi). When 4-AP was added, the IPSC was restored (bii) indicating that this is a monosynaptic pathway (n = 3 neurons, N = 2 mice). **c)** There was a significantly greater proportion of responding kisspeptin neurons receiving in *Nms-icre* mice that in *Avp-cre* or *Avp-cre*:Kiss-hrGFP mice (data from Figures 5.3 and 5.4). Fractions in bars indicate the number of responding neurons responses over the total number of recorded neurons. **** $p < 0.0001$. Traces displayed as 10 sweeps with the average overlaid in red. Scale bars = 200 ms/50 pA. *Avp-cre:* N = 6 mice, *Avp-cre:Kiss1-hrGFP:* N = 12 mice, *Nms-cre:Kiss1-hrGFP:* N = 3 mice. Representative brain slice taken from Franklin and Paxinos (2008).

could be evoked, TTX was bath applied to block sodium channels, and thus action potential propagation. This will essentially block blue light-evoked synaptic transmission. When TTX is coupled with the potassium channel blocker, 4-AP, potassium is unable to be extruded from the cell. This results in a build-up of intracellular K^+ which increases the net positive charge, increasing the excitability of the neuron, as well as inhibiting the K^+-mediated repolarisation. ChR2 activation at the synaptic terminal allows the influx of cations to further depolarise the terminal. No action potentials are conducted, but the depolarisation is sufficient to activate voltage-gated calcium channels. The resulting calcium influx can then drive synaptic transmission in an action potential-independent manner.

When ChR2 is activated, there are two possible outcomes. The first is that the IPSC is recorded in the postsynaptic cell. This shows that there is no propagation of the signal through a second neuron and, as such, this is unequivocal evidence that this is a monosynaptic circuit from the SCN to the RP3V. The second is that no postsynaptic current is recorded at the kisspeptin neuron. As it has been shown that blue light-stimulation is sufficient to evoke IPSCs onto kisspeptin neurons, no IPSC recorded would suggest that activation of the *Nms-icre* terminals results in neurotransmitter release onto a second neuron, which then, in turn, would release GABA onto the kisspeptin neuron. Due to the presence of TTX, that second neuron would be unable to propagate the electrical signal (i.e. action potentials) and, therefore, it could not release neurotransmitter onto the kisspeptin neuron. Thus, no IPSC would be recorded, indicating that this is a polysynaptic circuit, with one or several interneurons between the SCN and RP3V.

In this experiment, the application of TTX inhibited the postsynaptic currents seen in response to the blue light (Figure 5.6bi). Co-application of 4-AP, however, was able to restore the postsynaptic currents indicating that neurotransmission could be driven in the absence of action potentials, revealing that this circuitry was monosynaptic (Figure 5.6bii; n = 3 neurons, N = 2 mice). These data show that activating ChR2 in the presynaptic terminal is sufficient to

drive neurotransmitter release. Further, it suggests an additional SCN input to RP3V kisspeptin neurons from a population expressing NMS, that are distinct from the *Avp-cre* neurons.

5.4 Discussion

Chapter 4 revealed a dense innervation of the RP3V by *Avp-cre* neurons and close appositions to kisspeptin neurons, suggestive of putative synaptic input. Here, however, it has been shown that despite this projection, and despite 60% of AVP neurons expressing the vGAT to package GABA into vesicles for release, SCN *Avp-cre* neurons rarely communicate by fast synaptic neurotransmission to RP3V kisspeptin neurons. These findings may reflect technical issues due to the methodology; a lack of synapses; or the presence of non-functional synapses that either lack presynaptic GABA release; or lack of postsynaptic $GABA_A$Rs. Each of these will now be discussed.

5.4.1 Technical considerations

Using CRACM, this study found minimal evidence for synaptic input from SCN *Avp-cre* neurons to RP3V kisspeptin neurons. One possibility for a lack of synaptic responses is a limitation of the CRACM method. All mice used in these experiments had mCherry-expressing neurons in the SCN determined by eye before experiments were carried out. Thus, it is unlikely that the ChR2 was not sufficiently expressed, although no specific counting or colocalisation was carried out. The ChR2 variant used here was found to faithfully respond to light stimulation over a variety of frequencies, including the 5 Hz used for the paired-pulse stimulation paradigm. However, recordings of ChR2 activity were made in the SCN, at the *Avp-cre* cell body. There is a chance that stimulation at the cell body does not accurately represent the activity of the ChR2 in the projection fibres. However, activation of projection fibres in the *Nms-icre* mouse model indicates that the ChR2 does indeed function to drive synaptic release (Figure 5.6). SCN

Nms-icre neurons were observed to readily communicate to RP3V kisspeptin neurons by fast-synaptic transmission. In contrast, it seems that the SCN *Avp-cre* neurons do not relay information to RP3V kisspeptin neurons by GABAergic fast-synaptic transmission.

5.4.2 Are the *Avp-cre* SCN neurons projecting to the RP3V GABAergic?

It has been well reported, across multiple species, that SCN neurons produce GABA (Card & Moore, 1984; Okamura *et al.*, 1989; Moore & Speh, 1993; Gao & Moore, 1996; Abrahamson & Moore, 2001). Interestingly, however, the secondary phenotype (i.e. coexpression of peptides) of these GABAergic neurons remains contentious. Initially, it was reported that nearly all SCN neurons produce GABA (Okamura *et al.*, 1989; Moore & Speh, 1993; Abrahamson & Moore, 2001). Castel and Morris (2000), however, suggest that at most, 70% of the SCN neurons produce GABA. Further, GABA preferentially colocalises with VIP, rather than AVP (Castel & Morris, 2000).

The data presented here shows expression of the transgenic reporter of vGAT in almost 60% of AVP-ir neurons in the SCN. This supports the idea that a majority of AVP neurons in the SCN can package GABA in vesicles. Whether these vesicles are shuttled to synaptic sites for release, however, is unknown. Indeed, electron microscopy studies have shown that although SCN AVP somata do produce GABA, small synaptic vesicles containing GABA are rare at AVP-expressing terminals (Buijs *et al.*, 1995; Castel & Morris, 2000). Instead, GABA is found co-packaged into large dense-core vesicles (LDCVs), typically thought to be neuropeptide specific (Castel & Morris, 2000). These GABA/peptide-containing LDCVs do not cluster at synaptic terminals, thus providing a mechanism whereby GABA could be released but not within a synaptic cleft. It is important to note that the terminals examined in these studies are intra-SCN microcircuits rather than projections to other brain regions.

For GABA to be packaged into LDCVs in projections, vGAT must still be present, however. Likewise, we cannot be certain that the projection fibres we see express vGAT. Cre expression is sufficient to turn on the tdTomato reporter throughout the neuron (in the *Vgat-cre:tdTomato* mouse line) as a whole but cannot tell us exactly where in the neuron vGAT is being expressed. Further, as discussed in Chapter 3, tdTomato expression is an indirect reporter of vGAT expression, and thus cre may have been expressed transiently prior to experimentation. Thus, whether these AVP neurons produce GABA may not entirely answer whether they are releasing it at these RP3V projections.

Using an anterograde tracer, like that in Chapter 4, to label those SCN *Avp-cre* neurons projecting to the RP3V, coupled with immunohistochemistry for vGAT would provide strong evidence as to whether vGAT is expressed at the projections near to kisspeptin neurons. The possibility exists that the presence of vGAT may be to transport GABA to LDCVs rather than small synaptic vesicles. Further, GABA is also able to be packaged via a second mechanism, the vesicular monoamine transporter 2 (vMAT2) (Tritsch *et al.*, 2012), however, the presence of vMAT2 in the SCN itself appears to be minimal, if at all present (Allen Brain Atlas: http://mouse.brain-map.org/experiment/show/79591703).

5.4.3 Limited synaptic innervation by *Avp-cre* neurons

The study in this chapter suggests that although an anatomical projection from *Avp-cre* neurons was observed (Chapter 4), these fibres do not largely constitute functional synaptic connections between the SCN and RP3V. Advances in viral vector-mediated delivery by retrograde monosynaptic rabies viruses (Callaway & Luo, 2015; Kim *et al.*, 2016) allow for viral vectors to be carried across a synapse from a specific population of cells to transfect the presynaptic neuronal populations. This tool could be used to target kisspeptin neurons in the RP3V to reveal whether the SCN AVP projections were, in fact, forming synapses. A second approach would be to use a viral vector that targets cre-dependent fluorescent proteins to

synapses in an anterograde method. Thus, injection of this virus to *Avp-cre* neurons would reveal whether there are synapses adjacent to kisspeptin neurons.

The electrophysiological evidence here suggests minimal synaptic communication between SCN *Avp-cre* and RP3V neurons, however, this does not exclude the fact that synapses may be present but not functional. It could be that *Avp-cre*-to-kisspeptin synapses lack $GABA_A$Rs explaining the lack of fast synaptic transmission (Figure 5.7a). There is, however, clear evidence that kisspeptin neurons are receiving $GABA_A$R-mediated inputs. The recordings shown in Figures 5.3, 5.4 and 5.6, actively demonstrate IPSCs onto RP3V neurons, indicating that the neurons recorded do receive GABAergic synaptic inputs from afferent populations, and these are releasing GABA acting at $GABA_A$Rs (Figures 5.2, 5.3). Further, there is clear synaptic innervation of the RP3V kisspeptin neurons from SCN *Nms-icre* neurons. The possibility remains that *Avp-cre* projections are forming silent synapses (i.e. those lacking postsynaptic receptors). Silent synapses are typically glutamatergic synapses lacking postsynaptic glutamate receptors (Vincent-Lamarre *et al.*, 2018); however, a subtype known as 'mute synapses' where postsynaptic $GABA_A$Rs are present, but there is no presynaptic GABA (or presynaptic GABA is unable to be released) have also been identified (Figure 5.7b) (Losonczy *et al.*, 2004; Bekkers, 2005). We cannot rule out the possibility that these *Avp-cre* neurons are forming synapses but are unable to functionally cause synaptic transmission.

The final possibility is that *Avp-cre* neurons are producing and releasing GABA, just not at synapses. Packaging of GABA to LDCVs would suggest they are released at sites in *Avp-cre* projection away from a synapse (Figure 5.7c) (Morris & Pow, 1991). Further, these LDCVs would require greater stimulation for release, rather than the paired pulses used here (Salio *et al.*, 2006). It has been shown that LDCVs in the SCN can be released from both dendrites and the soma (Castel *et al.*, 1996). Dendrites of the magnocellular AVP populations can also

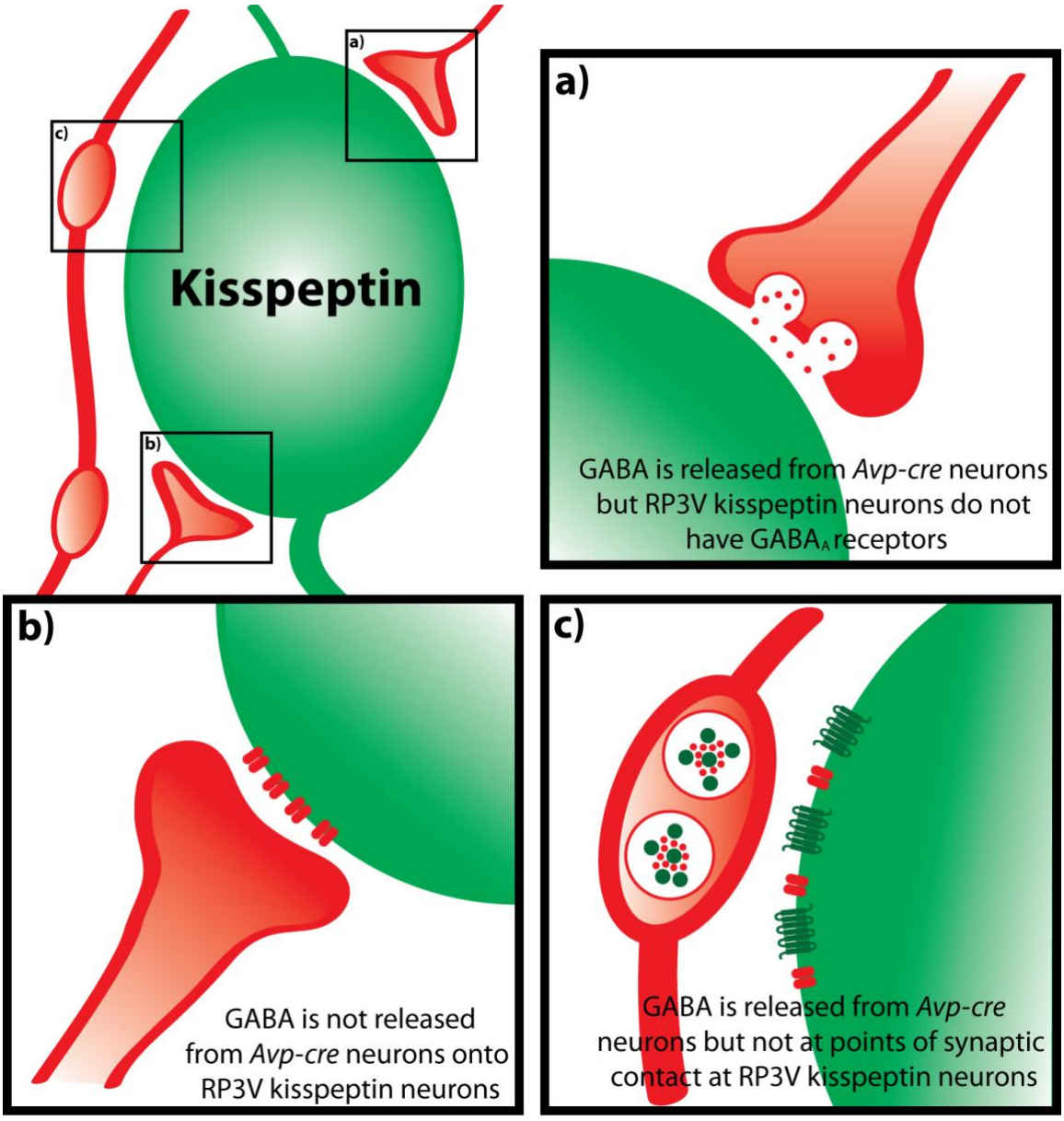

Figure 5.7: Potential mechanisms explaining minimal GABAergic synaptic transmission.

a) If synapses between *Avp-cre* neurons and kisspeptin neurons are present, they may be silent synapses where, even if GABA is released, the kisspeptin neuron cannot respond to it due to a lack of receptors. **b)** In contrast to that, the opposite may be true, where the kisspeptin neurons do have $GABA_AR$s, but GABA is not released from *Avp-cre* synapses. **c)** A third possibility is that the close appositions between *Avp-cre* projections and kisspeptin neurons are not synapses, but axonal swellings containing large dense-core vesicles (LDCVs). These vesicles may contain GABA, and $GABA_AR$s may be present at the kisspeptin neuron, however, the stimulation used here was not intense enough to drive the release of the LDCVs.

exocytose LDCVs containing AVP at distant nuclei (Pow & Morris, 1989; Ludwig & Leng, 2006; Son *et al.*, 2013). Thus, a possibility remains that these *Avp-cre* projections (whether dendritic or not remains unknown) could release GABA onto RP3V kisspeptin neurons away from synapses.

5.5 Summary

Despite robust anatomical evidence for innervation of RP3V kisspeptin neurons by SCN *Avp-cre* neurons, limited evidence was found for functional fast synaptic input. This suggests that these fibres may be sites of extrasynaptic release of GABA, or drive the activity of kisspeptin neurons through a mainly peptidergic mechanism. Interestingly, GABAergic synaptic transmission was seen from a second SCN population, comprised of *Nms-icre* neurons, to kisspeptin neurons. Of the 51 neurons recorded in the RP3V, only 3 exhibited *Avp-cre*-mediated inhibitory postsynaptic currents. Again, this is highly surprising as most of these *Avp-cre* neurons express vGAT, the membrane transporter that packages GABA into vesicles for release. As such, GABAergic synaptic transmission is not a means for SNC *Avp-cre* neurons to communicate with RP3V kisspeptin neurons. In the next chapter, the impact the SCN *Avp-cre* projections have on kisspeptin neurons must via the release of AVP was examined.

Chapter 6:

Regulation of Kisspeptin Neuron Action Potential Firing by SCN *Avp-cre* Neurons

6.1 Introduction

For successful ovulation in mammals, there must be a surge in the concentration of luteinising hormone (LH), occurring when oestradiol levels are highest. Kisspeptin neurons in the rostral periventricular region of the third ventricle (RP3V) are the key mediator of the LH surge, showing clear patterns of excitation in proestrus, at the time of the surge (Clarkson & Herbison, 2009). The integration of sex steroid feedback from the ovary, with a timing signal from the suprachiasmatic nucleus (SCN), makes kisspeptin neurons a key candidate in investigating the role that SCN-derived signals have at the RP3V, and how this may change throughout the oestrous cycle.

The key peptide from the SCN thought to drive an increase in the activity of kisspeptin neurons, prior to ovulation, is vasopressin (AVP). AVP can stimulate the LH surge in rodents lacking a functional SCN (Palm *et al.*, 2001; Miller *et al.*, 2006), and intracerebroventricular injection of an AVP receptor antagonist can significantly blunt the surge in intact animals (Funabashi *et al.*, 1999); although this has not been a consistent finding (Palm *et al.*, 2001; Miller *et al.*, 2006). There is evidence that changes in oestradiol concentrations affect AVP neuron interaction with kisspeptin neurons. Oestradiol treatment to ovariectomised (OVX) rodents increases the number of AVP-ir appositions to kisspeptin neurons (Vida *et al.*, 2010) and V1R gene expression in the RP3V (Kalamatianos *et al.*, 2004a; Smarr *et al.*, 2013). Further, AVP-mediated excitation of kisspeptin neurons is reduced following OVX, and enhanced in OVX mice treated with oestradiol (Piet *et al.*, 2015b), indicating that changes in oestradiol may underlie changes in functionality of the SCN to RP3V circuit. Together, these studies show that oestradiol is a critical regulator, to enhance the receptivity of this network. As oestradiol concentrations increase across the oestrous cycle, it could be that endogenous oestradiol feedback sets up, or primes this network at proestrus for optimal functionality at the time for the LH surge. However, little work has investigated how endogenous AVP released from SCN

neurons influences RP3V kisspeptin neurons, or how this may be dependent on oestrous cycle stage.

The studies in Chapter 4 of this thesis showed that *Avp-cre* projections from the SCN are in a prime position to release neuropeptides in the vicinity of the RP3V kisspeptin neurons. The studies in Chapter 5 showed that these projections rarely form functional GABAergic synapses onto RP3V kisspeptin neurons. Therefore, the experiments in this chapter sought to determine whether AVP is released from SCN *Avp-cre* projections in the RP3V, and how it influences the kisspeptin neuron activity over the oestrous cycle. The increase in oestradiol secretion from dioestrus to proestrus may drive changes in the excitability of the circuitry. Post ovulation, during oestrus, the drop in oestradiol secretion, and the rise in circulating progesterone, may also have an impact on the regulation of RP3V kisspeptin neuron activity by SCN AVP neurons. Measuring the functionality of this circuit across the oestrous cycle will determine how sex steroid feedback patterns may impact kisspeptin neuron responses to endogenous AVP release.

6.1.1 Frequency-dependent optogenetic stimulation

To drive the release of AVP from the projection fibres, a different stimulation protocol to that used in Chapter 5 was employed. AVP is packaged into large dense-core vesicles (LDCVs)which do not necessarily locate at synaptic release sites (Buijs *et al.*, 1999; Castel & Morris, 2000). The influx of calcium necessary to drive their release, therefore, must be greater than for small synaptic vesicles, which are adjacent to the membrane (van den Pol, 2012). Thus, a stimulation paradigm of greater frequency is necessary to drive the LDCV and, as such, AVP release. This has been shown previously to be necessary for neuropeptide release (Liu *et al.*, 2011; Schöne *et al.*, 2014; Qiu *et al.*, 2016; Piet *et al.*, 2018).

6.1.2 Hypothesis and aim

It was hypothesised that ***Avp-cre*** **neurons release AVP onto RP3V kisspeptin neurons and that the impact of this communication pathway fluctuates across the oestrous cycle such that RP3V kisspeptin neurons are optimally activated on the day the surge is generated**. The experiments carried out in this chapter aimed to **determine how stimulation of SCN *Avp-cre* projections impacts the action potential firing of RP3V kisspeptin neurons**. Further, the experiments aimed to determine **whether the effects vary throughout the oestrous cycle** in a manner consistent with a role for this circuit in activating RP3V kisspeptin neurons to generate the LH surge.

6.2 Methods

6.2.1 Animals

General animal information is outlined in Section 2.1. Adult female *Avp-cre:Kiss1-hrGFP* mice (2-6 months old) were used in this study. Oestrous cycles were determined by daily vaginal lavage and were used in stages outlined in each experiment.

6.2.2 Surgery

The general surgery procedures are outlined in Section 2.2. Here, mice were injected bilaterally with 400 nL/side of AAV-ChR2. Mice were left for at least two weeks to allow sufficient transduction of the viral vector prior to experimentation. Mice without transfection in the SCN due to an erroneous injection site were used as ‘off-target’ controls.

6.2.3 Acute brain slice preparation, identification of kisspeptin neurons and electrophysiology

The brain slicing procedure and electrophysiology has been outlined in Chapter 2. Identification of kisspeptin neurons has been outlined in Section 5.2.5. Prior to experimentation, the level of ChR2 transduction was determined by examining mCherry expression in the SCN. Mice were used for experiments when mCherry expressing neurons were easily visible in the SCN.

6.2.4 Optogenetic and electrophysiological protocols

The general brain slice electrophysiology procedure and recording configurations are outlined as part of Section 2.5.2. General optogenetic procedures are outlined in Chapter 5.

6.2.4.1 Neuropeptide bath application

Following patching of the kisspeptin neuron, baseline action potential activity was recorded for two minutes. AVP (500 nM; Sigma Aldrich) was then bath applied for two minutes to the brain slice. Recordings continued for another 9 minutes post-application.

6.2.4.2 Train optogenetic stimulation

As above, baseline kisspeptin neuron action potential activity was recorded for two minutes. Blue light was shone onto the RP3V for 60 s, at a frequency of 20 Hz (5 ms/pulse). Action potential frequency was then recorded for a further ten minutes post-stimulation.

6.2.5 Statistical analysis

General analysis methods are outlined in Section 2.7. Action potentials were analysed using threshold analysis in Clampex (see Section 2.5.2.1). In this chapter, where n-values are reported, n refers to neurons recorded, while N refers to the number of animals used in the experiments.

6.2.5.1 Analysis of kisspeptin neuron firing

Action potentials were grouped into 10-second bins and their average frequency in Hz was determined. The baseline frequency was the average frequency of the 120 s prior to the onset of stimulation or AVP wash. Immediate effects were considered those occurring during high-frequency light stimulation (HFLS) or the first 60 s of AVP wash. Delayed effects were those occurring within the five-minute period following the immediate effect period (Figure 6.1). Effects were qualified as either excitation (response exceeded baseline + 2 SD), inhibition (response exceeded baseline – 2 SD), or no change (response did not exceed baseline ± 2 SD). Where firing frequency varied by ≥ ± 2 SD of baseline firing rate in a single 10 s bin, two bins (20 s) immediately before and after were considered, and firing frequency over the entire 50 s period was averaged (Figure 6.1). In a number of recordings, multiple 10 s bins had changes greater than ± 2 SD of baseline. If those were not contiguous, the first bin varying by ≥ ± 2 SD of the 50 s averaged effect (Figure 6.1). If the bins were contiguous, the greatest change from baseline was considered the centre the 50 s average (Figure 6.1). The 50 s average was then compared to baseline to determine whether it still exceeded ± 2 SD; and was then considered either excitation, inhibition, or no change. No recording displayed responses comprised of both an inhibition and an excitation. Some recordings did not display a bin of greater than ± 2 SD. These cells were considered to not change. To determine the average response the bin with the greatest change (less than ± 2 SD) from baseline and the two contiguous bins either side were averaged and considered as the firing frequency in response to stimulation.

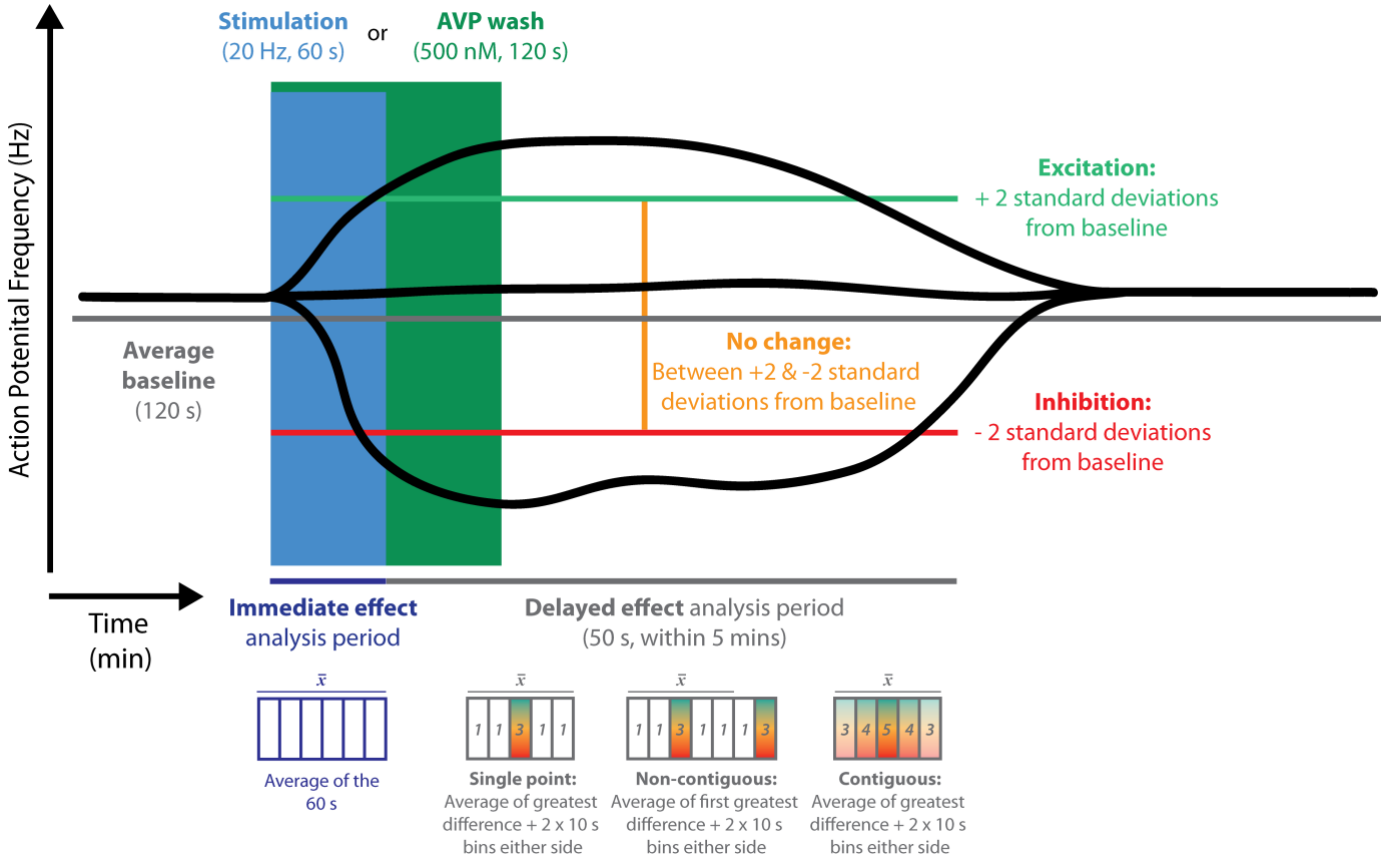

Figure 6.1: Analysis parameters for action potential frequency recordings over time.

Time course of experiments showing HFLS and AVP application. Analysis periods are marked, as well as criteria for effect. **Immediate effect:** The 60 s are averaged ($\bar{x}$) for the mean effect. **Delayed effect:** Responses either showed a single bin with the greatest frequency (denoted here by 3) exceeding ± 2 SD. The 2 bins either side were averaged with that point. If multiple bins displayed that greatest frequency but are not next to each other (non-contiguous), the first time it appears is considered the effect. If multiple bins next to each other (contiguous) exceed ± 2 SD, the greatest difference is the centre of the 50 s, and those either side are averaged.

6.2.5.2 Comparisons of firing rates

Action potential firing changes as a percent of baseline frequency were compared using a Friedman test with *post hoc* Dunn's multiple comparisons tests. Comparisons between oestrous cycle stages at specific time points were carried out using a Kruskal-Wallis test with *post hoc* Sidak test. Comparisons between oestrous cycle and bath application of drugs were carried out using Mann-Whitney tests. Comparisons of proportions of different neuron responses were carried out using a chi-squared test.

6.3 Results

6.3.1 Kisspeptin neurons do not change firing rate in response to high-frequency light stimulation in off-target control mice

First, to ensure that the ChR2 was able to be activated for 60 s, recordings of SCN *Avp-cre* neurons expressing ChR2 were made. Using on cell recordings of *Avp-cre* neurons with 60 s of 20 Hz light stimulation (Figure 6.2a) revealed that the ChR2 faithfully responded to blue light 86.7 ± 8.7% of the time (Figure 6.2b-c; n = 6 neurons, N = 2 mice).

Previous reports have suggested that HFLS of neuronal tissue can cause non-opsin mediated effects on neuronal activity (Stujenske *et al.*, 2015; Owen *et al.*, 2019). Thus, it was necessary to determine whether the HFLS used here would affect kisspeptin neuron activity. Dioestrous and proestrous *Avp-cre:Kiss1-hrGFP* mice, with off-target needle placement (i.e. AAV-ChR2 injected outside of the SCN resulting in no ChR2 expression in SCN *Avp-cre* neurons) were used to test this (Figure 6.3a).

None of the recorded neurons showed changes from baseline that met the criteria for excitation or inhibition (Table 6.1). Overall, HFLS of kisspeptin neurons did not change their

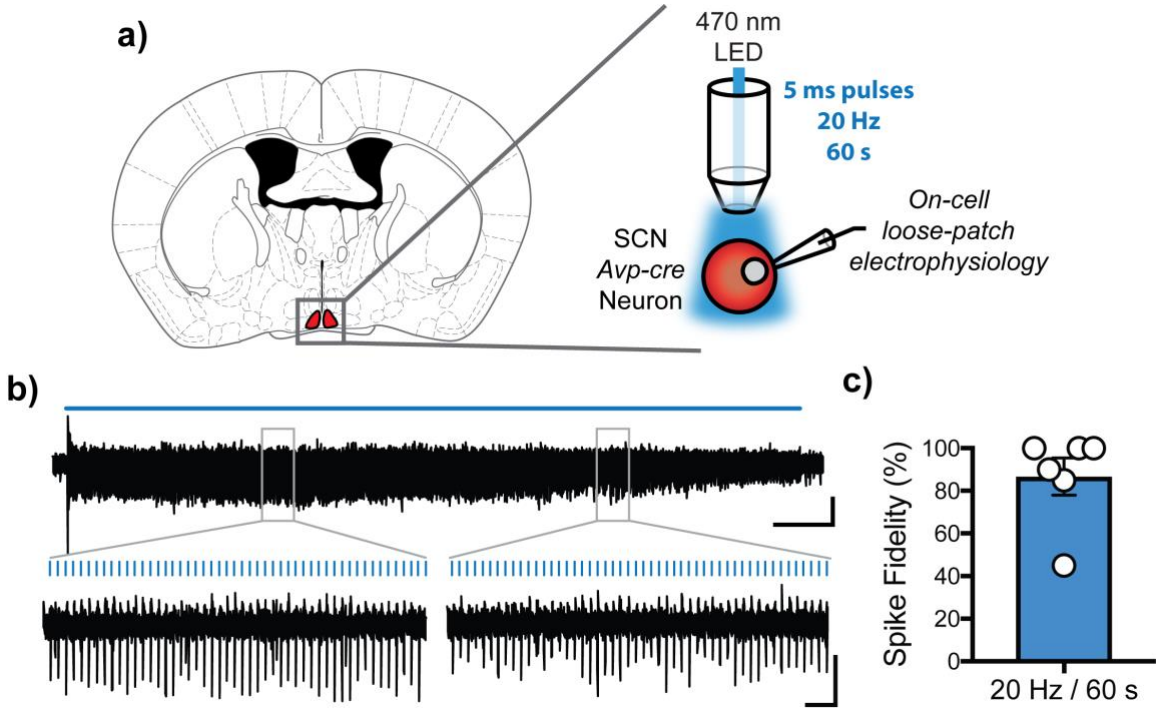

Figure 6.2: ChR2 function with high-frequency light stimulation.

a) Experimental setup. **b)** Example trace showing 60 s of 20 Hz stimulation of a ChR2-expressing *Avp-cre* neuron. Blue lines indicated 5 ms light pulses. Sharp deflections in the trace indicate action potential firing. **c)** Quantification of the fidelity of action potential firing at 20 Hz stimulation for 60 s. Scale bars = 20 pA/5 s (upper) and 20 pA/20 ms (lower). n = 6 neurons, N = 2 mice. Data shown as mean ± SEM. Representative brain slice taken from Franklin and Paxinos (2008).

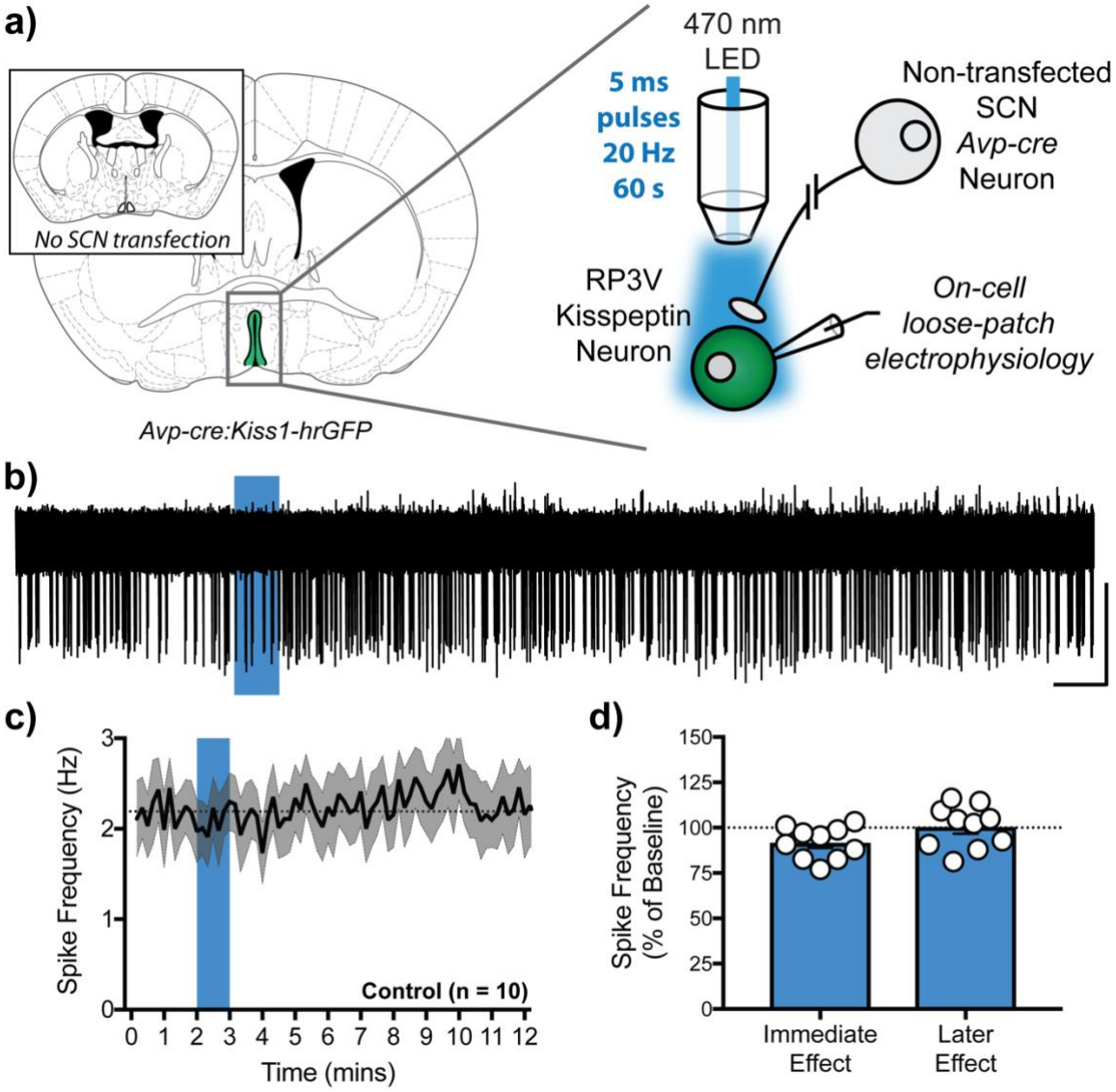

Figure 6.3: High-frequency light stimulation of *Avp-cre* neuron projections in animals with off target ChR2 transfection does not cause changes to kisspeptin action potential firing.

a) Experimental setup. **b)** Representative trace illustrating the effect of HFLS on action potential firing in a kisspeptin neuron in an *Avp-cre* mouse that had no detectable SCN transfection. **c)** Average time-course of action potential frequency over the recording period. **d)** Quantified changes of kisspeptin action potential frequency as a percentage of baseline frequency during the effect periods. Scale bars = 60 s/50 pA. Blue bars in b) and c) represent light stimulation. Data presented in c) and d) as mean ± SEM, dotted lines represent baseline. n = 10 neurons, N = 4 mice. Representative brain slice taken from Franklin and Paxinos (2008).

HFLS	Fig.	Immediate Effect				Delayed Effect			
		Excitation	No Change	Inhibition	Group mean	Excitation	No Change	Inhibition	Group mean
Control	6.3	0	10	0	91.7 ± 2.8%	0	10	0	100.4 ± 3.7%
Dioestrus	6.4	1	13	0	87.7 ± 7.3%	7	3	4	113.1 ± 13.8%
Proestrus	6.5	1	14	1	106.0 ± 12.8%	10	6	0	169.5 ± 16.9%
Proestrus + MC	6.6	0	10	1	90.6 ± 5.7%	2	8	1	109.9 ± 7.7%
Oestrus	6.7	0	3	9	57.3 ± 8.9%	0	11	1	78.4 ± 7.1%

Table 6.1: Individual and mean responses across the oestrous cycle to high frequency light stimulation.

The number of neurons showing responses in both the immediate and delayed effect periods, as per the criteria outlined in Section 6.2.6.3, are tabulated. The mean response from baseline from all the neurons recorded is also provided and presented as mean ± SEM. Yellow boxes indicate mean responses that are significantly different from baseline. Associated figures are referenced in the Fig. column.

firing rate in either the immediate or delayed response periods (Figure 6.3b-d; immediate: 91.7 ± 2.8% of baseline, p = 0.36; delayed: 100.4 ± 3.7% of baseline, p = 0.99; n = 10 neurons; N = 2 dioestrous and 2 proestrous mice; Friedman test with *post hoc* Dunn's multiple comparisons tests). These data show that the HFLS protocol used here, on its own, does not have any effect on RP3V kisspeptin neuron electrical activity.

6.3.2 Optogenetic stimulation of *Avp-cre* projections in dioestrus does not change kisspeptin neuron action potential firing

AAV-ChR2 was targeted to SCN *Avp-cre* neurons as shown previously (Figure 5.2). Although the *Avp-cre* projections were severed from the somata during brain slice preparation, ChR2-expressing fibres were still present in the RP3V (similar to the mCherry-expressing fibres shown in Chapter 4). Thus, HFLS of ChR2-expressing *Avp-cre* projections was carried out whilst recording RP3V kisspeptin neurons activity (Figure 6.4a).

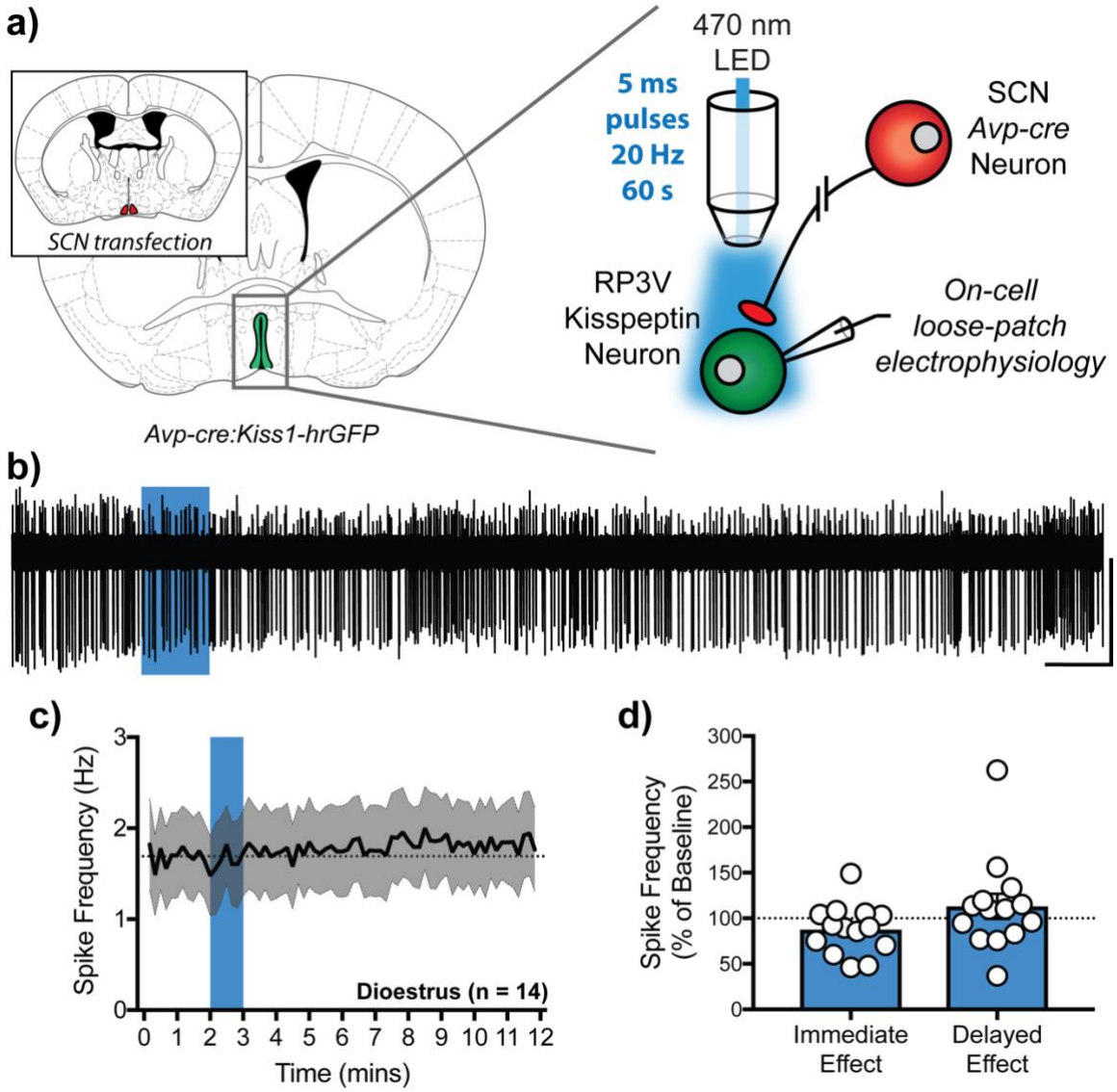

Figure 6.4: Kisspeptin neurons do not change action potential firing in response to high-frequency light stimulation of ChR2-expressing *Avp-cre* projections during dioestrus.

a) Experimental setup. **b)** Representative trace illustrating the effect of HFLS of ChR2-expressing *Avp-cre* projections on action potential firing from a kisspeptin neuron from a dioestrous mouse. **c)** Average time-course of action potential frequency over the recording period. **d)** Quantified changes of kisspeptin action potential frequency as a percentage of baseline frequency during the effect periods. Scale bars = 60 s/50 pA. Blue bars in b) and c) represent light stimulation. Data presented in c) and d) as mean ± SEM, dotted lines represent baseline. n = 14 neurons, N = 6 mice. Representative brain slice taken from Franklin and Paxinos (2008).

During the delayed effect period, there were varied effects of HFLS on kisspeptin neuron activity, with neurons some excited while others were inhibited (Table 6.1). Overall, HFLS did not result in significant changes to kisspeptin action potential firing in dioestrus (Figure 6.4b-d; immediate: 87.7 ± 7.3% of baseline, $p > 0.99$; delayed: 113.1 ± 13.8% of baseline, $p = 0.56$; $n = 14$ neurons; $N = 6$ mice; Friedman test with *post hoc* Dunn's multiple comparisons tests). These data suggest that while *Avp-cre* projections may either excite or inhibit individual RP3V kisspeptin neurons during dioestrus, the overall activity of the population is unaffected by HFLS of ChR2-expressing *Avp-cre* projections.

6.3.3 Optogenetic stimulation of *Avp-cre* projections in proestrus increases kisspeptin neuron action potential firing

The increasing oestradiol concentration and development of positive feedback in proestrus may increase the responsiveness of the RP3V kisspeptin neuron population. HFLS in proestrus caused the majority of kisspeptin neurons to be excited during the delayed period (Table 6.1). There was no group mean difference in action potential firing during the immediate response period (Figure 6.5; 106.0 ± 12.8% of baseline, $p > 0.99$, $n = 16$ neurons, $N = 7$ mice, Friedman test with *post hoc* Dunn's multiple comparisons test); however, there was a significant increase in the mean firing rate during the delayed response period (Figure 6.5; 169.5 ± 16.9% of baseline, $p = 0.001$, $n = 16$ neurons, $N = 7$ mice, Friedman test with *post hoc* Dunn's multiple comparisons test).

These data show that activating SCN *Avp-cre* projections excites RP3V kisspeptin neurons during proestrus.

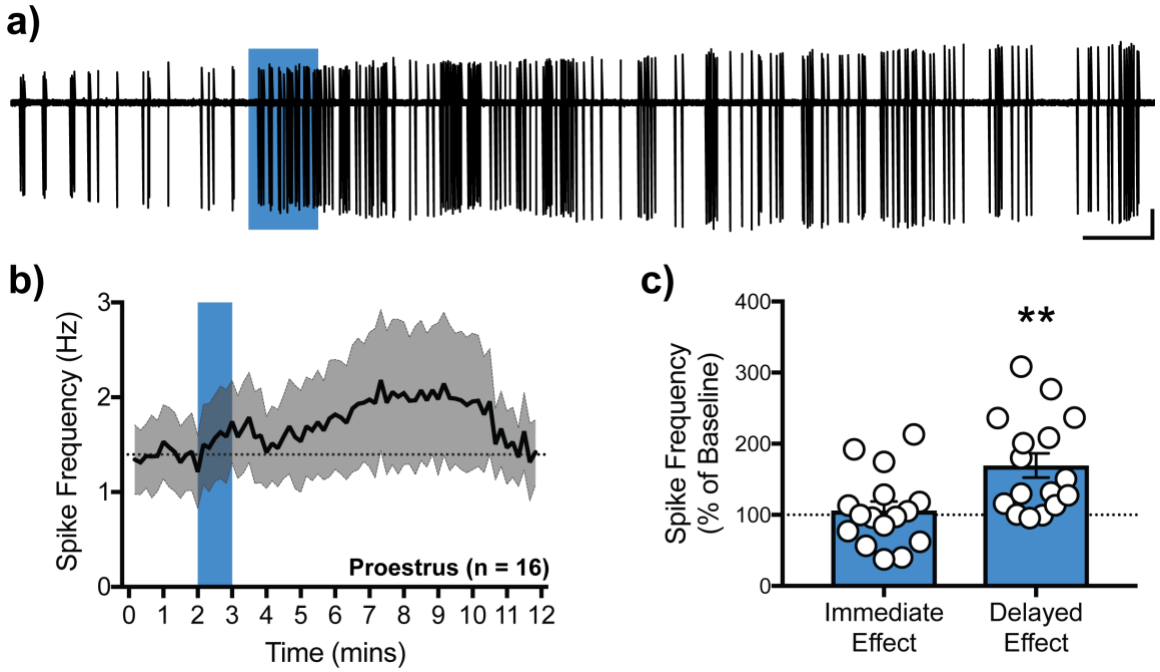

Figure 6.5: Kisspeptin neurons increase action potential firing in response to high-frequency light stimulation of ChR2-expressing *Avp-cre* projections during proestrus.

a) Representative trace illustrating the effect of HFLS of ChR2-expressing *Avp-cre* projections on action potential firing from a kisspeptin neuron from a proestrous mouse. **b)** Average time-course of action potential frequency over the recording period. **c)** Quantified changes of kisspeptin AP frequency as a percentage of baseline frequency during the effect periods. Scale bars = 60 s/50 pA. Blue bars in a) and b) represent light stimulation. Data presented in b) and c) as mean ± SEM, dotted lines represent baseline. n = 16 neurons, N = 7 mice. ** $p < 0.01$.

6.3.4 V1R antagonism prevents the increase in kisspeptin neuron action potential firing during proestrus

To address whether the activation of kisspeptin neurons in proestrus is due to AVP release, the V1R (and oxytocin receptor (OTR)) antagonist, Manning Compound (MC, 1 µM), was continuously bath applied to brain slices from proestrous *Avp-cre:Kiss1-hrGFP* mice throughout the recording period and the effect of HFLS tested. This experimental design was chosen due to the delayed and long-lasting nature of the effects seen in RP3V kisspeptin neurons in proestrus (Figure 6.5), which made repeated stimulation impractical.

During and following HFLS, the majority of kisspeptin neurons did not change their firing rate when ChR2-expressing SCN *Avp-cre* projections were stimulated in the presence of MC (Table 6.1; Figure 6.6a-c; immediate: 90.6 ± 5.7% of baseline, $p > 0.99$; delayed: 109.9 ± 7.7% of baseline, $p = 0.11$; $n = 11$ neurons; $N = 4$ mice; Friedman test with *post hoc* Dunn's multiple comparisons tests).

Furthermore, the delayed effect of HFLS in the presence of MC was significantly different to that seen in proestrus in the absence of the antagonist (Figure 6.6d; $p = 0.007$, Mann-Whitney test). There was also a non-significant trend towards a decrease in the proportion of kisspeptin neurons that were excited by HFLS in the presence of MC (Figure 6.6e; $p = 0.053$ vs proestrus, chi-squared test). These observations are consistent with the idea that AVP released from *Avp-cre* projections drives a delayed excitation of kisspeptin firing during proestrus.

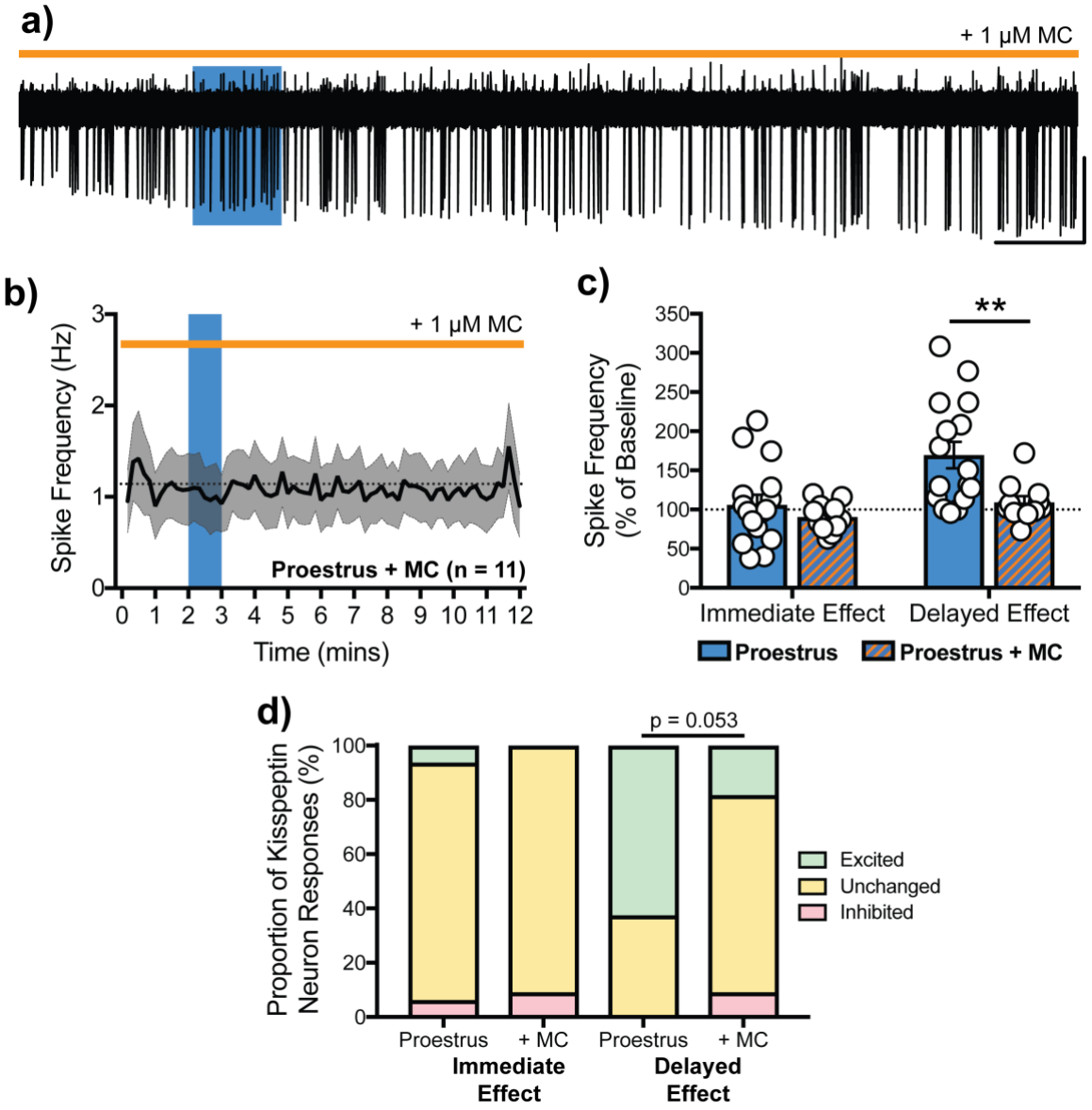

Figure 6.6: Manning Compound inhibits the increase in kisspeptin neuron action potential firing in response to high-frequency light stimulation of ChR2-expressing *Avp-cre* projections during proestrus.

a) Representative trace illustrating the effect of HFLS of ChR2-expressing *Avp-cre* projections on action potential firing from a kisspeptin neuron from a proestrus mouse in the presence of 1 µM Manning Compound (MC). **b)** Average time-course of action potential frequency over the recording period. **c)** Quantified changes of kisspeptin action potential frequency as a percentage of baseline frequency during the effect periods. **d)** The proportion of kisspeptin neurons responding in the absence or presence of MC, in proestrus. Data in proestrus from Figure 6.5. Scale bars = 60 s/50 pA. Blue bars in a) and b) represent light stimulation. Data presented in b), c) and d) as mean ± SEM, dotted lines represent baseline. Pro: n = 14 neurons, N = 6 mice; Pro + MC: n = 11 neurons, N = 4 mice. ** $p < 0.01$.

6.3.5 Optogenetic stimulation of *Avp-cre* projections in oestrus decreases kisspeptin neuron action potential firing

Next, it was investigated how kisspeptin neurons respond to HFLS of SCN *Avp-cre* projections during oestrus. First, it was noted that kisspeptin neurons in oestrus were predominantly silent (i.e. not firing action potentials). As such, only neurons that had a baseline firing frequency of 0.2 Hz or greater were used in this experiment.

The results seen following HFLS of SCN *Avp-cre* projections in oestrus were remarkably different to those seen in dioestrus and proestrus. During HFLS, 75% of kisspeptin neurons recorded were inhibited; this effect did not persist during the delayed period where hardly any neuron changed their firing frequency. No neuron was excited during or following HFLS (Table 6.1). This resulted in a significant decrease in kisspeptin action potential firing during the immediate effect period but not the delayed period following HFLS (Figure 6.7; immediate: 57.3 ± 8.9% of baseline, $p > 0.0002$; delayed: 78.4 ± 7.1% of baseline, $p = 0.063$; $n = 12$ neurons; $N = 5$ mice; Friedman test with *post hoc* Dunn's multiple comparisons tests)

These data indicate a switch in the impact of *Avp-cre* projections on RP3V kisspeptin neuron electrical activity: an inhibitory factor may rapidly dampen kisspeptin neuron firing, while released AVP may no longer stimulate their activity. These possibilities are addressed in later experiments.

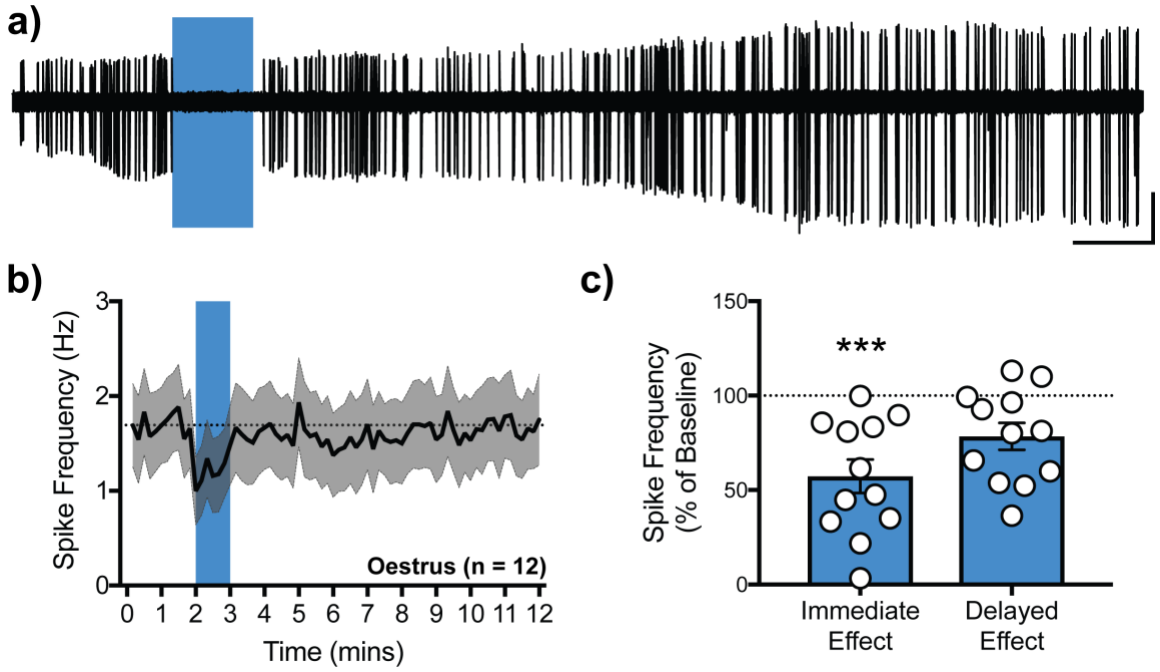

Figure 6.7: Kisspeptin neurons decrease action potential firing in response to high-frequency light stimulation of ChR2-expressing *Avp-cre* projections during oestrus.

a) Representative trace illustrating the effect of HFLS of ChR2-expressing *Avp-cre* projections on action potential firing from a kisspeptin neuron from an oestrous mouse. **b)** Average time-course of action potential frequency over the recording period. **c)** Quantified changes of kisspeptin AP frequency as a percentage of baseline frequency during the effect periods. Scale bars = 60 s/50 pA. Blue bars in a) and b) represent light stimulation. Data presented in b) and c) as mean ± SEM, dotted line at 100% represents baseline. n = 12 neurons, N = 5 mice. *** $p < 0.001$.

6.3.6 Oestrous cycle-dependent plasticity in RP3V kisspeptin neuron firing rates in response to light stimulation of SCN *Avp-cre* projections

The data presented thus far show differing responses throughout the oestrous cycle. There are two distinct response types with opposing effects on kisspeptin neuron electrical activity: an inhibitory response occurring during the light stimulation, almost exclusively during oestrus, and a delayed, excitatory response mediated by V1R activation mainly seen during proestrus. Figure 6.8 summarises these findings.

The immediate inhibitory response is significantly greater in oestrus than in proestrus (Figure 6.8a; $p = 0.015$, Kruskal-Wallis test with *post hoc* Dunn's multiple comparisons test). When looking at the proportions of cells which change their firing during this immediate period, there is a clear difference between oestrus and other experimental groups (Figure 6.8a; $p = 0.0003$ vs dioestrus, $p = 0.0008$ vs proestrus, chi-squared tests). There was no difference between the responses seen in dioestrus and proestrus (Figure 6.8a; $p = 0.64$, chi-squared test).

The delayed excitatory effect is significantly greater in proestrus compared with dioestrus or with oestrus (Figure 6.8b; $p = 0.013$ vs dioestrus, $p = 0.0006$, vs oestrus, Kruskal-Wallis test with *post hoc* Dunn's multiple comparisons tests). The proportions of neuron did not reach statistical significance between proestrus and dioestrus, (Figure 6.8b; $p = 0.061$, chi-squared test), although, responses in proestrus were significantly different compared to oestrus (Figure 6.8b; $p = 0.002$, chi-squared test). Further, the proportions of responses differed significantly between dioestrus and oestrus (Figure 6.8b; $p = 0.001$, chi-squared test).

Together, these data show a change in the patterns in which RP3V kisspeptin neurons respond to stimulation of SCN *Avp-cre* projections across the oestrous cycle.

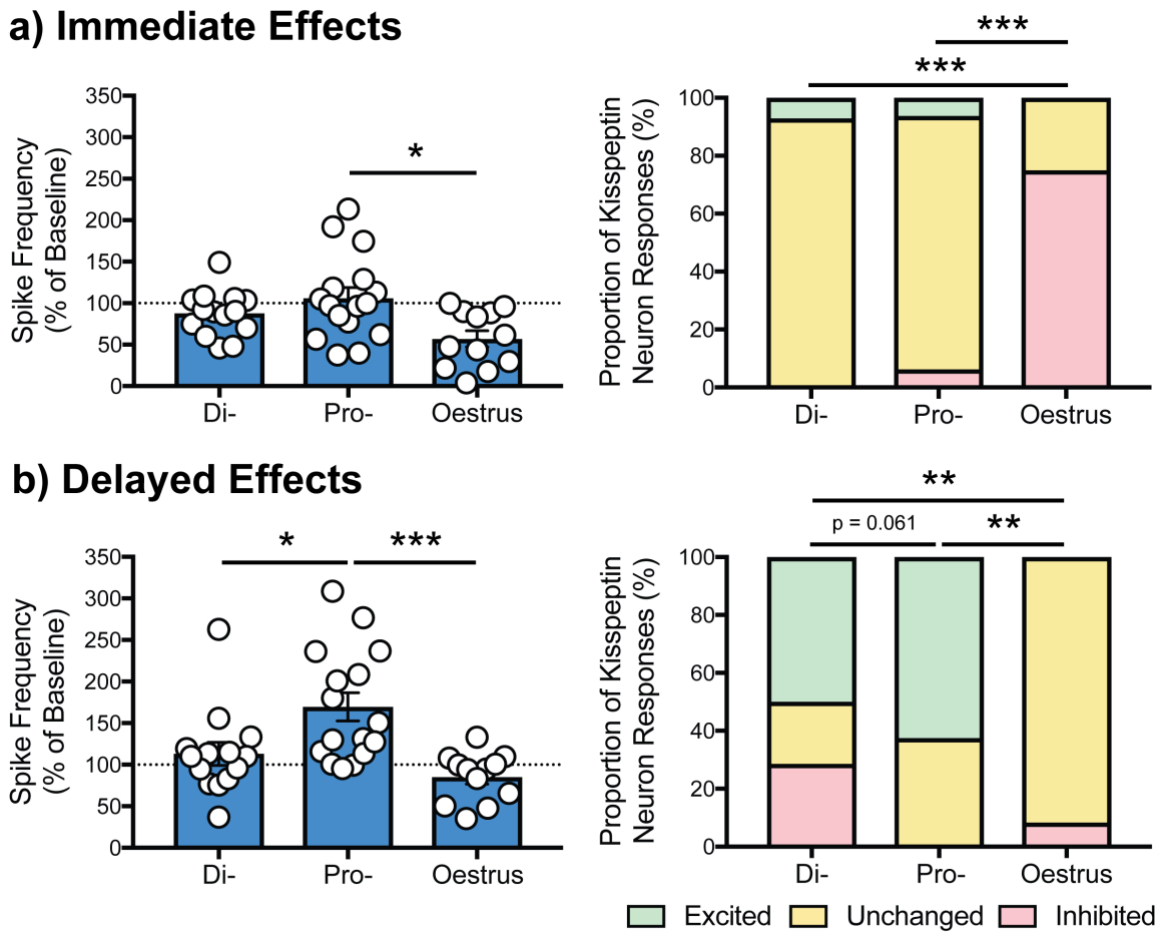

Figure 6.8: Summary of kisspeptin neuron response to HFLS of ChR2-expresing *Avp-cre* projections across the oestrous cycle.

a) During the immediate effect period, kisspeptin neurons in oestrus are inhibited by HFLS of ChR2-expressing *Avp-cre* projections. This response is significantly lower than that in proestrus. The proportion of neurons that are inhibited in oestrus is significantly higher than any response seen in neurons in di/proestrus. **b)** During the delayed effect period, kisspeptin neurons in proestrus are excited by HFLS of ChR2-expressing *Avp-cre* projections. This response is significantly greater than that seen in dioestrus and oestrus. The proportion of neurons that are excited in proestrus is significantly higher than the responses seen in oestrus. Data presented as mean ± SEM. Dotted line at 100% represents baseline. * $p < 0.05$, ** $p < 0.01$, *** $p < 0.001$.

6.3.7 $GABA_AR$ antagonism mitigates the decrease in kisspeptin neuron action potential firing in oestrus

Kisspeptin neurons in oestrus show an inhibition in their firing following HFLS of SCN *Avp-cre* projections with kinetics suggestive of amino acid neurotransmission (Schöne *et al.*, 2014; Piet *et al.*, 2018). As such, it was investigated whether the inhibitory neurotransmitter GABA, could be mediating this immediate effect. GABA has two main receptors, $GABA_A$ and $GABA_B$ receptors ($GABA_AR$, $GABA_BR$), both of which are expressed and have inhibitory effects in RP3V kisspeptin neurons (DeFazio *et al.*, 2002; Zhang *et al.*, 2013; Di Giorgio *et al.*, 2019). As the inhibitory response seen in oestrus is immediate, it is more likely that is it mediated by $GABA_AR$, a fast ion channel-mediated receptor, than by $GABA_BR$, a slow GPCR. Thus, the activation of $GABA_AR$ by *Avp-cre* projections during oestrus was investigated.

For this, a dual stimulation design was adopted, in which HFLS was carried out to identify kisspeptin neurons that were inhibited during light stimulation and was repeated in the absence or in the presence of 5 µM gabazine (GBZ), a $GABA_AR$ antagonist (Figure 6.9a, b). This allows for direct comparisons within the same recording of individual neurons. To ensure that the second stimulation was sufficient to drive inhibition of kisspeptin neurons, a second HFLS was repeated 12 minutes after the first HFLS in the absence of any drugs. Both the first and second HFLS resulted in action potential firing in RP3V kisspeptin neurons significantly inhibited below baseline, with no difference in the extent of inhibition between stimulations below baseline (Figure 6.9a, c; first: 72.7 ± 6.2% of baseline, $p = 0.028$; second: 77.2 ± 8.2% of baseline, $p = 0.028$, $n = 6$ neurons, $N = 3$ mice, Friedman test with *post hoc* Dunn's multiple comparisons tests). The ratio between the two stimulations was 1.05 ± 0.07 (Figure 6.9d).

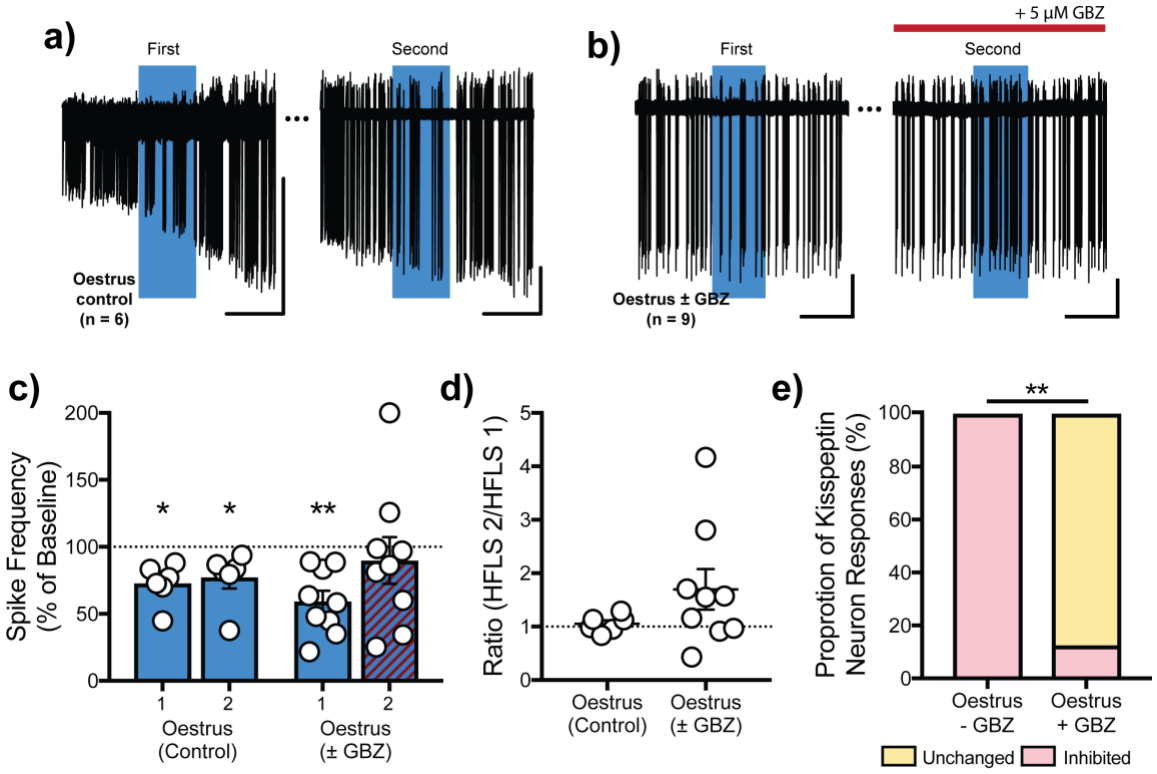

Figure 6.9: Gabazine reduces the decrease in kisspeptin neuron action potential firing in response to high-frequency light stimulation of ChR2-expressing *Avp-cre* projections during oestrus.

a) Representative trace illustrating the effect of two HFLS of ChR2-expressing *Avp-cre* projections on action potential firing from a kisspeptin neuron from an oestrous mouse (oestrus control). **b)** Representative trace illustrating the effect of two HFLS of ChR2-expressing *Avp-cre* projections on action potential firing from a kisspeptin neuron from an oestrous mouse, the second stimulation being in the presence of 5 µM gabazine (GBZ; oestrus ± GBZ). **c)** Quantified changes of kisspeptin AP frequency as a percentage of baseline frequency during the first (1) and second (2) HFLS in oestrus control and oestrus ± GBZ. **d)** Ratio of normalised firing rates comparing the second HFLS to the first. **e)** The proportion of kisspeptin neurons inhibited during HFLS in the presence of GBZ is significantly lower than without GBZ. Scale bars = 60 s/50 pA. Blue bars in a) and b) represent light stimulation. Data presented in c) and d) as mean ± SEM, dotted line in c) represents baseline, dotted line at 1 in d) indicates the value at which both first and second stimulations had an equal effect. Control: n = 6 neurons, N = 3 mice; ± GBZ: n = 9 neurons, N = 5 mice. * $p < 0.05$, ** $p < 0.01$.

HFLS	Immediate Effect			
	Excitation	No Change	Inhibition	Group mean
Oestrus - GBZ	0	0	9	59.2 ± 8.0%
Oestrus + GBZ	0	8	1	89.8 ± 17.4%

Table 6.2: Individual and mean responses during oestrus with and without gabazine, to high-frequency light stimulation.

The number of neurons showing responses in the immediate effect period, as per the criteria outlined in Section 6.2.6.3, are tabulated. The mean response from baseline from all the neurons recorded is also provided and presented as mean ± SEM. Yellow boxes indicate mean responses that are significantly different from baseline. This table is associated with Figure 6.9.

In a group of neurons, GBZ was bath applied after the first HFLS until the end of the recording (including throughout the second HFLS). While the first HFLS significantly decreased firing during the immediate period, the second HFLS in the presence of GBZ did not (Table 6.2, Figure 6.9b, c; first: 59.2 ± 8.0% of baseline, $p = 0.007$; second + GBZ: 89.8 ± 17.4% of baseline, $p = 0.19$, $n = 9$ neurons, $N = 5$ mice, Friedman test with *post hoc* Dunn's multiple comparisons tests). The ratio of the responses with and without GBZ was 1.70 ± 0.38 (Figure 6.9d). There was no difference between the extent of inhibition before and during GBZ application (Figure 6.9c; HFLS 1 vs HFLS 2: $p = 0.72$, Friedman test with *post hoc* Dunn's multiple comparisons test), nor between the response ratios in the two groups (Figure 6.9e; $p = 0.22$, Mann-Whitney test). There was a significant difference, however, in the proportion of neuron inhibited by HFLS (Figure 6.9e; $p = 0.0009$, chi-squared test).

Together the results of these experiments suggest that the immediate inhibition may be driven by activation of $GABA_AR$s.

6.3.8 AVP has oestrous cycle-dependent effects on kisspeptin neuron firing

The findings presented here show an effect for AVP released from SCN projections exciting kisspeptin neurons during proestrus. There is no delayed excitation seen in either dioestrus or oestrus. This could be due to either 1) AVP not being released, 2) AVP released

but not able to cause an effect by not interacting with receptors, 3) V1Rs not responding to released AVP because they are not present on the kisspeptin neurons, or due to impaired downstream signalling. To gain insight into this, kisspeptin neuron responsiveness to exogenous AVP across the oestrous cycle was investigated to test the third possibility.

As found previously (Piet *et al.*, 2015b), 500 nM AVP excited the majority of RP3V kisspeptin neurons in dioestrus and proestrus (Table 6.3). Both groups were similarly excited with significant increases in action potential firing following AVP application (Figure 6.10a, c, d, f, g; dioestrus: 228.8 ± 28.6% of baseline, n = 8 neurons, N = 3 mice, p = 0.004, proestrus: 184.2 ± 20.1% of baseline, n = 11 neurons, N = 3 mice, p = 0.0008, Friedman test with *post hoc* Dunn's multiple comparisons tests; dioestrus vs proestrus: p > 0.99, Kruskal-Wallis test on effect values with *post hoc* Dunn's multiple comparisons test; p = 0.91, chi-squared test on proportions responding).

During oestrus, however, a contrasting response was found, where kisspeptin neurons no longer responded to AVP application. While some kisspeptin neurons still responded to AVP during oestrus, the majority did not (Table 6.3). The mean response, however, was not significantly different to baseline (Figure 6.10b, e; 91.44 ± 16.5% of baseline, n = 10 neurons, N = 3 mice, p > 0.99, Friedman test with *post hoc* Dunn's multiple comparisons test). The response seen in oestrus was significantly lower than the responses seen in dioestrus and proestrus (Figure 6.10f; p = 0.002 vs dioestrus, p = 0.013 vs proestrus, Kruskal-Wallis test with *post hoc* Dunn's multiple comparisons test). When the proportions of neurons responding were compared, the proportion responding to AVP application was significantly lower in oestrus than dioestrus and proestrus (Figure 6.10g; p = 0.027 vs dioestrus, p = 0.045 vs proestrus, chi-squared tests).

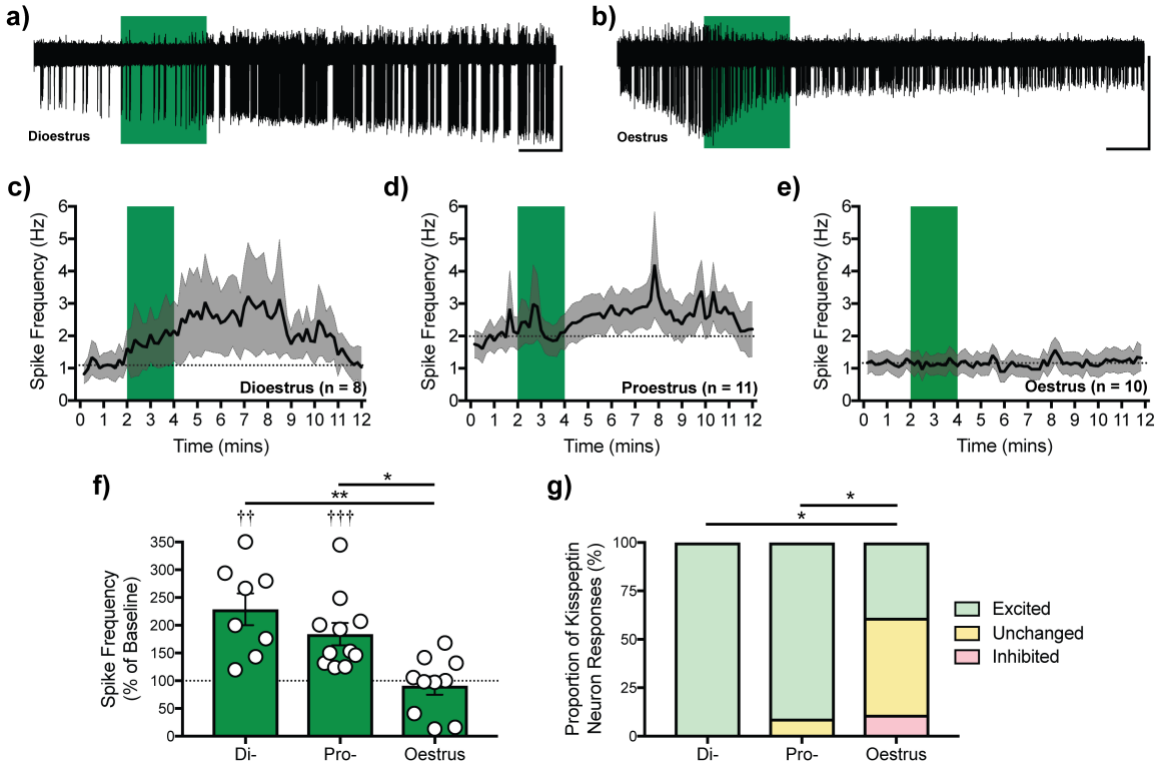

Figure 6.10: AVP application to kisspeptin neurons has different effects over the course of the oestrous cycle.

a) Representative trace illustrating the effect of 500 nM AVP on action potential firing from a kisspeptin neuron from a dioestrous mouse. **b)** Representative trace illustrating the effect of 500 nM AVP on action potential firing from a kisspeptin neuron from an oestrous mouse. **c-e)** Average time-course of action potential frequency over the recording period in dioestrus, proestrus and oestrus. **f)** Quantified changes of kisspeptin action potential frequency as a percentage of baseline frequency during the delayed effect period. **g)** The proportion of kisspeptin neuron responses to AVP, over the oestrous cycle. Scale bars = 60 s/50 pA. Green bars in a) to e) represent AVP application. Data presented in c) - f) as mean ± SEM, dotted lines represent baseline. Di: n = 8 neurons, N = 3 mice; Pro: n = 11 neurons, N = 3 mice; Oestrus: n = 10 neurons, N = 3 mice. †† $p < 0.01$ compared to baseline, ††† $p < 0.001$ compared to baseline, * $p < 0.05$ compared to other groups, ** $p < 0.01$ compared to other groups.

AVP Application	Delayed Effect			
	Excitation	No Change	Inhibition	Group mean
Dioestrus	8	0	0	228.8 ± 28.6%
Proestrus	10	1	0	184.2 ± 20.1%
Oestrus	4	5	1	91.4 ± 16.5%

Table 6.3: Individual and mean responses across the oestrous cycle to AVP application.

The number of neurons showing responses in both the immediate and delayed effect periods, as per the criteria outlined in Section 6.2.6.3, are tabulated. The mean response from baseline from all the neurons recorded is also provided and presented as mean ± SEM. Yellow boxes indicate mean responses that are significantly different from baseline. This table is associated with Figure 6.10.

As such, the data here show that kisspeptin neurons are less responsive to AVP in oestrus, compared to preovulatory cycle stages. This may explain the lack of a delayed response to HFLS in kisspeptin neurons in oestrus. In kisspeptin neurons in dioestrus, however, other mechanisms may be at play.

6.4 Discussion

The data presented in this chapter show contrasting responses of RP3V kisspeptin neuron action potential firing following stimulation of SCN *Avp-cre* neuron projections, throughout the murine oestrous cycle. In dioestrus, when sex steroids predominantly drive negative feedback, some kisspeptin neurons were excited in response to stimulation of SCN *Avp-cre* projections (Table 6.1; Figure 6.4), while in proestrus, when positive feedback occurs, a greater number of kisspeptin neuron increased their firing HFLS (Table 6.1; Figure 6.5). Following ovulation, the excitatory effects of stimulating SCN *Avp-cre* projections were lost, and a striking immediate inhibition of kisspeptin neurons occurs (Figure 6.7). During dioestrus, some neurons were inhibited by HFLS, although this inhibition was kinetically distinct to that seen in oestrus. This suggests that there is a cyclical, progressive shift in the different actions of SCN *Avp-cre* projections on RP3V kisspeptin neurons (Figure 6.11).

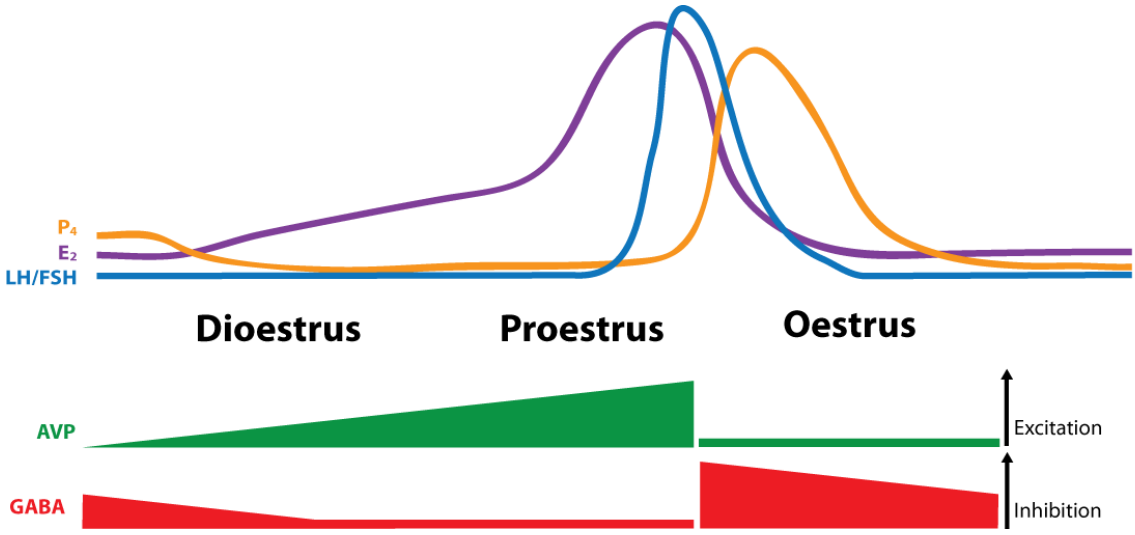

Figure 6.11: A working model of plastic changes in SCN AVP- and GABA-mediated effects occur over the oestrous cycle.

Dioestrus: There is a period of quiescence, where there is no overall change in the firing rate of the RP3V kisspeptin neuron population. **Proestrus:** As the concentration of E_2 rises, there is a concurrent increase in the proportion of RP3V kisspeptin neurons excited by AVP released from SCN neurons. This drives an overall excitation of the GnRH neuronal network to trigger the LH surge at the end of proestrus. **Oestrus:** As the concentration of E_2 falls, and the concentration of P_4 rises, there is a switch at the level of the SCN, whereby the projections begin releasing GABA. This results in an inhibition of the kisspeptin population, inhibiting the GnRH neuronal network.

The excitation seen at proestrus is mediated by action at the V1R (Figure 6.6). AVP application excited kisspeptin neurons to a similar extent between dioestrus and proestrus (Figure 6.10), indicating no change in V1R signalling in kisspeptin neurons prior to ovulation, but potentially a change in the AVP release from the SCN, or poor access to V1Rs in dioestrus. The immediate inhibition in oestrus is not seen in any other oestrous cycle stages. When SCN *Avp-cre* projections are stimulated in proestrus in the presence of Manning Compound, that immediate inhibition is not revealed. Thus, this suggests that is solely an effect at oestrus, rather than one masked by the AVP-mediated excitation. This inhibition at oestrus may be attributed to the release of GABA, acting at $GABA_A$Rs (Figure 6.9)

Together these data suggest a functionally plastic circuitry whereby SCN *Avp-cre* neurons can either excite or inhibit RP3V kisspeptin neurons in an oestrous cycle stage-dependent manner.

6.4.1 Technical caveats

To identify the kisspeptin neurons, blue light must be shone on the brain slice to excite GFP. The excitation spectrum of the GFP and that of ChR2 overlap, thus, it cannot be ruled out that visualising kisspeptin neurons may also drive electrical activity in ChR2-expressing terminals and, consequently, the release of neurotransmitters and neuropeptides. In order to overcome this, the intensity of blue light was different for identification of GFP-expressing cells (0.8 mW) and stimulation of ChR2-expressing axons (14.1 mW). Identification of the kisspeptin neurons may still drive neurotransmitter release due to activation of the ChR2. Between identification and recording, there was a wait period of 5-10 minutes before recording. This method has been used previously to ensure that no response to the initial light stimulus is ongoing when a loose-patch recording is formed (Piet *et al.*, 2018). Further, as the delayed excitation effect seen in Section 6.3.3 appears to last for less than ten minutes, this wait time

was likely sufficient for the neuron to recover from any stimulation of ChR2- expressing *Avp-cre* fibres.

Light sources in optogenetics have recently come under criticism for potential non-opsin-mediated effects due to heating of the tissue (Stujenske *et al.*, 2015; Owen *et al.*, 2019). These experiments have been carried out using LED lighting through a 40× immersion objective. Prolonged light stimulation can cause undesirable thermal effects due to heating of tissues (Stujenske *et al.*, 2015; Dong *et al.*, 2018), however, it appears that the light stimulation paradigm used in these experiments, 20 Hz for 60 s, does not result in negative effects of light stimulation (such as heat altering the activity of neurons). The control experiments carried out in Section 6.3.1 confirm that there are no unintended light-mediated effects. Interestingly, higher intensity light stimulation (53.9 mW, compared to 14.1 mW in these experiments) was found to completely inhibit kisspeptin neuron electrical activity (Appendix VIII), possibly due to heat or phototoxicity of neurons from the light source.

SCN neurons typically fire between 1-12 Hz (Green & Gillette, 1982; Pennartz *et al.*, 2002; Schaap *et al.*, 2003), peaking during the subjective afternoon of the light phase (Inouye & Kawamura, 1979; Green & Gillette, 1982; Schaap *et al.*, 2003). This afternoon increase in firing rate, is correlated to when AVP could be released, and potentially initiate the LH surge. The stimulation frequency used here can be considered paraphysiological, as it is above the expected peak firing rate, but can still reliably drive neuropeptide release without negatively affecting the tissue.

As this is a circadian network, one potentially important caveat to consider is the role of time as a confound. Prior work has not found a significant impact of time on how kisspeptin neurons respond to AVP (Piet *et al.*, 2015b), thus, it is unlikely that time is affecting how kisspeptin neurons respond to the endogenous AVP. As such, however, the expression of AVP is certainly circadian (van der Veen *et al.*, 2005; Maruyama *et al.*, 2010; Yoshikawa *et al.*, 2015). While these studies have examined AVP expression in the cell bodies of the SCN, there

is a possibility that export of the peptide occurs later in the day, closer to the time of the LH surge. As such, when brain slices were taken during the peak of AVP expression, export of AVP to projections in the RP3V may not be complete. As such, the responses seen here may be due to limited projection peptide content. If brain slices were taken later in the day, there is a possibility that the endogenous AVP release may drive greater effects, particularly in proestrus resulting in a more pronounced excitatory effect.

6.4.2 A delayed excitation of kisspeptin neurons is mediated by AVP

The results presented in this chapter show oestrous cycle-dependent changes in the manner that SCN *Avp-cre* projections can alter the activity of RP3V kisspeptin neurons. The experiments in Chapter 5 revealed that there is little or no functional synaptic input from SCN *Avp-cre* neurons to RP3V kisspeptin neurons, regardless of oestrous cycle stage. Taking this into consideration, the effects observed in this chapter must, therefore, be due to non-synaptic release of neuropeptides and neurotransmitters.

Fast synaptic neurotransmitters are localised near the synaptic membrane, thus individual action potentials are sufficient to cause low concentration calcium fluxes which drive their release at the synaptic terminal. This can be seen in Chapter 5 where single stimulations can evoke GABA release (Section 5.3.5). Neuropeptides, however, typically display a distinct uncoupled response to action potentials (Salio *et al.*, 2006). Due to neuropeptide packaging in LDCVs away from the synaptic membrane, a diffuse calcium signal due to repeated local depolarisation (i.e. multiple action potentials driving prolonged calcium influx) is necessary for their release. *In vitro*, short high-frequency stimulation of presynaptic terminals has been used to induce neuropeptide release (Liu *et al.*, 2011; Schöne *et al.*, 2014; Qiu *et al.*, 2016; Piet *et al.*, 2018)

Exocytosis of LDCVs away from synaptic membranes allows for neuromodulators to be released more diffusely to influence nearby neurons in a paracrine manner, rather than as a direct, synaptically targeted action (Morris & Pow, 1991). SCN neurons have been shown to release peptides from dendritic and axonal projections (Castel *et al.*, 1996), thus, it could be that the SCN *Avp-cre* neurons are releasing AVP from their projections identified in Chapter 4, which then diffuses to the nearby kisspeptin neurons. This is a feature that has been seen for AVP release by magnocellular AVP neurons from the PVN/SON onto their downstream targets (Ludwig & Leng, 2006; Son *et al.*, 2013).

Stimulation of SCN *Avp-cre* projections increased kisspeptin neuron firing, a response that was delayed and long-lasting, typical of GPCR-mediated effects. As the data presented in Chapter 4 indicate that PVN and SON neurons do not project to the RP3V, it is unlikely that this increase was mediated by anything other than a peptide released from SCN *Avp-cre* neurons. The excitation of kisspeptin neurons following HFLS of the *Avp-cre* projections is prevented in the presence of Manning Compound. Manning Compound is an antagonist of both V1Rs and the OTR (Manning *et al.*, 2012; Busnelli *et al.*, 2013). RP3V kisspeptin neurons express V1aRs (Williams *et al.*, 2011), but probably not V1bRs (Funabashi *et al.*, 2000a). Furthermore, previous electrophysiological studies suggest that RP3V kisspeptin neurons do not express OTRs (Piet *et al.*, 2015b). As the SCN does not synthesise oxytocin, it is, therefore, likely that this excitation is solely mediated by AVP.

The key question remaining is the mechanism behind how HFLS-induced excitation varies throughout the oestrous cycle. This could be due to several possibilities: changes in V1R function and/or expression on kisspeptin neurons, changes in the release of AVP from the SCN, or changes in the access of AVP to V1Rs on kisspeptin neurons. These will now be discussed in turn.

6.4.2.1 Changes in V1R expression across the oestrous cycle

Over the course of the oestrous cycle, the fluctuating hormone concentrations may be impacting the function and/or expression of V1R on the RP3V kisspeptin neurons. V1aRs have been shown to be present on kisspeptin neurons in oestradiol-treated hamsters (Williams *et al.*, 2011); as well as being responsive to AVP application at kisspeptin neurons (both here and by Piet *et al.* (2015b)). Interestingly, however, it appears that ovariectomy (OVX) is sufficient to inhibit the action of AVP at kisspeptin neurons, which is restored by oestradiol replacement (Piet *et al.*, 2015b). OVX is a blunt method of removing the influence of ovarian hormones, thus the loss of hormones, correlated to the loss of V1R signalling at the kisspeptin neurons suggests some sex steroid-mediated regulation of V1R expression. Kalamatianos *et al.* (2004a) provide some indication that V1aR in the RP3V restored by oestradiol replacement following OVX. Thus, it appears that the concentration of oestradiol may be a key driving factor in the expression of V1aRs.

Considering that kisspeptin neurons are able to respond to AVP application in dioestrus and proestrus to similar extents, the increasing oestradiol concentration does not appear to potentiate or upregulate V1R activity. However, the fall in oestradiol during oestrus may account for the loss of V1R-mediated effects at kisspeptin neurons. Oestrus is further characterised by a high progesterone concentration. However, no studies to date have addressed the effects of progesterone or its metabolites on V1R expression or function.

6.4.2.2 Changes in AVP synthesis and release across the oestrous cycle

A second possibility (although not an exclusive one) may be that the production and release of AVP from *Avp-cre* neurons fluctuates over the oestrous cycle. The data in dioestrus point to this possibility, as although RP3V kisspeptin neurons can respond to exogenous AVP, the release of endogenous AVP may not be driven by HFLS, like it can in proestrus. In oestrus, it is harder to determine how AVP release is impacted. In this case, V1R-mediated responses (as mentioned above) are the proxy for AVP release and action. As kisspeptin neurons no longer

respond to exogenous AVP in oestrus, the proxy to determine AVP release is no longer able to be used. Thus, it remains unknown whether AVP release is occurring in oestrus and is simply unable to exert an effect. Advances in sniffer cell techniques, where cells are transfected with V1Rs provides a fluorescent insight mediated by calcium flux as to whether AVP is released and acts at receptors (Son *et al.*, 2013; Gizowski *et al.*, 2016; Zaelzer *et al.*, 2018), would provide a more conclusive result as to changes in AVP release across the oestrous cycle.

The change in hormone profile across the oestrous cycle could be linked to changes in AVP production (Figure 6.12). If SCN AVP production is linked to oestradiol concentrations it must be through activation of ERβ. As mentioned, the SCN has little to no ERα (Shughrue *et al.*, 1997; Vida *et al.*, 2008). This is not unheard of, with AVP cells in culture increasing the production of *Avp* mRNA in response to ERβ activation (Shapiro *et al.*, 2000; Pak *et al.*, 2007). Thus, the increase in oestradiol towards proestrus could increase the amount of AVP produced. During oestrus, the rise in progesterone may also play a role in the inhibition of AVP release. Activation of PR in AVP neurons has been shown to inhibit the production of AVP (Auger & Vanzo, 2006), potentially acting as a second mechanism (along with the fall in oestradiol at oestrus) to stop the release of AVP. It is important to note here that these studies looking at hormone action on AVP production have predominantly been carried out on AVP neurons from elsewhere in the brain, rather than the SCN; however, this does not rule out the possibility that similar effects may happen at SCN AVP neurons.

A further point to consider is that AVP release from these projections may not have access to V1Rs. Vida *et al.* (2010) suggest that increased concentrations of oestradiol (similar to proestrus) may increase the number of appositions between kisspeptin and AVP-ir fibres. The fall in oestradiol concentration between proestrus and oestrus, may result in ultrastructural remodelling of the appositions resulting in their withdrawal (Figure 6.12). Thus, any AVP released in the extracellular fluid may not be able to diffuse far enough to act in a paracrine

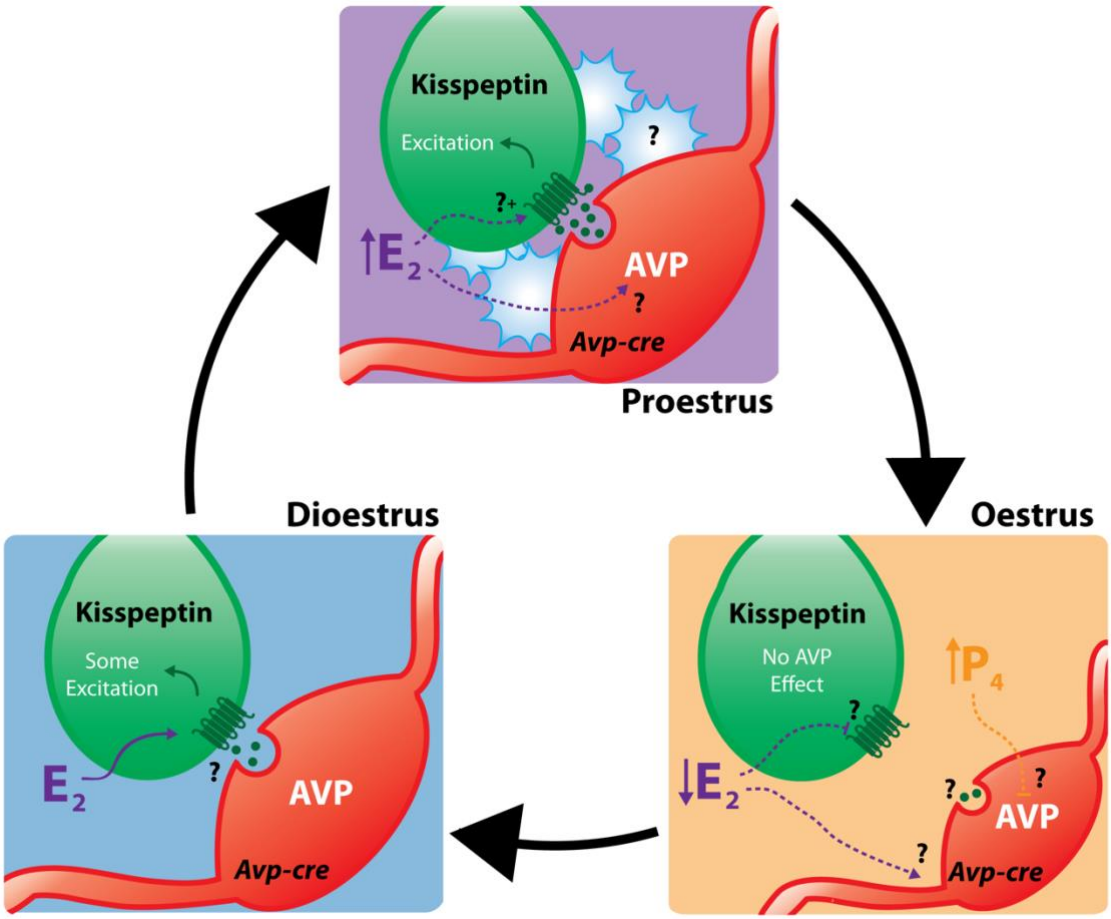

Figure 6.12: Potential changes to the SCN AVP system across the oestrous cycle.

Dioestrus: An intermediate period between oestrus and proestrus. The basal levels of E_2 maintain V1R expression on RP3V kisspeptin neurons. Some AVP is released from *Avp-cre* projections which is sufficient to excite some RP3V kisspeptin neurons, but the whole population overall. **Proestrus:** Increased E_2 concentrations may increase V1R expression on RP3V kisspeptin neurons, as well as increasing the production and release of AVP. Further, there is a possibility that increased astrocyte density in the RP3V forms a barrier to limit AVP diffusion targeting it to kisspeptin neurons. As a result, RP3V kisspeptin neurons are activated overall by SCN *Avp*-cre neurons. **Oestrus:** Post-ovulation, the fall in E_2 may decrease V1R expression on RP3V kisspeptin neurons. Further, it may also result in the withdrawal of AVP-producing appositions to the kisspeptin neurons, meaning that AVP, if it is released, cannot access the kisspeptin neurons. Increased P_4 in oestrus may inhibit AVP synthesis. It remains unknown what P_4 is doing to V1Rs, if anything. Overall, the kisspeptin neurons are no longer activated by SCN *Avp-cre* neurons.

manner. The change in hormones across the oestrous cycle may also be altering the glial coverage of neurons within the RP3V. Glia have been shown to increase their coverage of neurons in other brain regions at proestrus (Garcia-Segura *et al.*, 1994; Struble *et al.*, 2006; Arias *et al.*, 2009). Considering the extra synaptic release of AVP from the *Avp-cre* projections, it may be that increased glial coverage acts as a barrier to AVP diffusion (Figure 6.12). Released AVP would then be specifically concentrated towards RP3V kisspeptin neurons, rather than diffusing throughout the region.

6.4.3 An immediate inhibition of kisspeptin neurons is mediated by GABA

Potentially the most striking observation in this chapter is the appearance of an immediate inhibition, mediated by GABA acting at $GABA_A$Rs, during stimulation of the *Avp-cre* projections, in oestrus. As this response is not seen at any other stage of the oestrous cycle, it is likely specifically associated with the postovulatory phase. Studies of how hormones influence GABA synthesis have shown different effects in different brain regions (Weiland, 1992; Souza *et al.*, 2009; Noriega *et al.*, 2010), but changes in the SCN are unknown. Hormonal feedback may contribute to changes in SCN GABA synthesis (Figure 6.13). Here, however, the focus will be on how there may be changes in how GABA can act at kisspeptin neurons, or a change in how kisspeptin neurons respond across the oestrous cycle. Both of these will now be discussed in turn.

6.4.3.1 Changes in GABA action across the oestrous cycle

The most obvious idea for the appearance of an inhibition would be the oestrus-driven production and/or release of an inhibitory neurotransmitter. As the SCN AVP neurons are likely GABAergic, the release of GABA would make sense in this context. One other potential fast

inhibitory neurotransmitter that may be released is glycine. It has been suggested that SCN explants can release glycine (Shinohara *et al.*, 1998) which would act as an inhibitor at efferent targets. The glycine receptor acts as a chloride channel, similar to the $GABA_AR$ (Burgos *et al.*, 2016)**,** and can be inhibited by GBZ at high concentrations – albeit higher than those used here (Beato, 2008). Thus, it is more likely that this inhibition is GABA-mediated rather than glycine-mediated.

It is unlikely that there is GABA release in each cycle stage, which is being masked by the excitatory effect of AVP. As GABA and AVP show different response kinetics due to differences in their receptor mechanisms (ion channel vs. GPCR) the two responses would unlikely overlap. Further, the Manning Compound experiments in Section 6.3.4 do not reveal a masked immediate inhibition. Thus, the question remains, how is GABA being release at oestrus, but not during other oestrous cycle stages?

Being a small amino acid neurotransmitter, GABA is typically released from small synaptic vesicles into the synaptic cleft. Although GABAergic synaptic transmission from *Avp-cre* neurons onto the kisspeptin neurons was not detected, this could be due to several possibilities that have been outlined in Chapter 5. These, however, do not rule out the possibility that the release of GABA is occurring at synapses at distant dendritic zones where whole-cell recordings of IPSCs, like those in Chapter 5, would be unable to pick up the transient dendritic current. Despite this, however, a dendritic IPSC might still contribute to an overall inhibition of the kisspeptin neuron which would be recorded by the loose-patch configuration used in these experiments. Thus, if a dendritic synapse was constantly present (i.e. not plastic over the oestrous cycle), it would likely be detected here in dioestrus and proestrus.

It may be the case, however, that GABA is released extrasynaptically (Figure 6.13). GABA would, therefore, have to act at GABA receptors outside of a synaptic cleft. Extracellular $GABA_ARs$ are relatively common throughout the central nervous system and mediate a tonic inhibition of neuronal activity predominantly from synaptic cleft spill over

(Farrant & Nusser, 2005; Brickley & Mody, 2012). In saying this, $GABA_BRs$ are also found commonly in extrasynaptic regions, however, due to their action as a GPCR, this does not match the time course of the immediate inhibition seen here (Bowery *et al.*, 2002). GABA from an LDCV could drive the rapid and short-lasting inhibition that is seen here in recordings from oestrus kisspeptin neurons. The kisspeptin neurons at oestrus are not responding to AVP, thus it could be that the GABA takes a preferential effect. This would involve the co-packaging of AVP and GABA into LDCVs, which has been shown at SCN AVP neuron terminals (Castel & Morris, 2000). As the inhibitory response is not seen in any other oestrous cycle stage, however, it could be that there is a postovulatory drive in vGAT expression at the SCN *Avp-cre* neuron terminal to drive this co-packaging mechanism (Figure 6.13).

As the results here do not show a complete reduction of the inhibitory drive when GBZ is applied, the possibility remains that a second receptor might be present along with $GABA_AR$ to mediate the HFLS-induced decrease.

6.4.3.2 Changes in GABAR expression across the oestrous cycle

One key point differentiating oestrus from other oestrous cycle stages is the rise in levels of progesterone. Progesterone has been implicated in several studies concerning GABA, predominantly in its role of sensitising $GABA_ARs$. Once progesterone has been brought into a neuron, its metabolites act to sensitise and enhance GABAergic inhibitory currents (Callachan *et al.*, 1987; Brussard & Koksma, 2003; Wang, 2011). This would potentiate any GABAergic current that was present (Figure 6.13). Despite this, however, progesterone metabolites are likely to be washed from the slice in the bath solution. This does not exclude the role of astrocyte-derived neuroprogesterone that may still be causing an effect at the neurons (Micevych *et al.*, 2007). Progesterone administration has also been shown to increase the

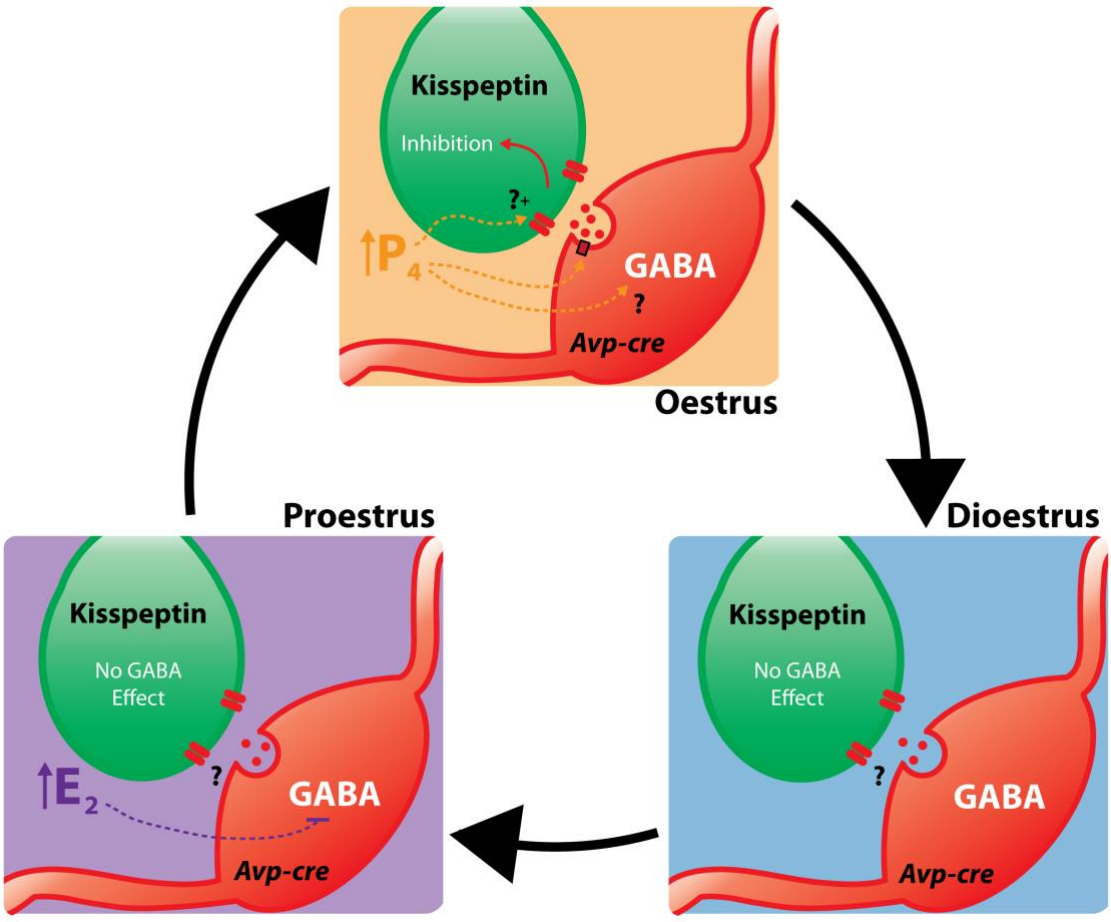

Figure 6.13: Potential changes to the SCN GABA system across the oestrous cycle.

Dioestrus: An intermediate period between oestrus and proestrus. Some GABA may be released from *Avp-cre* projections but does not drive an immediate inhibition. **Proestrus:** Increased E_2 concentrations may decrease GABA synthesis in SCN *Avp-cre* neurons. It remains unknown if GABA is released at all from the SCN *Avp-cre* neurons during proestrus. **Oestrus:** Post-ovulation, the increase in P_4 may increase vGAT expression on LDCVs in *Avp-cre* neuron projections. P_4 metabolites may also be enhancing $GABA_AR$ conductance and expression, as well as GABA synthesis.

transcription of $GABA_AR$ subunit mRNA in the hypothalamus, suggesting there may be greater numbers of $GABA_ARs$ (Noriega *et al.*, 2010).

6.5 Summary

The data presented in this chapter provide the first insight into how SCN *Avp-cre* projection fibres to the RP3V can influence the activity of kisspeptin neurons across the oestrous cycle. As oestradiol levels rise, the transition to positive feedback at proestrus correlates to AVP-mediated effects SCN *Avp-cre* projections acting at kisspeptin V1Rs, which can, in turn, drive an excitation of RP3V kisspeptin neurons. This has potentially uncovered a mechanism by which the onset of the LH surge, as driven by the central biological clock, can be driven. A novel finding was discovered during oestrus, where those same SCN *Avp-cre* neurons enact a second mechanism to inhibit the RP3V kisspeptin neurons. With the fall in oestradiol concentration, coupled to a rise in progesterone concentration, this inhibition may help to dampen the electrical activity of kisspeptin neurons in order to stop their further unnecessary activation following the LH surge. Between these stages, there appears to be a period of quiescence where there is little activation or inhibition of the kisspeptin neurons; essentially a transition period between the inhibition at oestrus, and the excitation at proestrus. This period correlates well to the period of oestradiol negative feedback necessary for maintaining the low level of LH secretion.

Together, these data suggest a model of bidirectional control of RP3V kisspeptin neuron electrical activity, involving two different neuromodulators, over the course of the murine oestrous cycle. The SCN AVP neurons, therefore, may act as a potential mechanism that gates the RP3V kisspeptin neurons to ensure the LH surge occurs during proestrus.

Chapter 7:

Alterations to the SCN *Avp-cre* Neuron Projection to RP3V Kisspeptin Neurons in a Mouse Model of Polycystic Ovary Syndrome

7.1 Introduction

The experiments carried out as part of the previous chapters have demonstrated the presence and functionality of the SCN *Avp-cre* neuron projection to the RP3V kisspeptin neurons. To determine the importance of this circuit for the LH surge, this projection was remapped in a mouse model of pathological subfertility which does not generate an endogenous LH surge. Understanding this circuit in a pathological condition provides a better understanding of its critical role in the neural regulation of the LH surge. The experiments in this chapter have thus been carried out using the prenatal androgen-treated (PNA) model of polycystic ovary syndrome (PCOS).

Polycystic ovary syndrome (PCOS) is the most common neuroendocrine disorder resulting in female sub- or infertility (Azziz *et al.*, 2004). It is typically characterised by hyperandrogenaemia, polycystic ovaries, and impaired ovulation; along with other distressing symptoms and comorbidities such as acne and hirsutism (Stein & Leventhal, 1935; Rotterdam, 2004). Despite the prevalence of PCOS and its symptoms, there remains no clear aetiology for its development. Prior animal work modelling PCOS has revealed disruptions in brain circuitry controlling the GnRH neuronal network (Sullivan & Moenter, 2004; Cernea *et al.*, 2015; Moore *et al.*, 2015; Porter *et al.*, 2019) suggesting a neuronal origin for the impairments in fertility seen in PCOS. As PCOS is associated with impaired ovulation, the SCN-to-RP3V circuit, critical to ovulation, may also be impaired.

7.1.1 The prenatally androgen-treated mouse model of PCOS

Prenatal androgen treatment involves the injection of androgens to the mother during pregnancy. While some groups use testosterone treatment, others (including the work presented in this chapter) use dihydrotestosterone (DHT) which is an androgen that cannot be aromatised (Santen, 1975; Steckelbroeck *et al.*, 2004). Aromatisation of androgens (particularly

testosterone) by the aromatase enzyme converts the androgens to oestrogen. Thus, the use of DHT in PNA models ensures that the resulting alterations to the developing brain are likely solely AR-mediated rather than ER-mediated. Further, DHT action solely at brain ARs is necessary to drive PCOS-like features (Caldwell *et al.*, 2017).

During foetal development, the developing brain is highly sensitive to circulating sex steroids (Schwarz & McCarthy, 2008). In mothers with hyperandrogenaemia, the high circulating androgen concentration is thought to alter the programming of the developing brain circuitry (Xita & Tsatsoulis, 2006). Thus, it is hypothesised that prenatal androgen exposure may underlie both the aetiology and pathophysiology of the PCOS. To investigate this, prenatal androgen treatment has been a key method to cause PCOS-like symptoms in animal models, and determine PNA-induced changes in the brain of the offspring (Stener-Victorin *et al.*, 2020).

Prenatal androgen treatment has modelled PCOS in several species to date including the mouse (Birch *et al.*, 2003; Sullivan & Moenter, 2004; Foecking *et al.*, 2005; Abbott *et al.*, 2008; Smith *et al.*, 2009; Wu *et al.*, 2010; Moore *et al.*, 2013). The PNA mouse model displays defects to the GnRH neuronal network which are consistent with the altered LH secretion seen in PCOS (Sullivan & Moenter, 2004; Moore *et al.*, 2015; Silva *et al.*, 2018; Silva *et al.*, 2019). Along with central alterations, PNA mice display thickened ovarian theca cell layers (potentially underlying an increase androgen production), hyperandrogenaemia and subfertility (Sullivan & Moenter, 2004; Moore *et al.*, 2013; Moore *et al.*, 2015; Silva *et al.*, 2018). Together these symptoms match the diagnostic criteria for PCOS in women (Rotterdam, 2004).

From a neuroendocrine perspective, the PNA mouse model has impaired oestrogen and progesterone feedback to the GnRH neuronal network (Moore *et al.*, 2013) as well as a loss of progesterone sensitivity (Moore *et al.*, 2015). Further, there is an increase in LH pulse frequency, similar to that seen in women with PCOS (Moore *et al.*, 2015). The PNA mouse model does not display regular oestrous cycles, instead remaining in one cycle stage for extended periods of time. Further, they rarely show a proestrous vaginal smear, indicating that

PNA mice are unlikely to naturally mount an LH surge (Sullivan & Moenter, 2004; Moore *et al.*, 2013; Silva *et al.*, 2018).

Although the PNA mouse model shows clear reproductive impairments, it does not fully recapitulate all the symptoms of PCOS. Despite the thickening of the theca cell layer surrounding the follicle, the PNA mouse model does not have cystic ovaries. Further, it does not display overt metabolic dysfunction (i.e. does not display obesity or insulin resistance) and, as such, is termed the lean PCOS phenotype (Moore *et al.*, 2013; Roland & Moenter, 2014). Despite this, however, the PNA mouse model allows for exquisite dissection of alterations in reproduction features without interference from metabolic effects, such as brain circuits that could be impaired in PCOS, resulting in disrupted ovulation.

7.1.2 Prenatal androgen treatment disrupts hypothalamic neural circuits

As mentioned, women with, and animal models of, PCOS display a heightened frequency of LH pulses (Coyle & Campbell, 2019). As such, the majority of work has focussed around disruption to the LH pulse generating ARN in PCOS. Prenatal androgen treatment has commonly shown an increase in GABAergic innervation of GnRH neurons, originating at least in part from the ARN (Moore *et al.*, 2015; Silva *et al.*, 2018), coupled with an increased GABAergic synaptic transmission to GnRH neurons (Sullivan & Moenter, 2004). This has also been shown in a model of PCOS induced by prenatal anti-Müllerian hormone treatment (Tata *et al.*, 2018). Activation of $GABA_A$Rs on GnRH neurons results in excitation (Herbison & Moenter, 2011), thus increased GABAergic drive in PNA models likely contributes to an increased excitation of GnRH neurons and, as such, heightened LH secretion.

ARN KNDy neurons are thought to be the pulse generator driving pulsatile GnRH and LH secretion (Clarkson *et al.*, 2017). There is disagreement about how they may change in

PCOS. Some animal models of PCOS report increased ARN kisspeptin cell number by immunohistochemistry (Aliabadi *et al.*, 2017; Osuka *et al.*, 2017) or increased *Kiss1* mRNA (Matsuzaki *et al.*, 2017). Other groups, however, using the same animal models report no change in ARN kisspeptin number (Cheng *et al.*, 2010) or *Kiss1* mRNA (Caldwell *et al.*, 2015). There is no data on the actual electrical activity of PCOS-like ARN kisspeptin neurons. There does, however, appear to be an increased GABAergic innervation to KNDy neurons, similar to the GnRH neurons (Porter *et al.*, 2019) along with a decrease in glutamatergic inputs (Cernea *et al.*, 2015).

Research on the RP3V kisspeptin population in PCOS-like animal models have reported either no change in their cell number (Cheng *et al.*, 2010; Caldwell *et al.*, 2015; Osuka *et al.*, 2017), or *Kiss1* mRNA (Caldwell *et al.*, 2015; Kauffman *et al.*, 2015; Matsuzaki *et al.*, 2017; Osuka *et al.*, 2017). Some groups, however, have reported a decrease in RP3V kisspeptin cell number (Brown *et al.*, 2012; Aliabadi *et al.*, 2017). With regard to the innervation of RP3V kisspeptin neuron, Cernea *et al.* (2015) report a decreased innervation (in the analogous region to the RP3V in the PNA sheep), likely from a GABAergic population, but do not specify from where it originates. While the sheep LH surge is not circadian in nature, relying on seasonal cues instead, this does not exclude the fact that the SCN may still project to the sheep RP3V analogue. Keeping in mind the anatomical projection from the SCN to RP3V, which is GABAergic, it could be that this circuit is diminished in the PNA model of PCOS.

7.1.3 Hypothesis and aim

As the SCN-to-RP3V circuitry is critical for the generation of the LH surge, it is important to see how the circuit may be affected in a model of pathology with ovulatory dysfunction. As the SCN-to-RP3V circuitry is critical for ovulation, it was hypothesised that **there would be a decrease in the innervation of the RP3V by SCN *Avp-cre* neurons**. The experiments carried out in this chapter aimed **to determine how the anatomy and**

functionality of the SCN *Avp-cre* projection to RP3V kisspeptin neurons may be impacted by subfertility, in a mouse model of PCOS.

7.2 Methods

7.2.1 Animals

General animal information is outlined in Section 2.1. Generation of prenatally androgen-treated animals is outlined in Section 2.1.2. Adult PNA and control oil vehicle-treated (VEH) female *Avp-cre* mice (2-6 months old) were used in this study. Oestrous cycles were determined by daily vaginal lavage and were used in dioestrus.

7.2.2 Other methods

Surgery, immunohistochemistry, microscopy, electrophysiology and optogenetics, and analyses have all been described previously in Chapters 2-6. Images shown herein are maximum projections of confocal Z-stack images unless stated otherwise. Where immunohistochemical data are reliant on the success of a viral injection, the range of upper and lower average values has been provided. For electrophysiology experiments in this chapter, where n-values are reported, n refers to neurons recorded, while N refers to the number of animals used in the experiments.

7.3 Results

7.3.1 SCN *Avp-cre* projections to the RP3V are reduced in the PNA mouse model

As in Section 4.3.1, viral-mediated tract-tracing of the SCN *Avp-cre* neurons to the RP3V was carried out to determine whether the projection was affected in the subfertile PNA mouse model. Due to the disruption in PNA mouse oestrous cycles (Figure 7.1), dioestrous PNA mice were compared to dioestrous VEH mice. In VEH mice, there was a clear fibre projection in the RP3V when SCN *Avp-cre* neurons were successfully transfected (Figure 7.2a). This lies in stark contrast to the PNA mice where SCN *Avp-cre* projections were reduced by about half (Figure 7.2b). There was a significantly reduced mCherry-ir fibre density in the RP3V of PNA mice, compared to their VEH counterparts (Figure 7.2c; VEH: 12.8 ± 2.2%, n = 8 mice, range = 7.1 – 25.0%; PNA: 7.0 ± 1.0%, n = 6 mice, range = 3.3 – 9.7%; $p = 0.043$, Mann-Whitney test). This is a particularly compelling finding when it is considered that the level of SCN transfection in those VEH and PNA animals is not significantly different (Figure 7.2d; VEH: 18.1 ± 2.1%, n = 8 mice, range = 10.5 – 27.6%; PNA: 16.1 ± 2.6%, n = 6 mice, range = 8.8 – 25.1%; $p = 0.66$, Mann-Whitney test).

Linear regression analysis revealed that both VEH and PNA mice showed significant positive correlations between the level of transfection in the SCN and the mCherry-ir fibres innervating the RP3V (Figure 7.2e; VEH: n = 9 mice, $p < 0.0001$, $R^2 = 0.84$; PNA: n = 9 mice, $p = 0.004$, $R^2 = 0.41$). Importantly, this correlation, as assessed by the slope of the fitted line, was significantly reduced in PNA mice (Figure 7.2e; PNA slope: 0.24 ± 0.07; VEH slope: 0.84 ± 0.09; $p < 0.0001$, linear regression slope comparison). These data suggest that the SCN *Avp-cre* projection is present but reduced in the PNA mouse model.

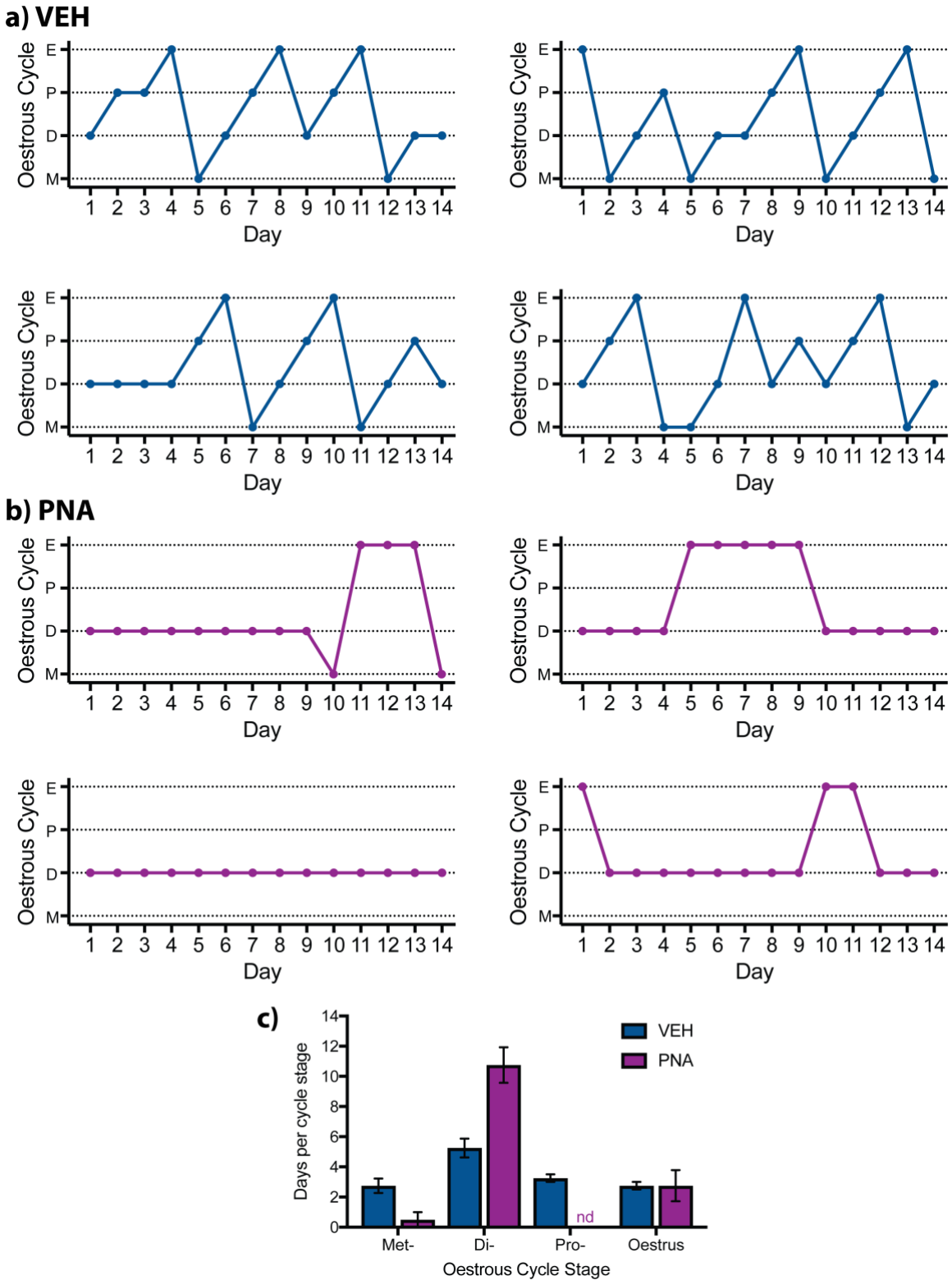

Figure 7.1: The PNA mouse model of PCOS is acyclic.

Four representative graphs of mouse oestrous cycles from VEH control mice (**a**) and PNA mice (**b**). The PNA mice tend to stay in one cycle stage for extended periods of time (usually dioestrus), where VEH mice show typical 4-5 day long oestrous cycles. **c**) Graphed data showing days spent in each cycle stage. Note also that PNA mice do not display proestrus. M = metoestrus, D = dioestrus, P = proestrus, E = oestrus. nd = not detected. Data shown as mean ± SEM.

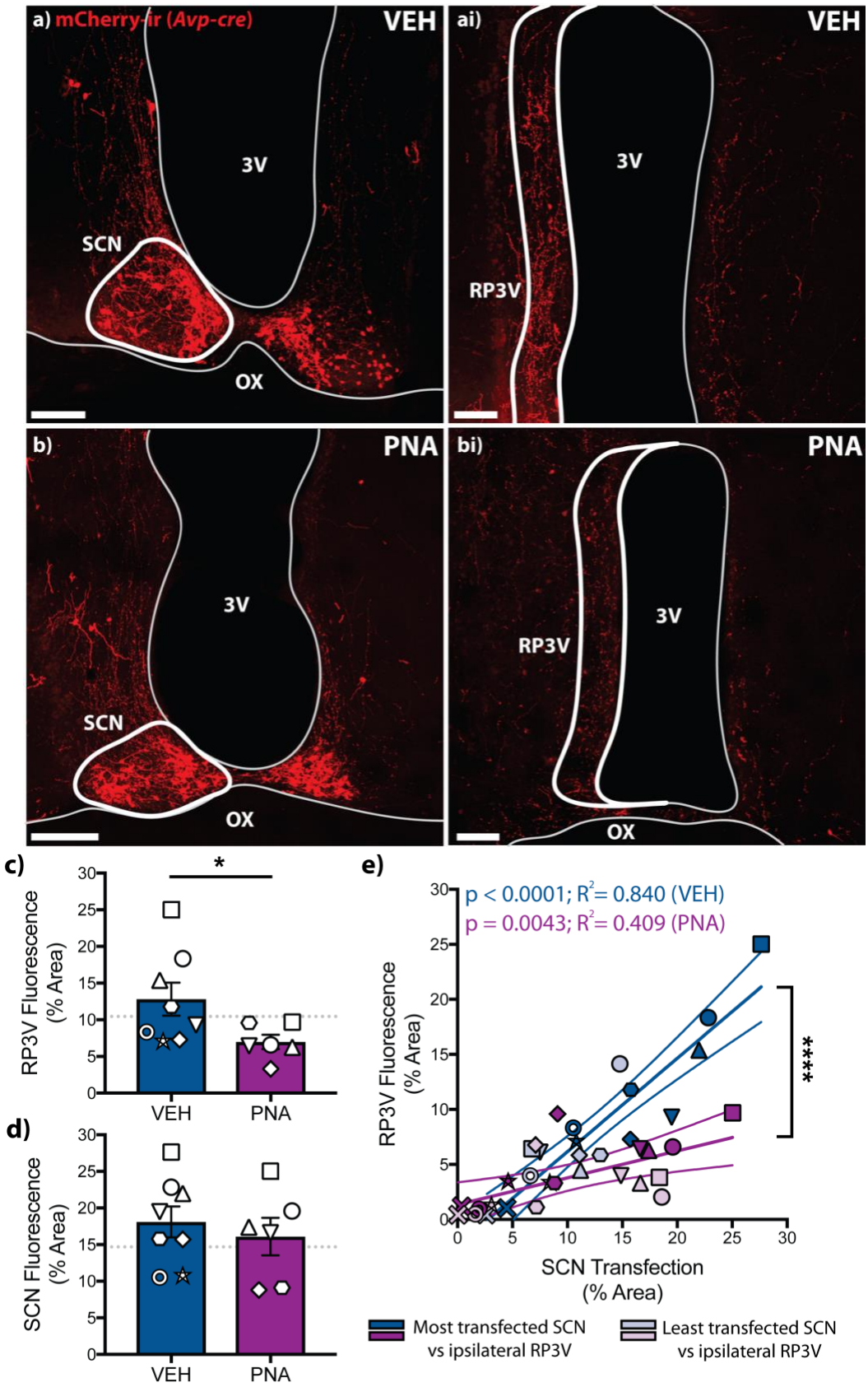

Figure legend overleaf

Figure 7.2: SCN *Avp-cre* projections in the RP3V are reduced in PCOS-like PNA female mice.

a, b) Confocal Z-stack images showing the innervation of the RP3V by mCherry-ir fibres in VEH and PNA mice; ai) and bi show the transfection in the SCN from the respective VEH or PNA animal. The thick white boundaries surrounding the ipsilateral RP3V and SCN represent the regions of interest used for pixel density analyses. **c, d)** RP3V innervation and SCN transfection in VEH and PNA mice. **e)** Correlation analysis of RP3V innervation and SCN transfection in VEH and PNA mice. Symbols represent individual mice; dark and light shades represent measurements ipsilateral to the most and least transfected side of the SCN, respectively. Data shown as line of best fit ± 95% confidence interval, or mean ± SEM. Dotted lines in d and e represent the average value for untreated animals presented in Chapter 4. Scale bars = 100 µm. * $p < 0.05$, **** $p < 0.0001$. 3V = third ventricle. OX = optic chiasm.

7.3.2 SCN *Avp-cre* appositions to RP3V kisspeptin neurons are reduced in the PNA mouse model

Given that the *Avp-cre* fibre projection is reduced in PNA mice compared to VEH, the potential innervation of the RP3V kisspeptin neurons was then assessed by looking at close *Avp-cre* appositions to kisspeptin neurons. Using dual fluorescence immunohistochemistry for mCherry and kisspeptin in animals with successful SCN transfection, it was found that there was a significant reduction in the proportion of kisspeptin neuron somata apposed by mCherry-ir fibres in PNA animals compared to VEH (Figure 7.3a-c; VEH: 44.3 ± 3.6%, n = 8 mice, range = 31.1 – 64.5%; PNA: 28.3 ± 4.3%, n = 6 mice, range = 18.2 – 44.9%; p = 0.020, Mann-Whitney test). Further, the average number of appositions per apposed neuron tended to be lower in PNA animals compared to VEH, although this did not reach statistical significance (Figure 7.3d; VEH: 1.65 ± 0.07/neuron, n = 8 animals, PNA: 1.45 ± 0.07/neuron, n = 6 animals, p = 0.059, Mann-Whitney test).

Similar to the untreated animals presented in Chapter 4, the VEH animals displayed a significant positive correlation between the proportion of RP3V kisspeptin neurons displaying close appositions by mCherry-ir fibres and transfection of the ipsilateral SCN (Figure 7.3e; n = 8 animals, p = 0.001, $R^2 = 0.55$). Interestingly, there was no correlation found for PNA animals (Figure 7.3e; n = 6 animals, p = 0.40, $R^2 = 0.07$, linear regression). In addition, the correlations were significantly different between the two groups (Figure 7.3e; PNA slope: -0.48 ± 0.55; VEH slope: 1.56 ± 0.37; p < 0.004, linear regression slope comparison). These data show that there is a lower proportion of RP3V kisspeptin neurons apposed by SCN *Avp-cre* projections in the PNA mouse model. This result cannot be explained by differences in SCN transfection rates, therefore, this indicates that the reduction is caused by prenatal androgen treatment.

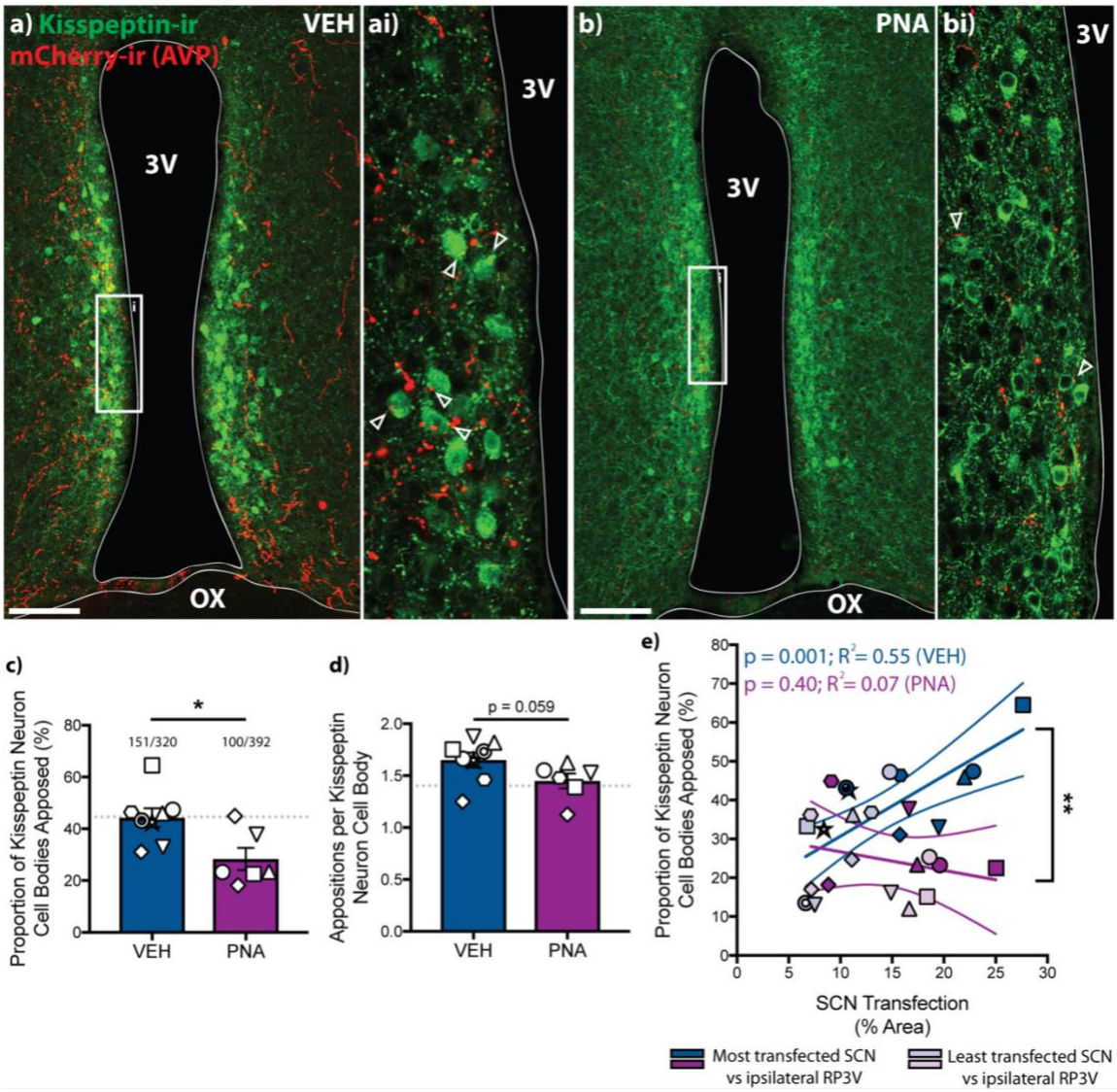

Figure 7.3: SCN *Avp-cre* close appositions to RP3V kisspeptin neurons are reduced in PNA mice.

a, b) Confocal Z stack images of the RP3V from VEH and PNA animals showing kisspeptin-ir neurons (green) with mCherry-ir fibres (red) innervating the region. **ai, bi)** Single plane images showing mCherry-ir fibres in close apposition to kisspeptin-ir neurons. Appositions to the somata of kisspeptin-ir neurons are marked with empty arrowheads. **c)** Summary graph of the proportion of kisspeptin-ir neurons apposed by mCherry-ir fibres in VEH and PNA mice. **d)** Summary graph of the number of appositions per kisspeptin neuron in VEH and PNA mice. **e)** Correlation analysis of the proportion of neurons apposed and SCN transfection in VEH and PNA mice. Symbols represent individual mice; dark and light shades represent measurements ipsilateral to the most and least transfected side of the SCN, respectively. Data shown as mean ± SEM, or linear regression ± 95% confidence interval. Dotted lines in c and d represent the average value for untreated animals presented in Chapter 4. Scale bars = 100 µm. * $p < 0.05$, ** $p < 0.01$. VEH = vehicle-treated. PNA = prenatal androgen-treated. 3V = third ventricle. OX = optic chiasm.

7.3.3 High-frequency light stimulation of *Avp-cre* projections does not alter the activity of kisspeptin neurons in the PNA mouse model

It was next investigated whether the reduction in RP3V kisspeptin neuron innervation in PNA mice had any effect on how SCN *Avp-cre* neurons regulate RP3V kisspeptin neuron firing rate. To test this, optogenetics was used, similar to Chapter 6. As PNA mice have disrupted oestrous cycles, tending to stay in dioestrus (Figure 7.1), the effect of optogenetic stimulation of SCN *Avp-cre* neurons on RP3V kisspeptin neuron electrical activity was determined in dioestrous VEH and PNA mice.

In dioestrous VEH control mice, there was no effect of HFLS on the activity of any RP3V kisspeptin neuron in the immediate period. As in Chapter 6, HFLS had varied effects on action potential firing rate in the delayed period (Table 7.1). Overall there was no change in the group mean firing rate during and following HFLS (Figure 7.4a, c, e; immediate: 108.1 ± 10.6% of baseline, $p > 0.99$; delayed: 111.3 ± 13.2% of baseline, $p > 0.99$; $n = 10$ neurons; $N = 3$ mice; Friedman test with *post hoc* Dunn's multiple comparisons tests).

HFLS	Immediate Effect				Delayed Effect			
	Excitation	No Change	Inhibition	Group mean	Excitation	No Change	Inhibition	Group mean
VEH	0	10	0	108.1 ± 10.6%	5	4	1	111.3 ± 13.2%
PNA	0	10	0	93.4 ± 12.7%	3	6	1	99.2 ± 11.0%

Table 7.1: Individual and mean responses between VEH and PNA mice to high frequency light stimulation.

The number of neurons showing responses in both the immediate and delayed effect periods, as per the criteria outlined in Section 6.2.6.3, are tabulated. The mean response from baseline from all the neurons recorded is also provided and presented as mean ± SEM. This table is associated with Figure 7.4.

Similarly, dioestrous PNA mice did not show any immediate changes to kisspeptin activity during HFLS and showed varied effects in the delayed period (Table 7.1). Overall,

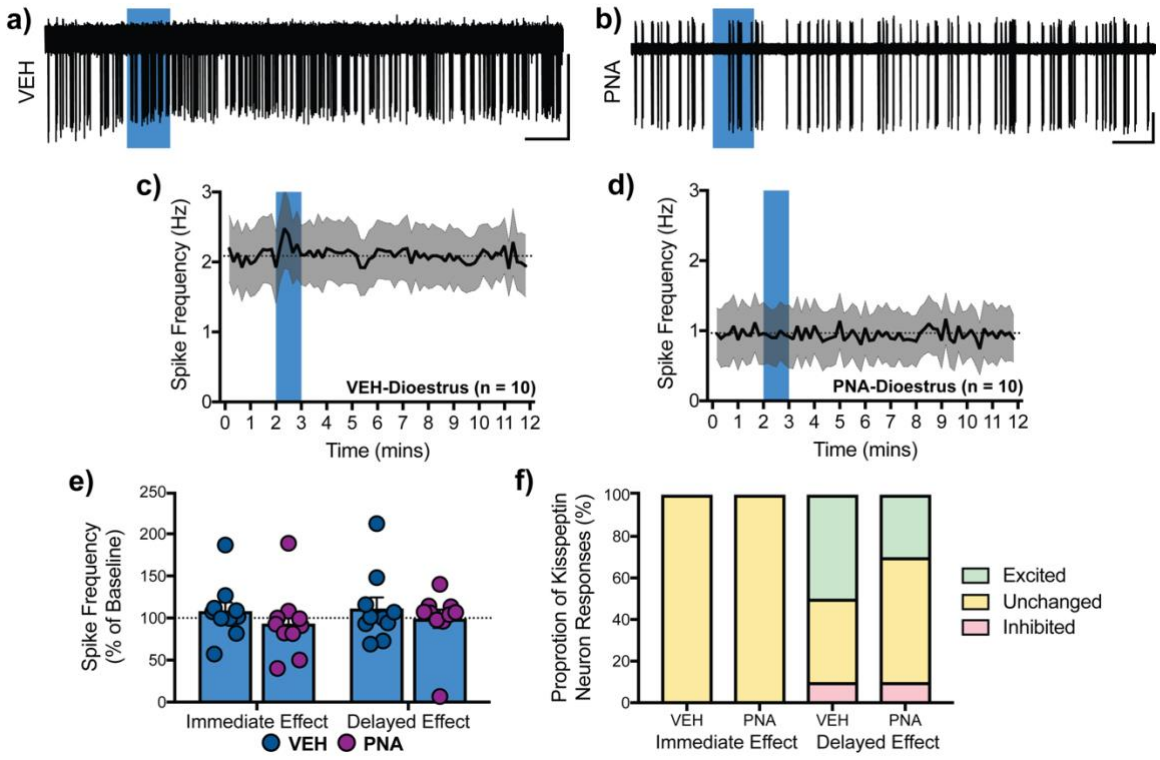

Figure 7.4: Kisspeptin neurons do not change action potential firing in response to high-frequency light stimulation of ChR2-expressing *Avp-cre* projections in dioestrous VEH and PNA mice.

a, b) Representative traces illustrating the effect of HFLS of ChR2-expressing *Avp-cre* projections on action potential firing from a kisspeptin neuron from a vehicle-treated (VEH) and prenatal androgen-treated (PNA) mouse. **c, d)** Average time-courses of action potential frequency over the recording periods. **e)** Quantified changes of kisspeptin action potential frequency as a percentage of baseline frequency during the effect periods following HFLS of ChR2-expressing *Avp-cre* projections in VEH and PNA mice. **f)** Proportions of neurons responding to HFLS of ChR2-expressing *Avp-cre* projections in VEH and PNA mice. Scale bars = 60 s/50 pA. Blue bars in a) – d) represent light stimulation. Data presented in c) – e) as mean ± SEM, dotted lines represent baseline. VEH: n = 10 neurons, N = 3 mice; PNA: n = 10 neurons, N = 3 mice.

there was no change in the group mean firing rate during and following HFLS (Figure 7.4b, d, e; immediate: 93.4 ± 12.7% of baseline, p = 0.68; delayed: 99.2 ± 11.0% of baseline, p > 0.99; n = 10 neurons; N = 3 mice; Friedman test with *post hoc* Dunn's multiple comparisons tests).

Comparisons between VEH and PNA groups showed no differences in how HFLS of SCN *Avp-cre* projections affected RP3V kisspeptin neuron firing rate (Figure 7.4e; immediate: p = 0.12, delayed: p = 0.74, Mann-Whitney tests); nor were there any differences between the proportion of kisspeptin neurons responding at either time period (Figure 7.4h, immediate: p > 0.99, delayed: p = 0.64, chi-squared tests).

These data show that there is no difference in the way SCN *Avp-cre* neurons influence the electrical activity of kisspeptin neurons in dioestrous VEH and PNA mice.

7.3.4 AVP application excites kisspeptin neurons similarly in PNA and VEH mice

For accuracy in comparisons, these experiments can only compare dioestrous PNA and VEH mice. As there was no effect of optogenetic stimulation of *Avp-cre* projections on kisspeptin action potential firing in dioestrus, it may be that those experiments were unable to detect any impairments in circuit function. As such, it was necessary to determine whether RP3V kisspeptin neurons from PNA mice were able to respond to AVP at all. Following 500 nM AVP application, all RP3V kisspeptin neurons sampled from VEH mice were excited (Table 7.2), with a significant increase in mean firing rate (Figure 7.5a, c, e; 216.7 ± 20.8% of baseline, n = 12 neurons, N = 3 mice, p < 0.0001, Friedman test with *post hoc* Dunn's multiple comparisons test). Similarly, AVP excited the majority of kisspeptin neurons from PNA mice (Table 7.2), and caused a significant increase in the group mean firing rate (Figure 7.5b, d, e; 310.8 ± 91.5% of baseline, n = 11 neurons, N = 3 mice, p = 0.005, Friedman test with *post hoc* Dunn's multiple comparisons test).

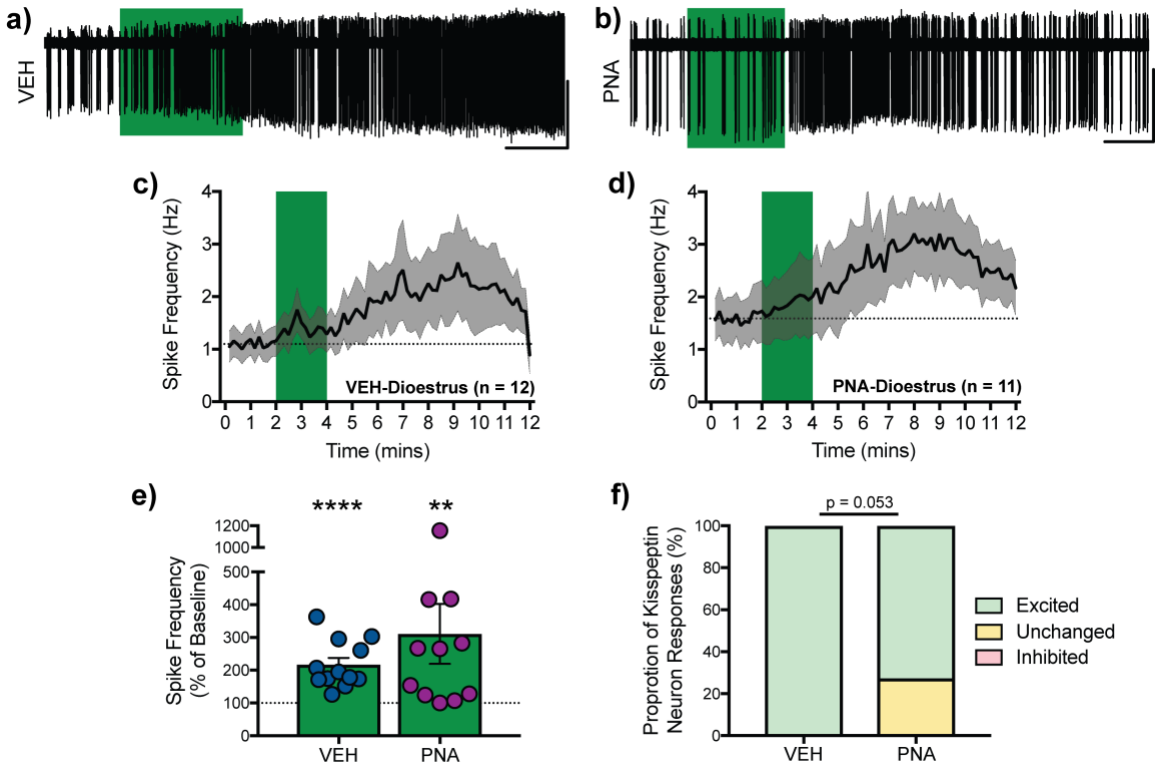

Figure 7.5: Kisspeptin neurons are excited by AVP application in dioestrous VEH and PNA mice.

a, b) Representative traces illustrating the effect of 500 nM AVP application on action potential firing from a kisspeptin neuron from a vehicle-treated (VEH) and prenatal androgen-treated (PNA) mouse. **c, d)** Average time-courses of action potential frequency over the recording periods. **e)** Quantified changes of kisspeptin action potential frequency as a percentage of baseline frequency following AVP application in VEH and PNA mice. **f)** Proportions of kisspeptin neurons responding to AVP in VEH and PNA mice. Scale bars = 60 s/50 pA. Green bars in a) – d) represent AVP wash. Data presented in c) – e) as mean ± SEM, dotted lines represent baseline. VEH: n = 12 neurons, N = 3 mice; PNA: n = 11 neurons, N = 3 mice. ** $p < 0.01$, **** $p < 0.0001$.

AVP Application	Delayed Effect			
	Excitation	No Change	Inhibition	Group mean
VEH	12	0	0	216.7 ± 20.8%
PNA	8	3	0	310.8 ± 91.5%

Table 7.2: Individual and mean responses between VEH and PNA mice to AVP application.
The number of neurons showing responses in both the immediate and delayed effect periods, as per the criteria outlined in Section 6.2.6.3, are tabulated. The mean response from baseline from all the neurons recorded is also provided and presented as mean ± SEM. Yellow boxes indicate mean responses that are significantly different from baseline. This table is associated with Figure 7.5.

When firing rates were compared between VEH and PNA mice, there was no difference between the extent of their excitation (Figure 7.5e, $p > 0.99$, Mann-Whitney test). There was, however, a trend towards a decrease in the proportion of PNA neurons responding to AVP application compared to VEH (Figure 7.5f; $p = 0.053$ chi-squared tests). These data suggest that RP3V kisspeptin neurons respond to AVP in both VEH and PNA mice.

7.4 Discussion

PCOS is a common endocrine disorder with potential origins in the brain. One of the key features of PCOS is ovulatory dysfunction. This chapter investigated the structure and function of the projection from the SCN *Avp-cre* neurons to the RP3V in a mouse model of PCOS. RP3V kisspeptin neurons are critical for ovulation and their innervation by SCN AVP neurons is suspected to be involved in generating the preovulatory LH surge. Thus, it was fascinating to discover that in mice with features of subfertility, including impaired ovulation (Moore *et al.*, 2013), there was a substantial reduction in the extent of this circuit. Decreased anatomical wiring did not coincide with changes to action potential firing following HFLS of *Avp-cre* projections, however. There was a trend towards RP3V kisspeptin neurons from PNA mice displaying a reduced receptivity to AVP, which did not reach significance. Together, these

data suggest a potential loss of a mechanism for driving an LH surge in the PNA mouse model, that potentially contributes to their ovulatory disfunction.

7.4.1 SCN *Avp-cre* fibres are reduced in the RP3V of PNA mice

Viral-tract tracing of the previously identified circuit between SCN *Avp-cre* neurons to RP3V kisspeptin neurons revealed that PNA mice have a significantly reduced *Avp-cre* fibre density in the RP3V compared to VEH control. This may be due to a change in the SCN *Avp-cre* projection to the RP3V in PNA mice. Wiring changes in PNA mice have been shown previously with ARN GABA neurons increasing their projections to GnRH neurons (Moore *et al.*, 2015), however, this is the first report of a PNA-induced change associated with SCN neurons.

Previous studies have shown increased neuronal wiring associated with PCOS (Moore *et al.*, 2015; Silva *et al.*, 2018); however, these have been focussed on ARN projections to GnRH neurons to address an increase in PNA pulse frequency. As such, the work presented here shows a contrasting change in wiring for a decreased response; where an increased pulse frequency correlates with increased wiring from the ARN (Moore *et al.*, 2015; Silva *et al.*, 2018), a loss in wiring to the LH surge-generating kisspeptin neurons correlates with a loss in the LH surge.

7.4.1.1 Is this a direct effect of prenatal androgen treatment?

To model PCOS, the pregnant dam is injected with the non-aromatisable androgen, DHT. It is likely that DHT action at the AR in the brain is critical for the development of PCOS-like features (Caldwell *et al.*, 2017).The distribution of AR expression specifically in the SCN throughout development is unknown. If it is similar to adulthood (i.e. distributed through the core, but not the shell (Iwahana *et al.*, 2008; Jahan *et al.*, 2015)), it is likely that AR activation

would not directly affect the SCN AVP neurons due to their lack of Ars (Karatsoreos *et al.*, 2007; Iwahana *et al.*, 2008). The SCN production of AVP is low through development and only develops to full expression across the first week postnatally (Hyodo *et al.*, 1992). Thus, it could be that AR-mediated actions at non-AVP SCN neurons subsequently repress the projections from AVP neurons.

Aside from action at the AR, there is a chance that the results seen here are due to activity at ERβ. Prenatal androgen treatment with DHT might result in the production of the DHT metabolite, 3β-androstanediol (Steckelbroeck *et al.*, 2004). 3β-androstanediol is a potent activator of ERβ (Handa *et al.*, 2008), which is abundant in the SCN (Shughrue *et al.*, 1996). It has been shown that DHT treatment activates ERβ on magnocellular vasopressin neurons in culture (Pak *et al.*, 2007). The activation of ERβ on these neurons, however, typically results in upregulation of AVP peptide and increased neuronal activity (Shapiro *et al.*, 2000; Pak *et al.*, 2007), somewhat in contrast to a reduction in the *Avp-cre* projections seen here.

Alternatively, prenatal androgen treatment may not affect the SCN, but rather act at the RP3V kisspeptin neurons. There in contrasting evidence about how the RP3V *Kiss1* mRNA or kisspeptin peptide are impacted in PCOS animal models: there is either no change to their expression (Cheng *et al.*, 2010; Caldwell *et al.*, 2015; Kauffman *et al.*, 2015; Matsuzaki *et al.*, 2017; Osuka *et al.*, 2017) or a decrease (Brown *et al.*, 2012; Aliabadi *et al.*, 2017). A decreased expression of kisspeptin may result in a decreased branching of *Avp-cre* fibres, for AVP release, that are seen in the RP3V. Critically, however, Cernea *et al.* (2015) report decreased appositions to preoptic kisspeptin neurons in the PNA sheep model, but do not identify from where these inputs are coming. Further, they identified these neurons as unlikely to be glutamatergic. As such, the decrease may be attributed to the reduced innervation by SCN AVP neurons.

Questions remain surrounding this circuit and how it is disrupted in the PNA model. Primarily, the ontogeny of the reduction in *Avp-cre* circuitry; is this circuit disrupted from birth, or disrupted by hyperandrogenaemia later in adulthood; or as suggested, has it withdrawn due

to a lack of kisspeptin neuron activity? Further, the plasticity in this circuit must be explored. It will be important to determine whether the reduction in the fibre density is permanent, or if restoration of hormone levels are sufficient to re-establish the projection.

7.4.1.2 Is the reduction in *Avp-cre* projections attributable to altered hormonal feedback?

One remaining possibility is that the loss in the *Avp-cre* fibre projection seen in the PNA mouse is not caused by excess androgen acting directly on the SCN *Avp-cre* neuron to RP3V kisspeptin neuron circuit, but rather due to impaired gonadal steroid hormone feedback. Essentially, the lack of positive feedback from the ovary is not priming the RP3V kisspeptin neurons for the surge.

Oestradiol is the key hormone necessary for the development of the LH surge (Karsch *et al.*, 1973; Legan *et al.*, 1975). PNA mice are no different to VEH mice in their serum oestradiol concentration in dioestrus (Moore *et al.*, 2015). However, the inability to progress into proestrus in PNA mice may be caused by failure of their ovaries to increase oestrogen production to levels necessary for positive feedback actions that generate the LH surge. Ovaries from PNA mice display decreased granulosa cell layer thickness (Moore *et al.*, 2015; Silva *et al.*, 2018). The elevated LH pulse frequency could be inhibiting the development of the granulosa cell layer, thus inhibiting the conversion of androgens to oestradiol. As kisspeptin neurons are highly oestradiol sensitive, this, in turn, would inhibit kisspeptin expression (Smith *et al.*, 2006), as well as ion channels necessary for the development of the LH surge (Piet *et al.*, 2013; Piet *et al.*, 2015a).

Interestingly, when oestradiol levels are artificially raised by implant, PNA mice are able to generate an LH surge at the expected time (Moore *et al.*, 2013)**,** indicating that the positive feedback mechanism can be restored. Further, women with PCOS treated with the partial ERα agonist, clomiphene citrate, display markedly increased ovulation (O'Herlihy *et*

al., 1981; López *et al.*, 2004), indicating that restoration ERα activation is sufficient to restore positive feedback. How this promotes an LH surge in PNA mice remains unknown, but data from Vida *et al.* (2010) suggest that the increased oestradiol levels may promote more AVP-ir fibres in the RP3V.

Thus, the prolonged dioestrus levels of oestradiol in PNA mice may be causing a withdrawal or removal of SCN *Avp-cre* fibres. This idea would, therefore, be a secondary effect, not due to direct androgen action at the SCN or RP3V.

7.4.2 SCN *Avp-cre* regulation of RP3V kisspeptin neuron electrical activity is not impaired in PNA mice

The data here showed that HFLS of SCN *Avp-cre* projections did not, overall, excite either dioestrous VEH or PNA mice. Based on the results outlined in Chapter 6, a more informative experiment would have been to compare the effect of HFLS in proestrous VEH and PNA mice. Unfortunately, PNA mice being typically acyclic, often remaining in dioestrus without ever displaying proestrus (Figure 7.1), there was little opportunity to test PNA mice in proestrus. What can be gleaned from these experiments, however, lies in the proportions of RP3V kisspeptin neurons responding to HFLS in VEH and PNA mice (Figure 7.4f). Although this was not significantly different, fewer neurons were excited in PNA mice, consistent with the decreased innervation by SCN *Avp-cre* neurons.

AVP application to the kisspeptin neurons indicated that there was no gross alteration in V1R function between VEH and PNA. VEH and PNA kisspeptin neurons were excited to similar extents, although a trend towards a lower proportion of RP3V kisspeptin neurons responding to AVP application was observed in PNA mice. These data suggest that it is unlikely that V1R expression and/or function on RP3V kisspeptin neurons is significantly altered in PNA mice. Given the reduction in fibre density, it may be that AVP is still released from the

remaining fibres into the extracellular fluid, but in lower concentrations. If it were possible to drive optogenetic stimulation of the SCN *Avp-cre* neurons in PNA mice, coupled with microdialysis of the RP3V, this would provide some evidence as to whether AVP is being released at the RP3V.

Besides subtle, non-significant changes in the response of RP3V kisspeptin neurons to HFLS and to exogenous AVP, these results indicate that PNA has little impact on the functionality of the SCN *Avp-cre* neuron to RP3V kisspeptin neuron circuit in dioestrus. This likely reflects the inability of these experiments to adequately interrogate the circuit in PNA mice due to their profoundly impaired oestrous cycles.

7.5 Summary

The experiments carried out in this chapter have revealed the surprising result that following prenatal androgen treatment, the projection from SCN *Avp-cre* neurons to RP3V kisspeptin neurons is significantly reduced. The disrupted oestrous cycles of the PNA mice prevented the undertaking of a meaningful assessment of the functionality of this circuit. The subtle changes that were noted did not amount to a significant result, however, these data provide the first evidence for a disruption of the circuits between the SCN and RP3V in a mouse model of a human fertility disorder, and potentially underpin changes in ovarian function in PCOS.

Chapter 8:

General Discussion

8.1 Background

This thesis focussed on investigating the circuitry between the SCN AVP neurons and the RP3V kisspeptin neurons to better understand how this network contributes to the development of the preovulatory LH surge. To address this, viral vector-mediated anterograde tract-tracing and optogenetics have been carried out to determine both the anatomy and the functionality of the SCN-to-RP3V network. Further, a mouse model of PCOS, which displays disrupted oestrous cycles, absence of ovulation and subfertility, has been used to investigate changes the anatomy and function of this circuit.

This chapter **summarises the main findings of each chapter** and **highlights how these studies contribute to the wider field**; also, the **limitations associated with this work are discussed**. The implications of this work will be put into perspective for both physiological and pathology. Lastly, this chapter **presents possible avenues for future research** that can be developed from the present findings.

8.2 Summary of the main findings

This work was made possible by a transgenic mouse model that allowed us to target and visualise AVP neurons in the SCN. Chapter 3 describes the characterisation of this model by crossing the *Avp-cre* strain to one expressing the fluorescent reporter, tdTomato. Immunohistochemistry for AVP revealed that tdTomato expression (i.e. cre-reporter expression) was restricted to known AVP-expressing populations within the brain (Rood & de Vries, 2011), particularly the PVN, SON, SCN and accessory AVP nuclei. As the focus of this thesis was the SCN, tdTomato reporter expression as a marker of where cre was present, even transiently throughout life, and virally transduced mCherry, as a marker of temporal cre expression, were characterised in colocalisation with AVP-ir neurons. The *Avp-cre* mouse reports approximately 60% of AVP neurons, although nearly half of reporter-expressing

neurons are not immunoreactive for AVP. While this may suggest other SCN neuronal phenotypes are reported in this model, the findings present indicate this is not likely; reporter-expressing neurons do not express VIP or GRP, two other major SCN peptides; and AAV-mediated labelling of *Avp-cre* neurons revealed a similar pattern of reporter expression, indicating that *Avp* and cre were likely expressed at that time but the peptide was below detectable levels. Although the *Avp-cre* model does not report of all the SCN AVP neurons, there was confidence in the specificity of the approach.

AAV-mediated tract-tracing in Chapter 4 revealed the extent of the SCN *Avp-cre* neuron projection to the RP3V, and how they interacted on an anatomical level with the RP3V kisspeptin neurons. mCherry-expressing *Avp-cre* projections were in apposition to approximately half of the RP3V kisspeptin neurons suggestive of sites for putative synaptic input. The correlation analysis of the projection density in the RP3V to reporter expression in AVP-expressing brain regions suggested that AVPergic innervation of the RP3V originates in the SCN.

Based on these findings, and due to the fact that SCN neurons are thought to express the amino acid neurotransmitter GABA, the experiments in Chapter 5 investigated the fast synaptic transmission between SCN *Avp-cre* neurons and the RP3V kisspeptin neurons. Channelrhodopsin-assisted circuit mapping revealed that there was very limited (~ 5%) GABAergic synaptic input from SCN *Avp-cre* to RP3V kisspeptin neurons. Control experiments using *Nms-icre* mice in Chapter 5 reveal that this result is likely not due to technical limitations.

Experiments in Chapter 6 investigated whether neuropeptide (i.e. AVP) release from *Avp-cre* projection may impact RP3V kisspeptin neuron activity. These studies revealed that at the individual cell level, activation of SCN *Avp-cre* projections increased action potential firing in RP3V kisspeptin neurons through the release of AVP. When considered as a population, the RP3V kisspeptin neurons were only excited in proestrus, but not dioestrus or oestrus.

Furthermore, during oestrus, it was found that the SCN *Avp-cre* projections, rather than exciting kisspeptin neurons, caused an inhibition. This inhibition was likely mediated by GABA, a fast-inhibitory neurotransmitter, rather than AVP. As such, these *Avp-cre* projections likely release two different chemicals depending on the stage of the oestrous cycle.

To investigate how pathological changes in ovarian hormone feedback may alter the SCN-to-RP3V circuit, Chapter 7 outlined how this circuit was changed in a model of subfertility caused by prenatal androgen treatment. The subfertile PNA mouse model of PCOS stood in stark contrast to the reproductively normal model, with a significantly reduced SCN *Avp-cre* projection to the RP3V and a limited anatomical interaction with the RP3V kisspeptin neurons. Stimulation of SCN *Avp-cre* projections in PNA mice did not alter the activity of the RP3V kisspeptin neurons compared to dioestrous VEH control counterparts. As PNA mice have severely disrupted oestrous cycles, it was only possible to interrogate the circuit in dioestrus, a cycle stage where activation of SCN *Avp-cre* projections does not have an overall significant effect on action potential firing in RP3V kisspeptin neurons. The reduction in SCN-to-RP3V circuitry may partially underlie ovulatory dysfunction in this animal model.

8.3 Contributions and limitations of this study

8.3.1 Anatomy of the SCN-to-RP3V circuitry

The studies carried out in this thesis provide conclusive evidence for the projection of SCN *Avp-cre* neurons to the RP3V. Previous studies used immunohistochemical, non-specific tracing, and electron microscopy methods (Vida *et al.*, 2010; Williams *et al.*, 2011) to explore this circuit. The experiments in this thesis have used a more selective, genetically-specific, method to confirm them. Thus, this work supports previous conclusions by providing direct anatomical evidence for an SCN-to-RP3V projection.

The specific genetically-targeted viral vector transduction of the mCherry reporter allows for visualisation of this circuit, however, it is limited by the *Avp-cre* mouse itself. While there is no better model available to explore this circuit it is important to remember that of the cre-expressing neurons that are phenotypically unaccounted for, they are unlikely to produce VIP or GRP. This study is limited by its inability to say that this projection is completely AVP-producing. Unpublished evidence from the Piet laboratory, along with others suggests that there is little to no VIP innervation of RP3V kisspeptin neurons (Vida *et al.*, 2010; Williams *et al.*, 2011), strengthening the idea that the projection seen is not confounded by other SCN peptides.

One remaining possibility is that although this circuit is present, it is not, in fact, solely an SCN-to-RP3V circuit; that is to say, it does not terminate at the RP3V. While axonal SCN projections (these projections have not been shown to be truly axonal, however) are necessary for maintaining the LH surge, (Wiegand *et al.*, 1980; Wiegand & Terasawa, 1982; Silver *et al.*, 1996); they may not terminate in synaptic contacts at kisspeptin neurons. Electron microscopy has revealed the presence of some AVP-ir synapses in the RP3V (Vida *et al.*, 2010), although this does not necessarily indicate the end of a projection. It could be that these projections (which can release AVP in a 'non-synaptic' manner) are continuing to elsewhere in the brain (Figure 8.1). Retrograde tracing studies reveal the SCN as the origin for RP3V projecting fibres, though this may be due to axonal uptake of tracing reagents rather than synaptic ones (Watts & Swanson, 1987). As such, the brain slices through the RP3V reveal the projection to the RP3V, but do not indicate where the fibres terminate. Whether the *Avp-cre* projection to the RP3V is solely and specifically to the RP3V, where they may continue from the RP3V, remains to be elucidated.

While it has been inferred throughout this thesis that the *Avp-cre* projection acts at kisspeptin neurons that go on to excite GnRH neurons, it could be that the kisspeptin neurons

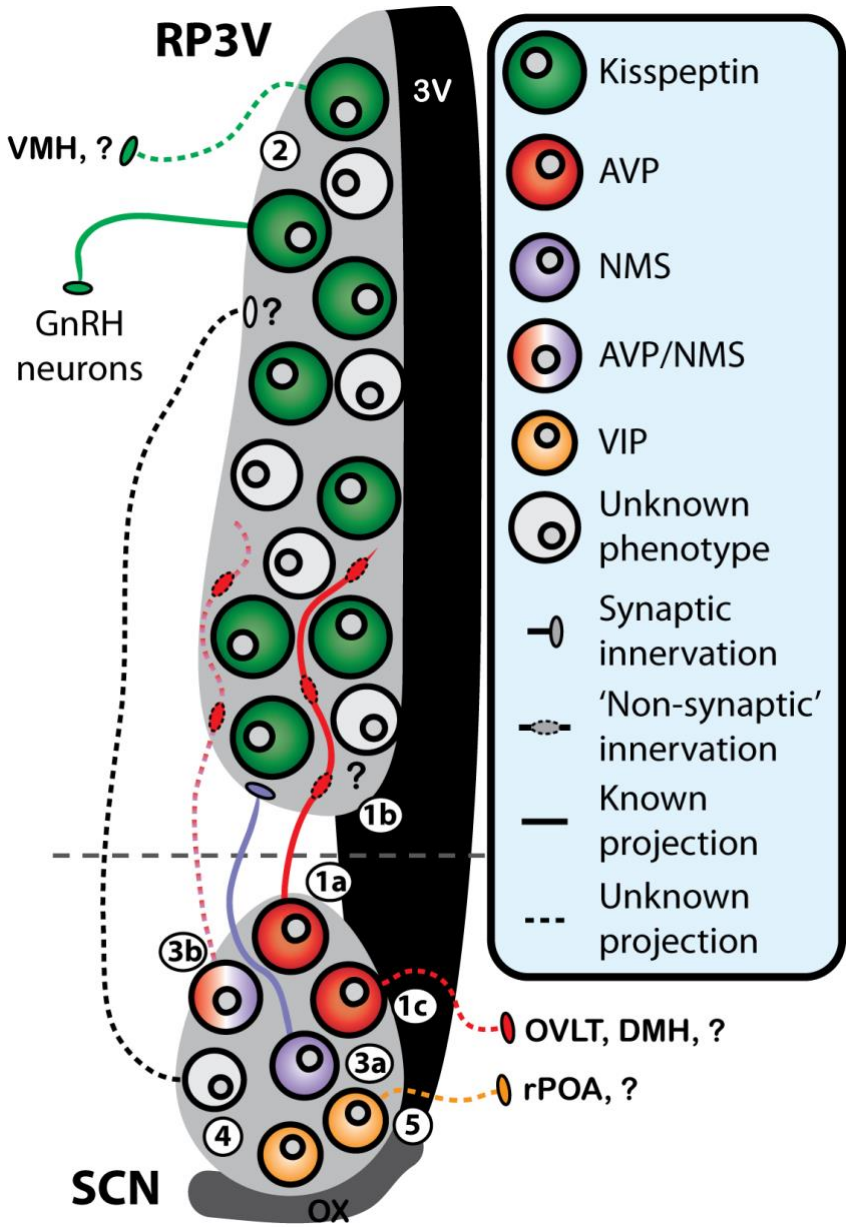

Figure 8.1: The SCN-to-RP3V circuit: Knowns and unknowns.

Schematic of the SCN-to-RP3V projection in the horizontal plane. This thesis demonstrates that SCN *Avp-cre* neurons project to the RP3V and influence the activity of RP3V kisspeptin neurons (**1a**). It remains unknown how this impacts other RP3V neurons (**1b)**. It also remains unknown whether SCN AVP neurons terminate in the RP3V, or go elsewhere, such as previously identified projection regions like the organum vasculosum of the lamina terminalis (OVLT), or dorsomedial hypothalamus (DMH) (**1c**). As they can influence the activity of kisspeptin neurons, it remains unknown whether these are the kisspeptin neurons that project to the GnRH neurons influencing the LH surge, or other groups of kisspeptin neurons projecting to the ventromedial hypothalamus (VMH) that influence sexual behaviour, for example (**2**). While SCN NMS neurons are synaptically linked with RP3V kisspeptin neurons (**3a**), it unlikely that these also coexpress AVP (**3b**). It remains unknown what other SCN neurons may influence the activity of the RP3V neurons (**4**), although it is unlikely that SCN VIP neurons are involved as they typically project elsewhere, such as the rostral preoptic area (rPOA) (**5**). Table 1.1 lists potential other projection patterns for SCN neurons. 3V = third ventricle, OX = optic chiasm.

influenced are those that do not impinge onto GnRH neurons. RP3V kisspeptin neurons have been shown to project to other regions in the hypothalamus such as the PVN, SON and VMH, among others (Clarkson & Herbison, 2006; Clarkson *et al.*, 2009; Lehman *et al.*, 2010b; Yeo *et al.*, 2016; Marraudino *et al.*, 2017; Seymour *et al.*, 2017; Hellier *et al.*, 2018). A cell-type specific tracing of the relationship between input and output (cTRIO) (Schwarz *et al.*, 2015) could be used to determine whether the *Avp-cre* input to RP3V kisspeptin neurons is specific to those that project to GnRH neurons or other regions. Broadly cTRIO involves labelling for the upstream projections to a population while only labelling those neurons that also project to a certain region (Schwarz *et al.*, 2015). As such, the kisspeptin neurons projecting to a known region could be traced while also revealing their inputs. Overlap with in the projection pattern with *Avp-cre* neurons would show that the SCN influences kisspeptin neurons that target certain regions. While many of the kisspeptin projections have not been fully characterised (and, as such, may also influence GnRH neurons as well as other targets), it could be that *Avp-cre* neurons act to impart circadian signals from the SCN to other regions of the brain, via RP3V kisspeptin neurons (Figure 8.1).

8.3.2 The functional impact of SCN *Avp-cre* projections onto RP3V kisspeptin neurons

Using electrophysiology and optogenetics, this work revealed that SCN *Avp-cre* neurons communicate with RP3V kisspeptin neurons through the release of AVP. This work is the first to address how endogenously released AVP from the SCN can impact the activity of RP3V kisspeptin neurons. Based on the anatomical tracing, it is likely that the only source of AVP that acts at the RP3V is from the SCN. Interestingly, these studies have revealed that AVP signalling is likely a plastic phenomenon occurring prior to ovulation, but not post-ovulation.

Post-ovulation, the SCN *Avp-cre* neurons appear to switch from releasing AVP to releasing GABA.

Although this work identified close appositions between SCN *Avp-cre* projections, some of which are likely to be synapses (Vida *et al.*, 2010), there was surprisingly limited fast synaptic innervation of the RP3V kisspeptin neurons by SCN *Avp-cre* neurons. As mentioned, it has been suggested that the proportion of AVP-ir appositions to RP3V kisspeptin neurons is correlated to oestradiol levels (Vida *et al.*, 2010). This suggests that there is a greater proportion of kisspeptin neurons receiving fast-synaptic input, however, as the data presented in Chapter 5 showed, there was no change across the oestrous cycle. As there is a GABAergic effect on the RP3V kisspeptin neurons at oestrus, the lack of fast-synaptic innervation suggests that either GABA is released extrasynaptically, or that there is a polysynaptic circuit influencing the activity of the kisspeptin neurons.

In terms of the LH surge, these results demonstrate a mechanism by which the SCN may shape surge onset and duration. SCN neurons are most active towards the end of the light phase (Green & Gillette, 1982; Schaap *et al.*, 2003), which coincides with the onset of the LH surge. If the increase in electrical activity results in AVP-mediated effects only in proestrus, this acts as a gate to the initiation of the LH surge. The coincident fall in oestradiol and rise in progesterone may act at the SCN to drive changes in the production of GABA, while downregulating V1Rs on the RP3V kisspeptin neurons (Figure 8.2). Studies looking at the time course of serum oestradiol and progesterone concentration across ovulation suggest that they decrease and increase, respectively, with ample time to exert effects at the brain (Kerdelhué *et al.*, 2002; McQuillan *et al.*, 2019). There is no data regarding a change in SCN AVP synthesis across the oestrous cycle, thus, the effect of this hormonal change on AVP signalling is still to be revealed. Either it is still be released, but due to the downregulation of V1Rs it is unable to exert its effects, similar to the reduced AVP-mediated effects at kisspeptin neurons seen here

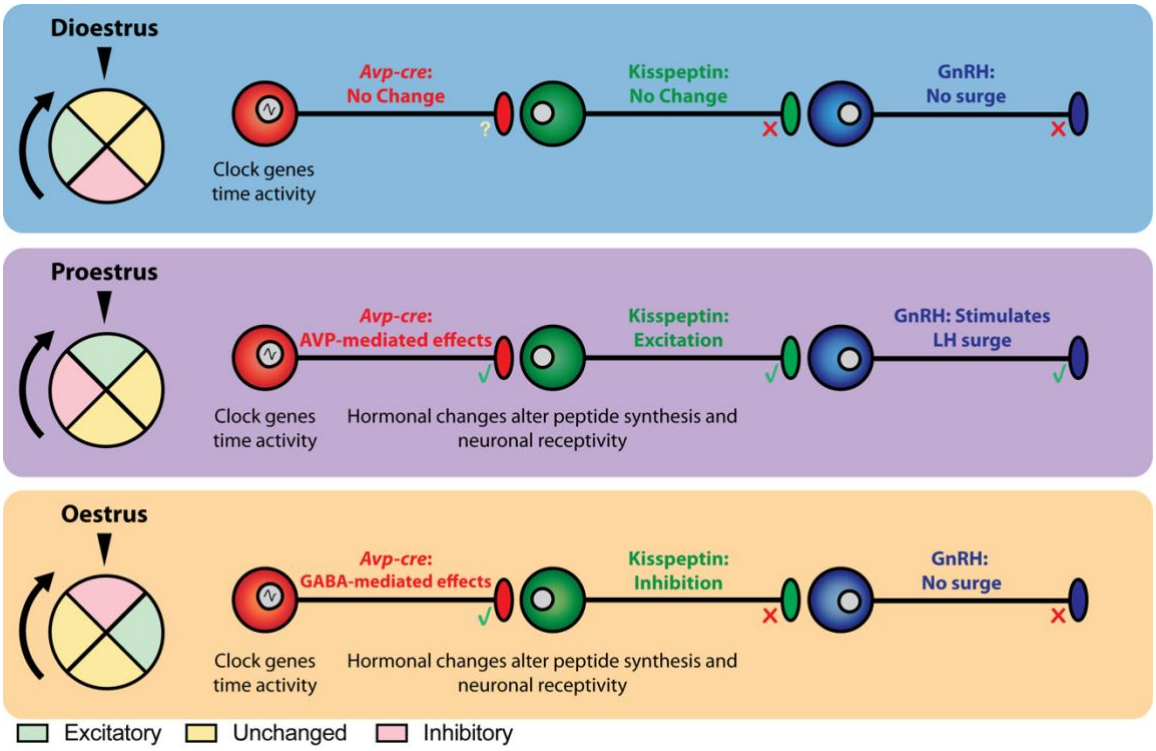

Figure 8.2: Changes in the SCN-to-RP3V circuit activity across the oestrous cycle direct the generation of the LH surge.

The SCN-to-RP3V circuit imparts different effects on LH surge generation across the oestrous cycle. The dial on the left-hand side indicates how the circuit impacts surge generation at each stage, with roughly 24 hours per stage. Clock genes in the SCN *Avp-cre* neurons influence their activity, and time excitation to mid-late afternoon. In **dioestrus**, the excited SCN *Avp-cre* neurons may release variable amounts of AVP or GABA which do not cause a change in the activity of RP3V kisspeptin neurons. No kisspeptin is released, and, as such, there is no excitation of GnRH neurons to generate the LH surge. In **proestrus**, the excited SCN *Avp-cre* neurons may release AVP that, in turn, excites RP3V kisspeptin neurons. The resulting release of kisspeptin excites GnRH neurons to generate the LH surge. In **oestrus**, the excited SCN *Avp-cre* neurons may release GABA that inhibits RP3V kisspeptin neurons. No kisspeptin is released, and, as such, there is no excitation of GnRH neurons to generate the LH surge. ✓ = hypothesised peptide release, **×** = no peptide release, **?** = unknown peptide release.

in oestrus; or AVP production is simultaneously downregulated in the SCN. Oestradiol-induced effects at the kisspeptin neurons, such as changes in ion channels (Piet *et al.*, 2015a) may persist due to the long-lasting genetic actions of ERs,. Thus, the oestrus change in *Avp-cre* neurons, to begin releasing GABA, would drive inhibition to the kisspeptin neurons and stop a repeated LH surge. It could be that this change in production (at the SCN) and responsiveness (at the kisspeptin neurons) is effectively timing the LH surge and is a mechanism to stop its recurrence, despite the daily circadian signal form the SCN.

A key limitation of this work is that experiments were carried out at a single time point. Even though RP3V kisspeptin neurons do not differ in their responsiveness to AVP over the day (Piet *et al.*, 2015b), this does not rule out a difference in AVP production or V1R function. The SCN produces AVP across the course of the day peaking during the morning (Jin *et al.*, 1999; Dardente *et al.*, 2004; van der Veen *et al.*, 2005; Maruyama *et al.*, 2010) As such, packaging and export of the peptide to the terminals may be delayed, and brain slices with severed projections would not contain AVP. There may be greater AVP available for release from projections later in the day, compared to in the morning. Thus, ChR2-mediated stimulation of *Avp-cre* projection fibres, from brain slices taken later in the day may result in a greater proportion of kisspeptin neurons excited by increased endogenous AVP release; while GABAergic inhibition of kisspeptin neurons might be less prominent towards the time when the surge may occur.

8.3.3 The relationship between subfertility and the SCN-to-RP3V circuit

Modelling subfertility by using the PNA mouse model of PCOS, these data have shown that the critical SCN-to-RP3V circuit is downregulated. This adds another abnormality to the GnRH neuronal network seen in the PNA mouse model, which may explain disrupted fertility

in PCOS patients, particularly in terms of ovulatory dysfunction. As PNA mice do not tend to display proestrus, it is not altogether surprising that the circuit is decreased. The ontogeny of this decrease in circuitry remains unknown, however. Two possibilities for this include an organisational effect whereby the SCN-to-RP3V circuit does not develop correctly (due to prenatal androgen excess); or an activational effect whereby impaired steroid hormone feedback disrupts the circuit in adulthood.

Androgen treatment during the prenatal period may be disrupting the development of the SCN *Avp-cre* projections, but the mechanism for how is less clear Androgen treatment can increase AR expression in the female SCN to a more male-like pattern (Iwahana *et al.*, 2008). Thus, the same thing may be occurring in the PNA mouse model, which in turn could inhibit the development of SCN projections (Figure 8.3). Androgenisation does not affect SCN AVP production (de Vries *et al.*, 1994). As there was no difference in SCN transfection levels, this suggests that prenatal androgen treatment does not affect cre expression, and therefore *Avp* expression levels. Thus, the reduction in mCherry-ir fibres, when looked at from an organisational perspective, would solely be a problem with the development of the *Avp-cre* projections from the SCN.

If the cause was activational (i.e. caused by impaired steroid feedback or hyperandrogenism later in life), rather than not developing in the first place, the projections may retract. The lack of oestradiol positive feedback to the RP3V kisspeptin neurons would fail to prime the RP3V kisspeptin neurons and, thus cause a reduction in their activity. This, in turn, may result in a reduction in their afferent wiring (Figure 8.3). As alluded to, the question remains as to whether this is truly an effect of androgen treatment, or whether it is a secondary effect of the loss of oestradiol feedback in PCOS. While Vida *et al.* (2010) suggest that oestradiol treatment increases AVP-ir fibres in the RP3V, the opposite may also be true; that decreases in oestradiol may result in AVP fibre withdrawal. Interestingly, PNA mice are able

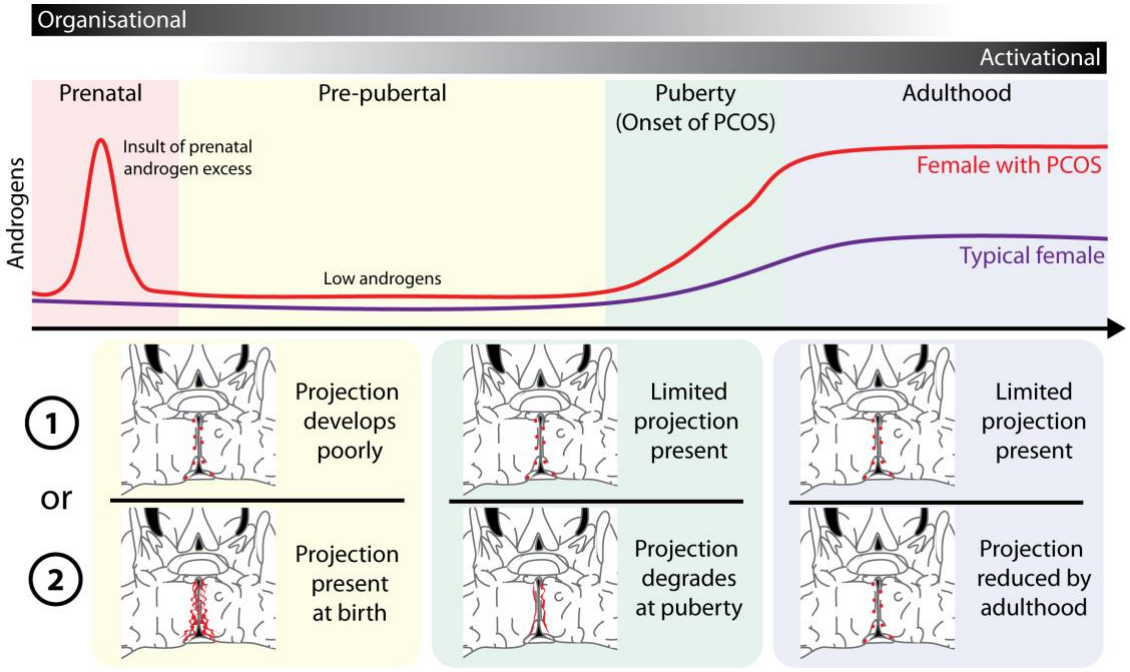

Figure 8.3: How might changes in androgen levels affect SCN-to-RP3V wiring?

Females exposed to prenatal androgens early in life display higher androgen levels throughout puberty and in adulthood, associated with the development of PCOS features. Both periods of high androgens may contribute to the reduction seen in *Avp-cre* mCherry fibre projections to the RP3V. If the prenatal androgen insult disrupts the development (**1**) then it may not be present from birth and be limited throughout life entirely. If the higher pubertal/adulthood androgens affect an already present projection, or the lack of gonadal steroid feedback supporting this network, (**2**) then it would degrade throughout adulthood. Figure adapted from Silva *et al.* (2018), representative brain slices taken from Franklin and Paxinos (2008).

to mount an LH surge when primed with oestradiol (Moore *et al.*, 2013) suggesting that oestradiol replacement may be able to restore the circuit. In saying this, it is important not to discount the effects of hyperandrogenism in these mice. Increased testosterone may be acting at SCN ARs to drive these reductions in fibre density, particularly if SCN AR expression is heightened in the PNA model. It will be necessary for future studies to correlate the projection density to the circulating oestradiol concentration; as well as comparing how dense the projection is in the PNA model to an ovariectomised model where endogenous oestrogens are removed. This will provide some evidence as to whether this is an effect of prenatal androgen treatment or an effect of decreased oestradiol feedback.

8.4 Relevance to human biology

The role of the GnRH neuronal network in the human LH surge has been debated with conflicting results about both its function and relevance, particularly as to whether human oestradiol positive feedback is mediated at the hypothalamus or solely at the pituitary gland (Hall *et al.*, 1994; Ottowitz *et al.*, 2008). Early work in the human hypothalamus did not identify significant kisspeptin populations outside of the infundibulum, the human analogue to the ARN (Rometo *et al.*, 2007). Optimisation of staining techniques, however, has revealed a kisspeptin population in the human equivalent to the RP3V (Hrabovszky *et al.*, 2010; Rumpler *et al.*, 2020) and, thus, the kisspeptin to GnRH circuit may be present in the human. Further, this population appears to be positively regulate by oestrogen feedback (Rumpler *et al.*, 2020). It remains unknown the extent at which this kisspeptin population influences the human LH surge. In saying this, it is important to note that kisspeptin treatment can induce surge-like LH levels and ovulatory responses (Dhillo *et al.*, 2007; Jayasena *et al.*, 2014; Romero-Ruiz *et al.*, 2019). While the literature surrounding the human LH surge suggests some aspect of timing particularly towards the early morning prior to waking (Edwards, 1981; Cahill *et al.*, 1998;

Kerdelhué *et al.*, 2002), although the mechanism behind this remains unknown. It could be that a homologous circuit of SCN-to-RP3V is present in the human, similar to the rodent, which relays a timing signal for the LH surge. The increase in LH appears to consistent with daily increases in cortisol (Kerdelhué *et al.*, 2002); suggesting some aspect of timing, potentially from the SCN.

The likelihood of a homologous SCN-to-RP3V circuit in humans is suggested by endocrine dysfunction in women with disrupted circadian rhythms (Gamble *et al.*, 2013). It may be that SCN stimulation of the human GnRH neuronal network is not occurring, or is occurring at inappropriate times. The activity of the SCN likely needs to be timed with individual clocks in downstream neurons (such as kisspeptin and GnRH), as well as peripheral tissues like the gonadotropes and ovary. Thus, asynchrony between these clocks caused by circadian disruption may impair gonadal hormone release and/or function (Gamble *et al.*, 2013; Stocker *et al.*, 2014; Goldstein & Smith, 2016). Interestingly, fertility in these women appears to be restored once normal circadian rhythms are reinstated (Gamble *et al.*, 2013; Stocker *et al.*, 2014). As such, this temporary subfertility may be due to inappropriate coordination of timing in multiple neuronal populations.

In women with PCOS, it is possible that hyperandrogenism is affecting the SCN circuitry which could contribute to their disrupted ovulation. PCOS patients treated with oestrogen receptor agonists and undergoing *in vitro* fertilisation, are highly amenable to ovulation induction, however. This suggests that exogenous steroid and gonadotropin administration may be able to override the GnRH neuronal network, and its potential timing mechanisms.

8.5 Future studies

8.5.1 Circuit mapping

The work presented here employs anterograde viral tract-tracing of the SCN *Avp-cre* neurons to define their relationship with RP3V kisspeptin neurons. While this method reveals projection fibres, it is limited by its anterograde nature. As mentioned, it remains unknown whether the *Avp-cre* projections seen in the RP3V are terminating fibres or simply *en passant* towards other regions of the brain. Coupling this anterograde tract-tracing with a tissue clearing method such as CLARITY or iDISCO (Chung *et al.*, 2013; Renier *et al.*, 2014), would allow for reconstruction of this circuit to visualise the extent of the projection. The reconstruction would then reveal the true extent of the fibre projection and give insight into where these projections are terminating.

If these fibres are terminating within the RP3V, it remains unclear as to why they rarely form functional synaptic innervation with the kisspeptin neurons. Thus, a marker of synaptic contacts could be used in conjunction with the immunohistochemistry presented here. Synaptophysin (Syp) is a marker of presynaptic vesicles in synaptic terminals (Calhoun *et al.*, 1996). An immunohistochemical stain of Syp in conjunction with mCherry (following AAV-mCherry injection) and kisspeptin could be carried out to identify synaptic contacts. Close apposition of Syp/mCherry/kisspeptin-ir would provide evidence as to whether the *Avp-cre* close appositions to kisspeptin neurons are in fact synaptic contacts. Knowing whether synapses are present or not would allow for further electrophysiological experiments to identify whether these are silent synapses as was discussed in Chapter 5 (Losonczy *et al.*, 2004; Bekkers, 2005; Vincent-Lamarre *et al.*, 2018).

Finally, an opposite approach could be taken whereby RP3V kisspeptin neurons are transfected with a viral-vector for monosynaptic retrograde tracing. This involves transfection in a mouse model expressing cre in kisspeptin neurons (Mayer *et al.*, 2010). The viral vector would then pass through synaptic contacts on the kisspeptin neurons and transfect the afferent neurons with a reporter. Immunohistochemistry for the reporter, as well as AVP, would provide irrefutable evidence as to whether SCN AVP neurons form synaptic contacts onto RP3V

kisspeptin neurons. Again, however, if SCN AVP neurons were forming synaptic contacts onto RP3V kisspeptin neurons, this does not indicate their functionality as shown by the electrophysiological data.

8.5.2 The role of hormonal feedback in AVP- and GABA-mediated communication from the SCN

The switch between AVP- and GABA-mediated communication from SCN *Avp-cre* neurons across proestrus to oestrus is an interesting and previously unknown finding. The key change across ovulation is the altered hormonal milieu of the animal, thus, it is likely that hormonal changes (i.e. the fall in oestradiol and increased progesterone) are driving a change from AVP to GABA release.

To investigate this, several relatively simple experiments can be carried out. The first, would involve determining whether there are changes across the oestrous cycle in either the presynaptic release of AVP or GABA, or looking at how the receptors for these chemicals might differ. Sniffer cell techniques can reveal whether AVP is released from projections (Son *et al.*, 2013; Zaelzer *et al.*, 2018), and would be important to test whether AVP is released at oestrous, when kisspeptin neurons do not respond. While GABA release specifically from these neurons is harder to examine, anatomical studies of GABA immunoreactivity could be carried out to determine whether there is colocalisation of GABA-ir with mCherry-ir in *Avp-cre* projections. Alternatively, a sniffer patch expressing $GABA_A$Rs could be used to determine whether GABA was released in brain slice experiments (Christensen *et al.*, 2014). RP3V kisspeptin neurons clearly respond to GABA across the oestrous cycle (as seen with background inhibitory postsynaptic currents recorded in Chapter 5); although, it may be that increases in progesterone at oestrus are sensitising $GABA_A$Rs. Bath application of $GABA_A$R agonists such as muscimol onto RP3V kisspeptin neurons would determine whether there was a difference in $GABA_A$R

activity across the oestrous cycle, that may begin to respond to extrasynaptic GABA released by *Avp-cre* projections.

Following this, it will be important to determine whether individual hormones may alter the *Avp-cre* projections. Repeating the ChR2-mediated stimulation of *Avp-cre* projections whilst recording kisspeptin neuron activity (as per Chapter 6) could be carried out in an OVX mouse. OVX abolishes the vast majority of oestradiol synthesis and therefore all oestradiol-mediated feedback. OVX will provide an indication as to what the circuit function might be without any hormonal feedback. The loss of oestradiol entirely would be problematic as oestradiol may be linked to AVP production (Shapiro *et al.*, 2000; Pak *et al.*, 2007), V1R expression and function (Kalamatianos *et al.*, 2004a; Piet *et al.*, 2015b), and RP3V kisspeptin neuron activity (Frazão *et al.*, 2013; Piet *et al.*, 2013). Thus, OVX alone would likely disrupt multiple points of the SCN-to-RP3V circuit. To maintain a stable baseline, low level oestradiol replacement to the OVX mouse (OVX + E) could be used, mimicking a dioestrus mouse. Comparing this to a mouse with low oestradiol, given a high oestradiol bolus (OVX+E+E) to mimic proestrus, would allow for potential oestrogen-mediated differences in the system to be interrogated. This may reveal an oestrogen-dependent switch to greater excitation of kisspeptin neurons by SCN *Avp-cre* neurons, as seen here in proestrus mice.

The transition to oestrus and the GABA-mediated inhibition is harder to investigate. It can be hypothesised that increased progesterone levels may be acting to drive changes in chemical release from the SCN *Avp-cre* neurons. Progesterone has been implicated in the suppression of AVP production (Auger & Vanzo, 2006), as well as the potentiation of $GABA_A$Rs (Callachan *et al.*, 1987; Brussard & Koksma, 2003; Wang, 2011). The role of progesterone on GABA synthesis is unclear, with reports showing increases and decreases in GABA synthetic enzymes in different brain regions (Weiland, 1992; Souza *et al.*, 2009; Noriega *et al.*, 2010). As progesterone receptor expression is driven by oestrogen levels (Moffatt *et al.*, 1998; Wagner *et al.*, 2001), however, OVX with progesterone replacement

would not be sufficient to interrogate the role of progesterone action in the SCN-to-RP3V circuit. Thus, an OVX mouse with low oestradiol and high progesterone replacement (OVX+E+P) could be used to model oestrus. As such, it could be expected that the increased progesterone levels may drive a predominantly GABAergic effect from the SCN *Avp-cre* neurons onto RP3V kisspeptin neurons.

8.5.3 An *in vivo* investigation of the AVP-mediated effects on the LH surge

The role of SCN AVP neurons *in vivo* on the generation of the LH surge remains somewhat unclear. While this thesis has shown that *Avp-cre* neurons exert a biphasic drive on kisspeptin activity (i.e. excitation by AVP prior to, and inhibition by GABA post-ovulation), there has been no specific *in vivo* experiments looking at this circuit. Early lesion studies have revealed that the SCN, and by extension the SCN AVP neurons, are necessary for the generation of the LH surge (Wiegand *et al.*, 1980; Wiegand & Terasawa, 1982). These were followed by showing that AVP injections can generate a surge (Palm *et al.*, 1999, 2001), although these have been hampered by studies showing conflicting results on whether V1R inhibition can inhibit the surge (Funabashi *et al.*, 2000a; Palm *et al.*, 2001; Miller *et al.*, 2006).

Modern neuroscientific techniques provide a better method to investigate the role of the SCN AVP neurons *in vivo. In vivo* optogenetic stimulation of *Avp-cre* neurons coupled with repeated blood sampling for LH levels would provide key evidence as to whether their stimulation is sufficient to induce a surge. Appendix 9.9 of this thesis presents preliminary results and a discussion from a pilot study designed to address this experiment. A similar approach utilising designer receptors exclusively activated by designer drugs (DREADDs) could be carried out. Injection of a viral vector carrying a modified human M3 muscarinic receptor activated by exogenous clozapine-N-oxide (Roth, 2016), could be used to stimulate

the *Avp-cre* neurons, whilst taking blood samples for LH detection, potentially showing that increases in SCN *Avp-cre* neuron activity drive downstream LH release. The reverse experiments may also be considered. During proestrus at the expected time of the surge, either inhibitory opsins could be stimulated resulting in suppression of *Avp-cre* neuron activity; or activation of an inhibitory DREADD could be used to see whether the expected LH surge is inhibited. These experiments would provide evidence as to whether the SCN AVP neurons were sufficient and necessary for the development of the LH surge.

8.5.4 Understanding the aetiology of the reduction in SCN-to-RP3V circuitry in the PNA mouse model

There was a clear reduction in the SCN-to-RP3V circuit in the PNA mouse model. While it remains unknown what causes this decrease, several experiments can be designed to address its aetiology.

Using an *Avp-cre:tdTomato* mouse, that reports cre expression from whenever the *Avp* gene has been active, the SCN-to-RP3V circuit from PNA and VEH mice could be examined at different time points prior to puberty to determine whether the projection is present, and how different levels of androgens over time may cause it to change. The development of this circuit in untreated animals remains unknown, thus, experiments could be designed to test how heightened androgen levels at different time points may be affecting it through prenatal exposure, or through puberty.

It would be important to determine the time point at which the SCN-to-RP3V circuit develops, to determine when it may be impacted by heightened androgens. It is unlikely that the RP3V kisspeptin neurons are present before puberty (Clarkson & Herbison, 2006; Mohr *et al.*, 2016), thus, the circuit may not be set up *in utero* and could be unaffected by the prenatal androgen treatment. Silva *et al.* (2018) suggest that androgen levels in the offspring are not

significantly elevated until puberty, thus, it would next be important to see whether the increase in androgen levels at puberty either delay the circuits development or drive its regression. Investigation of the circuit anatomy at these two time points could provide some indication as to whether the reduction in fibre density seen here is either an organisational, or activational effect of the prenatal androgen treatment.

As mentioned, the reduction in the circuitry may not be directly from androgen action, but rather from a loss in oestradiol-mediated feedback. An experiments could be developed to test the hypothesis that removing androgen effects to restore oestradiol feedback would restore the *Avp-cre* projection to the RP3V. The first would involve OVX of PNA mice, whereby the androgen overproducing ovary was removed, and oestradiol was implanted to restore oestradiol-mediated feedback. The circuit could then be investigated in these PNA mice to determine whether oestradiol replacement is sufficient to re-establish the circuit.

8.6 Concluding remarks

The work presented in this thesis confirms previous anatomical studies suggesting the presence of a circuit from SCN AVP neurons to RP3V kisspeptin neurons. Using genetically-mediated viral anterograde tract tracing, the density of this circuit and its anatomical interaction with kisspeptin neurons has been characterised, with the findings suggesting it is more extensive than previously thought. Selective optogenetic stimulation of this projection has been shown to alter the activity of identified kisspeptin neurons in a manner consistent with the generation of the LH surge: prior to ovulation, during proestrus, the circuit acts to excite kisspeptin neurons, while post ovulation, during oestrus, this circuit inhibits kisspeptin neuron activity. Thus, this circuitry appears to be critical in the development of the preovulatory LH surge. Finally, the SCN-to-RP3V circuit was interrogated in a clinically-relevant mouse model of PCOS, a pathology where ovulation is disrupted. It was found that there was a reduction in

the SCN AVP neuron to RP3V kisspeptin neuron circuit, underlying a potential cause for ovulatory dysfunction in PCOS.

Specifics about this circuit remain to be defined, particularly 1) how the activity of steroid hormones can influence its anatomy and 2) how they may drive changes in its function, and 3) whether changes to the circuit driven by diminished fertility are plastic and can be restored. The studies presented in this thesis have given novel insight into the regulation of the GnRH neuronal network by focussing on the afferent biological clock. Ultimately, this has provided us with a unique insight into how the brain is able to regulate and integrate both circadian and hormonal cues to precisely time ovulation.

Chapter 9:

Appendices

9.1 Appendix I: List of chemical reagents

No.	Solution	Reagents	pH
1.1	0.1 M Phosphate buffer (PBS)	H_2O 0.1 M Na_2HPO_4 0.1 M $NaH_2PO_4 \cdot 2H_2O$	 7.6
1.2	4% Paraformaldehyde	0.1 M Phosphate buffer 4% (w/v) Paraformaldehyde	 7.6
1.3	Tris-buffered saline (TBS)	H_2O 0.5 M Tris-HCl 0.5 M Tris-base 0.15 M NaCl	 7.6
1.4	30% Sucrose	TBS 30% (w/v) sucrose	 7.6
1.5	Cryoprotectant (stored at -20ºC)	1.0 M phosphate buffer 0.9% (w/v) NaCl 30% (w/v) sucrose 1% (w/v) polyvinylpyrrolidone (PVP-40) 30% (w/v) ethylene glycol	 7.6
1.6	Immunohistochemistry blocking solution	TBS 0.25% (w/v) Triton-X-100 0.3% (w/v) bovine serum albumin (BSA) 2% (w/v) normal goat serum (NGS)	 7.6
1.7	Immunohistochemistry incubation solution	TBS 0.25% (w/v) Triton-X-100 0.3% (w/v) bovine serum albumin (BSA)	 7.6
1.8	Slicing solution for *ex vivo* brain slicing	H_2O 87 mM NaCl 2.5 mM KCl 25 mM $NaHCO_3$ 1.25 mM NaH_2PO_4 0.5 mM $CaCl_2$ 6 mM $MgCl_2$ 25 mM D-glucose 75 mM sucrose	
1.9	Artificial cerebrospinal fluid	H_2O 125 mM NaCl 2.5 mM KCl 26 mM $NaHCO_3$ 1.25 mM NaH_2PO_4 2.5 mM $CaCl_2$ 1.2 mM $MgCl_2$ 11 mM D-glucose	

No.	Solution	Reagents	pH
1.9	Potassium chloride pipette internal solution	H_2O 130 mM KCl 10 mM HEPES 0.2 mM Na_2-GTP 2 mM Mg-ATP 1 mM QX314-Cl KOH for pH Sucrose for osmolarity to ~290 mOsM	 7.3
1.10	PBS-tween	0.1 M phosphate buffer 0.05% tween-20	 7.4
1.11	Citrate buffer	H_2O 1.03% (w/v) citric acid monohydrate 1.816% (w/v) sodium phosphate	 5.0
1.12	ELISA blocking solution	0.1 M phosphate buffer 0.05% tween-20 5% skim milk powder	 7.4

Table 9.1: List of chemical solutions, and their composite reagents, used in this thesis.

9.2 Appendix II: Antibodies

Product No.	Antibody	Source
Primary Antibodies		
T-5048.0050	Guinea pig anti-vasopressin	Peninsula Laboratories International, Inc. (CA, USA)
20077	Rabbit anti-vasoactive intestinal peptide	Immunostar (WI, USA)
20073	Rabbit anti-gastrin releasing peptide	Immunostar (WI, USA)
ab167453	Rabbit anti-mCherry	AbCam (Cambridge, UK)
AC053	Sheep anti-kisspeptin	Prof. A. Caraty (French National Institute for Agricultural Research, Paris, France)
GA04	Guinea pig anti-GnRH	Prof. G. Anderson (University of Otago, Dunedin, New Zealand)
Secondary Antibodies		
706-545-148	Donkey anti-guinea pig Alexa Fluor 488	Jackson ImmunoResearch Laboratories, Inc. (PY, USA)
A21206	Donkey anti-rabbit Alexa Fluor 488	ThermoFisher Scientific (MA, USA)
A10042	Donkey anti-rabbit Alexa Fluor 568	ThermoFisher Scientific (MA, USA)
A16045	Biotinylated donkey anti-sheep	ThermoFisher Scientific (MA, USA)
Tertiary Antibodies		
S11223	Streptavidin, Alexa Fluor 488 conjugate	ThermoFisher Scientific (MA, USA)
Antibodies used for ELISA		
518B7	Bovine LHβ monoclonal	Dr. L. Sibley (UC Davis, CA, USA)
AFP240580Rb	Rabbit polyclonal LH	Dr. A. Parlow (National Hormone and Pituitary Program, Torrence, CA, USA)
P0448	Goat anti-rabbit IgG/HRP	DAKO (CA, USA)

Table 9.2: List of antibodies, and their sources, used in this thesis.

9.3 Appendix III: Viral vectors

In text as:	Full Virus Name	Titre	Source
AAV-mCherry	AAV-DJ-EF1-DIO-mCherry	5.05×10^{13} GC/mL	Stanford Vector Core
AAV-ChR2	AAV-DJ-EF1 DIO hChR2 (E123T/T159C)-p2a-mCherry-WPRE	1.60×10^{13} GC/mL	Stanford Vector Core

Table 9.3: List of viral vectors, and their sources, used in this thesis.

9.4 Appendix IV: LED light intensity

LED Intensity (%)	Blue light power (466 ± 40 nm; mW)	Green light power (562 ± 40 nm; mW)
4× Objective (0.1 NA)		
100	100.3	43.3
90	95.0	40.1
80	88.5	36.5
75	85.1	34.8
70	81.5	33.0
60	73.6	29.2
50	64.9	25.3
40	54.8	21.0
30	43.1	16.5
25	36.9	14.1
20	29.7	11.5
10	14.8	6.0
5	6.6	3.0
2	1.7	1.1
1	0.1	0.4
40× Objective (0.8 NA)		
100	53.9	19.6
90	50.1	18.2
80	46.0	16.9
75	44.0	16.1
70	41.8	15.3
60	37.0	13.6
50	32.0	11.8
40	26.4	9.8
30	20.4	7.7
25	17.4	6.6
20	14.1	5.4
10	7.0	2.9
5	3.1	1.4
2	0.8	0.5
1	0.1	0.2

Table 9.4: Details of light intensity from LED lights used in this thesis.

9.5 Appendix V: Drugs used in electrophysiology

Product No.	Drug	Source
1262	Gabazine	Tocris Bioscience (Bristol, UK)
T-550	Tetrodotoxin	Alomone Labs (Jerusalem, Israel)
275875	4-Aminopyridine	Sigma-Aldrich (MO, USA)
3377	Manning Compound; catalogued as: $(d(CH_2)_5^1,Tyr(Me)^2,Arg^8)$-Vasopressin	Tocris Bioscience (Bristol, UK)
2935	Vasopressin; catalogued as: $[Arg^8]$-Vasopressin	Tocris Bioscience (Bristol, UK)

Table 9.5: List of drugs used in electrophysiological experiments, and their sources, used in this thesis.

9.6 Appendix VI: Surgery does not affect oestrous cycles

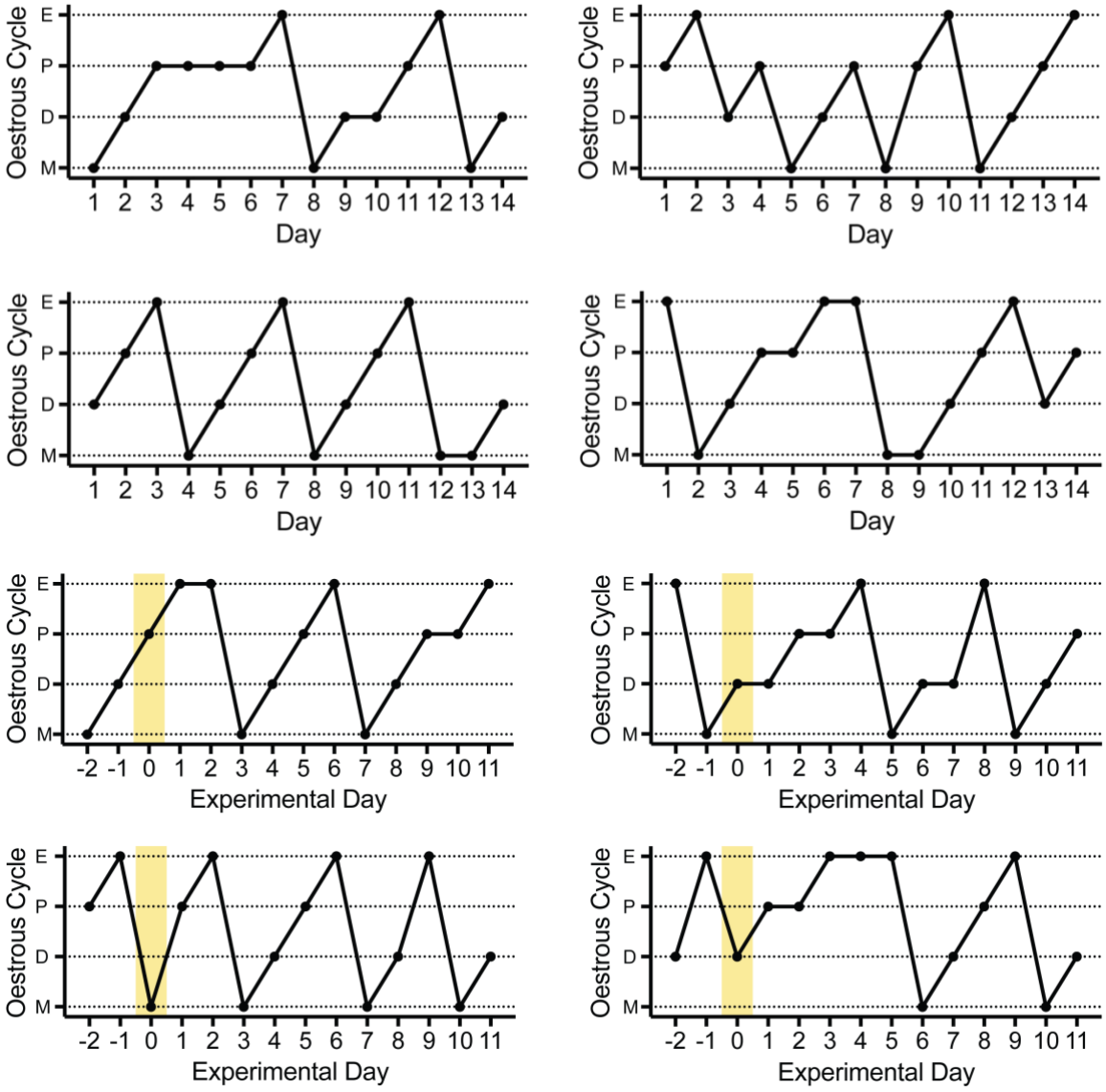

Figure 9.1: Oestrous cycles of mice undergoing stereotaxic surgery.

Upper: Four representative examples of typical mouse oestrous cycles. **Lower:** Four representative examples of mouse oestrous cycles before and after stereotaxic surgery. Surgery took place on experimental day 0 outlined by the yellow bar. Surgery did not affect oestrous cycles. M = metoestrus, D = dioestrus, P = proestrus, E = oestrus.

9.7 Appendix VII: GFP characterisation in the female *Kiss1-hrGFP* mouse model

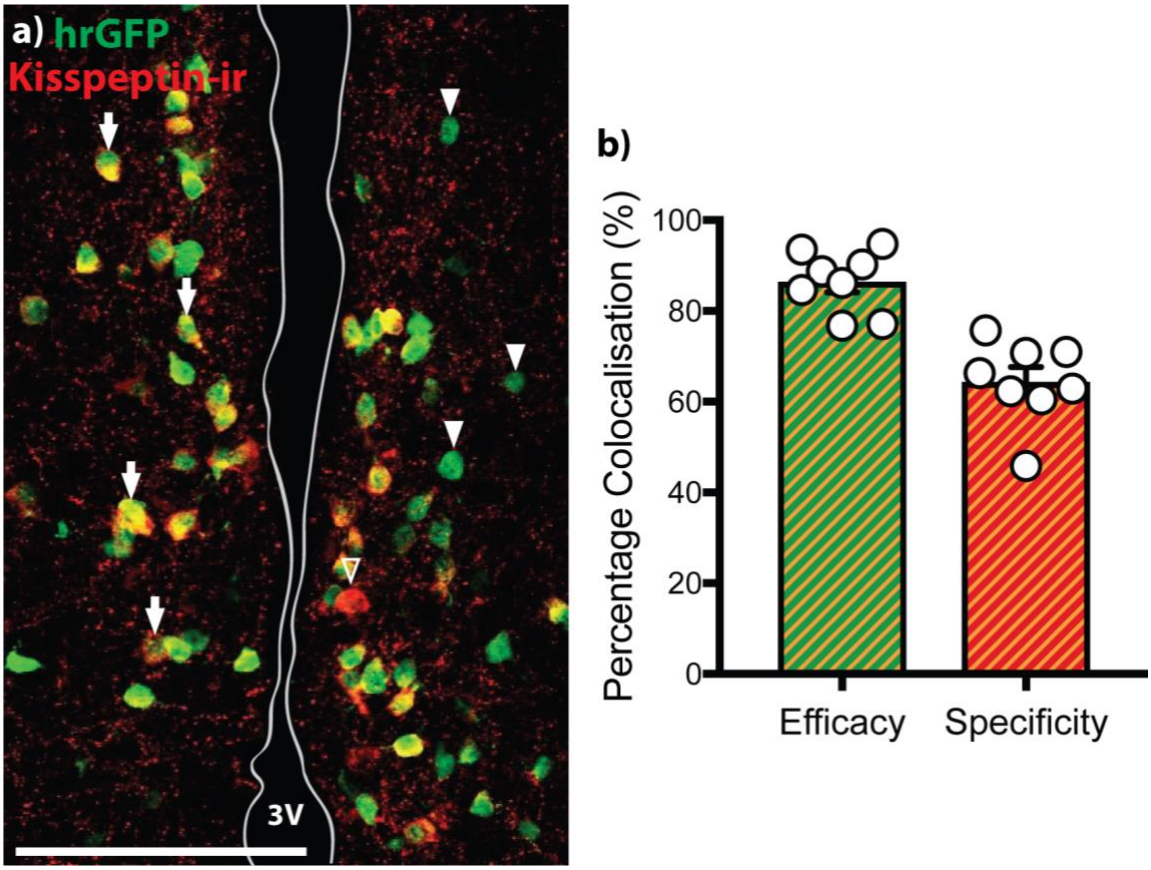

Figure 9.2: Characterisation of GFP expression in the *Kiss-hrGFP* mouse model.

a) Maximum projection image of a confocal Z-stack showing immunofluorescence staining for kisspeptin (red) and endogenous hrGFP fluorescence (green) in the RP3V. Overlap of the two labels indicates colocalisation (orange). Filled arrowheads indicate hrGFP expressing cells. Empty arrowheads indicate kisspeptin-ir cells. Arrows indicate colocalised cells. **b)** The efficacy is the proportion of the kisspeptin-ir population expressing hrGFP; while the specificity is the proportion of hrGFP cells with kisspeptin-ir. Data shown as mean ± SEM. Scale bar = 100 µm. 3V = third ventricle. This work was carried out at the University of Otago by Anaëlle K. Braine (2018).

9.8 Appendix VIII: High power light intensity inhibits kisspeptin neuron activity

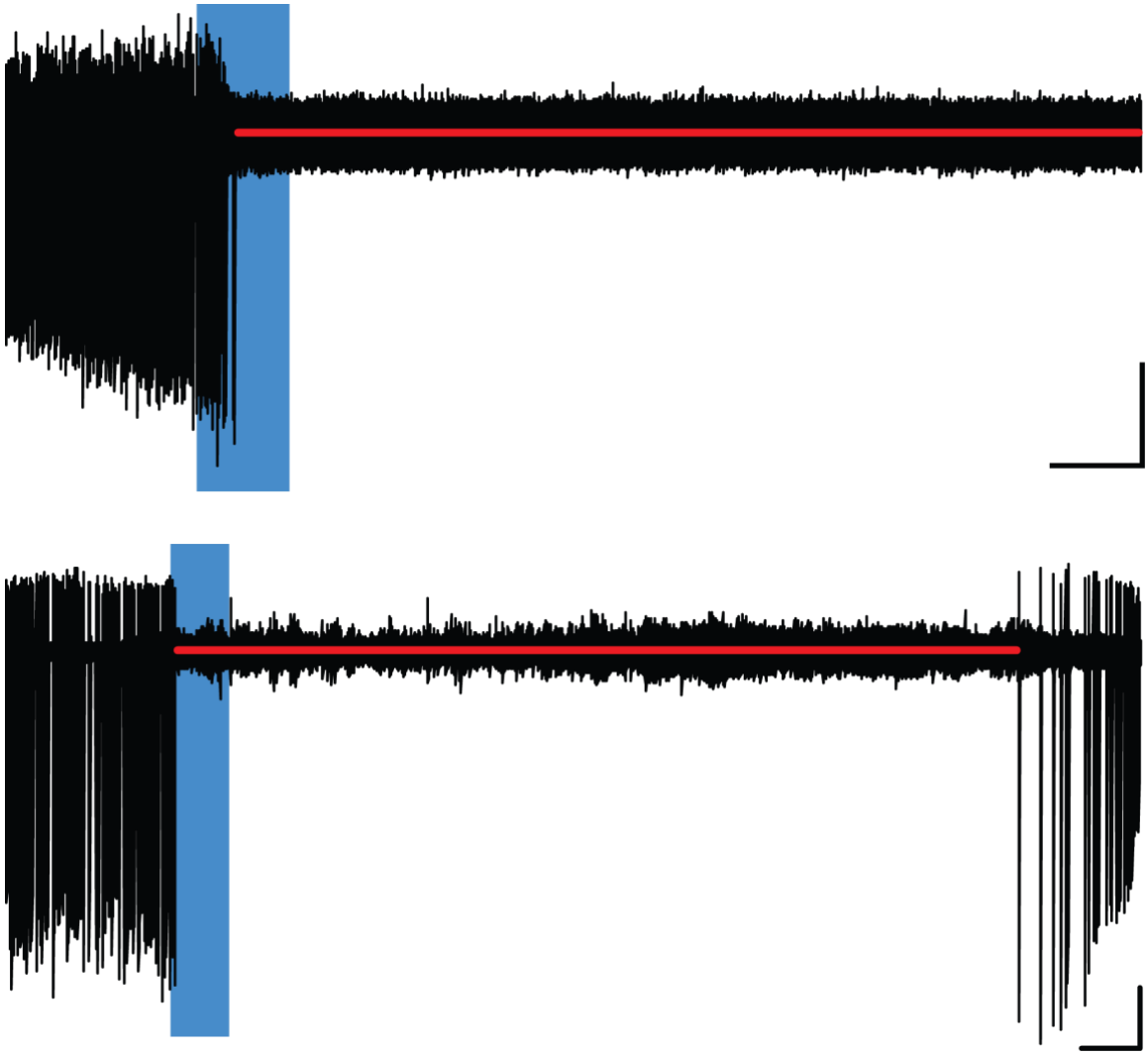

Figure 9.3: Inhibition of kisspeptin activity by 60 s of high LED power HFLS.

Two representative recordings of kisspeptin neurons with high-frequency light stimulation of *Avp-cre* projections at 53.9 mW power. This results in complete and prolonged inhibition of the neurons. Because this is not seen with lower power stimulations it is likely due to light-induced unwanted effects. The red lines indicate ~ 10 and ~ 12 minutes of inactivity, respectively. Scale bars = 60 s/50 pA.

9.9 A pilot study testing the effect of *in vivo* optogenetic stimulation of SCN *Avp-cre* neurons on the LH surge

9.9.1 Introduction

The surge of LH, necessary for ovulation, is closely timed in mammals to occur towards the end of the afternoon in proestrus (Everett & Sawyer, 1950; Murr *et al.*, 1973; Legan *et al.*, 1975; Bronson & vom Saal, 1979). The timing is thought to rely on a daily signal from the SCN coincident with rises in oestradiol which both impinge on the GnRH neuronal network (Everett & Sawyer, 1950; Legan *et al.*, 1975; Legan & Karsch, 1975; Wiegand *et al.*, 1980; Wiegand & Terasawa, 1982; Christian *et al.*, 2005; Miller *et al.*, 2006). As mentioned in Chapter 8, the sufficiency of the circuit between SCN and RP3V in the generation of the LH surge can only be conclusively confirmed by *in vivo* stimulation. *In vivo* optogenetic studies of the SCN are limited, with most looking at how stimulation of the SCN changes entrainment (Jones *et al.*, 2015; Mazuski *et al.*, 2018); only one study has optogenetically stimulated AVP projections originating from the SCN (Gizowski *et al.*, 2016). The results in this thesis have identified a functional output from SCN *Avp-cre* neurons that can excite RP3V kisspeptin neurons. Further, it is consistent with the idea of the SCN gating the surge to only occur on proestrus. Thus, it is important to determine whether the circuit is sufficient alone to trigger the LH surge *in vivo*.

9.9.1.1 Hypothesis and aim

As stimulation of SCN *Avp-cre* neurons *in vitro* can excite RP3V kisspeptin neurons at proestrus, it was hypothesised that **stimulation of this circuit is sufficient to trigger the LH surge given the appropriate hormonal environment**. As oestrogenic feedback is necessary for the development of the LH surge (Legan *et al.*, 1975), this was carried out in a model of

positive feedback used by others, previously (Bronson, 1981; Wintermantel *et al.*, 2006; Czieselsky *et al.*, 2016). To more accurately determine whether stimulation of the SCN *Avp-cre* neurons was sufficient to trigger an LH surge, these experiments were carried out mid-morning, to see whether SCN *Avp-cre* neuron stimulation could phase-advance the LH surge. As such, this pilot study aimed **to optogenetically stimulate the SCN *Avp-cre* neurons, while taking blood samples to determine the output of LH**.

9.9.2 Methods

Most methods are described elsewhere. Supplementary methods are listed below.

9.9.2.1 Stereotaxic fibre-optic implantation

Following stereotaxic injection of AAV-ChR2 into female *Avp-cre* mice, bilateral optical fibres were inserted above the SCN. Following surgery set up (as per Section 2.2), fur covering the scalp was trimmed using small scissors, and 4% hibitane was applied to the exposed skin. A midline incision was made in the skin using scissors, and the connective tissue covering the skull was cut. Using a small drill bit, the skull was etched to roughen up the periosteal surface. Etching gel (Scotchbond, ESPE, 3M) was then applied to the skull and left for 60 seconds, before removal with cotton buds and water. One small hole was drilled through the skull at the anterior end of the scalp incision, and two at the posterior end; and small screws were then inserted halfway into each hole.

The virus was then injected into the brain at the level of the SCN, as outlined in Section 2.2.1. Once the virus was injected and the needle removed, a thin layer of primer (Unitek, 3M) was applied to the exposed skull surface. The bilateral fibre-optic cannula was then lowered 5.7 mm into the brain (to sit above the SCN) through the hole made for virus injection. The cannulae

used were dual 6 mm flat-tip fibre-optics. The fibre-optics were 200 µm wide each, with a 0.5 mm inter-fibre distance (Doric Lenses, QC, Canada)**.**

With the fibre-optic *in situ*, Transbond XT adhesive (Unitek, 3M) was applied to surround the cannula and the screws. The 0.3 mm gap between the cannula ferrule and skull was also filled with adhesive. Once in place, blue LED light was used to set the adhesive. Following adhesion to the skull, two surgical sutures (Mersilk, Ethicon) were placed anterior and posterior to the glued region (Figure 9.4a). The mice were individually housed following surgery and left to recover. Postoperative management procedures, outlined by the University of Otago Animal Ethics Committee, were carried out following surgery.

9.9.2.2 Ovariectomy, capsule implantation and hormonal positive feedback

Mice used in *in vivo* optogenetic experiments underwent ovariectomy and capsule implantation six days prior to blood sampling. Following surgery set up (as per Section 2.2), mice were placed prone on a heating pad, and the lower back fur was shaved. Four percent hibitane was applied to the exposed skin. A small midline cut was made through the skin. The cut was moved laterally to expose the dorsal musculature, and a second cut was made through the muscle. The ovary and uterine horn were exteriorised, and the distal uterine horn was clamped with a haemostat, just below the ovary. The ovary was then excised. The uterine horn was placed back into the abdominal cavity, and the procedure was repeated on the contralateral side.

Following bilateral removal of the ovaries, a SILASTIC capsule of 17β-oestradiol mixed with medical-grade adhesive (0.1 mg/mL adhesive) into SILASTIC tubing (0.1 mm internal diameter, 2.13 mm external diameter) was implanted subcutaneously. Implants were cut to 1 cm/20 g body weight to provide 1 µg oestradiol/20 g body weight. Finally, the skin was closed with one to two wound staples (EZ Clip, Soelting Co.).

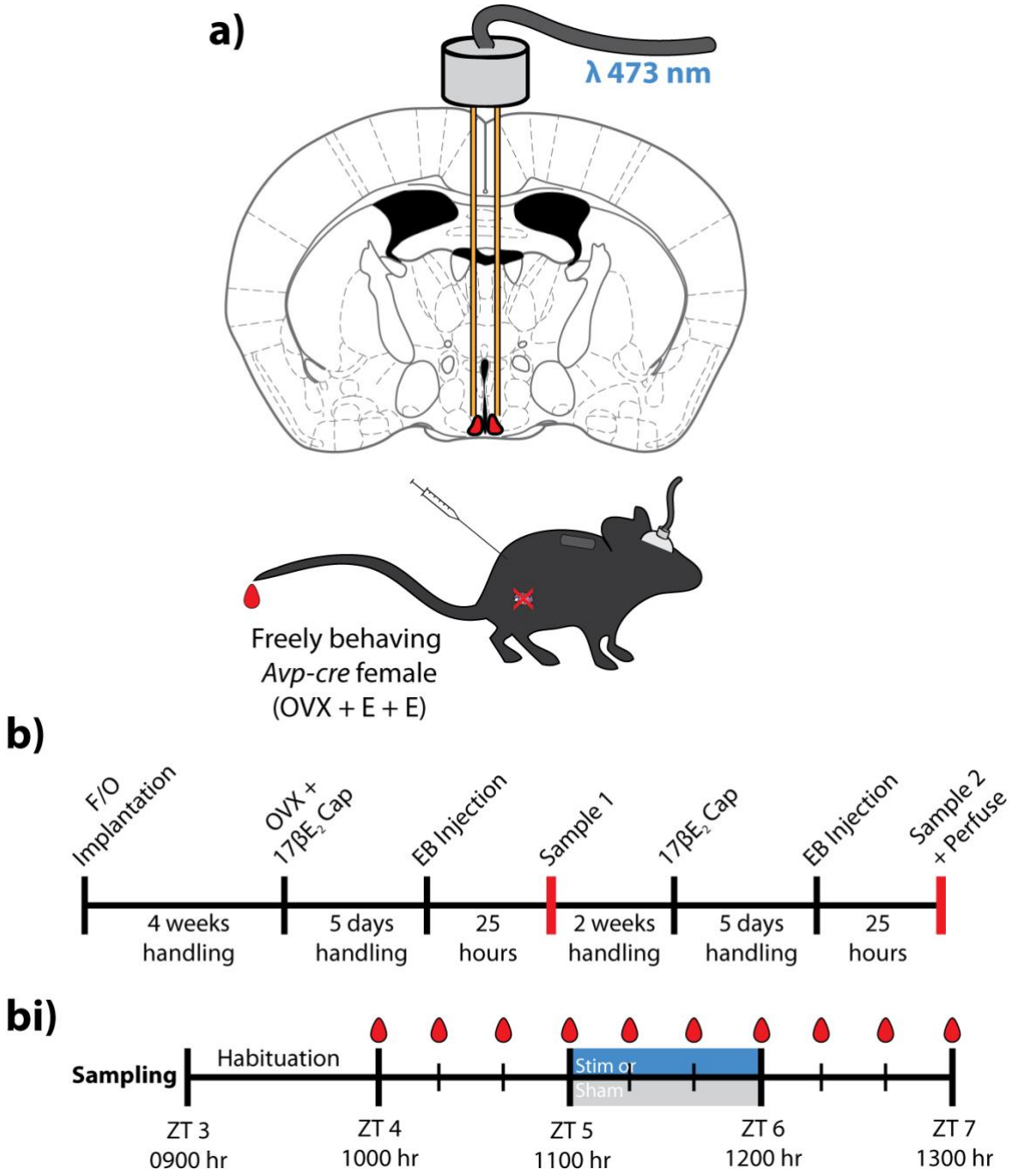

Figure 9.4: Experimental protocol for *in vivo* optogenetic pilot experiments.

a) Experimental setup. Bilateral optical fibres (F/O) are implanted above the SCN to shine blue light onto ChR2-expressing *Avp-cre* neurons (red). Mice in this experiment are ovariectomised (OVX) and implanted with a capsule of 17β-oestradiol ($17\beta E_2$ Cap). One day prior to blood sampling, mice receive oestradiol benzoate subcutaneously (EB). This primes mice for an LH surge (OVX+E+E) on the day of blood sampling. **b)** Time course of experimentation showing surgeries and injection times. Blue bars represent experiment times. **bi)** Time course of blood sampling. Red drops indicate when blood samples are taken (20 min intervals). Blue or grey box indicates an hour of optogenetic stimulation, or sham stimulation with the laser turned off.

Postoperative management procedures, outlined by the University of Otago Animal Ethics Committee, were carried out following surgery.

Five days post-implantation, mice received a subcutaneous injection of oestradiol benzoate (1 µg/ 20 g body weight) to raise serum oestradiol to positive feedback levels (Bronson, 1981) (Figure 9.4b).

9.9.2.3 *In vivo* optogenetic protocol

Mice were randomly assigned to either stimulation or sham protocol. Sham protocols were carried out in exactly the same manner as stimulation, but the laser was not turned on. At ZT3 on the day of the experimentation, mice were connected via the fibre-optic cannulae to a laser (IkeCool Corporation). At ZT5, the laser was turned on to deliver 5 ms pulses of 473 nm wavelength light at 20 Hz for 6 seconds every 12 seconds (based on Piet *et al.* (2018)), for 60 mins (Figure 9.4bi). Between ZT4-ZT7 serial blood samples were collected from the tail tip as outlined below.

Following experimentation, mice were then reassigned to the opposite group (i.e. stimulation became sham). A second implant and injection (as outlined above) were given, and the experiment was repeated at a later date based on the mouse's new grouping. Thus, each animal underwent both stimulation and sham stimulation. At the end of the second experiment, the mice were transcardially perfused (Section 2.3.1) so ChR2 expression and optical fibre placement could be determined.

9.9.2.4 Serial blood sample collection

Mice used for *in vivo* optogenetic experiments were habituated to daily handling for 2-5 weeks prior to blood sampling, to avoid stress when taking blood. Mice were kept in a quiet room in open-top cages during this handling procedure. Blood samples were taken from a small

cut at the tip of the mouse's tail. Three µL of blood was taken every 20 minutes during the experimental period (Figure 9.4bi). Whole blood samples were then diluted in 57 µL of phosphate-buffered saline (PBS)-tween (Appendix I, 1.10) and immediately frozen on dry ice. Blood samples were stored at -20ºC for *post hoc* hormone assays.

9.9.2.5 LH sandwich enzyme-linked immunosorbent assay (ELISA)

An established sandwich ELISA for LH (Steyn *et al.*, 2013; Czieselsky *et al.*, 2016) was used to determine the concentration of LH in the small blood samples taken as per Section 2.7. A 96-well high-affinity binding plate (Corning**)** was coated with bovine LHβ518B7 monoclonal antibody (50 µL/well; 1:1000 in PBS; Dr. L. Sibley, UC Davis, CA, USA). All incubations following, were carried out in a humidified chamber on an orbital shaker. Following overnight incubation at 4ºC, wells were filled with 200 µL of blocking buffer (Appendix I, 1.12) and were incubated for 120 minutes at room temperature. The plate was then washed with 0.05% PBS-Tween (Appendix I, 1.10), 3 times for 3 minutes each. Samples, along with standards and positive controls, were added to the plate and incubated at room temperature for 120 minutes. The standard curve for LH detection was produced by serial dilution of mouse LH-RP reference peptide (Dr. A. Parlow, National Hormone and Pituitary Program, Torrence, CA, USA). Following this, plates were washed as described previously. Fifty µL/well of rabbit LH detection primary antibody (1:10000 in PBS; Dr. A. Parlow, National Hormone and Pituitary Program, Torrence, CA, USA) were added to the well for 90 mins and incubated at room temperature. This was followed by washing, and incubation with 50 µL/well of horseradish peroxidase-conjugated polyclonal goat anti-rabbit IgG secondary antibody (1:1000 in PBS; DAKO, Santa Clara, CA, USA) for 90 mins at room temperature. After another wash, 100 µL/well of H_2O_2 in citrate buffer (Appendix I, 1.11) with *o*-phenylenediamine (1 tablet, Invitrogen) was added, and incubated while protected from light for 30 mins. The reaction was ceased by addition of 50 µL/well of 3M hydrochloric acid. LH levels were then determined

using an absorbance plate reader (Molecular Devices) at 490 nm and 650 nm wavelengths. The sensitivity of the LH ELISA was 0.002 ng/mL.

9.9.2.6 Statistical analysis

General analysis methods are outlined in Section 2.7. LH concentrations were grouped into either baseline (1020 – 1100 hr), stimulation/sham (1120 – 1200 hr), or recovery (1220 – 1300 hr) periods. These were compared across experiments using a Friedman test with *post hoc* Dunn's multiple comparisons test. To compare between experiments, the stimulation or sham period was normalised to the baseline concentrations. The stimulation and sham periods were then compared using a Mann-Whitney test.

9.9.3 Preliminary results

Eight mice were sampled with either light stimulation of ChR2-expressing SCN *Avp-cre* neurons (stimulation), and then at another time with sham stimulation (laser not turned on; sham), or in the opposite order. Individual LH secretion profiles over the sampling periods are presented in Figure 9.5a. Throughout the experiment, some mice did not display any notable differences in LH secretion from baseline, in either stimulation (Figure 9.5a; examples: mice 4 and 5) or sham experiments (Figure 9.5a; examples: mice 6, 7 and 8). Others showed small peaks in LH concentration during stimulation (Figure 9.5a; examples - mice 1, 3 and 5). Similar peaks in LH concentration, however, were also seen in control experiments with sham stimulation (Figure 9.5a; examples - mice 1 and 2). The highest concentration of LH recorded during stimulation was 4.12 ng/mL (Figure 9.5a; mouse 7). The highest concentration of LH recorded during sham stimulation was 3.34 ng/mL (Figure 9.5a; mouse 4). Mouse 5 showed

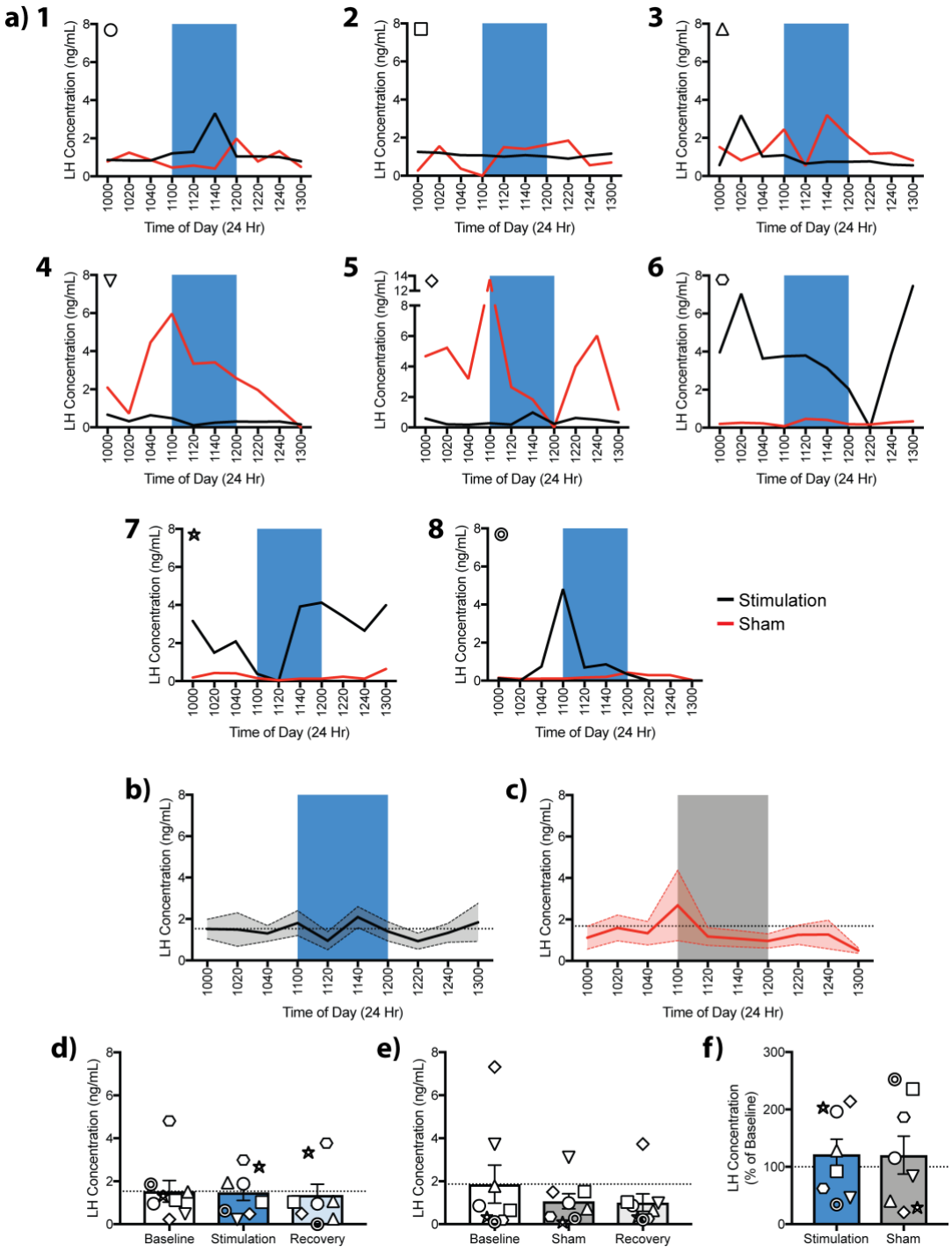

Figure 9.5: I*n vivo* optogenetic stimulation of SCN *Avp-cre* neurons does not change plasma LH concentration.

a) Plasma LH profiles in eight individual mice. Each was subjected to optogenetic stimulation, or to sham stimulation (laser off), in a randomised order. Blue bars represent the stimulation period. **b, c)** Averaged LH profiles from mice with optogenetic stimulation (b) or sham stimulation (c). **d, e)** Quantified data from the baseline, during the stimulation or during the sham stimulation, and the recovery period post-stimulation. **f)** There was no difference in LH concentration whether stimulation was on or off. Dotted lines represent baseline. Symbols represent individual mice and are shown on individual traces. Raw data shown in a). Data in b) – f) shown as mean ± SEM.

the highest peak in LH concentration at 13.53 ng/mL (Figure 9.5a), however, this peak was initiated before the onset of stimulation, and, therefore, could not have been caused by the excitation of ChR2-expressing neurons.

When the data are grouped (Figure 9.5b) there was no synchronised increase in LH secretion, suggesting that overall stimulation of ChR2-expressing SCN *Avp-cre* neurons did not trigger an LH surge (Figure 9.5b, d; baseline [LH]: 1.53 ± 0.50 ng/mL; stimulation [LH]: 1.48 ± 0.37 ng/mL, $p = 0.91$ compared to baseline; stimulation recovery [LH]: 1.37 ± 0.50 ng/mL, $p = 0.91$ compared to baseline; $n = 8$ mice; Friedman tests with *post hoc* Dunn's multiple comparisons tests). In sham experiments, there was also no change to LH concentration during or following light stimulation (Figure 9.5c, e; sham baseline [LH]: 1.87 ± 0.89 ng/mL; sham stimulation [LH]: 1.07 ± 0.35 ng/mL, $p > 0.99$ compared to baseline; sham recovery [LH]: 1.01 ± 0.41 ng/mL, $p > 0.99$ compared to baseline; $n = 8$ mice; Friedman tests with *post hoc* Dunn's multiple comparisons tests). Due to the difference in raw baseline LH concentrations, the stimulation concentrations were normalised to baseline levels before comparison. There was no difference between the normalised LH concentrations between stimulation and sham groups (Figure 9.5f; normalised stimulation [LH]: 122.0 ± 26.3% of baseline; normalised sham [LH]: 120.4 ± 33.0% of baseline; $p = 0.80$, Mann-Whitney test).

The data presented here suggest that *in vivo* optogenetic stimulation of ChR2-expressing SCN *Avp-cre* neurons may not be sufficient to trigger an LH surge out of phase.

9.9.4 Discussion

9.9.4.1 Limitations of this pilot study

There are multiple limitations to this experiment, which will now be considered. This experiment relies on multiple coincident successes to ensure that each step is carried out accurately. Firstly, the SCN *Avp-cre* neurons must be accurately targeted by the AAV injection

to ensure ChR2-expression is sufficient. The data presented here comes from animals with visible mCherry expression in the SCN, with optical fibres placed in the parenchyma above. There is little reason to suspect the function of the ChR2 differs *in vivo* compared to what has been shown in *in vitro* experiments carried out in Chapter 5. Following AAV injection, it was necessary to ensure that the fibreoptic placement accurately targeted the SCN. Practise experiments carried out show that the fibreoptic can be stereotaxically fitted above the SCN, however, the placement in these experiments remains unknown. Secondly, it remains unknown as to how the light from the fibreoptic illuminates the SCN. While it was placed above the SCN, it may be that the light does not reach all the ChR2-expressing neurons, and thus, fewer neurons are stimulated than would be effective *in vivo*. Thirdly, while the OVX+E+E protocol has been shown to induce positive feedback in mice necessary for an LH surge (Bronson & vom Saal, 1979; Czieselsky *et al.*, 2016), it has not been tested whether this protocol is able to reliably induce a normally-timed LH surge in these mice. Finally, serial blood sampling from freely behaving animals is anecdotally difficult when mice may be experiencing even the slightest amount of stress. Stress hormones can inhibit the LH surge from occurring (Roozendaal *et al.*, 1995; Wagenmaker & Moenter, 2017). While the mice in this study had been habituated to daily handling and manipulation of the tail similar to being bled for at least 4 weeks before the end prior to any experimentation, there is a possibility that the stress of the experiments may have inhibited the development of an LH surge. As such, all of these factors may have contributed to the outcome presented here.

While the *in vivo* experiments have been designed to replicate the *in vitro* work carried out in Chapter 6, there are differences between them that may contribute to the findings presented here. Due to brain slices being taken for experiments in Chapter 6, stimulation of ChR2-expressing *Avp-cre* projections was carried out, whilst here, stimulation is targeted at the cell bodies. The stimulation paradigm used here is based off that by Piet *et al.* (2018) to stimulate kisspeptin neurons, adapted to 20 Hz, similar to the *in vitro* experiments in Chapter

6. As no studies have addressed the stimulation frequency at the SCN needed to trigger hormone release from neurons efferent to SCN projections, this frequency was chosen based on what could accurately be used to induce AVP release as per Chapter 6. Green and Gillette (1982) suggest that the late-afternoon firing frequency (when the LH surge is expected) of the SCN is approximately 10-12 Hz, thus, it could be that a stimulation frequency closer to that range may be necessary.

In saying this, the frequencies reported are for the entire SCN, rather than SCN AVP neurons. Whether the frequency accurately represents SCN AVP neuron activity, however, would make little difference if AVP was not being produced. One possibility is that as these experiments were carried out in the mid-late morning, AVP would not have been synthesised or exported to the RP3V. Thus, the SCN itself may not be geared to trigger an LH surge.

9.9.4.2 Downstream mechanisms of timekeeping

The above limitations are related to the SCN and *Avp-cre* neurons to explain our observations. It may be that downstream of SCN neurons, timekeeping mechanisms, which have not been considered in this experiment, may also play a role. These include mechanisms in the kisspeptin and GnRH neurons, as well as gonadotrophs in the anterior pituitary gland.

Both kisspeptin neurons and GnRH neurons express clock genes (Hickok & Tischkau, 2010; Chassard *et al.*, 2015) potentially gating their receptivity to upstream signals. Kisspeptin neurons display daily oscillations in clock genes (Chassard *et al.*, 2015); but how this correlates to their activity or output is unknown. There may be a circadian pattern of kisspeptin expression (Xu *et al.*, 2011) although this could be due oestrogenic feedback and signals from the SCN (Robertson *et al.*, 2009; Smarr *et al.*, 2012). Circadian V1R expression in kisspeptin neurons specifically has not been addressed. There may be, however, circadian expression of V1R in the RP3V (Smarr *et al.*, 2013), although this has not been a consistent finding (Kalamatianos *et al.*, 2004a). Despite this, RP3V kisspeptin neurons can respond to AVP similar extents

throughout the day (Piet *et al.*, 2015b) suggesting that V1R expression is not regulated in a circadian manner. While AVP may be able to stimulate kisspeptin neurons throughout the day, the amount of kisspeptin peptide synthesised at the stimulation time here, may not be high enough to trigger GnRH activity (Robertson *et al.*, 2009). Immortalised GnRH neurons show circadian rhythmic patterns of Kiss1R expression further gating their responsiveness to kisspeptin (Tonsfeldt *et al.*, 2011). Finally, studies of anterior pituitary gonadotropes show that there may also be gating the activity of GnRH peptide, with circadian regulation of GnRHRs (Schirman-Hildesheim *et al.*, 2006; Resuehr *et al.*, 2007). In saying this, however, gonadotrope-specific knock-out of BMAL1 does not affect the LH surge (Chu *et al.*, 2013). Interestingly, kisspeptin, Kiss1R and GnRHR are all likely to be most highly expressed in the mid-afternoon when the onset of the LH surge is expected (Schirman-Hildesheim *et al.*, 2006; Robertson *et al.*, 2009; Hickok & Tischkau, 2010; Tonsfeldt *et al.*, 2011; Xu *et al.*, 2011).

Thus, the stimulation of SCN *Avp-cre* neurons *in vivo*, may be able to drive their excitation, the multiple downstream gating mechanisms discussed above could prevent this signal propagating through the GnRH neuronal network to the GnRH neurons and gonadotropes, precluding the generation of the LH surge.

9.9.5 Summary

In this pilot study, an LH surge was not triggered by *in vivo* stimulation of SCN *Avp-cre* neurons. There are a number of technical factors, and downstream biological mechanism which remain to be validated, that hinder interpreting the results seen here. This study paves the way for significant follow-up work. Future experiments could test stimulation of the entire SCN to trigger a surge, rather than the cre-expressing subpopulation; whether stimulation of the *Avp-cre* neurons at a different time of could drive the initiation of the LH surge, or whether the downstream kisspeptin and GnRH neurons may have gating mechanisms for time-locking the LH surge to a specific time point.

References

Abbara A, Ratnasabapathy R, Jayasena CN & Dhillo WS. (2013). The effects of kisspeptin on gonadotropin release in non-human mammals. *Advances in Experimental and Medical Biology* **784,** 63-87.

Abbott DH, Barnett DK, Levine JE, Padmanabhan V, Dumesic DA, Jacoris S & Tarantal AF. (2008). Endocrine antecedents of polycystic ovary syndrome in fetal and infant prenatally androgenized female rhesus monkeys. *Biology of Reproduction* **79,** 154-163.

Abrahamson EE & Moore RY. (2001). Suprachiasmatic nucleus in the mouse: Retinal innervation, intrinsic organization and efferent projections. *Brain Research* **915,** 172-191.

Ahn T, Fergani C, Coolen LM, Padmanabhan V & Lehman MN. (2015). Prenatal testosterone excess decreases neurokinin 3 receptor immunoreactivity within the arcuate nucleus KNDy cell population. *Journal of Neuroendocrinology* **27,** 100-110.

Akasu T, Shoji S & Hasuo H. (1993). Inward rectifier and low-threshold calcium currents contribute to the spontaneousfiring mechanism in neurons of the rat suprachiasmatic nucleus. *Pflügers Archive* **425,** 109-116.

Akema T, Hashimoto R & Kimura F. (1988). Preoptic injection of VIP, but not of secretin or PHI, inhibits LH and stimulates prolactin secretion in the ovariectomized rat. *Brain Research* **441,** 367-370.

Alexander MJ, Clifton DK & Steiner RA. (1985). Vasoactive intestinal polypeptide effects a central inhibition of pulsatile luteinizing hormone secretion in ovariectomized rats. *Endocrinology* **117,** 2134-2139.

Aliabadi E, Namavar MR, Mortezaee K, Toolee H, Keshtgar S, Mirkhani H, Akbari M, Rastegar T & Solhjoo S. (2017). Kisspeptin expression features in the arcuate and anteroventral periventricular nuclei of hypothalamus of letrozole-induced polycystic ovarian syndrome in rats. *Archives of Gynecology and Obstetrics* **296,** 957-963.

Anderson GM, Relf HL, Rizwan MZ & Evans JJ. (2009). Central and peripheral effects of RFamide-related peptide-3 on luteinizing hormone and prolactin secretion in rats. *Endocrinology* **150,** 1834-1840.

Apridonidze T, Essah PA, Iuorno MJ & Nestler JE. (2005). Prevalence and characteristics of the metabolic syndrome in women with polycystic ovary syndrome. *Journal of Clinical Endocrinology and Metabolism* **90,** 1929-1935.

Arendt J & Broadway J. (1987). Light and melatonin as zeitgebers in man. *Chronobiology International* **4,** 273-282.

Arias C, Zepeda A, Hernandez-Ortega K, Leal-Galicia P, Lojero C & Camacho-Arroyo I. (2009). Sex and estrous cycle-dependent differences in glial fibrillary acidic protein immunoreactivity in the adult rat hippocampus. *Hormones and Behvaiour* **55,** 257-263.

Armstrong SM, Cassone VM, Chesworth MJ, Redman JR & Short RV. (1986). Synchronization of mammalian circadian rhythms by melatonin. *Journal of Neural Transmission Supplementum* **21,** 375-394.

Asunción M, Calvo RM, San Millán JL, Sancho J, Avila S & Escobar-Morrale HF. (2000). A prospective study of the prevalence of the polycystic ovary syndrome in unselected Caucasian women from Spain. *Journal of Clinical Endocrinology and Metabolism* **85,** 2434-2438.

Atkinson SE, Maywood ES, Chesham JE, Wozny C, Colwell CS, Hastings MH & Williams SR. (2011). Cyclic AMP signaling control of action potential firing rate and molecular circadian pacemaking in the suprachiasmatic nucleus. *Journal of Biological Rhythms* **26,** 210-220.

Aton SJ, Colwell CS, Harmar AJ, Waschek J & Herzog ED. (2005). Vasoactive intestinal polypeptide mediates circadian rhythmicity and synchrony in mammalian clock neurons. *Nature Neuroscience* **8,** 476-483.

Auger CJ & Vanzo RJ. (2006). Progesterone treatment of adult male rats suppresses arginine vasopressin expression in the bed nucleus of the stria terminalis and the centromedial amygdala. *Journal of Neuroendocrinology* **18,** 187-194.

Azziz R, Woods KS, Reyna R, Key TJ, Knochenhauer ES & Yildiz BO. (2004). The prevalence and features of the polycystic ovary syndrome in an unselected population. *Journal of Clinical Endocrinology and Metabolism* **89,** 2745-2749.

Baldissera SF, Motta LDC, Almeida MC & Antunes-Rodrigues J. (1991). Proposal of an experimental model for the study of polycystic ovaries. *Brazilian Journal of Medical and Biological Research* **24,** 747-751.

Bankir L. (2001). Antidiuretic action of vasopressin: Quantitative aspects and interaction between V1a and V2 receptor-mediated effects. *Cardiovascular Research* **51,** 372-390.

Beato M. (2008). The time course of transmitter at glycinergic synapses onto motoneurons. *Journal of Neuroscience* **28,** 7412-7425.

Bekkers JM. (2005). Presynaptically silent GABA synapses in hippocampus. *Journal of Neuroscience* **25,** 4031-4039.

Belchetz PE, Plant TM, Nakai Y, Keogh EJ & Knobil E. (1978). Hypophysial responses to continuous and intermittent delivery of hypopthalamic gonadotropin-releasing hormone. *Science* **202,** 631-633.

Belle MDC, Diekman CO, Forger DB & Piggins HD. (2009). Daily electrical silencing in the mammalian circadian clock. *Science* **326,** 281-284.

Berg T, Silveira MA & Moenter SM. (2018). Prepubertal development of GABAergic transmission to gonadotropin-releasing hormone (GnRH) neurons and postsynaptic response are altered by prenatal androgenization. *Journal of Neuroscience* **38,** 2283-2293.

Berndt A, Schoenenberger P, Mattis J, Tye KM, Deisseroth K, Hegemann P & Oertner TG. (2011). High-efficiency channelrhodopsins for fast neuronal stimulation at low light levels. *Proceedings of the National Academy of Sciences of the United States of America* **108,** 7595-7600.

Berson DM, Dunn FA & Takao M. (2002). Phototransduction by retinal ganglion cells that set the circadian clock. *Science* **295,** 1070-1073.

Besson J, Sarrieau A, Vial M, Marie J-C, Rosselin G & Rostene W. (1986). Characterization and autoradiographic distribution of vasoactive intestinal peptide binding sites in the rat central nervous system. *Brain Research* **398,** 329-336.

Betley JN & Sternson SM. (2011). Adeno-associated viral vectors for mapping, monitoring, and manipulating neural circuits. *Human Gene Therapy* **22,** 669-677.

Biello SM, Golombek DA, Schak KM & Harrington ME. (1997). Circadian phase shifts to neuropeptide Y *in vitro*: Cellular communication and signal transduction. *Journal of Neuroscience* **17,** 8468-8475.

Bilban M, Ghaffari-Tabrizi N, Hintermann E, Bauer S, Molzer S, Zoratti C, Malli R, Sharabi A, Hiden U, Graier W, Knofler M, Andreae F, Wagner O, Quaranta V & Desoye G. (2004). Kisspeptin-10, a KiSS-1/metastin-derived decapeptide, is a physiological invasion inhibitor of primary human trophoblasts. *Journal of Cell Science* **117,** 1319-1328.

Birch RA, Padmanabhan V, Foster DL, Unsworth WP & Robinson JE. (2003). Prenatal programming of reproductive neuroendocrine function: Fetal androgen exposure produces progressive disruption of reproductive cycles in sheep. *Endocrinology* **144,** 1426-1434.

Bittman EL. (2019). Circadian function in multiple cell types in necessary for proper timimng of the preovulatory LH surge. *Journal of Biological Rhythms* **34,** 622-633.

Blake CA & Sawyer CH. (1974). Effects of hypothalamic deafferentation on the pulsatile rhythm in plasma concentrations of luteinizing hormone in ovariectomized rats. *Endocrinology* **94,** 730-736.

Boer GJ, van Esseveldt KE, van der Geest BAM, Duindam H & Rietveld WJ. (1999). Vasopressin-deficient suprachiasmatic nucleus grafts re-instate circadian rhythmicity in suprachiasmatic nucleus-lesioned arrhythmic rats. *Neuroscience* **89,** 375-385.

Bonzini M, Palmer KT, Coggon D, Carugno M, Cromi A & Ferrario MM. (2011). Shift work and pregnancy outcomes: A systematic review with meta-analysis of currently available epidemiological studies. *British Journal of Obstetrics and Gynaecology* **118,** 1429-1437.

Bouabe H & Okkenhaug K. (2013). Gene targeting in mice: A review. *Methods in Molecular Biology* **1064,** 315-336.

Bowery NG, Bettler B, Froestl W, Gallagher JP, Marshall F, Raiteri M, Bonner TI & Enna SJ. (2002). International Union of Pharmacology. XXXIII. Mammalian ɣ-aminobutyric acid$_B$ receptors: Structure and function. *Pharmacological Reviews* **54,** 247-264.

Brayman MJ, Pepa PA, Berdy SE & Mellon PL. (2012). Androgen receptor repression of GnRH gene transcription. *Molecular Endocrinology* **26,** 2-13.

Brickley SG & Mody I. (2012). Extrasynaptic GABA$_A$ receptors: Their function in the CNS and implications for disease. *Neuron* **73,** 23-34.

Bronson FH. (1981). The regulation of luteinizing hormone secretion by estrogen: Relationships among negative feedback, surge potential, and male stimulation in juvenile, peripubertal, and adult female mice. *Endocrinology* **108,** 506-516.

Bronson FH & vom Saal FS. (1979). Control of the preovulatory release of luteinizing hormone by steroids in the mouse. *Endocrinology* **104,** 1247-1255.

Brown MH & Nunez AA. (1986). Hypothalamic circuits and circadian rhythms: Effects of knife cuts vary with their placement within the suprachiasmatic area. *Brain Research Bulletin* **16,** 705-711.

Brown RE, Wilkinson DA, Imran SA, Caraty A & Wilkinson M. (2012). Hypothalamic *kiss1* mRNA and kisspeptin immunoreactivity are reduced in a rat model of polycystic ovary syndrome (PCOS). *Brain Research* **1467,** 1-9.

Brown TM, Colwell CS, Waschek JA & Piggins HD. (2007). Disrupted neuronal activity rhythms in the suprachiasmatic nuclei of vasoactive intestinal polypeptide-deficient mice. *Journal of Neurophysiology* **97,** 2553-2558.

Brussard AB & Koksma J-J. (2003). Conditional regulation of neurosteroid sensitivity of GABA $_A$ receptors. *Annals of the New York Academy of Science* **1007,** 29-38.

Buijs RM, Hermes MHLJ & Kalsbeek A. (1999). The suprachiasmatic nucleus—paraventricular nucleus interactions: A bridge to the neuroendocrine and autonomic nervous system. *Progress in Brain Research* **119,** 365-382.

Buijs RM, Wortel J & Hou Y-X. (1995). Colocalization of ɣ-aminobutyric acid with vasopressin, vasoactive intestinal peptide, and somatostatin in the rat suprachiasmatic nucleus. *Journal of Comparative Neurology* **358,** 343-352.

Burgos CF, Yevenes GE & Aguayo LG. (2016). Structure and pharmacologic modulation of inhibitory glycine receptors. *Molecular Pharmacology* **90,** 318-325.

Burke MC, Letts PA, Krajewski SJ & Rance NE. (2006). Coexpression of dynorphin and neurokinin B immunoreactivity in the rat hypothalamus: Morphologic evidence of interrelated function within the arcuate nucleus. *Journal of Comparative Neurology* **498,** 712-726.

Busnelli M, Bulgheroni E, Manning M, Kleinau G & Chini B. (2013). Selective and potent agonists and antagonists for investigating the role of mouse oxytocin receptors. *Journal of Pharmacology and Experimental Therapeutics* **346,** 318-327.

Butler WR, Malven PV, Willett LB & Bolt DJ. (1972). Patterns of pituitary release and cranial output of LH and prolactin in ovariectomized ewes. *Endocrinology* **91,** 793-801.

Cahill DJ, Wardle PG, Harlow CR & Hull MGR. (1998). Onset of the preovulatory luteinizing hormone surge: Diurnal timing and critical follicular prerequisites. *Fertility and Sterility* **70,** 56-59.

Cai W, Rambaud J, Teboul M, Masse I, Benoit G, Gustafsson J-Å, Delaunay F, Laudet V & Pongratz I. (2008). Expression levels of estrogen receptor beta are modulated by components of the molecular clock. *Molecular and Cellular Biology* **28,** 784-793.

Caldwell AS, Eid S, Kay CR, Jimenez M, McMahon AC, Desai R, Allan CM, Smith JT, Handelsman DJ & Walters KA. (2015). Haplosufficient genomic androgen receptor signaling is adequate to protect female mice from induction of polycystic ovary syndrome features by prenatal hyperandrogenization. *Endocrinology* **156,** 1441-1452.

Caldwell ASL, Edwards MC, Desai R, Jimenez M, Gilchrist RB, Handelsman DJ & Walters KA. (2017). Neuroendocrine androgen action is a key extraovarian mediator in the development of polycystic ovary syndrome. *Proceedings of the National Academy of Sciences of the United States of America* **114,** E3334-E3343.

Calhoun ME, Jucker M, Martin LJ, Thinakaran G, Price DL & Mouton PR. (1996). Comparative evaluation of synaptophysin-based methods for quantification of syanpses. *Journal of Neurocytology* **25,** 821-828.

Caligioni CS. (2009). Assessing reproductive status/stages in mice. *Current Protocols in Neuroscience* **Supplement 48,** 1-8.

Callachan H, Cottrell GA, Hather NY, Lambert JJ, Nooney JM & Peters JA. (1987). Modulation of the $GABA_A$ receptor by progesterone metabolites. *Proceedings of the Royal Society B: Biological Sciences* **231,** 359-369.

Callaway EM & Luo L. (2015). Monosynaptic circuit tracing with glycoprotein-deleted rabies viruses. *Journal of Neuroscience* **35,** 8979-8985.

Campbell RE, Ducret E, Porteous R, Liu X, Herde MK, Wellerhaus K, Sonntag S, Willecke K & Herbison AE. (2011). Gap junctions between neuronal inputs but not gonadotropin-releasing hormone neurons control estrous cycles in the mouse. *Endocrinology* **152,** 2290-2301.

Campbell RE, Gaidamaka G, Han SK & Herbison AE. (2009). Dendro-dendritic bundling and shared synapses between gonadotropin-releasing hormone neurons. *Proceedings of the National Academy of Sciences of the United States of America* **106,** 10835-10840.

Caraty A & Locatelli A. (1988). Effect of time after castration on secretion of LHRH and LH in the ram. *Journal of Reproduction and Fertility* **82,** 263-269.

Card JP & Moore RY. (1982). Ventral lateral geniculate nucleus efferents to the rat suprachiasmatic nucleus exhibit avian pancreatic polypeptide-like immunoreactivity. *Journal of Comparative Neurology* **206,** 390-396.

Card JP & Moore RY. (1984). The suprachiasmatic nucleus of the golden hamster: Immunohistochemical analysis of cell and fiber distribution. *Neuroscience* **13,** 415-431.

Cariboni A, Maggi R & Parnavelas JG. (2007). From nose to fertility: The long migratory journey of gonadotropin-releasing hormone neurons. *Trends in Neuroscience* **30,** 638-644.

Castel M & Morris JF. (2000). Morphological heterogeneity of the GABAergic network in the suprachiasmatic nucleus, the brain's circadian pacemaker. *Journal of Anatomy* **196,** 1-13.

Castel M, Morris JF & Belenky M. (1996). Non-synaptic and dendritic exocytosis from dense-cored vesicles in the suprachiasmatic nucleus. *NeuroReport* **7,** 543-547.

Cernea M, Padmanabhan V, Goodman RL, Coolen LM & Lehman MN. (2015). Prenatal testosterone treatment leads to changes in the morphology of KNDy neurons, their inputs, and projections to GnRH cells in female sheep. *Endocrinology* **156,** 3277-3291.

Chappel PE, Lydon JP, Conneely OM, O'Malley BW & Levine JE. (1997). Endocrine defects in mice carrying a null mutation for the progesterone receptor gene. *Endocrinology* **138,** 4147-4152.

Chappel PE, White RS & Mellon PL. (2003). Circadian gene expression regulates pulsatile gonadotropin-releasing hormone (GnRH) secretory patterns in the hypothalamic GnRH-secreting GT1–7 cell line. *Journal of Neuroscience* **23,** 11202-11213.

Chassard D, Bur I, Poirel VJ, Mendoza J & Simonneaux V. (2015). Evidence for a putative circadian Kiss-clock in the hypothalamic AVPV in female mice. *Endocrinology* **156,** 2999-3011.

Chen D, Buchanan GF, Ding JM, Hannibal J & Gillette MU. (1999). Pituitary adenylyl cyclase-activating peptide: A pivotal modulator of glutamatergic regulation of the suprachiasmatic circadian clock. *Proceedings of the National Academy of Sciences of the United States of America* **96,** 13468-13473.

Cheng G, Coolen LM, Padmanabhan V, Goodman RL & Lehman MN. (2010). The kisspeptin/neurokinin B/dynorphin (KNDy) cell population of the arcuate nucleus: Sex differences and effects of prenatal testosterone in sheep. *Endocrinology* **151,** 301-311.

Cheng MY, Bullock CM, Li C, Lee AG, Bermak JC, Belluzzi J, Weaver DR, Leslie FM & Zhou QY. (2002). Prokineticin 2 transmits the behavioural circadian rhythm of the suprachiasmatic nucleus. *Nature* **417,** 405-410.

Cheong RY, Porteous R, Chambon P, Abraham I & Herbison AE. (2014). Effects of neuron-specific estrogen receptor (ER) α and ERβ deletion on the acute estrogen negative feedback mechanism in adult female mice. *Endocrinology* **155,** 1418-1427.

Choe HK, Kim HD, Park SH, Lee HW, Park JY, Seong JY, Lightman SL, Son GH & Kim K. (2013). Synchronous activation of gonadotropin-releasing hormone gene transcription and secretion by pulsatile kisspeptin stimulation. *Proceedings of the National Academy of Sciences of the United States of America* **110,** 5677-5682.

Christensen RK, Petersen AV, Schmitt N & Perrier JF. (2014). Fast detection of extrasynaptic GABA with a whole-cell sniffer. *Frontiers in Cellular Neuroscience* **8,** 133.

Christian CA, Mobley JL & Moenter SM. (2005). Diurnal and estradiol-dependent changes in gonadotropin-releasing hormone neuron firing activity. *Proceedings of the National Academy of Sciences of the United States of America* **102,** 15682-15687.

Christian CA & Moenter SM. (2008). Vasoactive intestinal polypeptide can excite gonadotropin-releasing hormone neurons in a manner dependent on estradiol and gated by time of day. *Endocrinology* **149,** 3130-3136.

Chu A, Zhu L, Blum ID, Mai O, Leliavski A, Fahrenkrug J, Oster H, Boehm U & Storch KF. (2013). Global but not gonadotrope-specific disruption of *Bmal1* abolishes the luteinizing hormone surge without affecting ovulation. *Endocrinology* **154,** 2924-2935.

Chung K, Wallace J, Kim SY, Kalyanasundaram S, Andalman AS, Davidson TJ, Mirzabekov JJ, Zalocusky KA, Mattis J, Denisin AK, Pak S, Bernstein H, Ramakrishnan C, Grosenick L, Gradinaru V & Deisseroth K. (2013). Structural and molecular interrogation of intact biological systems. *Nature* **497,** 332-337.

Clarke IJ, Burman KJ, Doughton BW & Cummins JT. (1986). Effects of constant infusion of gonadotrophin-releasing hormone in ovariectomized ewes with hypothalamo-pituitary disconnection: Further evidence for differential control of LH and FSH secretion and the lack of a priming effect. *Journal of Endocrinology* **111,** 43-49.

Clarke IJ & Cummins JT. (1982). The temporal relationship between gonadotropin releasing hormone (GnRH) and luteinizing hormone (LH) secretion in ovariectomized ewes. *Endocrinology* **111,** 1737-1739.

Clarkson J, d'Anglemont de Tassigny X, Colledge WH, Caraty A & Herbison AE. (2009). Distribution of kisspeptin neurones in the adult female mouse brain. *Journal of Neuroendocrinology* **21,** 673-682.

Clarkson J, d'Anglemont de Tassigny X, Moreno AS, Colledge WH & Herbison AE. (2008). Kisspeptin-GPR54 signaling is essential for preovulatory gonadotropin-releasing hormone neuron activation and the luteinizing hormone surge. *Journal of Neuroscience* **28,** 8691-8697.

Clarkson J, Han SY, Piet R, McLennan T, Kane GM, Ng J, Porteous RW, Kim JS, Colledge WH, Iremonger KJ & Herbison AE. (2017). Definition of the hypothalamic GnRH pulse generator in mice. *Proceedings of the National Academy of Sciences of the United States of America* **114,** E10216-E10223.

Clarkson J & Herbison AE. (2006). Postnatal development of kisspeptin neurons in mouse hypothalamus; sexual dimorphism and projections to gonadotropin-releasing hormone neurons. *Endocrinology* **147,** 5817-5825.

Clarkson J & Herbison AE. (2009). Oestrogen, kisspeptin, GPR54 and the pre-ovulatory luteinising hormone surge. *Journal of Neuroendocrinology* **21,** 305-311.

Colwell CS. (2000). Rhythmic coupling among cells in the suprachiasmatic nucleus. *Journal of Neurobiology* **43,** 379-388.

Colwell CS. (2011). Linking neural activity and molecular oscillations in the SCN. *Nature Reviews Neuroscience* **12,** 553-569.

Colwell CS, Michel S, Itri J, Rodriguez W, Tam J, Lelievre V, Hu Z, Liu X & Waschek JA. (2003). Disrupted circadian rhythms in VIP- and PHI-deficient mice. *American Journal of Physiology Regulatory, Integrative and Comparative Physiology* **285,** 939-949.

Constantin S, Iremonger KJ & Herbison AE. (2013). *In vivo* recordings of GnRH neuron firing reveal heterogeneity and dependence upon $GABA_A$ receptor signaling. *Journal of Neuroscience* **33,** 9394-9401.

Couse JF & Korach KS. (1999). Estrogen receptor null mice: What have we learned and where will they lead us? *Endocrine Reviews* **20,** 358-417.

Couse JF, Yates MM, Walker VR & Korach KS. (2003). Characterization of the hypothalamic-pituitary-gonadal axis in estrogen receptor (ER) null mice reveals hypergonadism and endocrine sex reversal in females lacking ERα but not ERβ. *Molecular Endocrinology* **17,** 1039-1053.

Coyle C & Campbell RE. (2019). Pathological pulses in PCOS. *Molecular and Cellular Endocrinology* **498,** 110561.

Cravo RM, Frazão R, Perello M, Osborne-Lawrence S, Williams KW, Zigman JM, Vianna C & Elias CF. (2013). Leptin signaling in Kiss1 neurons arises after pubertal development. *PLoS One* **8,** e58698.

Cutler DJ, Haraura M, Reed HE, Shen S, Sheward WJ, Morrison CF, Marston HM, Harmar AJ & Piggins HD. (2003). The mouse VPAC2 receptor confers suprachiasmatic nuclei cellular rhythmicity and responsiveness to vasoactive intestinal polypeptide *in vitro*. *European Journal of Neuroscience* **17,** 197-204.

Czieselsky K, Prescott M, Porteous R, Campos P, Clarkson J, Steyn FJ, Campbell RE & Herbison AE. (2016). Pulse and surge profiles of luteinizing hormone secretion in the mouse. *Endocrinology* **157,** 4794-4802.

d'Anglemont de Tassigny X, Fagg LA, Dixon JP, Day K, Leitch HG, Hendrick AG, Zahn D, Franceschini I, Caraty A, Carlton MB, Aparicio SA & Colledge WH. (2007). Hypogonadotropic hypogonadism in mice lacking a functional *Kiss1* gene. *Proceedings of the National Academy of Sciences of the United States of America* **104,** 10714-10719.

d'Occhio MJ, Schanbacher BD & Kinder JE. (1983). Individual differences in LH and FSH responses to orchidectomy and testosterone replacement therapy in rams. *Journal of Andrology* **4,** 210-215.

Dahlman-Wright K, Cavailles V, Fuqua SA, Jordan VC, Katzenellenbogen JA, Korach KS, Maggi A, Muramatsu M, Parker MG & Gustafsson J-Å. (2006). International Union of Pharmacology. LXIV. Estrogen Receptors. *Pharmacological Reviews* **58,** 773-781.

Dardente H, Menet JS, Challet E, Tournier BB, Pevet P & Masson-Pevet M. (2004). Daily and circadian expression of neuropeptides in the suprachiasmatic nuclei of nocturnal and diurnal rodents. *Molecular Brain Research* **124,** 143-151.

de Croft S, Boehm U & Herbison AE. (2013). Neurokinin B activates arcuate kisspeptin neurons through multiple tachykinin receptors in the male mouse. *Endocrinology* **154,** 2750-2760.

de Croft S, Piet R, Mayer C, Mai O, Boehm U & Herbison AE. (2012). Spontaneous kisspeptin neuron firing in the adult mouse reveals marked sex and brain region differences but no support for a direct role in negative feedback. *Endocrinology* **153,** 5384-5393.

de Jeu MTG & Pennartz CMA. (1997). Functional characterization of the H-current in SCN neurons in subjective day and night: A whole-cell patch-clamp study in acutely prepared brain slices. *Brain Research* **767,** 72-80.

de la Iglesia HO, Blaustein JD & Bittman EL. (1995). The suprachiasmatic area in the femal hampster projects to neurons containing estrogen receptors and GnRH. *NeuroReport* **6,** 1715-1722.

de la Iglesia HO, Blaustein JD & Bittman EL. (1999). Oestrogen receptor-α-immunoreactive neurones project to the suprachiasmatic nucleus of the female syrian hamster. *Journal of Neuroendocrinology* **11,** 481-490.

de la Iglesia HO, Meyer J & Schwartz WJ. (2003). Lateralization of circadian pacemaker output: Activation of left- and right-sided luteinizing hormone–releasing hormone neurons involves a neural rather than a humoral pathway. *Journal of Neuroscience* **23,** 7412-7414.

de Roux N, Genin E, Carel JC, Matsuda F, Chaussain JL & Milgrom E. (2003). Hypogonadotropic hypogonadism due to loss of function of the KiSS1-derived peptide receptor GPR54. *Proceedings of the National Academy of Sciences of the United States of America* **100,** 10972-10976.

de Vries GJ, Wang Z, Bullock NA & Numan S. (1994). Sex differences in the effects of testosterone and its metabolites on vasopressin messenger RNA levels in the bed nucleus of the stria terminalis of rats. *Journal of Neuroscience* **14,** 1789-1794.

DeFazio RA, Heger S, Ojeda SR & Moenter SM. (2002). Activation of A-type ɣ-aminobutyric acid receptors excites gonadotropin-releasing hormone neurons. *Molecular Endocrinology* **16,** 2872-2891.

Dhillo WS, Chaudhri OB, Thompson EL, Murphy KG, Patterson M, Ramachandran R, Nijher GK, Amber V, Kokkinos A, Donaldson M, Ghatei MA & Bloom SR. (2007). Kisspeptin-54 stimulates gonadotropin release most potently during the preovulatory phase of the menstrual cycle in women. *Journal of Clinical Endocrinology and Metabolism* **92,** 3958-3966.

Di Giorgio NP, Bizzozzero Hiriart M, Surkin PN, Lopez PV, Bourguignon NS, Dorfman VB, Bettler B, Libertun C & Lux-Lantos V. (2019). Multiple failures in the lutenising hormone surge generating system in GABAB1KO female mice. *Journal of Neuroendocrinology* **31,** e12765.

Dickmeis T. (2009). Glucocorticoids and the circadian clock. *Journal of Endocrinology* **200,** 3-22.

Dierschke DJ, Bhattachayra AN, Atkinson LE & Knobil E. (1970). Circhoral oscillations of plasma LH levels in the ovariectomized rhesus monkey. *Endocrinology* **87,** 850-853.

Dolatshad H, Campbell EA, O'Hara L, Maywood ES, Hastings MH & Johnson MH. (2006). Developmental and reproductive performance in circadian mutant mice. *Human Reproduction* **21,** 68-79.

Dong N, Berlinguer-Palmini R, Soltan A, Ponon N, O'Neil A, Travelyan A, Maaskant P, Degenaar P & Sun X. (2018). Opto-electro-thermal optimization of photonic probes for optogenetic neural stimulation. *Journal of Biophotonics* **11,** e201700358.

Drouyer E, LeSauter J, Hernandez AL & Silver R. (2010). Specializations of gastrin-releasing peptide cells of the mouse suprachiasmatic nucleus. *Journal of Comparative Neurology* **518,** 1249-1263.

Ducret E, Anderson GM & Herbison AE. (2009). RFamide-related peptide-3, a mammalian gonadotropin-inhibitory hormone ortholog, regulates gonadotropin-releasing hormone neuron firing in the mouse. *Endocrinology* **150,** 2799-2804.

Dudley TE, DiNardo LA & Glass JD. (1998). Endogenous rregulation of serotonin release in the hamster suprachiasmatic nucleus. *Journal of Neuroscience* **19,** 5045-5052.

Dulka EA, Burger LL & Moenter SM. (2020). Ovarian androgens maintain high GnRH neuron firing rate in adult prenatally-androgenized female mice. *Endocrinology* **161**.

Dulka EA & Moenter SM. (2017). Prepubertal development of gonadotropin-releasing hormone neuron activity is altered by sex, age, and prenatal androgen exposure. *Endocrinology* **158,** 3943-3953.

Edwards RG. (1981). Test-tube babies, 1981. *Nature* **293,** 253-256.

Eide EJ, Woolf MF, Kang H, Woolf P, Hurst W, Camacho F, Vielhaber EL, Giovanni A & Virshup DM. (2005). Control of mammalian circadian rhythm by CKIε-regulated proteasome-mediated PER2 degradation. *Molecular and Cellular Biology* **25,** 2795-2807.

Evans NP, Dahl GE, Mauger D & Karsch FJ. (1995). Estradiol induces both qualitative and quantitative changes in the pattern of gonadotropin-releasing hormone secretion during the presurge period in the ewe. *Endocrinology* **136,** 1603-1609.

Evans NP, Dahl GE, Padmanabhan V, Thrun LA & Karsch FJ. (1997). Estradiol requirements for induction and maintenance of the gonadotropin-releasing hormone surge: Implications for the neuroendocrine processing of the estradiol signal. *Endocrinology* **138,** 5408-5414.

Everett JW & Sawyer CH. (1950). A 24-hour periodicity in the "LH release apparatus" of female rats, disclosed by barbituate sedation. *Endocrinology* **47,** 198-218.

Farrant M & Nusser Z. (2005). Variations on an inhibitory theme: Phasic and tonic activation of $GABA_A$ receptors. *Nature Reviews Neuroscience* **6,** 215-229.

Fenno L, Yizhar O & Deisseroth K. (2011). The development and application of optogenetics. *Annual Review of Neuroscience* **34,** 389-412.

Fernandez DC, Chang YT, Hattar S & Chen SK. (2016). Architecture of retinal projections to the central circadian pacemaker. *Proceedings of the National Academy of Sciences of the United States of America* **113,** 6047-6052.

Fernández-Guasti A, Kruijver FPM, Fodor M & Swaab DF. (2000). Sex differences in the distribution of androgen receptors in the human hypothalamus. *Journal of Comparative Neurology* **425,** 422-435.

Fink G. (1988). Oestrogen and progesterone interactions in the control of gonadotrophin and prolactin secretion. *Journal of Steroid Biochemistry* **30,** 169-178.

Flourakis M, Kula-Eversole E, Hutchison AL, Han TH, Aranda K, Moose DL, White KP, Dinner AR, Lear BC, Ren D, Diekman CO, Raman IM & Allada R. (2015). A conserved bicycle model for circadian clock control of membrane excitability. *Cell* **162,** 836-848.

Foecking EM, Szabo M, Schwartz NB & Levine JE. (2005). Neuroendocrine consequences of prenatal androgen exposure in the female rat: Absence of luteinizing hormone surges, suppression of progesterone receptor gene expression, and acceleration of the gonadotropin-releasing hormone pulse generator. *Biology of Reproduction* **72,** 1475-1483.

Foley NC, Tong TY, Foley D, Lesauter J, Welsh DK & Silver R. (2011). Characterization of orderly spatiotemporal patterns of clock gene activation in mammalian suprachiasmatic nucleus. *European Journal of Neuroscience* **33,** 1851-1865.

Franklin K & Paxinos G. (2008). *The Mouse Brain in Stereotaxic Coordinates*, 3 edn. Elsevier.

Frazão R, Cravo RM, Donato Jr. J, Ratra DV, Clegg DJ, Elmquist JK, Zigman JM, Williams KW & Elias CF. (2013). Shift in Kiss1 cell activity requires estrogen receptor α. *Journal of Neuroscience* **33,** 2807-2820.

Fujiyama F, Hioki H, Tomioka R, Taki K, Tamamaki N, Nomura S, Okamoto K & Kaneko T. (2003). Changes of immunocytochemical localization of vesicular glutamate transporters in the rat visual system after the retinofugal denervation. *Journal of Comparative Neurology* **465,** 234-249.

Funabashi T, Aiba S, Sano A, Shinohara K & Kimura F. (1999). Intracerebroventricular injection of arginine-vasopressin V1 receptor antagonist attenuates the surge of luteinizing hormone and prolactin secretion in proestrous rats. *Neuroscience Letters* **260,** 37-40.

Funabashi T, Shinohara K, Mitsushima D & Kimura F. (2000a). Estrogen increases arginine-vasopressin V1a receptor mRNA in the preoptic area of young but not of middle-aged female rats. *Neuroscience Letters* **285,** 205-208.

Funabashi T, Shinohara K, Mitsushima D & Kimura F. (2000b). Gonadotropin-releasing hormone exhibits circadian rhythm in phase with arginine-vasopressin in co-cultures of the female rat preoptic area and suprachiasmatic nucleus. *Journal of Neuroendocrinology* **12,** 521-528.

Funabashi T, Suyama K, Uemura T, Hirose M, Hirahara F & Kimura F. (2001). Immortalized gonadotropin-releasing hormone neurons (GT1-7 cells) exhibit synchronous bursts of action potentials. *Neuroendocrinology* **73,** 157-165.

Funes S, Hedrick JA, Vassileva G, Markowitz L, Abbondanzo S, Golovko A, Yang S, Monsma FJ & Gustafson EL. (2003). The KiSS-1 receptor GPR54 is essential for the development of the murine reproductive system. *Biochemical and Biophysical Research Communications* **312,** 1357-1363.

Gal A, Lin PC, Cacioppo JA, Hannon PR, Mahoney MM, Wolfe A, Fernandez-Valdivia R, Lydon JP, Elias CF & Ko C. (2016). Loss of fertility in the absence of progesterone receptor expression in kisspeptin neurons of female mice. *PLoS One* **11,** e0159534.

Gamble KL, Resuehr D & Johnson CH. (2013). Shift work and circadian dysregulation of reproduction. *Frontiers in Endocrinology* **4,** 92.

Gao B & Moore RY. (1996). Glutamic acid decarboxylase message isoforms in muman suprachiasmatic nucleus. *Journal of Biological Rhythms* **11,** 172-179.

Garcia-Segura LM, Luquín S, Párducz A & Naftolin F. (1994). Gonadal hormone regulation of glial fibrillary acidic protein immunoreactivity and glial ultrastructure in the rat neuroendocrine hypothalamus. *Glia* **10,** 59-69.

Garzo VG & Dorrington JH. (1984). Aromatase activity in human granulosa cells during follicular development and the modulation by follicle-stimulating hormone and insulin. *American Journal of Obestetrics and Gynecology* **148,** 657-662.

Gay VL & Sheth NA. (1972). Evidence for a periodic release of LH in castrated male and female rats. *Endocrinology* **90,** 158-162.

Gekakis N, Staknis D, Nguyen HB, Davis FC, Wilsbacher LD, King DP, Takahashi JS & Weitz CJ. (1998). Role of the CLOCK protein in the mammalian circadian mechanism. *Science* **280,** 1564-1569.

Gerhold LM, Rosewell KL & Wise PM. (2005). Suppression of vasoactive intestinal polypeptide in the suprachiasmatic nucleus leads to aging-like alterations in cAMP rhythms and activation of gonadotropin-releasing hormone neurons. *J Neurosci* **25,** 62-67.

Gibson EM, Humber SA, Jain S, Williams WP, 3rd, Zhao S, Bentley GE, Tsutsui K & Kriegsfeld LJ. (2008). Alterations in RFamide-related peptide expression are coordinated with the preovulatory luteinizing hormone surge. *Endocrinology* **149,** 4958-4969.

Gillette MU & McArther AJ. (1996). Circadian actions of melatonin at the suprachiasmatic nucleus. *Behavioural Brain Research* **73,** 135-139.

Ginther OJ, Pinaffi FL, Khan FA, Duarte LF & Beg MA. (2013). Circadian influence on the preovulatory LH surge, ovulation, and prolactin concentrations in heifers. *Theriogenology* **79,** 528-533.

Gizowski C, Zaelzer C & Bourque CW. (2016). Clock-driven vasopressin neurotransmission mediates anticipatory thirst prior to sleep. *Nature* **537,** 685-688.

Glass JD, DiNardo LA & Ehlen JC. (2000). Dorsal raphe nuclear stimulation of SCN serotonin release and circadian phase-resetting. *Brain Research* **859,** 224-232.

Glidewell-Kenney C, Hurley LA, Pfaff L, Weiss J, Levine JE & Jameson JL. (2007). Nonclassical estrogen receptor α signaling mediates negative feedback in the female mouse reproductive axis. *Proceedings of the National Academy of Sciences of the United States of America* **104,** 8173-8177.

Goldsmith PC, Boggan JE & Thind KK. (1997). Estrogen and progesterone receptor expression in neuroendocrine and related neurons of the pubertal female monkey hypothalamus. *Neuroendocrinology* **65,** 325-334.

Goldstein CA & Smith YR. (2016). Sleep, circadian rhythms, and fertility. *Current Sleep Medicine Reports* **2,** 206-217.

Goodman RL & Karsch FJ. (1980). Pulsatile secretion of luteinizing hormone: Differential suppression by ovarian steroids. *Endocrinology* **107**.

Goodman RL, Lehman MN, Smith JT, Coolen LM, de Oliveira CV, Jafarzadehshirazi MR, Pereira A, Iqbal J, Caraty A, Ciofi P & Clarke IJ. (2007). Kisspeptin neurons in the arcuate nucleus of the ewe express both dynorphin A and neurokinin B. *Endocrinology* **148,** 5752-5760.

Gottsch ML, Cunningham MJ, Smith JT, Popa SM, Acohido BV, Crowley WF, Seminara S, Clifton DK & Steiner RA. (2004). A role for kisspeptins in the regulation of gonadotropin secretion in the mouse. *Endocrinology* **145,** 4073-4077.

Green DJ & Gillette R. (1982). Circadian rhythm of firing rate recorded from single cells in the rat suprachiasmatic brain slice. *Brain Research* **245**.

Grino PB, Griffin JE & Wilson JD. (1990). Testosterone at high concentrations interacts with the human androgen receptor similarly to dihydrotestosterone. *Endocrinology* **126,** 1165-1172.

Groblewski TA, Nunez AA & Gold RM. (1981). Circadian rhythms in vasopressin deficient rats. *Brain Research Bulletin* **6,** 125-130.

Halász B & Gorski RA. (1967). Gonadotrophic hormone secretion in female rats After partial or total interruption of neural afferents to the medial basal hypothalamus. *Endocrinology* **80,** 608-622.

Hall JE, Taylor AE, Martin KA, Rivier J, Schoenfeld DA & Crowley Jr. WF. (1994). Decreased release of gonadotropin-releasing hormone during the preovulatory midcycle luteinzing hormone surge in normal women. *Proceedings of the National Academy of Sciences of the United States of America* **91,** 6894-6898.

Han SK, Gottsch ML, Lee KJ, Popa SM, Smith JT, Jakawich SK, Clifton DK, Steiner RA & Herbison AE. (2005). Activation of gonadotropin-releasing hormone neurons by kisspeptin as a neuroendocrine switch for the onset of puberty. *Journal of Neuroscience* **25,** 11349-11356.

Han SY, Clarkson J, Piet R & Herbison AE. (2018). Optical approaches for interrogating neural circuits controlling hormone secretion. *Endocrinology* **159,** 3822-3833.

Handa RJ, Pak TR, Kudwa AE, Lund TD & Hinds L. (2008). An alternate pathway for androgen regulation of brain function: Activation of estrogen receptor beta by the metabolite of dihydrotestosterone, 5α-androstane 3β, 17β diol. *Hormones and Behvaiour* **53,** 741-752.

Hannibal J. (2002). Neurotransmitters of the retino-hypothalamic tract. *Cell and Tissue Research* **309,** 73-88.

Hannibal J, Ding JM, Chen D, Fahrenkrug J, Larsen PJ, Gillette MU & Mikkelsen JD. (1997). Pituitary adenylate cyclase-activating peptide (PACAP) in the retinohypothalamic tract: A potential daytime regulator of the biological clock. *Journal of Neuroscience* **17,** 2637-2644.

Harmar AJ, Marston HM, Shen S, Spratt C, West KM, Sheward WJ, Morrison CF, Dorin JR, Piggins HD, Reubi J-C, Kelly JS, Maywood ES & Hastings MH. (2002). The $VPAC_2$ receptor is essential for circadian function in the mouse suprachiasmatic nuclei. *Cell* **109,** 497-508.

Harney JP, Scarbrough K, Rosewell KL & Wise PM. (1996). *In vivo* antisense antagonism of vasoactive intestinal peptide in the suprachiasmatic nuclei causes aging-like changes in the estradiol-induced luteinizing hormone and prolactin surges. *Endocrinology* **137,** 3696-3701.

Harrington ME, Hoque S, Hall A, Golombek D & Biello S. (1999). Pituitary adenylate cyclase activating peptide phase shifts circadian rhythms in a manner similar to light. *Journal of Neuroscience* **19,** 6637-6642.

Harris JA, Hirokawa KE, Sorensen SA, Gu H, Mills M, Ng LL, Bohn P, Mortrud M, Ouellette B, Kidney J, Smith KA, Dang C, Sunkin S, Bernard A, Oh SW, Madisen L & Zeng H. (2014). Anatomical characterization of cre driver mice for neural circuit mapping and manipulation. *Frontiers in Neural Circuits* **8,** 76.

Hastings MH, Maywood ES & Brancaccio M. (2018). Generation of circadian rhythms in the suprachiasmatic nucleus. *Nature Reviews Neuroscience* **19,** 453-469.

Hattar S, Kumar M, Park A, Tong P, Tung J, Yau KW & Berson DM. (2006). Central projections of melanopsin-expressing retinal ganglion cells in the mouse. *Journal of Comparative Neurology* **497,** 326-349.

Hattar S, Liao H-W, Takao M, Berson DM & Yau K-W. (2002). Melanopsin-containing retinal ganglion cells: Architecture, projections, and intrinsic photosensitivity. *Science* **295,** 1065-1070.

Hay-Schmidt A, Vrang N, Larsen PJ & Mikkelsen JD. (2003). Projections from the raphe nuclei to the suprachiasmatic nucleus of the rat. *Journal of Chemical Neuroanatomy* **25,** 293-310.

Hellier V, Brock O, Candlish M, Desroziers E, Aoki M, Mayer C, Piet R, Herbison A, Colledge WH, Prevot V, Boehm U & Bakker J. (2018). Female sexual behavior in mice is controlled by kisspeptin neurons. *Nature Communications* **9,** 400.

Henningsen JB, Ancel C, Mikkelsen JD, Gauer F & Simonneaux V. (2017). Roles of RFRP-3 in the daily and seasonal regulation of reproductive activity in female syrian hamsters. *Endocrinology* **158,** 652-663.

Herbison AE. (2008). Estrogen positive feedback to gonadotropin-releasing hormone (GnRH) neurons in the rodent: The case for the rostral periventricular area of the third ventricle (RP3V). *Brain Research Reviews* **57,** 277-287.

Herbison AE. (2015). Physiology of the adult gonadotropin-releasing hormone neuronal network. In *Knobil and Neill's Physiology of Reproduction*, 4 edn, ed. Plant TM & Zeleznik AJ, pp. 399-467. Elsevier.

Herbison AE, d'Anglemont de Tassigny X, Doran J & Colledge WH. (2010). Distribution and postnatal development of Gpr54 gene expression in mouse brain and gonadotropin-releasing hormone neurons. *Endocrinology* **151,** 312-321.

Herbison AE & Moenter SM. (2011). Depolarising and hyperpolarising actions of $GABA_A$ receptor activation on gonadotrophin-releasing hormone neurones: Towards an emerging consensus. *Journal of Neuroendocrinology* **23,** 557-569.

Herbison AE & Theodosis DT. (1992). Localization of oestrogen receptors in preoptic neurons containing neurotensin but not tyrosine hydroxylase, cholecystokinin or leuteinizing hormone-releasing hormone in the male and female rat. *Neuroscience* **50,** 283-298.

Herde MK, Iremonger KJ, Constantin S & Herbison AE. (2013). GnRH neurons elaborate a long-range projection with shared axonal and dendritic functions. *Journal of Neuroscience* **33,** 12689-12697.

Herzog ED, Aton SJ, Numano R, Sakaki Y & Tei H. (2004). Temporal precision in the mammalian circadian system: A reliable clock from less reliable neurons. *Journal of Biological Rhythms* **19,** 35-46.

Hickok JR & Tischkau SA. (2010). *In vivo* circadian rhythms in gonadotropin-releasing hormone neurons. *Neuroendocrinology* **91,** 110-120.

Hoff JD, Quigley ME & Yen SSC. (1983). Hormonal dynamics at midcycle: A reevaluation. *Journal of Clinical Endocrinology and Metabolism* **57,** 792-796.

Hoffman GE & Gibbs FP. (1982). LHRH pathways in rat brain: 'Deafferentiation' spares a sub-chiasmatic LHRH projection to the median eminence. *Neuroscience* **7,** 1979-1993.

Hoffman GE, Smith MS & Verbalis JG. (1993). c-Fos and related immediate early gene products as markers of activity in neuroendocrine systems. *Frontiers in Neuroendocrinology* **14,** 173-213.

Horvath TL, Cela V & van der Beek EM. (1998). Gender-specific apposition between vasoactive intestinal peptide-containing axons and gonadotrophin-releasing hormone-producing neurons in the rat. *Brain Research* **795,** 277-281.

Hou-You A, Lamme AT, Zimmerman EA & Silverman A-J. (1986). Comparative distribution of vasopressin and oxytocin neurons in the rat-brain using a double-label procedure. *Neuroendocrinology* **44,** 235-246.

Hrabovszky E, Ciofi P, Vida B, Horvath MC, Keller E, Caraty A, Bloom SR, Ghatei MA, Dhillo WS, Liposits Z & Kalló I. (2010). The kisspeptin system of the human hypothalamus: Sexual dimorphism and relationship with gonadotropin-releasing hormone and neurokinin B neurons. *European Journal of Neuroscience* **31,** 1984-1998.

Huang X & Harlan RE. (1993). Absence of androgen receptors in LHRH immunoreactive neurons. *Brain Research* **624,** 309-311.

Hunzicker-Dunn M & Mayo KE. (2014). Gonadotropin signaling in the ovary. In *Knobil and Neill's Physiology of Reproduction*, 4 edn, ed. Plant TM & Zeleznik AJ, pp. 895-946. Elsevier.

Hyodo S, Yamada C, Takezawa T & Urano A. (1992). Expression of provasopressin gene during ontogeny in the hypothalamus of developing mice. *Neuroscience* **46,** 241-250.

Inouye S-IT & Kawamura H. (1979). Persistence of circadian rhythmicity in a mammalian hypothalamic "island" containing the suprachiasmatic nucleus. *Proceedings of the National Academy of Sciences of the United States of America* **76,** 5962-5966.

Iwahana E, Karatsoreos I, Shibata S & Silver R. (2008). Gonadectomy reveals sex differences in circadian rhythms and suprachiasmatic nucleus androgen receptors in mice. *Hormones and Behvaiour* **53,** 422-430.

Jackson AC, Yao GL & Bean BP. (2004). Mechanism of spontaneous firing in dorsomedial suprachiasmatic nucleus neurons. *Journal of Neuroscience* **24,** 7985-7998.

Jacobs DC, Veitch RE & Chappell PE. (2016). Evaluation of immortalized AVPV- and arcuate-specific neuronal kisspeptin cell lines to elucidate potential mechanisms of estrogen responsiveness and temporal gene expression in females. *Endocrinology* **157,** 3410-3419.

Jahan MR, Kokubu K, Islam MN, Matsuo C, Yanai A, Wroblewski G, Fujinaga R & Shinoda K. (2015). Species differences in androgen receptor expression in the medial preoptic and anterior hypothalamic areas of adult male and female rodents. *Neuroscience* **284,** 943-961.

Jasoni CL, Todman MG, Han SK & Herbison AE. (2005). Expression of mRNAs encoding receptors that mediate stress signals in gonadotropin-releasing hormone neurons of the mouse. *Neuroendocrinology* **82,** 320-328.

Jayasena CN, Abbara A, Comninos AN, Nijher GM, Christopoulos G, Narayanaswamy S, Izzi-Engbeaya C, Sridharan M, Mason AJ, Warwick J, Ashby D, Ghatei MA, Bloom SR, Carby A, Trew GH & Dhillo WS. (2014). Kisspeptin-54 triggers egg maturation in women undergoing *in vitro* fertilization. *Journal of Clinical Investigation* **124,** 3667-3677.

Jiang Z-G, Yang Y-Q & Allen CN. (1997). Tracer and electrical coupling of rat suprachiasmatic nucleus neurons. *Neuroscience* **77,** 1059-1066.

Jiang-Xie LF, Yin L, Zhao S, Prevosto V, Han BX, Dzirasa K & Wang F. (2019). A common neuroendocrine substrate for diverse general anesthetics and sleep. *Neuron* **102,** 1053-1065 e1054.

Jin X, Shearman LP, Weaver DR, Zylka MJ, de Vries GJ & Reppert SM. (1999). A molecular mechanism regulating rhythmic output from the suprachiasmatic circadian clock. *Cell* **96,** 57-68.

Johnson MH. (2007a). Actions of steroid hormones in the adult. In *Johnson & Everitt's Essential Reproduction*, 6 edn, ed. Johnson MH & Everitt BJ, pp. 146-167. Blackwell Publishing.

Johnson MH. (2007b). Ovarian function in the adult. In *Johnson & Everitt's Essential Reproduction*, 6 edn, ed. Johnson MH & Everitt BJ, pp. 80-101. Blackwell Publishing.

Jones JR, Tackenberg MC & McMahon DG. (2015). Manipulating circadian clock neuron firing rate resets molecular circadian rhythms and behavior. *Nature Neuroscience* **18,** 373-375.

Kalamatianos T, Kalló I, Goubillon M-L & Coen CW. (2004a). Cellular expression of V_{1a} vasopressin receptor mRNA in the female rat preoptic area: Effects of oestrogen. *Journal of Neuroendocrinology* **16,** 525-533.

Kalamatianos T, Kalló I, Piggins HD & Coen CW. (2004b). Expression of VIP and/or PACAP receptor mRNA in peptide synthesizing cells within the suprachiasmatic nucleus of the rat and in its efferent target sites. *Journal of Comparative Neurology* **475,** 19-35.

Kalló I, Kalamatianos T, Wiltshire N, Shen S, Sheward J, Harmar AJ & Coen CW. (2004). Transgenic approach reveals expression of the $VPAC_2$ receptor in phenotypically defined neurons in the mouse suprachiasmatic nucleus and in its efferent target sites. *European Journal of Neuroscience* **19,** 2201-2211.

Kalra PS & McCann SM. (1975). The stimulatory effect on gonadotropin release of implants of estradiol or progesterone in certain sites in the central nervous system. *Neuroendocrinology* **19,** 289-302.

Kalsbeek A & Buijs RM. (2002). Output pathways of the mammalian suprachiasmatic nucleus: Coding circadian time by transmitter selection and specific targeting. *Cell and Tissue Research* **309,** 109-118.

Kalsbeek A, Buijs RM, van Heerikhuize JJ, Arts M & van der Woude TP. (1992). Vasopressin-containing neurons of the suprachiasmatic nuclei inhibit corticosterone release. *Brain Research* **580,** 62-67.

Kalsbeek A, Teclemariam-Mesbah R & Padgaonkar NA. (1993). Efferent projections of the suprachiasmatic nucleus in the golden hamster (*Mesocricetus auratus*). *Journal of Comparative Neurology* **332,** 293-314.

Kalsbeek A, van der Vliet J & Buijs RM. (1996a). Decrease of endogenous vasopressin release necessary for expression of the circadian rise in plasma corticosterone: A reverse microdialysis study. *Journal of Neuroendocrinology* **8,** 299-307.

Kalsbeek A, van Heerikhuize JJ, Wortel J & Buijs RM. (1996b). A diurnal rhythm of stimulatory input to the hypothalamo–pituitary–adrenal system as revealed by timed intrahypothalamic administration of the vasopressin V_1 antagonist. *Journal of Neuroscience* **16,** 5555-5565.

Karatsoreos IN & Silver R. (2007). Minireview: The neuroendocrinology of the suprachiasmatic nucleus as a conductor of body time in mammals. *Endocrinology* **148,** 5640-5647.

Karatsoreos IN, Wang A, Sasanian J & Silver R. (2007). A role for androgens in regulating circadian behavior and the suprachiasmatic nucleus. *Endocrinology* **148,** 5487-5495.

Karsch FJ, Weick RF, Butler WR, Dierschke DJ, Krey LC, Weiss G, Hotchkiss J, Yamaji T & Knobil E. (1973). Induced LH surges in the rhesus monkey: Strength-duration characteristics of the estrogen stimulus. *Endocrinology* **92,** 1740-1747.

Kauffman AS, Gottsch ML, Roa J, Byquist AC, Crown A, Clifton DK, Hoffman GE, Steiner RA & Tena-Sempere M. (2007). Sexual differentiation of Kiss1 gene expression in the brain of the rat. *Endocrinology* **148,** 1774-1783.

Kauffman AS, Thackray VG, Ryan GE, Tolson KP, Glidewell-Kenney CA, Semaan SJ, Poling MC, Iwata N, Breen KM, Duleba AJ, Stener-Victorin E, Shimasaki S, Webster NJ & Mellon PL. (2015). A novel letrozole model recapitulates both the reproductive and netabolic phenotypes of polycystic ovary syndrome in memale mice. *Biology of Reproduction* **93,** 69.

Kerdelhué B, Brown S, Lenoir V, Queenan Jr. JT, Seegar Jones G, Scholler R & Jones Jr. HW. (2002). Timing and initiation of the preovulatory luteinizing hormone surge and its relationship with the circadian corisol rhythm in the human. *Neuroendocrinology* **75,** 158-163.

Kim EJ, Jacobs MW, Ito-Cole T & Callaway EM. (2016). Improved monosynaptic neural circuit tracing using engineered rabies virus glycoproteins. *Cell Reports* **15,** 692-699.

Kim K & Ramirez VD. (1982). *In vitro* progesterone stimulates the release of luteinizing hormone-releasing hormone from superfused hypothalamic tissue from ovariectomized estradiol-primed prepuberal rats. *Endocrinology* **111,** 750-757.

Kimura F, Mitsugi N, Arita J, Akema T & Yoshida K. (1987). Effects of preoptic injections of gastrin, cholecystokinin, secretin, vasoactiveintestinal peptide and PHI on the secretion of luteinizing hormone and prolactin in ovariectomized estrogen-primed rats. *Brain Research* **410,** 315-322.

King JC & Anthony ELP. (1984). LHRH neurons and their projections in humans and other mammals: Species comparisons. *Peptides* **5,** 195-207.

Kinoshita M, Tsukamura H, Adachi S, Matsui H, Uenoyama Y, Iwata K, Yamada S, Inoue K, Ohtaki T, Matsumoto H & Maeda K. (2005). Involvement of central metastin in the regulation of preovulatory luteinizing hormone surge and estrous cyclicity in female rats. *Endocrinology* **146,** 4431-4436.

Kirilov M, Clarkson J, Liu X, Roa J, Campos P, Porteous R, Schütz G & Herbison AE. (2013). Dependence of fertility on kisspeptin-Gpr54 signaling at the GnRH neuron. *Nature Communications* **4,** 2492.

Knutsson A. (2003). Health disorders of shift workers. *Occupational Medicine* **53,** 103-108.

Kononenko NI, Shao L-R & Dudek FE. (2004). Riluzole-sensitive slowly inactivating sodium current in rat suprachiasmatic nucleus neurons. *Journal of Neurophysiology* **91,** 710-718.

Koshimizu TA, Nakamura K, Egashira N, Hiroyama M, Nonoguchi H & Tanoue A. (2012). Vasopressin V1a and V1b receptors: From molecules to physiological systems. *Physiological Reviews* **92,** 1813-1864.

Kotani M, Detheux M, Vandenbogaerde A, Communi D, Vanderwinden JM, Le Poul E, Brezillon S, Tyldesley R, Suarez-Huerta N, Vandeput F, Blanpain C, Schiffmann SN, Vassart G & Parmentier M. (2001). The metastasis suppressor gene KiSS-1 encodes kisspeptins, the natural ligands of the orphan G protein-coupled receptor GPR54. *Journal of Biological Chemistry* **276,** 34631-34636.

Kramer A, Yang F-C, Snodgrass P, Xiaodong Li, Scammell TE, Davis FC & Weitz CJ. (2001). Regulation of daily locomotor activity and sleep by hypothalamic EGF receptor signaling. *Science* **294,** 2511-2515.

Krege JH, Hodgin JB, Couse JF, Enmark E, Warner M, Mahler JF, Sar M, Korach KS, Gustafsson J-Å & Smithies O. (1998). Generation and reproductive phenotypes of mice lacking estrogen receptor β. *Proceedings of the National Academy of Sciences of the United States of America* **95,** 15677-15682.

Kriegsfeld LJ, Leak RK, Yackulic CB, LeSauter J & Silver R. (2004). Organization of suprachiasmatic nucleus projections in Syrian hamsters (*Mesocricetus auratus*): An anterograde and retrograde analysis. *Journal of Comparative Neurology* **468,** 361-379.

Kriegsfeld LJ, Mei DF, Bentley GE, Ubuka T, Mason AO, Inoue K, Ukena K, Tsutsui K & Silver R. (2006). Identification and characterization of a gonadotropin-inhibitory system in the brains of mammals. *Proceedings of the National Academy of Sciences of the United States of America* **103,** 2410-2415.

Kriegsfeld LJ & Silver R. (2006). The regulation of neuroendocrine function: Timing is everything. *Hormones and Behvaiour* **49,** 557-574.

Kriegsfeld LJ, Silver R, Gore AC & Crews D. (2002). Vasoactive intestinal polypeptide contacts on gonadotropin-releasing hormone neurones increase following puberty in female rats. *Journal of Neuroendocrinology* **14,** 685-690.

Kruijver FPM & Swaab DF. (2002). Sex hormone receptors are present in the human suprachiasmatic nucleus. *Neuroendocrinology* **75,** 296-305.

Kuhlman SJ & McMahon DG. (2004). Rhythmic regulation of membrane potential and potassium current persists in SCN neurons in the absence of environmental input. *European Journal of Neuroscience* **20,** 1113-1117.

Kumar P & Sait SF. (2011). Luteinizing hormone and its dilemma in ovulation induction. *Journal of Human Reproductive Sciences* **4,** 2-7.

Lall GS & Biello SM. (2003). Attenuation of circadian light induced phase advances and delays by neuropeptide Y and a neuropeptide Y Y1/Y5 receptor agonist. *Neuroscience* **119,** 611-618.

Langub Jr. MC, Maley BE & Watson Jr. RE. (1994). Estrous cycle-associatedaxosomatic synaptic plasticity upon estrogen receptive neurons in the rat preoptic area. *Brain Research* **641,** 303-310.

Lawton IE & Schwartz NB. (1967). Pituitary-ovarian function in rats exposed to constant light: A chronological study. *Endocrinology* **81,** 497-508.

Leak RK, Card JP & Moore RY. (1999). Suprachiasmatic pacemaker organization analyzed by viral transynaptic transport. *Brain Research* **819,** 23-32.

Leak RK & Moore RY. (2001). Topographic organization of suprachiasmatic nucleus projection neurons. *Journal of Comparative Neurology* **433,** 312-334.

Lee IT, Chang AS, Manandhar M, Shan Y, Fan J, Izumo M, Ikeda Y, Motoike T, Dixon S, Seinfeld JE, Takahashi JS & Yanagisawa M. (2015). Neuromedin S-producing neurons act as essential pacemakers in the suprachiasmatic nucleus to couple clock neurons and dictate circadian rhythms. *Neuron* **85,** 1086-1102.

Lee J-H, Miele ME, Hicks DJ, Phillips KK, Trent JM, Wiessman BE & Welch DR. (1996). KiSS-1, a novel human malignant melanoma metastasis-suppressor gene. *Journal of the National Cancer Institute* **88,** 1731-1737.

Lee W-S, Smith MS & Hoffman GE. (1990). Luteinizing hormone-releasing hormone neurons express Fos protein during the proestrous surge of luteinizing hormone. *Proceedings of the National Academy of Sciences of the United States of America* **87,** 5163-5167.

Legan SJ, Coon GA & Karsch FJ. (1975). Role of estrogen as initiator of daily LH surges in the ovariectomized rat. *Endocrinology* **96,** 50-56.

Legan SJ & Karsch FJ. (1975). A daily signal for the LH surge in the rat. *Endocrinology* **96,** 57-62.

Lehman MN, Coolen LM & Goodman RL. (2010a). Kisspeptin/neurokinin B/dynorphin (KNDy) cells of the arcuate nucleus: A central node in the control of gonadotropin-releasing hormone secretion. *Endocrinology* **151,** 3479-3489.

Lehman MN, Merkley CM, Coolen LM & Goodman RL. (2010b). Anatomy of the kisspeptin neural network in mammals. *Brain Res* **1364,** 90-102.

Levine JE, Pau K-YF, Ramirez VD & Jackson GL. (1982). Simultaneous measurement of luteinizing hormone-releasing hormone and luteinizing hormone release in unanesthetized, ovariectomized sheep. *Endocrinology* **111,** 1449-1455.

Li JD, Burton KJ, Zhang C, Hu SB & Zhou QY. (2009). Vasopressin receptor V1a regulates circadian rhythms of locomotor activity and expression of clock-controlled genes in the suprachiasmatic nuclei. *American Journal of Physiology Regulatory, Integrative and Comparative Physiology* **296,** R824-830.

Li JD, Hu WP, Boehmer L, Cheng MY, Lee AG, Jilek A, Siegel JM & Zhou QY. (2006). Attenuated circadian rhythms in mice lacking the *prokineticin 2* gene. *Journal of Neuroscience* **26,** 11615-11623.

Lim AJ, Huang Z, Chua SE, Kramer MS & Yong EL. (2016). Sleep duration, exercise, shift work and polycystic ovarian syndrome-related outcomes in a healthy population: A cross-sectional study. *PLoS One* **11,** e0167048.

Lim DH, Ledue J, Mohajerani MH, Vanni MP & Murphy TH. (2013). Optogenetic approaches for functional mouse brain mapping. *Frontiers in Neuroscience* **7,** 54.

Liou SY, Shibata S, Iwasaki K & Ueki S. (1986). Optic nerve stimulation-induced increase of release of ^{3}H-glutamate and ^{3}H-aspartate but not ^{3}H-GABA from the suprachiasmatic nucleus in slices of rat hypothalamus. *Brain Research Bulletin* **16,** 527-531.

Liu C, Weaver DR, Jin X, Shearman LP, Pieschl RL, Gribkoff VK & Reppert SM. (1997). Molecular dissection of two disctinct actions of melatonin on the suprachiasmatic circadian clock. *Neuron* **19,** 91-102.

Liu X & Herbison AE. (2011). Estrous cycle- and sex-dependent changes in pre- and postsynaptic GABAB control of GnRH neuron excitability. *Endocrinology* **152,** 4856-4864.

Liu X, Lee K & Herbison AE. (2008). Kisspeptin excites gonadotropin-releasing hormone neurons through a phospholipase C/calcium-dependent pathway regulating multiple ion channels. *Endocrinology* **149,** 4605-4614.

Liu X, Porteous R, d'Anglemont de Tassigny X, Colledge WH, Millar R, Petersen SL & Herbison AE. (2011). Frequency-dependent recruitment of fast amino acid and slow neuropeptide neurotransmitter release controls gonadotropin-releasing hormone neuron excitability. *Journal of Neuroscience* **31,** 2421-2430.

Loh DH, Kuljis DA, Azuma L, Wu Y, Truong D, Wang HB & Colwell CS. (2014). Disrupted reproduction, estrous cycle, and circadian rhythms in female mice deficient in vasoactive intestinal peptide. *Journal of Biological Rhythms* **29,** 355-369.

Lokshin M, LeSauter J & Silver R. (2015). Selective distribution of retinal input to mouse SCN revealed in analysis of sagittal sections. *Journal of Biological Rhythms* **30,** 251-257.

Long MA, Jutras MJ, Connors BW & Burwell RD. (2005). Electrical synapses coordinate activity in the suprachiasmatic nucleus. *Nature Neuroscience* **8,** 61-66.

López E, Gunby J, Daya S, Parrilla JJ, Abad L & Balasch J. (2004). Ovulation induction in women with polycystic ovary syndrome: Randomized trial of clomiphene citrate versus low-dose recombinant FSH as first line therapy. *Reproductive BioMedicine Online* **9,** 382-390.

Losonczy A, Biró AA & Nusser Z. (2004). Persistently active cannabinoid receptors mute a subpopulation of hippocampal interneurons. *Proceedings of the National Academy of Sciences of the United States of America* **101,** 1362-1367.

Lubahn DB, Moyer JS, Golding TS, Couse JF, Korach KS & Smithies O. (1993). Alteration of reproductive function but not prenatal sexual development after insertional disruption of the mouse estrogen receptor gene. *Proceedings of the National Academy of Sciences of the United States of America* **90**.

Luborsky-Moore JL, Poliakoff SJ & Worthington Jr WC. (1975). Ultrastructural observation of anterior pituitary gonadotrophs following hypophysial portal vessel infusion of luteinizing hormone-releasing hormone. *American Journal of Anatomy* **144,** 549-555.

Ludwig M & Leng G. (2006). Dendritic peptide release and peptide-dependent behaviours. *Nature Reviews Neuroscience* **7,** 126-136.

Lydon JP, DeMayo FJ, Funk CR, Mani SK, Hughes AR, Montgomery Jr CA, Shyamala G, Conneely OM & O'Malley BW. (1995). Mice lacking progesterone receptor exhibit pleiotropic reproductive abnormalities. *Genes and Development* **9,** 2266-2278.

Madisen L, Zwingman TA, Sunkin SM, Oh SW, Zariwala HA, Gu H, Ng LL, Palmiter RD, Hawrylycz MJ, Jones AR, Lein ES & Zeng H. (2010). A robust and high-throughput Cre reporting and characterization system for the whole mouse brain. *Nature Neuroscience* **13,** 133-140.

Mahoney MM & Smale L. (2005). Arginine vasopressin and vasoactive intestinal polypeptide fibers make appositions with gonadotropin-releasing hormone and estrogen receptor cells in the diurnal rodent *Arvicanthis niloticus*. *Brain Research* **1049,** 156-164.

Manning M, Misicka A, Olma A, Bankowski K, Stoev S, Chini B, Durroux T, Mouillac B, Corbani M & Guillon G. (2012). Oxytocin and vasopressin agonists and antagonists as research tools and potential therapeutics. *Journal of Neuroendocrinology* **24,** 609-628.

March WA, Moore VM, Willson KJ, Phillips DI, Norman RJ & Davies MJ. (2010). The prevalence of polycystic ovary syndrome in a community sample assessed under contrasting diagnostic criteria. *Human Reproduction* **25,** 544-551.

Marraudino M, Miceli D, Farinetti A, Ponti G, Panzica G & Gotti S. (2017). Kisspeptin innervation of the hypothalamic paraventricular nucleus: Sexual dimorphism and effect of estrous cycle in female mice. *Journal of Anatomy* **230,** 775-786.

Marshall CJ, Desroziers E, McLennan T & Campbell RE. (2017). Defining subpopulations of arcuate nucleus GABA neurons in male, female, and prenatally androgenized female mice. *Neuroendocrinology* **105,** 157-169.

Maruyama T, Ohbuchi T, Fujihara H, Shibata M, Mori K, Murphy D, Dayanithi G & Ueta Y. (2010). Diurnal changes of arginine vasopressin-enhanced green fluorescent protein fusion transgene expression in the rat suprachiasmatic nucleus. *Peptides* **31,** 2089-2093.

Matsuzaki T, Tungalasuvd A, Iwasa T, Munkhzaya M, Yanagihara R, Tokui T, Yano K, Mayila Y & Kato T. (2017). Kisspeptin mRNA expression is increased in the posterior hypothalamus in the rat model of polycystic ovary syndrome. *Endocrine Journal* **64,** 7-14.

Mayer C, Acosta-Martinez M, Dubois SL, Wolfe A, Radovick S, Boehm U & Levine JE. (2010). Timing and completion of puberty in female mice depend on estrogen receptor alpha-signaling in kisspeptin neurons. *Proceedings of the National Academy of Sciences of the United States of America* **107,** 22693-22698.

Maywood ES, Chesham JE, O'Brien JA & Hastings MH. (2011). A diversity of paracrine signals sustains molecular circadian cycling in suprachiasmatic nucleus circuits. *Proceedings of the National Academy of Sciences of the United States of America* **108,** 14306-14311.

Mazuski C, Abel JH, Chen SP, Hermanstyne TO, Jones JR, Simon T, Doyle FJ, 3rd & Herzog ED. (2018). Entrainment of circadian rhythms depends on firing rates and neuropeptide release of VIP SCN neurons. *Neuron* **99,** 555-563 e555.

McElhinny TL, Sisk CL, Holekamp KE & Smale L. (1999). A morning surge in plasma luteinizing hormone coincides with elevated Fos expression in gonadotropin-releasing hormone-immunoreactive neurons in the diurnal rodent, *Arvicanthis niloticus*. *Biology of Reproduction* **61,** 1115-1122.

McElhinny TL, Smale L & Holekamp KE. (1997). Patterns of body temperature, activity, and reproductive behavior in a tropical murid rodent, *Arvicanthis niloticus*. *Physiology and Behaviour* **61,** 91-96.

McQuillan HJ, Han SY, Cheong I & Herbison AE. (2019). GnRH pulse generator activity across the estrous cycle of female mice. *Endocrinology* **160,** 1480-1491.

Merchenthaler I, Setalo G, Csontos C, Petrusz P, Flerko B & Negro-Vilar A. (1989). Combined retrograde tracing and immunocytochemical identification of luteinizing hormone-releasing hormone- and somatostatin-containing neurons projecting to the median eminence of the rat. *Endocrinology* **125,** 2812-2821.

Mereness AL, Murphy ZC & Sellix MT. (2015). Developmental programming by androgen affects the circadian timing system in female mice. *Biology of Reproduction* **92,** 88.

Messager S, Chatzidaki EE, Ma D, Hendrick AG, Zahn D, Dixon J, Thresher RR, Malinge I, Lomet D, Carlton MB, Colledge WH, Caraty A & Aparicio SA. (2005). Kisspeptin directly stimulates gonadotropin-releasing hormone release via G protein-coupled receptor 54. *Proceedings of the National Academy of Sciences of the United States of America* **102,** 1761-1766.

Meyer-Bernstein EL, Blanchard JH & Morin LP. (1997). The serotonergic projection from the median raphe nucleus to the suprachiasmatic nucleus modulates activity phase onset, but not other circadian rhythm parameters. *Brain Research* **755,** 112-120.

Meyer-Bernstein EL, Jetton AE, Matsumoto S-I, Markuns JF, Lehman MN & Bittman EL. (1999). Effects of suprachiasmatic transplants on circadian rhythms of neuroendocrine function in golden hamsters. *Endocrinology* **140,** 207-218.

Micevych P & Sinchak K. (2011). The neurosteroid progesterone underlies estrogen positive feedback of the LH surge. *Frontiers in Endocrinology* **2,** 90.

Micevych P, Sinchak K, Mills RH, Tao L, LaPolt P & Lu JK. (2003). The luteinizing hormone surge is preceded by an estrogen-induced increase of hypothalamic progesterone in ovariectomized and adrenalectomized rats. *Neuroendocrinology* **78,** 29-35.

Micevych PE, Chaban V, Ogi J, Dewing P, Lu JK & Sinchak K. (2007). Estradiol stimulates progesterone synthesis in hypothalamic astrocyte cultures. *Endocrinology* **148,** 782-789.

Micevych PE & Kelly MJ. (2012). Membrane estrogen receptor regulation of hypothalamic function. *Neuroendocrinology* **96,** 103-110.

Miller BH, Olson SL, Levine JE, Turek FW, Horton TH & Takahashi JS. (2006). Vasopressin regulation of the proestrous luteinizing hormone surge in wild-type and *Clock* mutant mice. *Biology of Reproduction* **75,** 778-784.

Miller BH, Olson SL, Turek FW, Levine JE, Horton TH & Takahashi JS. (2004). Circadian *Clock* mutation disrupts estrous cyclicity and maintenance of pregnancy. *Current Biology* **14,** 1367-1373.

Mintz EM & Albers HE. (1997). Microinjection of NMDA into the SCN region mimics the phase shifting effect of light in hamsters. *Brain Research* **758,** 245-259.

Mintz EM, Marvel CL, Gillespie CF, Price KM & Albers HE. (1999). Activation of NMDA receptors in the suprachiasmatic nucleus produces light-like phase shifts of the circadian clock *in vivo*. *Journal of Neuroscience* **19,** 5124-5130.

Moenter SM, Brand RM, Midgley AR & Karsch FJ. (1992). Dynamics of gonadotropin-releasing hormone release during a pulse. *Endocrinology* **130,** 503-510.

Moffatt CA, Rissman EF, Shupnik MA & Blaustein JD. (1998). Induction of progestin receptors by estradiol in the forebrain of estrogen receptor-α gene-disrupted mice. *Journal of Neuroscience* **18,** 9556-9563.

Mohawk JA & Takahashi JS. (2011). Cell autonomy and synchrony of suprachiasmatic nucleus circadian oscillators. *Trends in Neuroscience* **34,** 349-358.

Mohr MA, Garcia FL, DonCarlos LL & Sisk CL. (2016). Neurons and glial cells are added to the female rat anteroventral periventricular nucleus during puberty. *Endocrinology* **157,** 2393-2402.

Moore AM & Campbell RE. (2017). Polycystic ovary syndrome: Understanding the role of the brain. *Frontiers in Neuroendocrinology* **46,** 1-14.

Moore AM, Prescott M & Campbell RE. (2013). Estradiol negative and positive feedback in a prenatal androgen-induced mouse model of polycystic ovarian syndrome. *Endocrinology* **154,** 796-806.

Moore AM, Prescott M, Marshall CJ, Yip SH & Campbell RE. (2015). Enhancement of a robust arcuate GABAergic input to gonadotropin-releasing hormone neurons in a model of polycystic ovarian syndrome. *Proceedings of the National Academy of Sciences of the United States of America* **112,** 596-601.

Moore RY & Eichler VB. (1972). Loss of a circadian adrenal corticosterone rhythm following suprachiasmatic lesions in the rat. *Brain Research* **42,** 201-206.

Moore RY & Lenn NJ. (1972). A retinohypothalamic projection in the rat. *Journal of Comparative Neurology* **146,** 1-14.

Moore RY & Speh JC. (1993). GABA is the principal neurotransmitter of the circadian system. *Neuroscience Letters* **150,** 112-116.

Morin LP. (2013). Neuroanatomy of the extended circadian rhythm system. *Experimental Neurology* **243,** 4-20.

Morin LP & Allen CN. (2006). The circadian visual system, 2005. *Brain Research Reviews* **51,** 1-60.

Morin LP, Blanchard J & Moore RY. (1992). Intergeniculate leaflet and suprachiasmatic nucleus organization and connections in the golden hamster. *Visual Neuroscience* **8,** 219-230.

Morin LP & Blanchard JH. (2005). Descending projections of the hamster intergeniculate leaflet: Relationship to the sleep/arousal and visuomotor systems. *Journal of Comparative Neurology* **487,** 204-216.

Morin LP, Goodless-Sanchez N, Smale L & Moore RY. (1994). Projections of the suprachiasmatic nuclei, subparaventricular zone and retrochiasmatic area in the golden hamster. *Neuroscience* **61,** 391-410.

Morin LP, Shivers KY, Blanchard JH & Muscat L. (2006). Complex organization of mouse and rat suprachiasmatic nucleus. *Neuroscience* **137,** 1285-1297.

Morris JF & Pow DV. (1991). Widespread release of peptides in the central nervous system: Quantification of tannic acid-captured exocytoses. *The Anatomical Record* **231,** 437-445.

Murr SM, Geschwind II & Bradford GE. (1973). Plasma LH and FSH during different oestrous cycle conditions in mice. *Journal of Reproduction and Fertility* **32,** 221-230.

Nankin HR & Troen P. (1971). Repetitive luteinizing hormone elevations in serum of normal men. *Journal of Clinical Endocrinology and Metabolism* **33,** 558-560.

Navarro VM, Gottsch ML, Chavkin C, Okamura H, Clifton DK & Steiner RA. (2009). Regulation of gonadotropin-releasing hormone secretion by kisspeptin/dynorphin/neurokinin B neurons in the arcuate nucleus of the mouse. *Journal of Neuroscience* **29,** 11859-11866.

Navarro VM, Gottsch ML, Wu M, Garcia-Galiano D, Hobbs SJ, Bosch MA, Pinilla L, Clifton DK, Dearth A, Rønnekleiv OK, Braun RE, Palmiter RD, Tena-Sempere M, Alreja M & Steiner RA. (2011). Regulation of NKB pathways and their roles in the control of Kiss1 neurons in the arcuate nucleus of the male mouse. *Endocrinology* **152,** 4265-4275.

Ndefo UA, Eaton A & Green MR. (2013). Polycystic ovary syndrome: A review of treatment options with a focus on pharmacological approaches. *Pharmacology and Therapeutics* **38,** 336-355.

Noriega NC, Eghlidi DH, Garyfallou VT, Kohama SG, Kryger SG & Urbanski HF. (2010). Influence of 17β-estradiol and progesterone on GABAergic gene expression in the arcuate nucleus, amygdala and hippocampus of the rhesus macaque. *Brain Research* **1307,** 28-42.

Nunemaker CS, DeFazio RA, Guesz ME, Herzog ED, Pitts GR & Moenter SM. (2001). Long-term recordings of networks of immortalized GnRH neurons reveal episodic patterns of electrical activity. *Journal of Neurophysiology* **86,** 86-93.

O'Herlihy C, Pepperell RJ, Brown JB, Smith MA, Sandri L & McBain JC. (1981). Incremental clomiphene therapy: A new method for treating persistent anovulation. *Obstetrics & Gynecology* **58,** 535-542.

Ohtsuka S, Miyake A, Nishizaki T, Tasaka K & Tanizawa O. (1988). Vasoctive intestinal peptide stimulates gonadotropin-releasing hormone release from rat hypothalamus *in vitro*. *Acta Endocrinologica* **117,** 399-402.

Okamura H, Bérod A, Julien J-F, Geffard M, Kitahama K, JacquesMallet & Bobillier P. (1989). Demonstration of GABAergic cell bodies in the suprachiasmaticnucleus: *In situ* hybridization of glutamic acid decarboxylase(GAD) mRNA and immunocytochemistry of GAD and GABA. *Neuroscience Letters* **102,** 131-136.

Olcese J, McArdle CA, Middendorff R & Greenland K. (1997). Pituitary adenylate cyclase-activating peptide and vasoactive intestinal peptide receptor expression in immortalized LHRH neurons. *Journal of Neuroendocrinology* **9,** 937-943.

Orban PC, Chui D & Marth JD. (1992). Tissue- and site-specific DNA recombination in transgenic mice. *Proceedings of the National Academy of Sciences of the United States of America* **89,** 6861-6865.

Ördög T & Knobil E. (1995). Estradiol and the inhibition of hypothalamic gonadotropin-releasing hormone pulse generator activity in the rhesus monkey. *Proceedings of the National Academy of Sciences of the United States of America* **92,** 5813-5816.

Osuka S, Iwase A, Nakahara T, Kondo M, Saito A, Bayasula, Nakamura T, Takikawa S, Goto M, Kotani T & Kikkawa F. (2017). Kisspeptin in the hypothalamus of 2 rat models of polycystic ovary syndrome. *Endocrinology* **158,** 367-377.

Ottowitz WE, Dougherty DD, Fischman AJ & Hall JE. (2008). [^{18}F]2-fluoro-2-deoxy-D-glucose positron emission tomography demonstration of estrogen negative and positive feedback on luteinizing hormone secretion in women. *Journal of Clinical Endocrinology and Metabolism* **93,** 3208-3214.

Owen SF, Liu MH & Kreitzer AC. (2019). Thermal constraints on *in vivo* optogenetic manipulations. *Nature Neuroscience* **22,** 1061-1065.

Pak TR, Chung WC, Hinds LR & Handa RJ. (2007). Estrogen receptor-β mediates dihydrotestosterone-induced stimulation of the arginine vasopressin promoter in neuronal cells. *Endocrinology* **148,** 3371-3382.

Palm IF, van der Beek EM, Wiegant VM, Buijs RM & Kalsbeek A. (1999). Vasopressin induces an luteinizing hormone surge in ovariectomized, estradiol-treated rats with lesions of the suprachiasmatic nucleus. *Neuroscience* **93,** 659-666.

Palm IF, van der Beek EM, Wiegant VM, Buijs RM & Kalsbeek A. (2001). The stimulatory effect of vasopressin on the luteinizing hormone surge in ovariectomized, estradiol-treated rats is time-dependent. *Brain Research* **902,** 109-116.

Partch CL, Green CB & Takahashi JS. (2014). Molecular architecture of the mammalian circadian clock. *Trends in Cell Biology* **24,** 90-99.

Pelletier G, Peillon F & Vila-Porcile E. (1971). An ultrastructural study of sites of granual extrusion in the anterior pituitary of the rat. *Zeitschrift für Zellforschung und Mikroskopische Anatomie* **115,** 501-507.

Pennartz CMA, Bos NPA, de Jeu MTG, Geurtsen AMS, Mirmiran M, Slutter AA & Buijs RM. (1998). Membrane properties and morphology of vasopressin neurons in slices of rat suprachiasmatic nucleus. *Journal of Neurophysiology* **80,** 2710-2717.

Pennartz CMA, de Jeu MTG, Bos NPA, Schaap J & Geurtsen AMS. (2002). Diurnal modulation of pacemaker potentials and calcium current in the mammalian circadian clock. *Nature* **416,** 286-290.

Petersen SL, Cheuk C, D. HR & Barraclough CA. (1989). Medial preoptic microimplants of the antiestrogen, keoxifene, affect luteinizing hormone-releasing hormone mRNA levels, median eminence luteinizing hormone-releasing hormone concentrations and luteinizing hormone release in ovariectomized, estrogen-treated rats. *Journal of Neuroendocrinology* **1,** 279-283.

Petreanu L, Huber D, Sobczyk A & Svoboda K. (2007). Channelrhodopsin-2-assisted circuit mapping of long-range callosal projections. *Nature Neuroscience* **10,** 663-668.

Petreanu L, Mao T, Sternson SM & Svoboda K. (2009). The subcellular organization of neocortical excitatory connections. *Nature* **457,** 1142-1145.

Pezük P, Mohawk JA, Wang LA & Menaker M. (2012). Glucocorticoids as entraining signals for peripheral circadian oscillators. *Endocrinology* **153,** 4775-4783.

Pickard GE & Silverman A-J. (1981). Direct retinal projections to the hypothalamus, piriform cortex, and accessory optic nuclei in the golden hamster as demonstrated by a sensitive anterograde horseradish peroxidase technique. *Journal of Comparative Neurology* **196,** 155-172.

Piet R, Boehm U & Herbison AE. (2013). Estrous cycle plasticity in the hyperpolarization-activated current ih is mediated by circulating 17β-estradiol in preoptic area kisspeptin neurons. *Journal of Neuroscience* **33,** 10828-10839.

Piet R, de Croft S, Liu X & Herbison AE. (2015a). Electrical properties of kisspeptin neurons and their regulation of GnRH neurons. *Frontiers in Neuroendocrinology* **36,** 15-27.

Piet R, Dunckley H, Lee K & Herbison AE. (2016). Vasoactive intestinal peptide excites GnRH neurons in male and female mice. *Endocrinology* **157,** 3621-3630.

Piet R, Fraissenon A, Boehm U & Herbison AE. (2015b). Estrogen permits vasopressin signaling in preoptic kisspeptin neurons in the female mouse. *Journal of Neuroscience* **35,** 6881-6892.

Piet R & Herbison AE. (2018). Electrophysiology of rodent GnRH neurons. In *The GnRH Neuron and its Control*, ed. Herbison AE & Plant TM, pp. 117-202. John Wiley & Sons.

Piet R, Kalil B, McLennan T, Porteous R, Czieselsky K & Herbison AE. (2018). Dominant neuropeptide cotransmission in kisspeptin-GABA regulation of GnRH neuron firing driving ovulation. *Journal of Neuroscience* **38,** 6310-6322.

Pigny P, Merlen E, Robert Y, Cortet-Rudelli C, Decanter C, Jonard S & Dewailly D. (2003). Elevated serum level of anti-Müllerian hormone in patients with polycystic ovary syndrome: Relationship to the ovarian follicle excess and to the follicular arrest. *Journal of Clinical Endocrinology and Metabolism* **88,** 5957-5962.

Pitts GR, Ohta H & McMahon DG. (2006). Daily rhythmicity of large-conductance Ca^{2+}-activated K^{+} currents in suprachiasmatic nucleus neurons. *Brain Research* **1071,** 54-62.

Plant TM. (2012). A comparison of the neuroendocrine mechanisms underlying the initiation of the preovulatory LH surge in the human, Old World monkey and rodent. *Frontiers in Neuroendocrinology* **33,** 160-168.

Plant TM. (2015). Neuroendocrine control of the onset of puberty. *Frontiers in Neuroendocrinology* **38,** 73-88.

Plant TM, Krey LC, Moossy J, McCormack JT, Hess DL & Knobil E. (1978). The arcuate nucleus and the control of gonadotropin and prolactin secretion in the female rhesus monkey (*Macaca mulatta*). *Endocrinology* **102,** 52-62.

Polston EK & Simerly RB. (2006). Ontogeny of the projections from the anteroventral periventricular nucleus of the hypothalamus in the female rat. *Journal of Comparative Neurology* **495,** 122-132.

Porter DT, Moore AM, Cobern JA, Padmanabhan V, Goodman RL, Coolen LM & Lehman MN. (2019). Prenatal testosterone exposure alters GABAergic synaptic inputs to GnRH and KNDy neurons in a sheep model of polycystic ovarian syndrome. *Endocrinology* **160,** 2529-2542.

Pow DV & Morris JF. (1989). Dendrites of hypothalamic magnocellular neurons release neurohypophysial peptides by exocytosis. *Neuroscience* **32,** 435-439.

Proaño SB, Morris HJ, Kunz LM, Dorris DM & Meitzen J. (2018). Estrous cycle-induced sex differences in medium spiny neuron excitatory synaptic transmission and intrinsic excitability in adult rat nucleus accumbens core. *Journal of Neurophysiology* **120,** 1356-1373.

Prossnitz ER, Arterburn JB & Sklar LA. (2007). GPR30: A G protein-coupled receptor for estrogen. *Molecular and Cellular Endocrinology* **256-266,** 138-142.

Qiu J, Nestor CC, Zhang C, Padilla SL, Palmiter RD, Kelly MJ & Rønnekleiv OK. (2016). High-frequency stimulation-induced peptide release synchronizes arcuate kisspeptin neurons and excites GnRH neurons. *Elife* **5**.

Ramaswamy S, Seminara SB, Ali B, Ciofi P, Amin NA & Plant TM. (2010). Neurokinin B stimulates GnRH release in the male monkey (*Macaca mulatta*) and is colocalized with kisspeptin in the arcuate nucleus. *Endocrinology* **151,** 4494-4503.

Ramaswamy S & Weinbauer GF. (2015). Endocrine control of spermatogenesis: Role of FSH and LH/testosterone. *Spermatogenesis* **4,** e996025.

Raskin K, de Gendt K, Duittoz A, Liere P, Verhoeven G, Tronche F & Mhaouty-Kodja S. (2009). Conditional inactivation of androgen receptor gene in the nervous system: Effects on male behavioral and neuroendocrine responses. *Journal of Neuroscience* **29,** 4461-4470.

Rawlings NC & Cook SJ. (1993). LH secretion around the time of the preovulatory gonadotrophin surge in the ewe. *Animal Reproduction Science* **30,** 289-299.

Renier N, Wu Z, Simon DJ, Yang J, Ariel P & Tessier-Lavigne M. (2014). iDISCO: A simple, rapid method to immunolabel large tissue samples for volume imaging. *Cell* **159,** 896-910.

Resuehr D, Wildemann U, Sikes H & Olcese J. (2007). E-box regulation of gonadotropin-releasing hormone (GnRH) receptor expression in immortalized gonadotrope cells. *Molecular and Cellular Endocrinology* **278,** 36-43.

Rhodes CH, Morrell JI & Pfaff DW. (1981). lmmunohistochemical analysis of magnocellular elements in rat hypothalamus: Distribution and numbers of cells containing neurophysin, oxytocin, and vasopressin. *Journal of Comparative Neurology* **198,** 45-64.

Robben JH, Knoers NVAM & Deen PMT. (2004). Regulation of the vasopressin V2 receptor by vasopressin in polarized renal collecting duct cells. *Molecular Biology of the Cell* **15,** 5693-5699.

Robertson JL, Clifton DK, de la Iglesia HO, Steiner RA & Kauffman AS. (2009). Circadian regulation of *Kiss1* neurons: Implications for timing the preovulatory gonadotropin-releasing hormone/luteinizing hormone surge. *Endocrinology* **150,** 3664-3671.

Roland AV & Moenter SM. (2014). Reproductive neuroendocrine dysfunction in polycystic ovary syndrome: Insight from animal models. *Frontiers in Neuroendocrinology* **35,** 494-511.

Romero-Ruiz A, Skorupskaite K, Gaytan F, Torres E, Perdices-Lopez C, Mannaerts BM, Qi S, Leon S, Manfredi-Lozano M, Lopez-Rodriguez C, Avendaño MS, Sanchez-Garrido MA, Vazquez MJ, Pinilla L, van Duin M, Kohout TA, Anderson RA & Tena-Sempere M. (2019). Kisspeptin treatment induces gonadotropic responses and rescues ovulation in a subset of preclinical models and women with polycystic ovary syndrome. *Human Reproduction* **34,** 2495-2512.

Rometo AM, Krajewski SJ, Voytko ML & Rance NE. (2007). Hypertrophy and increased kisspeptin gene expression in the hypothalamic infundibular nucleus of postmenopausal women and ovariectomized monkeys. *Journal of Clinical Endocrinology and Metabolism* **92,** 2744-2750.

Rood BD & de Vries GJ. (2011). Vasopressin innervation of the mouse (*Mus musculus*) brain and spinal cord. *Journal of Comparative Neurology* **519,** 2434-2474.

Roozendaal MM, Swarts HJM, Wiegant VM & Mattheij JAM. (1995). Effect of restraint stress on the preovulatory luteinizing hormone profile and ovulation in the rat. *European Journal of Endocrinology* **133,** 347-353.

Roth BL. (2016). DREADDs for neuroscientists. *Neuron* **89,** 683-694.

Rotterdam EA-SPCWG. (2004). Revised 2003 consensus on diagnostic criteria and long-term health risks related to polycystic ovary syndrome. *Fertility and Sterility* **81,** 19-25.

Ruka KA, Burger LL & Moenter SM. (2013). Regulation of arcuate neurons coexpressing kisspeptin, neurokinin B, and dynorphin by modulators of neurokinin 3 and kappa-opioid receptors in adult male mice. *Endocrinology* **154,** 2761-2771.

Rumi MAK, Singh P, Roby KF, Zhao X, Iqbal K, Ratri A, Lei T, Cui W, Borosha S, Dhakal P, Kubota K, Chakraborty D, Vivian JL, Wolfe MW & Soares MJ. (2017). Defining the role of estrogen receptor β in the regulation of female fertility. *Endocrinology* **158,** 2330-2343.

Rumpler É, Skrapits K, Takács S, Göcz B, Trinh SH, Rácz G, Matolcsy A, Kozma Z, Ciofi P, Dhillo WS & Hrabovszky E. (2020). Characterization of kisspeptin neurons in the human rostral hypothalamus. *Neuroendocrinology*.

Russo KA, La JL, Stephens SB, Poling MC, Padgaonkar NA, Jennings KJ, Piekarski DJ, Kauffman AS & Kriegsfeld LJ. (2015). Circadian control of the female reproductive axis through gated responsiveness of the RFRP-3 system to VIP signaling. *Endocrinology* **156,** 2608-2618.

Sadun AA, Schaechter JD & Smith LH. (1984). A retinohypothalamic pathway in man: Light mediation of circadian rhythms. *Brain Research* **302,** 371-377.

Salio C, Lossi L, Ferrini F & Merighi A. (2006). Neuropeptides as synaptic transmitters. *Cell and Tissue Research* **326,** 583-598.

Samson WK, Burton KP, Reeves JP & McCann SM. (1981). Vasoactive-intestinal peptide stimulates luteinizing hormone-releasing hormone release from median eminence synaptosomes. *Regulatory Peptides* **2,** 253-264.

Santen RJ. (1975). Is aromatization of testosterone to estradiol required for inhibition of luteinizing hormone secretion in men? *Journal of Clinical Investigation* **56,** 1555-1563.

Savoy-Moore RT & Swartz KH. (1987). Several GnRH stimulation frequencies differentially release FSH and LH from isolated, perfused rat anterior pituitary cells. *Advances in Experimental and Medical Biology* **219,** 641-645.

Schaap J, Pennartz CM & Meijer JH. (2003). Electrophysiology of the circadian pacemaker in mammals. *Chronobiology International* **20,** 171-188.

Schanbacher BD. (1980). Testosterone regulation of luteinizing hormone and follicle stimulating hormone in young male lambs. *Journal of Animal Science* **51,** 679-684.

Scharfman HE, Mercurio TC, Goodman JH, Wilson MA & MacLusky NJ. (2003). Hippocampal excitability increases during the estrous cycle in the rat: A potential role for brain-derived neurotrophic factor. *Journal of Neuroscience* **23,** 11641-11652.

Schirman-Hildesheim TD, Ben-Aroya N & Koch Y. (2006). Daily GnRH and GnRH-receptor mRNA expression in the ovariectomized and intact rat. *Molecular and Cellular Endocrinology* **252,** 120-125.

Schöne C, Apergis-Schoute J, Sakurai T, Adamantidis A & Burdakov D. (2014). Coreleased orexin and glutamate evoke nonredundant spike outputs and computations in histamine neurons. *Cell Reports* **7,** 697-704.

Schwartz MD, Urbanski HF, Nunez AA & Smale L. (2011). Projections of the suprachiasmatic nucleus and ventral subparaventricular zone in the Nile grass rat (*Arvicanthis niloticus*). *Brain Research* **1367,** 146-161.

Schwartz WJ, Coleman RJ & Reppert SM. (1983). A daily vasopressin rhythm in rat cerebrospinal fluid. *Brain Research* **263,** 105-112.

Schwarz JM & McCarthy MM. (2008). Steroid-induced sexual differentiation of the developing brain: Multiple pathways, one goal. *Journal of Neurochemistry* **105,** 1561-1572.

Schwarz LA, Miyamichi K, Gao XJ, Beier KT, Weissbourd B, DeLoach KE, Ren J, Ibanes S, Malenka RC, Kremer EJ & Luo L. (2015). Viral-genetic tracing of the input–output organization of a central norepinephrine circuit. *Nature* **524,** 88-92.

Seibel MM, Shine W, Smith DM & Taymor ML. (1982). Biological rhythm of the luteinizing hormone surge in women. *Fertility and Sterility* **37,** 709-711.

Sellix MT, Murphy ZC & Menaker M. (2013). Excess androgen during puberty disrupts circadian organization in female rats. *Endocrinology* **154,** 1636-1647.

Seminara SB, Messager S, Chatzidaki EE, Thresher RR, James S. Acierno J, Shagoury JK, Bo-Abbas Y, Kuohung W, Schwinof KM, Hendrick AG, Zahn D, Dixon J, Kaiser UB, Slaugenhaupt SA, Gusella JF, O'Rahilly S, Carlton MBL, William F. Crowley J, Aparicio SAJR & Colledge WH. (2003). The GPR54 gene as a regulator of puberty. *New England Journal of Medicine* **349,** 1614-1627.

Seymour AJ, Scott V, Augustine RA, Bouwer GT, Campbell RE & Brown CH. (2017). Development of an excitatory kisspeptin projection to the oxytocin system in late pregnancy. *Journal of Physiology* **595,** 825-838.

Shapiro RA, Xu C & Dorsa DM. (2000). Differential transcriptional regulation of rat vasopressin gene expression by estrogen receptor α and β. *Endocrinology* **141,** 4056-4064.

Sharma TP, Blache D & Martin GB. (1999). Aromatase and 5α-reductase pathways and their interaction with nutrition in the control of pulsatile secretion of LH in male sheep. *Proceedings of the Australian Society of Reproductive Biology* **30,** 96.

Shaw ND, Histed SN, Srouji SS, Yang J, Lee H & Hall JE. (2010). Estrogen negative feedback on gonadotropin secretion: Evidence for a direct pituitary effect in women. *Journal of Clinical Endocrinology and Metabolism* **95,** 1955-1961.

Shibata S, Liou SY & Ueki S. (1986). Influence of excitatory amino acid receptor antagonists and of baclofen on synaptic transmission in the optic nerve to the suprachiasmatic nucleus in slices of rat hypothalamus. *Neuropharmacology* **25,** 403-409.

Shinohara K, Honma S, Katsuno Y, Abe H & Honma K-I. (1998). Circadian release of amino acids in the suprachiasmatic nucleus *in vitro*. *NeuroReport* **9,** 137-140.

Shughrue PJ, Komm B & Merchenthaler I. (1996). The distribution of estrogen receptor-β mRNA in the rat hypothalamus. *Steroids* **61,** 678-681.

Shughrue PJ, Lane MV & Merchenthaler I. (1997). Comparative distribution of estrogen receptor-α and -β mRNA in the rat central nervous system. *Journal of Comparative Neurology* **388,** 507-525.

Silva MS, Prescott M & Campbell RE. (2018). Ontogeny and reversal of brain circuit abnormalities in a preclinical model of PCOS. *JCI Insight* **3**.

Silva MSB, Desroziers E, Hessler S, Prescott M, Coyle C, Herbison AE & Campbell RE. (2019). Activation of arcuate nucleus GABA neurons promotes luteinizing hormone secretion and reproductive dysfunction: Implications for polycystic ovary syndrome. *EBioMedicine* **44,** 582-596.

Silver R, LeSauter J, Tresco PA & Lehman MN. (1996). A diffusible coupling signal from the transplanted suprachiasmatic nucleus controlling circadian locomotor rhythms. *Nature* **382**.

Silverman A-J, Antunes JL, Abrams GM, Nilaver G, Thau R, Robinson JA, Ferin M & Krey LC. (1982). The luteinizing hormone-releasing hormone pathways in rhesus (*Macaca mulatta*) and pigtailed (*Macaca nemestrina*) monkeys: New observations on thick, unembedded sections. *Journal of Comparative Neurology* **211,** 309-317.

Silverman A-J, Jhamandas J & Renaud LP. (1987). Localization of luteinizing hormone-releasing hormone (LHRH) neurons that project to the median eminence. *Journal of Neuroscience* **7,** 2312-2319.

Simonneaux V & Piet R. (2018). Neuroendocrine pathways driving daily rhythms in the hypothalamic pituitary gonadal axis of female rodents. *Current Opinion in Physiology* **5,** 99-108.

Skinner DC, Caraty A & Allingham R. (2001). Unmasking the progesterone receptor in the preoptic area and hypothalamus of the ewe: No colocalization with gonadotropin-releasing neurons. *Endocrinology* **142,** 573-579.

Skinner DC, Evans NP, Delaleu B, Goodman RL, Bouchard P & Caraty A. (1998). The negative feedback actions of progesterone on gonadotropin- releasing hormone secretion are transduced by the classical progesterone receptor. *Proceedings of the National Academy of Sciences of the United States of America* **95,** 10978-10983.

Smarr BL, Gile JJ & de la Iglesia HO. (2013). Oestrogen-independent circadian clock gene expression in the anteroventral periventricular nucleus in female rats: Possible role as an integrator for circadian and ovarian signals timing the luteinising hormone surge. *Journal of Neuroendocrinology* **25,** 1273-1279.

Smarr BL, Morris E & de la Iglesia HO. (2012). The dorsomedial suprachiasmatic nucleus times circadian expression of Kiss1 and the luteinizing hormone surge. *Endocrinology* **153,** 2839-2850.

Smith JT, Cunningham MJ, Rissman EF, Clifton DK & Steiner RA. (2005a). Regulation of Kiss1 gene expression in the brain of the female mouse. *Endocrinology* **146,** 3686-3692.

Smith JT, Dungan HM, Stoll EA, Gottsch ML, Braun RE, Eacker SM, Clifton DK & Steiner RA. (2005b). Differential regulation of KiSS-1 mRNA expression by sex steroids in the brain of the male mouse. *Endocrinology* **146,** 2976-2984.

Smith JT, Popa SM, Clifton DK, Hoffman GE & Steiner RA. (2006). *Kiss1* neurons in the forebrain as central processors for generating the preovulatory luteinizing hormone surge. *Journal of Neuroscience* **26,** 6687-6694.

Smith MJ, Jennes L & Wise PM. (2000). Localization of the VIP_2 protein on GnRH neurons in the female rat. *Endocrinology* **141,** 4317-4320.

Smith MS, Freeman ME & Neill JD. (1975). The control of progesterone secretion during the estrous cycle and early pseudopregnancy in the rat: Prolactin, gonadotropin and steroid Levels associated with rescue of the corpus luteum of pseudopregnancy. *Endocrinology* **96,** 219-226.

Smith P, Steckler TL, Veiga-Lopez A & Padmanabhan V. (2009). Developmental programming: Differential effects of prenatal testosterone and dihydrotestosterone on follicular recruitment, depletion of follicular reserve, and ovarian morphology in sheep. *Biology of Reproduction* **80,** 726-736.

Sofroniew MV, Weindl A, Schinko I & Wetzstei R. (1979). The distribution of vasopressin-, oxytocin-, and neurophysin-producing neurons in the guinea pig brain. *Cell and Tissue Research* **196,** 367-384.

Son SJ, Filosa JA, Potapenko ES, Biancardi VC, Zheng H, Patel KP, Tobin VA, Ludwig M & Stern JE. (2013). Dendritic peptide release mediates interpopulation crosstalk between neurosecretory and preautonomic networks. *Neuron* **78,** 1036-1049.

Soper BD & Weick RF. (1980). Hypothalamic and extrahypothalamic mediation of pulsatile discharges of luteinizing hormone in the ovariectomized rat. *Endocrinology* **106,** 348-355.

Souza MF, Toniazo VM, Frazzon APG & Barros HMT. (2009). Influence of progesterone on GAD65 and GAD67 mRNA expression in the dorsolateral striatum and prefrontal cortex of female rats repeatedly treated with cocaine. *Brazilian Journal of Medical and Biological Research* **42,** 1068-1075.

Stamp JA, Piggins HD, Rusak B & Semba K. (1997). Distribution of ionotropic glutamate receptor subunit immunoreactivity in the suprachiasmatic nucleus and intergeniculate leaflet of the hamster. *Brain Research* **756,** 215-224.

Steckelbroeck S, Jin Y, Gopishetty S, Oyesanmi B & Penning TM. (2004). Human cytosolic 3α-hydroxysteroid dehydrogenases of the aldo-keto reductase superfamily display significant 3β-hydroxysteroid dehydrogenase activity: Implications for steroid hormone metabolism and action. *Journal of Biological Chemistry* **279,** 10784-10795.

Stein IF & Leventhal ML. (1935). Amenorrhea associated with bilateral polycystic ovaries. *American Journal of Obstetrics and Gynecology* **29,** 181-191.

Stener-Victorin E, Padmanabhan V, Walters KA, Campbell RE, Benrick A, Giacobini P, Dumesic DA & Abbott DH. (2020). Animal models to understand the etiology and pathophysiology of polycystic ovary syndrome. *Endocrine Reviews*.

Stephan FK & Zucker I. (1972). Circadian rhythms in drinking behavior and locomotor activity of rats are eliminated by hypothalamic lesions. *Proceedings of the National Academy of Sciences of the United States of America* **69,** 1583-1586.

Stephens SB, Tolson KP, Rouse ML, Jr., Poling MC, Hashimoto-Partyka MK, Mellon PL & Kauffman AS. (2015). Absent progesterone signaling in kisspeptin neurons disrupts the LH surge and impairs fertility in female mice. *Endocrinology* **156,** 3091-3097.

Stetson MH & Watson-Whitmyre M. (1976). Nucleus suprachiasmaticus: The biological clock in the hamster? *Science* **191**.

Steyn FJ, Wan Y, Clarkson J, Veldhuis JD, Herbison AE & Chen C. (2013). Development of a methodology for and assessment of pulsatile luteinizing hormone secretion in juvenile and adult male mice. *Endocrinology* **154,** 4939-4945.

Stocker LJ, Macklon NS, Cheong YC & Bewley SJ. (2014). Influence of shift work on early reproductive outcomes: A systematic review and meta-analysis. *Obstetrics & Gynecology* **124,** 99-110.

Stoynev AG & Nagai K. (1996). Lack of effect of suprachiasmatic infusion of a vasopressin antagonist on the circadian rhythm of wheel-running activity in rats. *Acta Physiologica et Pharmacologica Bulgarica* **22,** 39-43.

Struble RG, Afridi S, Beckman-Randall S, Li M, Cady C, Nathan B & McAsey ME. (2006). Neocortical and hippocampal glial fibrillary acidic protein immunoreactivity shows region-specific variation during the mouse estrous cycle. *Neuroendocrinology* **83,** 325-335.

Stujenske JM, Spellman T & Gordon JA. (2015). Modeling the spatiotemporal dynamics of light and heat Propagation for *in vivo* optogenetics. *Cell Reports* **12,** 525-534.

Sullivan SD & Moenter SM. (2004). Prenatal androgens alter GABAergic drive to gonadotropin-releasing hormone neurons: Implications for a common fertility disorder. *Proceedings of the National Academy of Sciences of the United States of America* **101,** 7129-7134.

Swaab DF, Pool CW & Nijveldt F. (1975). Immunofluorescence of vasopressin and oxytocin in the rat hypothalamo-neurohypophyseal system. *Journal of Neural Transmission* **36,** 195-215.

Tagliaferri V, Romualdi D, Scarinci E, Cicco S, Florio CD, Immediata V, Tropea A, Santarsiero CM, Lanzone A & Apa R. (2018). Melatonin treatment may be able to restore menstrual cyclicity in women with PCOS: A pilot study. *Reproductive Sciences* **25,** 269-275.

Tanoue A, Ito S, Honda K, Oshikawa S, Kitagawa Y, Koshimizu TA, Mori T & Tsujimoto G. (2004). The vasopressin V1b receptor critically regulates hypothalamic-pituitary-adrenal axis activity under both stress and resting conditions. *Journal of Clinical Investigation* **133,** 302-309.

Tata B, Mimouni NEH, Barbotin AL, Malone SA, Loyens A, Pigny P, Dewailly D, Catteau-Jonard S, Sundstrom-Poromaa I, Piltonen TT, Dal Bello F, Medana C, Prevot V, Clasadonte J & Giacobini P. (2018). Elevated prenatal anti-Müllerian hormone reprograms the fetus and induces polycystic ovary syndrome in adulthood. *Nature Medicine* **24,** 834-846.

Taylor AE, McCourt B, Martin KA, Anderson EJ, Adams JM, Schoenfeld D & Hall JE. (1997). Determinants of abnormal gonadotropin secretion in clinically defined women with polycystic ovary syndrome. *Journal of Clinical Endocrinology and Metabolism* **82,** 2248-2256.

Terasawa E, Keen KL, Mogi K & Claude P. (1999a). Pulsatile release of luteinizing hormone-releasing hormone (LHRH) in cultured LHRH neurons derived from the embryonic olfactory placode of the rhesus monkey. *Endocrinology* **140,** 1432-1441.

Terasawa E, Schanhofer WK, Keen KL & Luchansky L. (1999b). Intracellular Ca^{2+} oscillations in luteinizing hormone-releasing hormone neurons derived from the embryonic olfactory placode of the rhesus monkey. *Journal of Neuroscience* **19,** 5898-5909.

Testart J, Frydman R & Roger M. (1982). Seasonal influence of diurnal rhythms in the onset of the plasma luteinizing hormone surge in women. *Journal of Clinical Endocrinology and Metabolism* **55,** 374-377.

Thompson EL, Patterson M, Murphy KG, Smith KL, Dhillo WS, Todd JF, Ghatei MA & Bloom SR. (2004). Central and peripheral administration of kisspeptin-10 stimulates the hypothalamic-pituitary-gonadal axis. *Journal of Neuroendocrinology* **16,** 850-858.

Tobin VA, Millar RP & Canny BJ. (1997). Testosterone acts directly at the pituitary to regulate gonadotropin-releasing hormone-induced calcium signals in male rat gonadotropes. *Endocrinology* **138,** 3314-3319.

Tonsfeldt KJ, Goodall CP, Latham KL & Chappell PE. (2011). Oestrogen induces rhythmic expression of the kisspeptin-1 receptor GPR54 in hypothalamic gonadotrophin-releasing hormone-secreting GT1-7 cells. *Journal of Neuroendocrinology* **23,** 823-830.

Topaloglu AK, Tello JA, Kotan LD, Ozbek MN, Yilmaz MB, Erdogan S, Gurbuz F, Temiz F, Millar RP & Yuksel B. (2012). Inactivating *KISS1* mutation and hypogonadotropic hypogonadism. *New England Journal of Medicine* **366**.

Tousson E & Meissl H. (2004). Suprachiasmatic nuclei grafts restore the circadian rhythm in the paraventricular nucleus of the hypothalamus. *Journal of Neuroscience* **24,** 2983-2988.

Tritsch NX, Ding JB & Sabatini BL. (2012). Dopaminergic neurons inhibit striatal output through non-canonical release of GABA. *Nature* **490,** 262-266.

Tsang AH, Barclay JL & Oster H. (2014). Interactions between endocrine and circadian systems. *Journal of Molecular Endocrinology* **52,** R1-16.

Tsutsui K, Saigoh E, Ukena K, Teranishi H, Fujisawa Y, Kikuchi M, Ishii S & Sharp PJ. (2000). A novel avian hypothalamic peptide inhibiting gonadotropin release. *Biochemical and Biophysical Research Communications* **275,** 661-667.

Umetsu Y, Tenno T, Goda N, Shirakawa M, Ikegami T & Hiroaki H. (2011). Structural difference of vasoactive intestinal peptide in two distinct membrane-mimicking environments. *Biochimica et Biophysica Acta* **1814,** 724-730.

Usdin TB, Bonner TI & Mezey E. (1994). Two receptors for vasoactive intestinal polypeptide with similar specificity and complementary distributions. *Endocrinology* **135,** 2662-2680.

van den Pol AN. (1980). The hypothalamic suprachiasmatic nucleus of rat: Intrinsic anatomy. *Journal of Comparative Neurology* **191,** 661-702.

van den Pol AN. (1991). Glutamate and aspartate immunoreactivity in hypothalamic presynaptic axons. *Journal of Neuroscience* **11,** 2087-2101.

van den Pol AN. (2012). Neuropeptide transmission in brain circuits. *Neuron* **76,** 98-115.

van der Beek EM, Horvath TL, Wiegant VM, van den Hurk R & Buijs RM. (1997). Evidence for a direct neuronal pathway from the suprachiasmatic nucleus to the gonadotropin-releasing hormone system: Combined tracing and light and electron microscope immunocytochemical studies. *Journal of Comparative Neurology* **384,** 569-579.

van der Beek EM, Swarts HJM & Wiegant VM. (1999). Central administration of antiserum to vasoactive intestinal peptide delays and reduces luteinizing hormone and prolactin surges in ovariectomized, estrogen-treated rats. *Neuroendocrinology* **69,** 227-237.

van der Veen DR, Castillo MR, van der Zee EA, Jansen K, Gerkema MP & Bult-Ito A. (2005). Circadian dynamics of vasopressin in mouse selection lines: Translation and release in the SCN. *Brain Research* **1060,** 16-25.

van der Zee EA & Bult A. (1995). Distribution of AVP and Ca^{2+}-dependent PKC-isozymes in the suprachiasmatic nucleus of the mouse and rabbit. *Brain Research* **701,** 99-107.

van der Zee EA, Roman V, Ten Brinke O & Meerlo P. (2005). TGFα and AVP in the mouse suprachiasmatic nucleus: Anatomical relationship and daily profiles. *Brain Research* **1054,** 159-166.

Veldhuis JD, Urban RJ & Dufau ML. (1993). Evidence that androgen negative feedback regulates hypothalamic gonadotropin-releasing hormone impulse strength and the burst-like secretion of biologically active luteinizing hormone in men. *Journal of Clinical Endocrinology and Metabolism* **74,** 1227-1235.

Vida B, Deli L, Hrabovszky E, Kalamatianos T, Caraty A, Coen CW, Liposits Z & Kalló I. (2010). Evidence for suprachiasmatic vasopressin neurones innervating kisspeptin neurones in the rostral periventricular area of the mouse brain: Regulation by oestrogen. *Journal of Neuroendocrinology* **22,** 1032-1039.

Vida B, Hrabovszky E, Kalamatianos T, Coen CW, Liposits Z & Kalló I. (2008). Oestrogen receptor α and β immunoreactive cells in the suprachiasmatic nucleus of mice: Distribution, sex differences and regulation by gonadal hormones. *Journal of Neuroendocrinology* **20,** 1270-1277.

Vijayan E, Samson WK, Said SI & McCann SM. (1979). Vasoactive intestinal peptide: Evidence for a hypothalamic site of action to release growth hormone, luteinizing hormone, and prolactin in conscious ovariectomized rats. *Endocrinology* **104,** 53-57.

Vincent-Lamarre P, Lynn M & Beique JC. (2018). The eloquent silent synapse. *Trends in Neuroscience* **41,** 557-559.

Volpi S, Rabadan-Diehl C & Aguilera G. (2004). Regulation of vasopressin V1b receptors and stress adaptation. *Annals of the New York Academy of Science* **1018,** 293-301.

Vong L, Ye C, Yang Z, Choi B, Chua S, Jr. & Lowell BB. (2011). Leptin action on GABAergic neurons prevents obesity and reduces inhibitory tone to POMC neurons. *Neuron* **71,** 142-154.

Vosko AM, Schroeder A, Loh DH & Colwell CS. (2007). Vasoactive intestinal peptide and the mammalian circadian system. *General and Comparative Endocrinology* **152,** 165-175.

Vrang N, Larsen PJ & Mikkelsen JD. (1995). Direct projection from the suprachiasmatic nucleus to hypophysiotrophic corticotropin-releasing factor immunoreactive cells in the paraventricular nucleus of the hypothalamus demonstrated by means of *Phaseolus vulgaris*-leucoagglutinin tract tracing. *Brain Research* **684,** 61-69.

Wagenmaker ER & Moenter SM. (2017). Exposure to acute psychosocial stress disrupts the luteinizing hormone surge independent of estrous cycle alterations in female mice. *Endocrinology* **158,** 2593-2602.

Wagner CK, Pfau JL, De Vries GJ & Merchenthaler IJ. (2001). Sex differences in progesterone receptor immunoreactivity in neonatal mouse brain depend on estrogen receptor α expression. *Journal of Neurobiology* **47,** 176-182.

Walker VR & Korach KS. (2004). Estrogen receptor knockout mice as a model for endocrine research. *ILAR Journal* **45,** 455-461.

Wang L, DeFazio RA & Moenter SM. (2016). Excitability and burst generation of AVPV kisspeptin neurons are regulated by the estrous cycle via multiple conductances modulated by estradiol action. *eNeuro* **3**.

Wang L, Vanacker C, Burger LL, Barnes T, Shah YM, Myers MG & Moenter SM. (2019). Genetic dissection of the different roles of hypothalamic kisspeptin neurons in regulating female reproduction. *Elife* **8**.

Wang M. (2011). Neurosteroids and GABA-A Receptor Function. *Frontiers in Endocrinology* **2,** 44.

Wang YC & Huang RC. (2006). Effects of sodium pump activity on spontaneous firing in neurons of the rat suprachiasmatic nucleus. *Journal of Neurophysiology* **96,** 109-118.

Warren SG, Humphreys AG, Juraska JM & Greenough WT. (1995). LTP varies across the estrous cycle: Enhanced synaptic plasticity in proestrus rats. *Brain Research* **703,** 26-30.

Watanabe K, Vanecek J & Yamaoka S. (2000). *In vitro* entrainment of the circadian rhythm of vasopressin-releasing cells in suprachiasmatic nucleus by vasoactive intestinal polypeptide. *Brain Research* **877,** 361-366.

Watson Jr. RE, Langub Jr. MC, Engle MG & Maley BE. (1995). Estrogen-receptive neurons in the anteroventral periventricular nucleus are synaptic targets of the suprachiasmatic nucleus and peri-suprachiasmatic region. *Brain Research* **689**.

Watts AG, Sheward WJ, Whale D & Fink G. (1989). The effects of knife cuts in the sub-paraventricular zone of the female rat hypothalamus on oestrogen-induced diurnal surges of plasma prolactin and LH, and circadian wheel-running activity. *Journal of Endocrinology* **112,** 593-604.

Watts AG & Swanson LW. (1987). Efferent projections of the suprachiasmatic nucleus: II. Studies using retrograde transport of fluorescent dyes and simultaneous peptide immunohistochemistry in the rat. *Journal of Comparative Neurology* **258,** 230-252.

Watts AG, Swanson LW & Sanchez-Watts G. (1987). Efferent projections of the suprachiasmatic nucleus: I. Studies using anterograde transport of *Phaseolus vulgaris* leucoagglutinin in the rat. *Journal of Comparative Neurology* **258,** 204-229.

Weiland NG. (1992). Glutamic acid decarboxylase messenger ribonucleic acid is regulated by estradiol and progesterone in the hippocampus. *Endocrinology* **131,** 2697-2702.

Welsh DK, Logothetis DE, Meister M & Reppert SM. (1995). Individual neurons dissociated from rat suprachiasmatic nucleus express independently phased circadian firing rhythms. *Neuron* **14,** 697-706.

Wiegand SJ & Terasawa E. (1982). Discrete lesions reveal functional hetereogeneity of suprachiasmatic structures in regulation of gonadotropin secretion in the female rate. *Neuroendocrinology* **34,** 395-404.

Wiegand SJ, Terasawa E, Bridson WE & Goy RW. (1980). Effects of discrete lesions of preoptic suprachiasmatic structures in the female rat: Alterations in the feedback regulation of gonadotropin secretion. *Neuroendocrinology* **31,** 147-157.

Wildt L, Häusler A, Marshall G, Hutchinson JS, Plant TM, Belchetz PE & Knobil E. (1981). Frequency and amplitude of gonadotropin-releasing hormone stimulation and gonadotropin secretion in the rhesus monkey. *Endocrinology* **109,** 376-385.

Williams WP, 3rd, Jarjisian SG, Mikkelsen JD & Kriegsfeld LJ. (2011). Circadian control of kisspeptin and a gated GnRH response mediate the preovulatory luteinizing hormone surge. *Endocrinology* **152,** 595-606.

Williams WP, 3rd & Kriegsfeld LJ. (2012). Circadian control of neuroendocrine circuits regulating female reproductive function. *Frontiers in Endocrinology* **3,** 60.

Wintermantel TM, Campbell RE, Porteous R, Bock D, Grone HJ, Todman MG, Korach KS, Greiner E, Perez CA, Schutz G & Herbison AE. (2006). Definition of estrogen receptor pathway critical for estrogen positive feedback to gonadotropin-releasing hormone neurons and fertility. *Neuron* **52,** 271-280.

Wu SS, Nathanielsz PW & McDonald TJ. (1995). Immunocytochemical distribution of androgen receptors in the hypothalamus and pituitary of the fetal baboon in late gestation. *Developmental Brain Research* **84,** 278-281.

Wu X-Y, Li Z-L, Wu C-Y, Liu Y-M, Lin H, Wang S-H & Xiao W-F. (2010). Endocrine traits of polycystic ovary syndrome in prenatally androgenized female Sprague-Dawley rats. *Endocrine Journal* **57,** 201-209.

Xita N & Tsatsoulis A. (2006). Fetal programming of polycystic ovary syndrome by androgen excess: Evidence from experimental, clinical, and genetic association studies. *Journal of Clinical Endocrinology and Metabolism* **91,** 1660-1666.

Xu Z, Kaga S, Tsubomizu J, Fujisaki J, Mochiduki A, Sakai T, Tsukamura H, Maeda K, Inoue K & Adachi AA. (2011). Circadian transcriptional factor DBP regulates expression of *Kiss1* in the anteroventral periventricular nucleus. *Molecular and Cellular Endocrinology* **339,** 90-97.

Yamaguchi Y, Suzuki T, Mizoro Y, Kori H, Okada K, Chen Y, Fustin J-M, Yamazaki F, Mizuguchi N, Zhang J, Dong X, Tsujimoto G, Okuno Y, Doi M & Okamura H. (2013). Mice genetically deficient in vasopressin V1a and V1b receptors are resistant to jet lag. *Science* **342,** 85-90.

Yan L, Karatsoreos I, LeSauter J, Welsh DK, Kay S, Foley D & Silver R. (2007). Exploring spatiotemporal organization of SCN circuits. *Cold Spring Harbor Symposia on Quantitative Biology* **72,** 527-541.

Yeo SH, Kyle V, Morris PG, Jackman S, Sinnett-Smith LC, Schacker M, Chen C & Colledge WH. (2016). Visualisation of Kiss1 neurone distribution using a Kiss1-CRE transgenic mouse. *Journal of Neuroendocrinology* **28**.

Yeung CM, Chan CB, Leung PS & Cheng CH. (2006). Cells of the anterior pituitary. *International Journal of Biochemistry & Cell Biology* **38,** 1441-1449.

Yildiz BO, Bozdag G, Yapici Z, Esinler I & Yarali H. (2012). Prevalence, phenotype and cardiometabolic risk of polycystic ovary syndrome under different diagnostic criteria. *Human Reproduction* **27,** 3067-3073.

Yip SH, Boehm U, Herbison AE & Campbell RE. (2015). Conditional viral tract tracing delineates the projections of the distinct kisspeptin neuron populations to gonadotropin-releasing hormone (GnRH) neurons in the mouse. *Endocrinology* **156,** 2582-2594.

Yizhar O, Fenno LE, Davidson TJ, Mogri M & Deisseroth K. (2011). Optogenetics in neural systems. *Neuron* **71,** 9-34.

Yoshikawa T, Nakajima Y, Yamada Y, Enoki R, Watanabe K, Yamazaki M, Sakimura K, Honma S & Honma K. (2015). Spatiotemporal profiles of arginine vasopressin transcription in cultured suprachiasmatic nucleus. *European Journal of Neuroscience* **42,** 2678-2689.

Young JM & McNeilly AS. (2010). Theca: The forgotten cell of the ovarian follicle. *Reproduction* **140,** 489-504.

Yung Y, Aviel-Ronen S, Maman E, Rubinstein N, Avivi C, Orvieto R & Hourvitz A. (2014). Localization of luteinizing hormone receptor protein in the human ovary. *Molecular Human Reproduction* **20,** 844-849.

Zaelzer C, Gizowski C, Salmon CK, Murai KK & Bourque CW. (2018). Detection of activity-dependent vasopressin release from neuronal dendrites and axon terminals using sniffer cells. *Journal of Neurophysiology* **120,** 1386-1396.

Zhang C, Roepke TA, Kelly MJ & Rønnekleiv OK. (2008). Kisspeptin depolarizes gonadotropin-releasing hormone neurons through activation of TRPC-like cationic channels. *Journal of Neuroscience* **28,** 4423-4434.

Zhang C, Rønnekleiv OK & Kelly MJ. (2013). Kisspeptin inhibits a slow afterhyperpolarization current via protein kinase C and reduces spike frequency adaptation in GnRH neurons. *American Journal of Physiology Endocrinology and Metabolism* **304,** E1237-1244.